NUREG/CR—4905
SAND85—1263
R3
Printed June 1987

Detonability of H_2-Air-Diluent Mixtures

Sheldon R. Tieszen, Martin P. Sherman
William B. Benedick, Marshall Berman

Prepared by
Sandia National Laboratories
Albuquerque, New Mexico 87185 and Livermore, California 94550
for the United States Department of Energy
under Contract DE-AC04-76DP00789

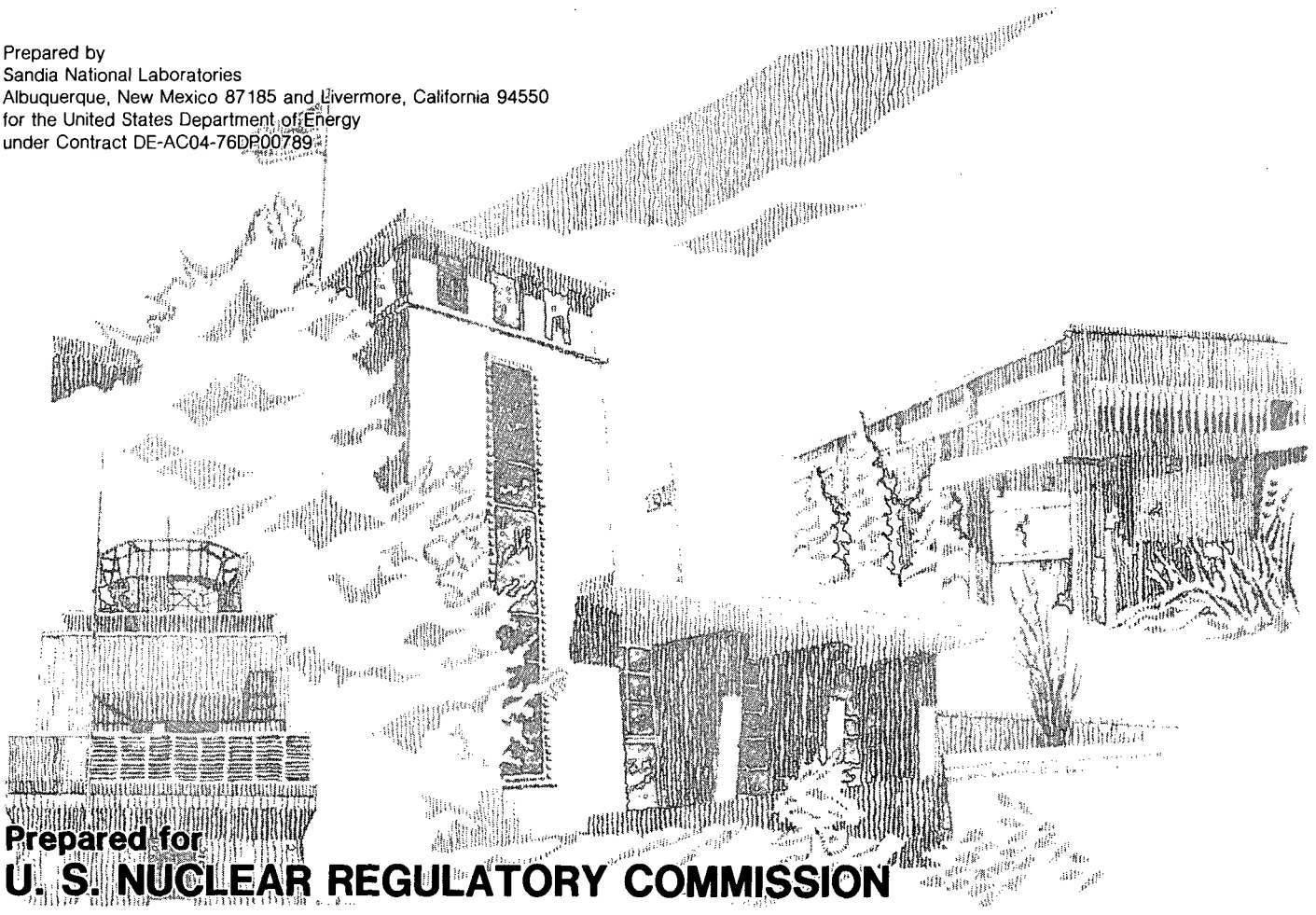

Prepared for
U. S. NUCLEAR REGULATORY COMMISSION

SF2900Q(8-81)

NOTICE

This report was prepared as an account of work sponsored by an agency of the United States Government. Neither the United States Government nor any agency thereof, or any of their employees, makes any warranty, expressed or implied, or assumes any legal liability or responsibility for any third party's use, or the results of such use, of any information, apparatus product or process disclosed in this report, or represents that its use by such third party would not infringe privately owned rights.

Available from

Superintendent of Documents
U.S. Government Printing Office
Post Office Box 37082
Washington, D.C. 20013-7082

and

National Technical Information Service
Springfield, VA 22161

NUREG/CR-4905
SAND85-1263
R-3

DETONABILITY OF H_2-AIR-DILUENT MIXTURES

Sheldon R. Tieszen
Martin P. Sherman
William B. Benedick
Marshall Berman

June 1987

Sandia National Laboratories
Albuquerque, New Mexico 87185
Operated by
Sandia Corporation
for the
U.S. Department of Energy

Prepared for
Division of Reactor System Safety
Office of Nuclear Regulatory Research
U.S. Nuclear Regulatory Commission
Washington, DC 20555
Under Memorandum of Understanding DOE 40-550-75
NRC FIN No. A-1246

ABSTRACT

This report describes the Heated Detonation Tube (HDT). Detonation cell width and velocity results are presented for H_2-air mixtures, undiluted and diluted with CO_2 and H_2O for a range of H_2 concentration, initial temperature and pressure. The results show that the addition of either CO_2 or H_2O significantly increases the detonation cell width and hence reduces the detonability of the mixture. The results also show that the detonation cell width is reduced (detonability is increased) for increased initial temperature and/or pressure.

TABLE OF CONTENTS

	Page
ABSTRACT	iii/iv
Preface	xiii
ACKNOWLEDGMENTS	xiv
EXECUTIVE SUMMARY	1
CHAPTER 1 - INTRODUCTION	1-1
1.1 PURPOSE OF THE FACILITY	1-1
1.2 LITERATURE	1-1
1.3 REFERENCES FOR CHAPTER 1	1-9
CHAPTER 2 - FACILITY DESCRIPTION	2-1
2.1 DESIGN CONSIDERATIONS	2-1
2.2 HDT DESCRIPTION	2-2
2.3 REFERENCES FOR CHAPTER 2	2-10
CHAPTER 3 - PROCEDURE	3-1
CHAPTER 4 - RESULTS	4-1
4.1 DETONATION CELL WIDTH, λ	4-1
4.1.1 Modeling	4-9
4.1.2 H_2-Air; P,T = Constant (Test Series #1)	4-10
4.1.3 H_2-Air-CO_2; P,T = Constant (Test Series #2)	4-11
4.1.4 H_2-Air-Steam; ρ_{air},T = Constant (Test Series #3,4)	4-12
4.1.5 H_2-Air; ρ_{air},T = Constant(Test Series #5)	4-13
4.1.6 H_2-Air; X_{H2},P = Constant (Test Series #6) ρ = Constant (Test Series #7)	4-13
4.2 DETONATION VELOCITY MEASUREMENTS	4-14
4.3 REFERENCES FOR CHAPTER 4	4-19
CHAPTER 5 - DISCUSSION AND CONCLUSIONS	5-1
5.1 DISCUSSION	5-1
5.2 CONCLUSIONS	5-2
5.3 FUTURE WORK	5-4
5.4 REFERENCES FOR CHAPTER 5	5-5

Page

APPENDICES

APPENDIX A - DETAILS OF THE EXPERIMENTAL APPARATUS A-1

A.1 STRUCTURE A-1
A.1.1 The Main Tube A-1
A.1.2 The Secondary Piping A-6
A.1.3 The Structural Supports A-9
A.2 ELECTRICAL A-13
A.2.1 General Power A-13
A.2.2 Detonation Tube Heating System A-13
A.3 THERMAL ASPECTS A-25
A.3.1 Insulation A-26
A.3.2 Temperature Monitoring Thermocouples A-26
A.3.3 Thermal Limits A-27
A.4 EXPLOSIVE INITIATOR CIRCUIT A-28
A.5 INSTRUMENTATION A-30
A.5.1 Static Pressure Instrumentation A-30
A.5.2 Temperature Instrumentation A-31
A.5.3 Smoked Foil Instrumentation A-31
A.5.4 Dynamic Pressure Instrumentation A-39
A.5.5 Humidity Instrumentation A-40
A.6 REFERENCES FOR APPENDIX A A-48

APPENDIX B - DETAILS OF PROCEDURE B-1

B.1 TEST SERIES #1 B-2
B.2 TEST SERIES #2 B-3
B.3 TEST SERIES #3, 4 B-4
B.4 TEST SERIES #5 B-5
B.5 TEST SERIES #6 B-5
B.6 TEST SERIES #7 B-6

APPENDIX C - TABULATED DATA C-1

APPENDIX D - ESTIMATE OF UNCERTAINTY BOUNDS D-1

D.1 DETONATION CELL WIDTH D-1
D.1.1 Comparison Between Test Apparatus D-2
D.1.2 Uncertainty Bounds for Detonation Cell Width Measurements D-6
D.1.2.1 Comparison Between Test Apparatus D-7
D.1.2.2 Multiple Observers D-7
D.1.3 Bounds on the HDT Test Series D-10
D.2 DETONATION PRESSURE D-11
D.3 DETONATION VELOCITY D-17
D.4 THERMODYNAMIC STATE D-19
D.4.1 Variance Estimates for Measured Variables D-23
D.4.1.1 Temperature Standard Deviation Estimate D-24

Page

D.4.1.2 Pressure Standard Deviation Estimate D-25
D.4.1.3 Uncertainty in the Uniformity of the Gas Mixture D-26
D.4.1.4 Steady State Criteria D-27
D.4.2 Standard Deviation Estimates of ρ_{air}, ϕ, X_{H2O}, and X_{CO2} D-28
D.4.3 Standard Deviation Estimates of Detonation Cell Width and Velocity Due Initial Thermodynamic State D-36
D.5 REFERENCES FOR APPENDIX D D-37

APPENDIX E - THERMODYNAMICS AND CELL WIDTH E-1

E.1 THERMODYNAMIC RELATIONS E-1
E.2 GENERAL FUNCTIONAL RELATIONSHIP E-5
E.3 EFFECT OF TEMPERATURE E-6

APPENDIX F - ANALYSIS OF THE TEMPERATURE DISTRIBUTION AND THERMAL TRANSIENT RESPONSE OF THE HDT F-1

F.1 NOMENCLATURE F-1
F.2 DERIVATION OF THE MODEL F-3
F.3 SOLUTION TO PROBLEM #1 - HEATERS FULL ON F-5
F.4 SOLUTION TO PROBLEM #2 - HEATERS AT CONSTANT TEMPERATURE, T_r F-9
F.5 COMPARISON BETWEEN THE MODEL AND THE HDT F-15

APPENDIX G - DATA ACQUISITION SYSTEM DETAILS G-1

G.1 HARDWARE G-1
G.1.1 Tektronix 7612D Transient Digitizers G-1
G.1.2 CAMAC Transient Digitizers G-2
G.1.3 Storage/Processing Hardware G-2
G.2 SOFTWARE G-2
G.2.1 HDT Control Program G-2
G.2.2 Data Acquisition Programs G-3
G.2.3 Data Storage Formats G-3
G.2.4 Data Processing Programs G-3
G.3 REFERENCES FOR APPENDIX G G-4

LIST OF FIGURES

Figure		Page
1-1	Percent Hydrogen Concentration vs. Percent Metal-Water Reaction for Various Plants.	1-3
1-2	Early Prediction of the Detonability Limits of H_2-Air-Steam Mixtures.	1-4
1-3	Cellular Pattern Left on Sooted Plate from Passing Detonation Wave in Argon Diluted Fuel/Oxygen.	1-6
1-4	Effect of Geometry on Propagation of Detonation Waves.	1-7
1-5	Detonation Cell Pattern on a Smoked Foil for a H_2-Air Mixture. Note "irregular" structure compared to Figure 1-3.	1-8
2-1	Heated Detonation Tube without Thermal Insulation.	2-3
2-2	Heated Detonation Tube with Thermal Insulation Layer	2-4
2-3	Schematic of the Secondary Piping	2-5
2-4	Schematic of the Heater Control Circuit.	2-7
4-1	Typical Smoked Foil from HDT	4-2
4-2	Detonation Cell Width vs. Equivalence Ratio for Test Series #1. (H_2-Air at P=1 atm, T=20°C)	4-3
4-3	Detonation Cell Width vs. Equivalence Ratio for Test Series #2. (H_2-Air-CO_2 at P=1 atm, T=20°C)	4-4
4-4	Detonation Cell Width vs. Equivalence Ratio for Test Series #3, 4. (H_2-Air-H_2O at ρ_{air}=41.6 moles/m^3, T=100°C	4-5
4-5	Effect of Initial Conditions on Detonation Cell Width of H_2-Air Mixtures	4-6
4-6	Detonation Cell Width vs. Temperature for Test Series #6, 7. (H_2-Air at X_{H2}=0.17)	4-7
4-7	Uncertainty Ranges for the HDT Data in Figure 4-5.	4-8

Figure		Page
4-8	Detonation Velocity vs. Equivalence Ratio for Test Series #1, 2. (H_2-Air-CO_2 at P=1 atm, T=20°)	4-15
4-9	Detonation Velocity vs. Equivalence Ratio for Test Series #3, 4. (H_2-Air-H_2O at ρ_{air}=41.6 moles/m^3, T=100°C)	4-16
4-10	Effect of Initial Conditions on Detonation Velocity of H_2-Air Mixtures	4-17
4-11	Detonation Velocity vs. Temperature for Test Series #6,7. (H_2-Air at X_{H2}=0.17)	4-18
5-1	Constant Detonation Cell Width on Mixture Coordinates (for T = 100°C, Air Density = 41.6 mole/m^3)	5-2
5-2	Effect of Geometry on Propagation of Detonation Waves.	5-3
5-3	Detonation Cell Width vs. Equivalence Ratio for Test Series #3,4. (H_2-Air-H_2O at ρ_{air}=41.6 moles/m^3, T=100°C)	5-5
A-1	Cross-Section of a Gas Recirculation Penetration	A-2
A-2	Cross-Section of a Transducer Penetration	A-3
A-3	Cross-Section of a Pipe Flange	A-4
A-4	Schematic of the Secondary Piping	A-7
A-5	Detonation Tube Supports	A-10
A-6	Tube Support V-Block Positioning Device	A-11
A-7	Heater Section Schematic - Long Pipe Section, Sides and Bottom	A-15
A-8	Heater Section Schematic - Long Pipe Section, Top	A-17
A-9	Heater Section Schematic - Pipe to Pipe Flanges	A-18
A-10	Heater Section Schematic - Short Pipe	A-19
A-11	Heater Section Schematic - Endplates, Flanges	A-21

Figure		Page
A-12	Heater Control Circuit Schematic	A-23
A-13	High Explosive Initiator	A-29
A-14	Transducer Fitting Cross-Section	A-47
D-1	Detonation Cell Width Measurement (a) Use of High Contrast Individual Cells (b) Use of High Contrast Long Running Lines	D-2
D-2	Detonation Cell Width Measurements for HDT Test Series #3 (H_2-Air, ρ_{air}=41.6 moles/m^3, T=100°C).	D-4
D-3	Detonation Cell Width Measurements for HDT Test Series #5 (H_2-Air, ρ_{air}=41.6 moles/m^3, T=20°C).	D-5
D-4	Comparison of Detonation Cell Width Data Between the HDT and McGill University. (HDT Test Series #1, P=1 atm, T=25°C).	D-8
D-5	Normalized Detonation Cell Width (λ Author/λ Knystautas) vs. HDT Test Number.	D-9
D-6	Typical PCB Pressure Trace - Small Cell Width (λ = 5 mm , Test HT-84).	D-13
D-7	Typical Kistler Pressure Trace - Small Cell Width (λ = 5 mm , Test HT-84).	D-14
D-8	Typical PCB Pressure Trace - Large Cell Width (λ = 400 mm , Test HT-96).	D-15
D-9	Typical Kistler Pressure Trace - Large Cell Width (λ = 400 mm , Test HT-96).	D-16
F-1	Control Volume for the 1-D Unsteady Fin Model.	F-4
F-2	Comparison of Temperature Distribution and Transient Response of the HDT and 1-D Unsteady Fin Model	F-16

LIST OF TABLES

Table		Page
3-1 -	Test Series	3-2
4-1 -	Equivalence Ratio as a Function of Steam and H_2 Concentrations in Total Mixture by Volume	4-10
A-1 -	Temperature Limits of Detonation Tube Components	A-27
A-2 -	Axial Location of Instrumentation Ports Relative to the Initiation Endplate Inside Face	A-30
A-3 -	Type and Location of Initial Thermodynamic State Measurements	A-32
A-4 -	Temperature, Pressure and Humidity Instrumentation	A-37
A-5 -	Type, Number and Digitizing Frequency for Dynamic Pressure Measurement	A-41
A-6 -	Dynamic Pressure Instrumentation	A-46
B-1 -	Test Series	B-2
C-1 -	Tests in Each Series	C-2
C-2 -	Detonation Cell Width Data	C-3
C-3 -	Detonation Velocity Data	C-9
C-4 -	Initial Thermodynamic State	C-14
D-1 -	Effect of Initial Transient on Detonation Velocity	D-18
D-2 -	Upper and Lower Bounds on the Detonation Velocity	D-20
D-3 -	Variables Chosen to Specify the Initial Thermodynamic State of the Mixture	D-22
D-4 -	Measured Variables	D-22

Table		Page
D-5 -	Standard Deviation Estimates of Measured Variables. (Using Engineering Judgement)	D-24
F-1 -	Numerical Values of the Model Parameters	F-15

Preface

This document is intended to serve two purposes. First, it provides a complete summary of the Heated Detonation Tube test results for the general reader. Second, it completely documents, for scientific accuracy and archival purposes, the apparatus, procedures, and uncertainties associated with data from the Heated Detonation Tube Program. The appendices contain a detailed description of the apparatus, procedures and uncertainty analysis of the data.

ACKNOWLEDGMENTS

The authors would like to recognize the considerable contribution to the field of detonation research and its application to reactor safety by Professors John H. Lee and Romuald Knystautas of McGill University, Canada. They have assisted us throughout this project from its conceptual design to reviewing the results. The authors would also like to acknowledge valuable technical discussions with J. Shepherd who developed the model used to correlate the data in this report. The authors would like to thank NRC Contract Managers J. Larkins and P. Worthington. The authors also appreciate the technical support of C. J. Daniel, D. Montgomery, M. Oliver, D. Beeker, J. Lee and J. Barry in obtaining the data in this report.

EXECUTIVE SUMMARY

Hydrogen combustion as related to reactor safety has been studied since the accident at Three Mile Island. The recent accident at Chernobyl, during which a hydrogen detonation (or accelerated deflagration) may have occurred, strengthens the concern that hydrogen combustion can occur during a severe accident. It is important to understand the various modes of combustion which can occur, both in terms of the possibility and consequences. One mode of combustion is detonation.

This report documents test results from gaseous detonation studies in the Heated Detonation Tube (HDT). Detonations have peak pressures that are well above the quasi-static pressures associated with ordinary deflagrations. Should a detonation occur inside a reactor containment, both the containment and safety-related equipment could be severely damaged.

Test results reported are the detonation cell width, λ, and detonation velocity. λ is an intrinsic length scale that characterizes detonations. Highly detonable mixtures have small cell widths, while increasingly less detonable mixtures have increasingly larger cell widths. Previous research has shown that the limits of detonation propagation are related to the ratio of λ to a characteristic geometric length-scale. λ has been related to dynamic detonation parameters such as limits of propagation in tubes, channels, and other ducts, the transmission from a duct to an unconfined space, and initiation energy for a high-explosive charge. Detonation cell width measurements have been used to establish the relative detonability for a broad range of fuel-oxidizer mixtures.

The HDT is a 43-cm (17-in) inside diameter, 13-m (43-ft) long heated tube. It is designed to study H_2-air-steam mixtures. To the authors' knowledge, no prior experimental detonation data existed for this ternary mixture, which is the most likely mixture to occur in a severe accident. Further, much of the earlier detonation limit data for dry H_2-air mixtures are of limited relevance because of the small scale in which the experiments were done. Experimental results from the large diameter HDT have shown that H_2 will detonate for a broader range of concentrations than previously believed; a mixture as lean as 13% H_2 has detonated. Experiments show that the addition of steam to a H_2-air mixture at 100°C, with an air density of 41.6 moles/m^3 (standard density of air), significantly decreases the sensitivity of the mixture to detonate. The energy required to detonate a stoichiometric H_2-air mixture increases by factors of 220, 8000, and 2.2×10^5 for addition of 10%, 20%, and 30% steam, respectively.

Tests have also shown that the detonation cell width, and hence detonability, depends on the initial thermodynamic state of the mixture as well as on the gas composition. Changing the

temperature and pressure (or density) of the mixture affects the detonability of that mixture. Increasing the temperature or pressure of the mixture sensitizes the mixture making it more detonable.

Experimental results reported here can be applied directly to detonation safety analysis to answer the question, "Can a detonation propagate in a given mixture in a given geometry?" The results do not address related questions associated with the generation, transport and mixing of hydrogen in containment. Such additional information is necessary to better use the results of this report in a safety analysis. Further, this report does not address the question of how a detonation is initiated, i.e., the deflagration-to-detonation transition question, nor does it address possible damage from detonation overpressures.

CHAPTER 1

INTRODUCTION

1.1 PURPOSE OF THE FACILITY

The main purpose of the Heated Detonation Tube (HDT) facility is to study the detonability of hydrogen-air-steam mixtures. To the best of our knowledge, there have been no previous experimental studies of these ternary mixtures. Such mixtures can form in a severe nuclear-reactor accident involving core damage. Detonations cause peak loads in addition to the quasi-static loads of weak deflagrations. They pose a potential threat to the containment structure and to safety-related equipment. Detonability is related to detonation cell width, the primary measurement obtained from the HDT experiments.

In addition to studying detonations in hydrogen-air-steam mixtures, necessarily at elevated temperatures, the Heated Detonation Tube has been used to study dry hydrogen-air mixtures. Hydrogen-air mixtures have been studied at ambient and elevated temperatures, various densities, and at mixtures farther from stoichiometric than had been detonated at any other facility. Some studies with hydrogen-air-carbon dioxide were also made to confirm and extend previous data for this ternary mixture.

1.2 LITERATURE

Serious study of H_2-air detonations began after the Three-Mile-Island (TMI-2) accident during which a hydrogen deflagration occurred. The source of the burned hydrogen in containment was the oxidation of the zirconium cladding in the degraded core. The hydrogen mole fraction prior to combustion has been estimated to be about 8%. [1] If the concentration of hydrogen, even locally, were considerably higher, then there could exist the danger of a detonation.

Prior to the TMI-2 accident, the reactor safety community was concerned with design basis accidents where only a limited degree of metal-water reaction was specified. The relatively small amount of hydrogen produced from this type of accident, coupled with early research which indicated that at least 18% hydrogen was needed for a detonation, led many researchers to minimize the threat of a hydrogen-air detonation.

Research since the TMI-2 accident has identified, and in some cases quantified, several factors which play a role in determining the threat of detonation. Some of these factors are the rates and amounts of hydrogen released, the rate of transport and mixing of the hydrogen, the presence of diluents such as steam, the source and timing of ignition, the local turbulent environment where a deflagration might undergo a transition to a

detonation, the containment volume and design, and the location of safety-related equipment.

Fig. 1-1, from Ref. [2] shows the hydrogen concentration as a function of percent metal-water reaction for various nuclear reactor containments. Multi-compartment lumped-volume computer models developed for deflagration studies have shown that locally high concentrations of H_2 are possible in certain containments in certain accident scenarios, particularly in the upper plenum of an ice condenser PWR [3]. Research has also shown that detonations can result from confinement and turbulent interaction with a deflagration. Recent observations of Lee [4], Pförtner [5] and Sherman et al. [6] showed that turbulence-induced transition to detonation can occur even in off-stoichiometric H_2-air mixtures, not only under confined, but also under partially and even unconfined conditions.

The only prior work on hydrogen-air-steam mixtures appears to be an estimate of detonation limits in the report of Shapiro and Moffette [7], which was repeated in the WASH 1400 Reactor Safety Study [8] and the Core-Meltdown Review [9]. The "detonation limit" is defined as the limiting mixture ratios of fuel to oxidizer, at given pressure and temperature, that will propagate a detonation. In these reports a triangular diagram appeared, Fig. 1-2, in which "detonation limits" for hydrogen-air-steam mixtures were shown. For no steam, the limits are the 18% and 59% values quoted in the older combustion literature, e.g., [10]. It appears that the values for the limits with steam may have been estimated by drawing two lines nearly parallel to the axes and rounding off the intersection at about 32% steam mole fraction. This is equivalent to predicting that for steam mole fractions below about 25%, steam has a negligible effect on the lean and rich detonation limits for hydrogen.

Several experimental studies that have been completed in the last decade in dry H_2-air mixtures have shown that the classical 18% and 59% detonation limits are not correct [11,12,13,14,15, 16]. The entire idea of a detonation "limit" has undergone considerable review. It is now known that detonation limits are not fixed values of mixture composition, but depend on the ratio of geometric size to what is termed "detonation cell width (or size)."

1.2.1 Detonation Cell Width

Detonations are known not to be simple planar waves with a leading, normal shock wave closely followed by a rapid chemical reaction, as in the Zel'dovich-von Neumann-Doering (ZND) model developed in the 1940's. Gaseous detonations are composed of a complex pattern of transverse oblique shock waves with Mach triple-point intersections followed by chemical reactions (deflagrations). The locus of Mach triple-point intersections can be shown by the pattern a detonation makes passing over a smoked surface. A regular pattern of such diamond shapes is shown in

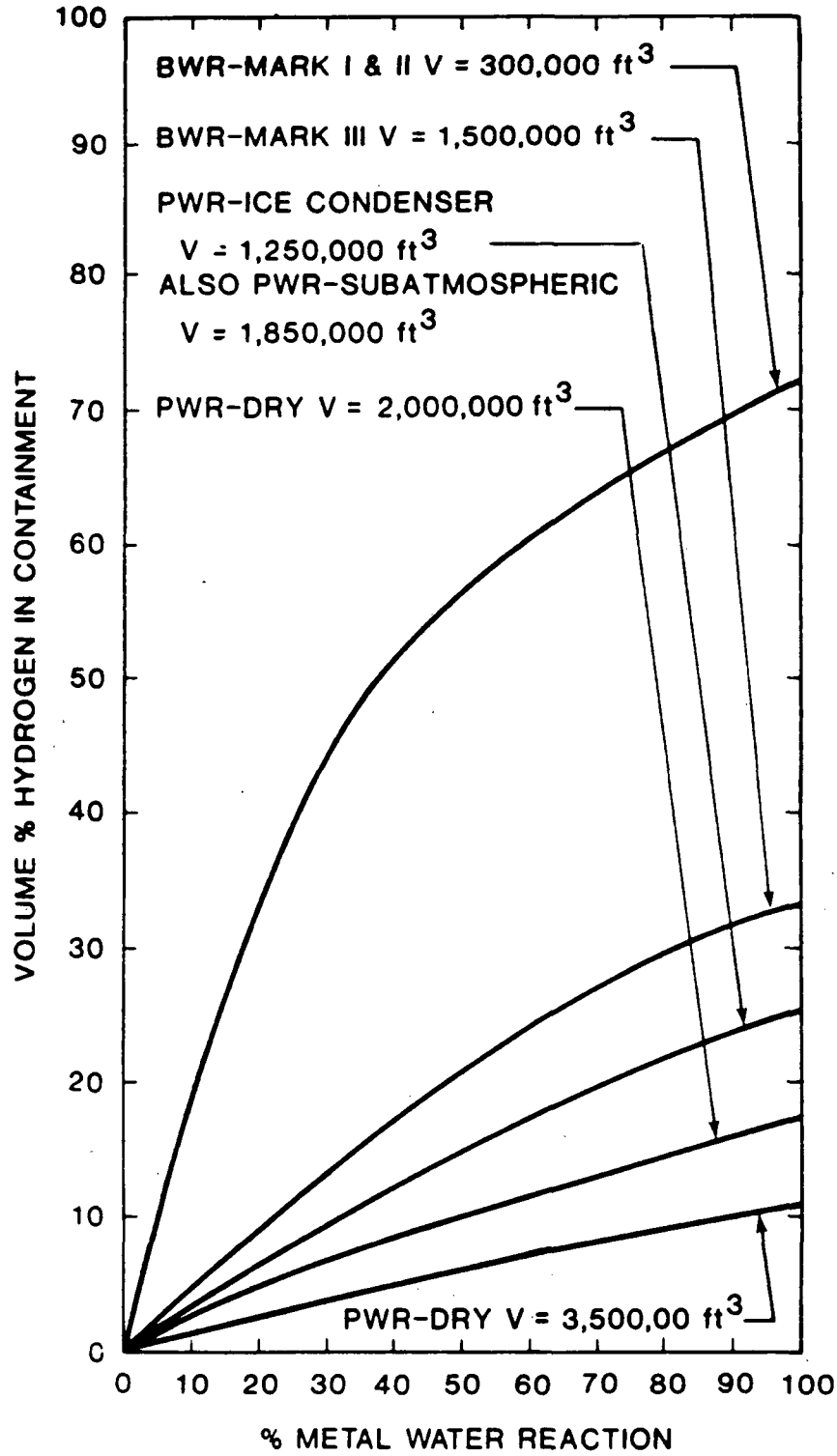

Figure 1-1. Percent Hydrogen Concentration vs. Percent Metal-Water Reaction for Various Plants.

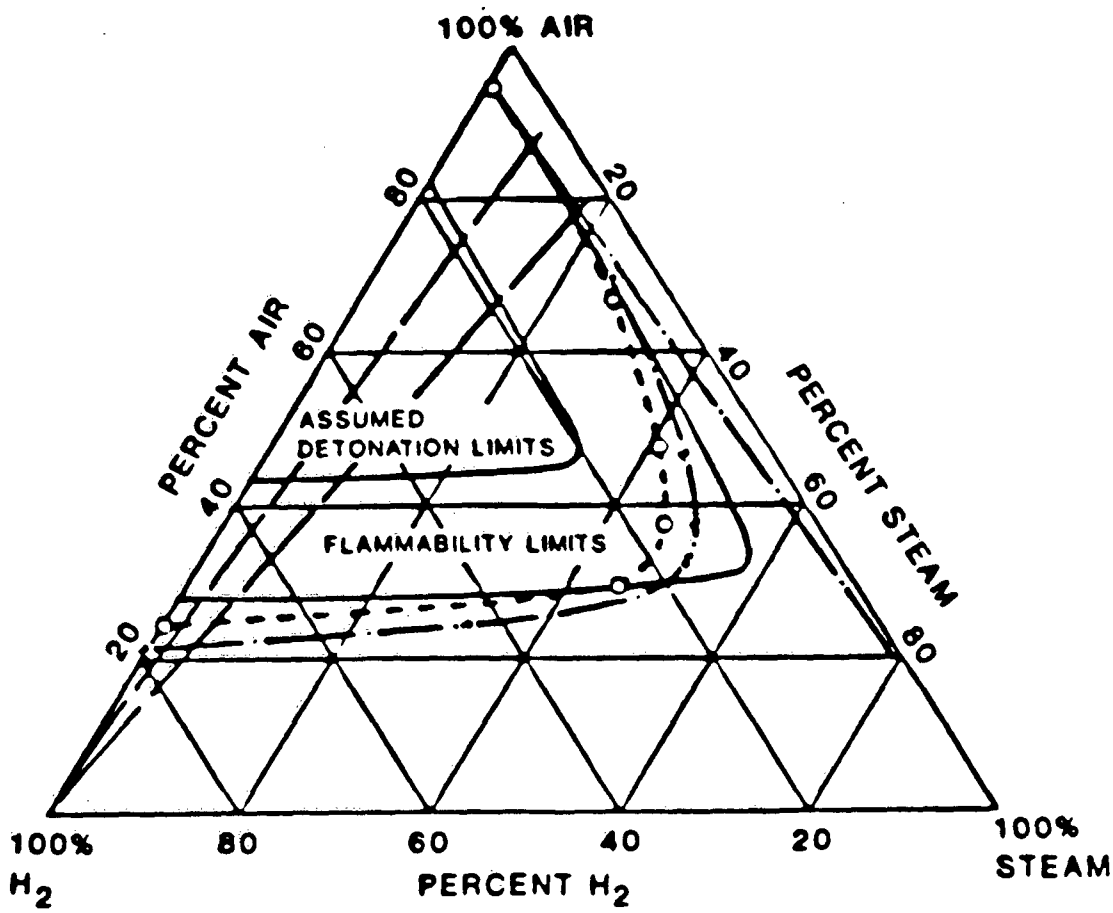

FLAMMABILITY LIMITS

——————— 75° F - 0 psig (24° C - 101 kPa)*

O— — — — — 300° F - 0 psig (149° C - 101 kPa)

⊙———•— 300° F - 100 psig (149° C - 792 kPa)

* Actual temperatures used in producing the data for this curve are 68°F - 187°F (20°C - 86°C)

Figure 1-2. Early Prediction of the Detonability Limits of H_2-Air-Steam Mixtures. [From Reference 7]

Fig. 1-3 from studies in argon diluted fuel-oxygen mixtures [17]. The width of these diamond patterns is the detonation cell width, λ.

The three-dimensional transverse wave structure which produces the diamond pattern is the direct consequence of the nonlinear coupling of the exothermic chemical reactions and the shock-induced hydrodynamic flow field. Extensive evidence shows that all self-sustaining gaseous detonation waves have this structure. The cell width is believed to be proportional to the chemical length scale of a given explosive mixture under detonating conditions and can be used to define the detonation sensitivity of that particular mixture. Moreover, in recent years the broader significance of the detonation cell width has been demonstrated via the quantitative links that have been established with the other "dynamic" detonation parameters [11,12] such as the critical initiation energy and the critical tube diameter. It also has direct relevance to establishing criteria for transmission of detonation [13], onset of transition [14], and definition of detonability limits [15]. Examples are shown in Fig. 1-4.

Other measures of detonation sensitivity exist, such as the critical tube diameter [18]. The critical tube diameter is the minimum diameter of a rigid tube or orifice from which a detonation in a given mixture will continue to propagate as it diffracts into an unconfined volume. In fuel-air mixtures the critical tube diameter can become quite large, on the order of meters, making measurements inconvenient. Further, when the desired initial conditions are other than ambient, measuring critical tube diameter becomes even more difficult.

Detonation cellular structure is relatively easy to record; however, there is a certain amount of irregularity that characterizes fuel-air mixtures, unlike the fuel-oxygen mixtures with high argon dilution shown in Fig. 1-3. This randomness, or irregularity, makes the interpretation of smoked foil records uncertain. A typical smoked foil record is shown in Fig. 1-5. It appears that a range of detonation cell widths exist. Typically, experimenters report only one detonation cell width for a given mixture. The rationale used is that there is only one intrinsic detonation cell width for a given mixture, and the randomness is due to the response of the detonation wave to external perturbations.

A few experimenters have assigned error estimates to their detonation cell width data [19,20]. Recently, there have been some questions raised concerning the validity of the rationale that there is only one intrinsic detonation cell width for a given mixture. It has been proposed that the irregularity of some of the smoked foil records indicates that a detonation wave in fuel-air mixtures has more than one detonation cell width or mode [20,21]. The causes of irregularities are currently an active area of research.

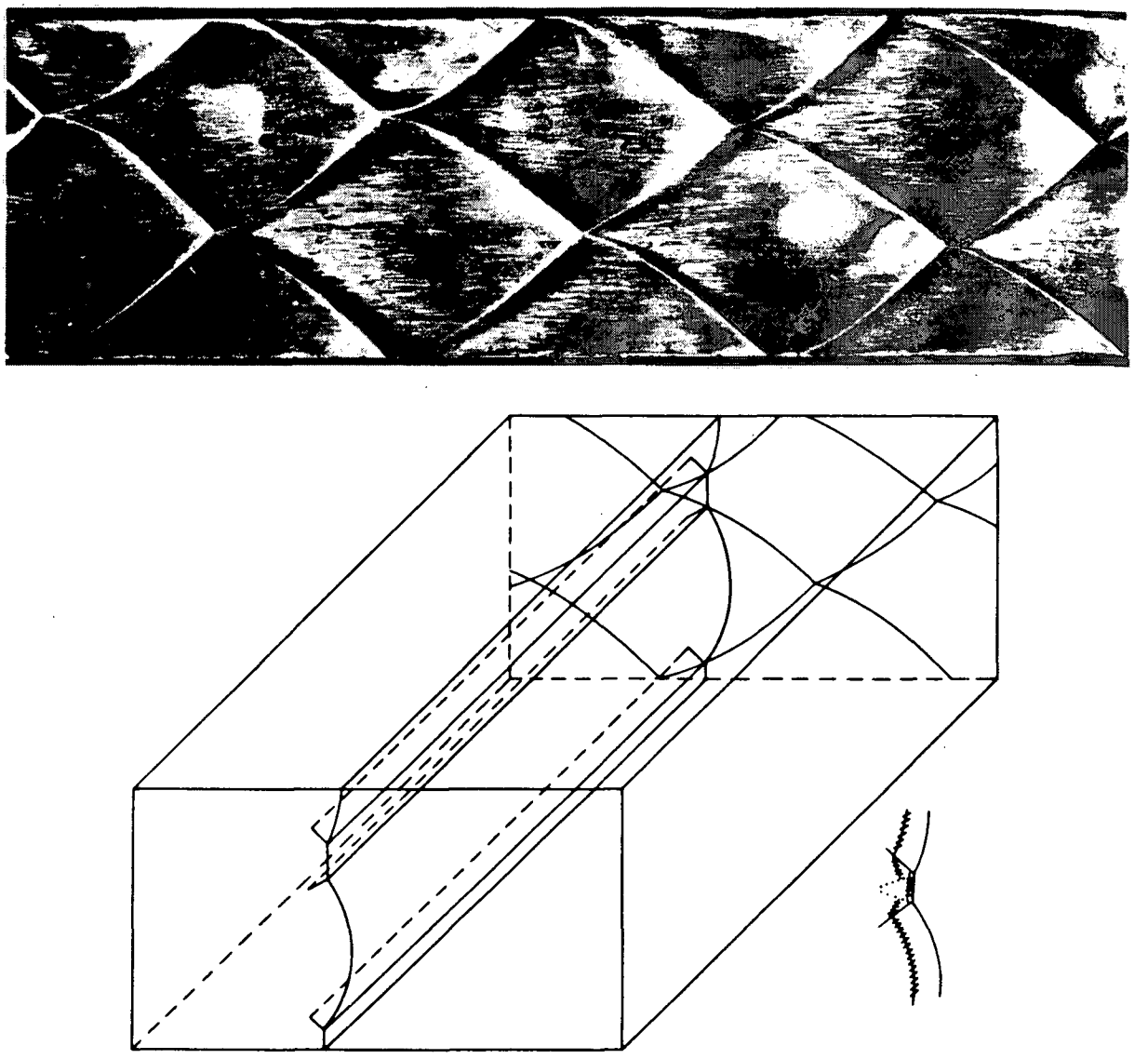

Figure 1-3 Cellular Pattern Left on Sooted Plate from Passing Detonation Wave in Argon-Diluted Fuel/Oxygen. [From Reference 17]

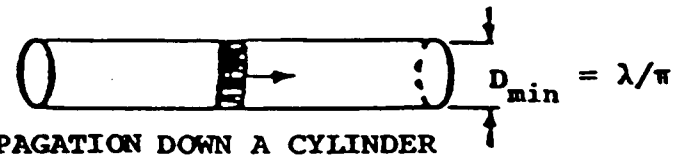

PROPAGATION DOWN A CYLINDER

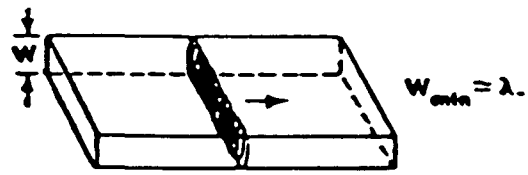

PROPAGATION DOWN A TWO-DIMENSIONAL CHANNEL

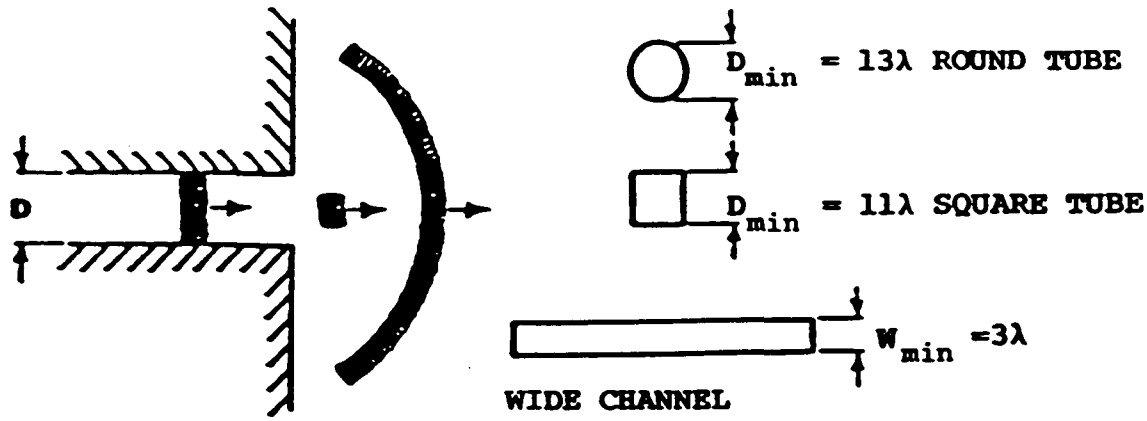

TRANSMISSION FROM A TUBE INTO A LARGE OPEN SPACE
"CRITICAL TUBE DIAMETER"

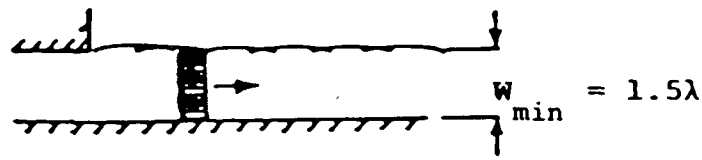

TRANSMISSION FROM A CHANNEL INTO A CLOUD
CONFINED ON ANY ONE SIDE

Figure 1-4. Effect of Geometry on Propagation of Detonation Waves.

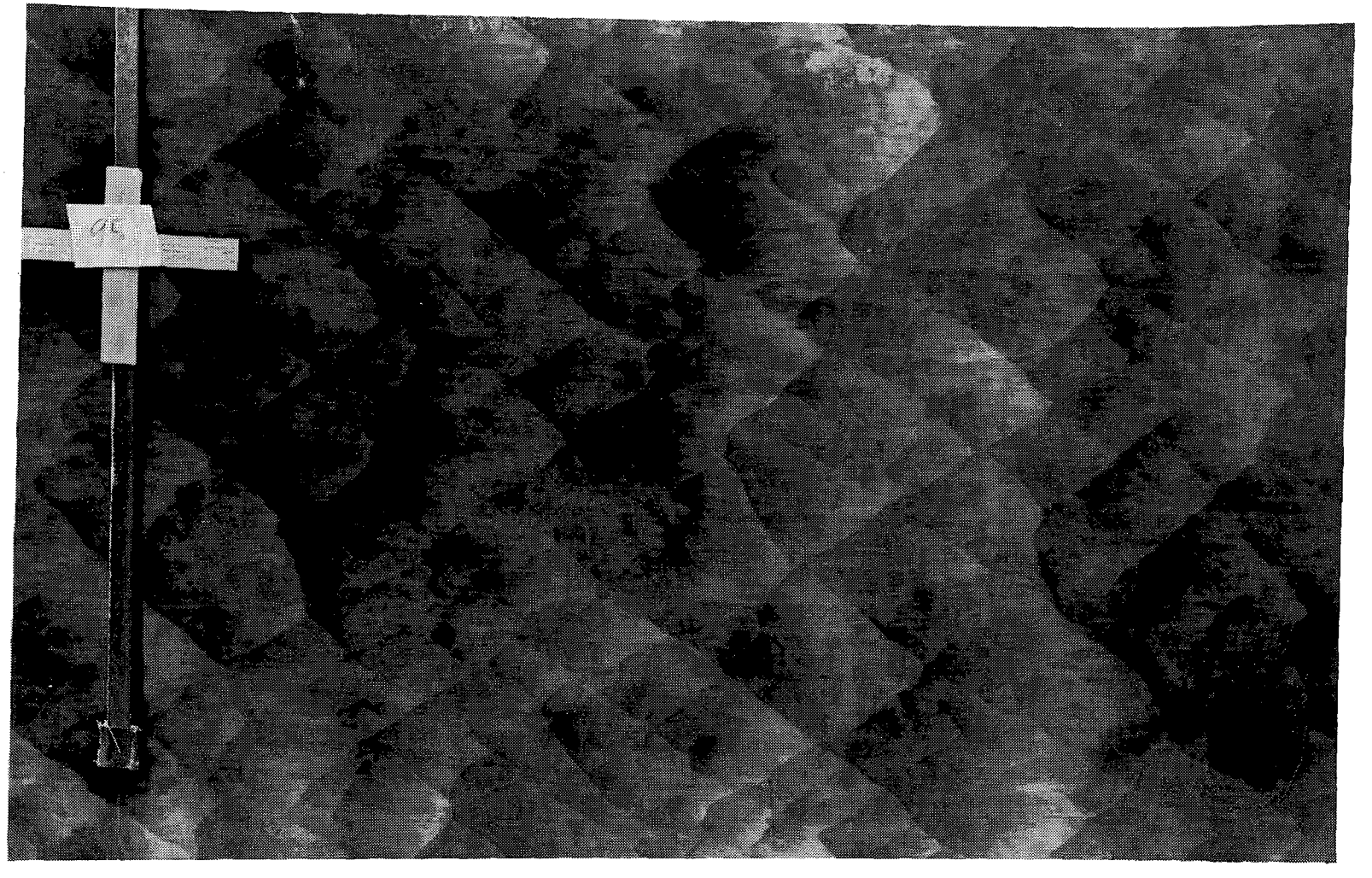

Figure 1-5. Detonation Cell Pattern on a Smoked Foil for a H_2-Air Mixture. Note "irregular" structure compared to Figure 1-3.

Older data on detonation limits, e.g., [10] were obtained in small diameter tubes, usually 2.5 cm (1 inch) or less in diameter. We now know that the old values represented the limit of propagation for that diameter tube. Larger tubes have produced wider limits and the large length scales associated with reactor containment buildings can be expected to have yet wider limits of propagation. Atkinson et al., have predicted that the limits in an infinite (unconfined) geometry would be 13% and 70% [22].

1.2.2 Modeling

The first successful attempt to model detonation waves was developed around the turn of the century. The theory was based on equilibrium thermodynamics and was proposed by Chapman and Jouguet (C-J). Extensive data from decades of research since the (C-J) theory was proposed have shown that detonations have pressures approximately 10 to 15% lower than the C-J predicted pressure and velocities typically 1% higher than the C-J values [23]. It has also been shown that the velocity is affected by the size of the detonation tube [24]. Measured velocities from small-diameter detonation tubes are lower than those in larger diameter tubes.

The next significant advancement in detonation modeling occurred in the 1940's with the proposals of Zel'dovich, von Neumann and Doering (ZND). They independently proposed that detonations are one-dimensional shock waves followed by deflagrations. This type of model is used to predict a characteristic length scale associated with the chemical reaction distance behind the shock waves. This model has been extended recently to include detailed chemical kinetics [25,26,27]. These models determine the distance behind the initial shock wave for the chemical reaction to reach an arbitrary degree of equilibrium. These models are termed "induction-length models" but usually the length scale defined by these models contains the reaction zone as well as the chemical-induction zone. These models are one-dimensional and, hence, do not predict detonation structure; it is assumed that they represent a spatial average of the actual detonation structure. Empirical relations are used to relate the induction-zone length to the detonation cell size.

Since the late 1970's, two-dimensional models have been developed to investigate the detonation wave structure [28,29]. These models are computationally intensive and hence have used simplified chemical kinetics. These models have shown the detonation cell pattern developing from a disturbed one-dimensional detonation wave.

1.3 REFERENCES FOR CHAPTER 1

1. Henrie, J. O. and Postma, A. K., Analysis of the Three Mile Island (TMI-2) Hydrogen Burn, Thermal-Hydraulics of Nuclear

Reactors, Vol. II. Amer. Nucl. Soc., LaGrange, IL, U.S. A.S.M.E., 1983, pp. 1157-1170.

2. Berman, M. and Cummings, J. C., "Hydrogen Behavior in Light-Water Reactors," Nuclear Safety, Vol. 25, No. 1, pp. 53-74, 1984.

3. Camp, A. L., Behr, V. L., and Haskin, F. E., "MARCH-HECTR Analysis of Selected Accidents in an Ice-Condenser Containment," NUREG/CR-3912, SAND83-0501, December 1984.

4. Lee, J. H., Knystautas, R., Chan, C. K., "Turbulent Flame Propagation in Obstacle Filled Tubes," Proceedings of the 20th Symposium (International) on Combustion, Published by the Combustion Institute, Pittsburgh, PA, pp. 1663-1672, 1984.

5. Pförtner, H., Schneider, H., Drenchen, W., Koch, C., "Flame Acceleration and Pressure Buildup in Free and Partially Confined Hydrogen-Air Clouds," presented at the Ninth International Colloquium on Dynamics of Explosions and Reactive Systems, Poiters, France, July, 1983.

6. Sherman, M. P., Tieszen, S. R., Benedick, W. B., Fisk, J. W., Carcassi, M., "The Effect of Transverse Venting on Flame Acceleration and Transition to Detonation in a Large Channel," AIAA Progress in Astronautics and Aeronautics Series, Vol. 106, pp. 66-89, 1986.

7. Shapiro, Z. M. and Moffette, T. R., Hydrogen Flammability Data and Application to PWR Loss-of-Coolant Accident, WAPD-SC-545, Bettis Plant, September 1957.

8. Reactor Safety Study, WASH-1400 (NUREG-75/014) U. S. Nuclear Regulatory Commission (October, 1975).

9. Core-Meltdown Experimental Review, SAND77-0382, Sandia National Laboratories, Albuquerque, March 1977.

10. Lewis, B., and Elbe, G. von, Combustion, Flames and Explosions of Gases, 2nd Ed., New York, Academic Press, 1961.

11. Lee, J. H. S.,"Dynamic Parameters of Gaseous Detonations," Annual Review of Fluid Mechanics, V. 16, pp. 311-336, 1984.

12. Knystautas, R., Guirao, C. M., Lee J. H., and Sulmistras A., "Measurements of Cell Size in Hydrocarbon-Air Mixtures and Predictions of Critical Tube Diameter, Critical Initiation Energy, and Detonability Limits," Progress in Astronautics & Aeronautics, Vol. 94, pp. 23-37, 1984.

13. Liu, Y. K., Lee, J. H. S., Knystautas, R., "Effect of Geometry on Transmission of Detonation Through an Orifice," Combustion and Flame V. 56, pp. 215-225, 1984.

14. Lee, J. H., Knystautas, R., Chan, C. K., "Turbulent Flame Propagation in Obstacle Filled Tubes," Proceedings of the 20th Symposium (International) on Combustion, Ann Arbor, (In Press).

15. Dupre, G., Knystautas, R., and Lee, J. H., "Near Limit Propagation of Detonation in Tubes," AIAA Progress in Astronautics and Aeronautics Series, Vol. 106, pp. 244-260, 1986.

16. Bull, D. C., "Concentration Limits to the Initiation of Unconfined Detonation in Fuel/Air Mixtures," Trans IChemE, Vol. 57, pp. 219-227, 1979.

17. Strehlow, R. A., Combustion Fundamentals, McGraw-Hill Series in Energy, Combustion & Environment, 1984.

18. Moen, I. O., Murray, S. B., Bjerketvedt, D., Rinnan, A., Knystautas, R., and Lee, J. H., "Diffraction of Detonation From Tubes Into A Large Fuel-Air Explosive Cloud," 19th Symp. (Int'l.) on Combustion, The Combustion Institute, Pittsburgh, PA, 1982, pp. 635 - 645.

19. Bull, D. C., Elsworth, J. E., Shuff, P. J.,"Detonation Cell Structures in Fuel/Air Mixtures," Combustion and Flame, V. 45, 1982, pp. 7-22.

20. Moen, I. O., Funk, J. W., Ward, S. A.,Rude, G. M. and Thibault, P. A., "Detonation Length Scales for Fuel-Air Explosives," AIAA Progress in Astronautics and Aeronautics, Vol. 94, 1984, pp. 55-79.

21. Moen, I. O., Sulmistras, A., Thomas, G. O., Bjerketvedt, D., and Thibault, P. A., "The Influence of Cellular Regularity on the Behavior of Gaseous Detonations," AIAA Progress in Astronautics and Aeronautics, Vol. 106, pp. 220-243, 1986.

22. Atkinson, R., Bull, D. C., Shuff, P. J., "Initiation of Spherical Detonation In Hydrogen/Air," Combustion and Flame, V. 39, 1980, pp. 287-300.

23. Fickett & Davis, Detonations, Univ. of California Press, Berkeley, CA, 1979, Chapter 1A.

24. Manson, N., Brochet, C., Brossard, J. and Pujol, T., Ninth Symposium (International) on Combustion, Academic Press, New York, 1963, p. 461.

25. Westbrook, C. K., and Urtiew, P. A., "Chemical Kinetic Prediction of Critical Parameters in Gaseous Detonation,"

19th Symp. (Int'l.) on Combustion, The Combustion Institute, Pittsburgh, PA, 1982, pp. 615 - 623.

26. Shepherd, J. E., "Chemical Kinetics and Hydrogen-Air-Diluent Detonations," AIAA Progress in Astronautics and Aeronautics Series, Vol. 106, pp. 263-293, 1986.

27. Tarver, C. M., "Chemical Energy Release in One-Dimensional Detonation Waves in Gaseous Explosives," Combustion and Flame, Vol 46, pp, 111-133, 1982.

28. Oran, E. S., et al., "Numerical Simulations of Detonations in Hydrogen-Air and Methane-Air Mixtures," Eighteenth Symposium (International) on Combustion, pp. 1641-1647, 1981.

29. Hiramatsu, K., Fujiwara, T., and Taki, S., "A Computational Study of Transmission of Gaseous Detonations to Unconfined Space," presented at the Twentieth Symposium (International) on Combustion, Ann Arbor, Michigan, USA, August 12-17, 1984.

CHAPTER 2

HDT FACILITY DESCRIPTION

This section briefly describes the HDT facility and its design. A detailed description of the facility appears in Appendix A.

2.1 DESIGN CONSIDERATIONS

At the time (1982) that construction of the Heated Detonation Tube (HDT) was proposed, it was known that composition limits for detonation propagation were not fixed quantities but appeared to depend on the ratio of a characteristic geometric size to detonation cell width. Because we were interested in obtaining information on the detonation of leaner mixtures than previously tested and extrapolating the results to reactor containment scales, a decision was made to build a larger diameter tube than had been used in previous studies. To minimize corrosion due to steam, stainless steel tubing was selected. To initiate the detonation, a thin sheet of high-explosive was selected. We chose a 43-cm (17-in)-inner-diameter tube with a length-to-diameter ratio of about 30 to provide adequate distance for the initiation transient to decay prior to recording the detonation cell width. The selection of a large diameter tube for the HDT has proved to have advantages beyond those originally considered. Results from small diameter detonation tubes are affected by boundary layer effects. Small values of velocity deficit obtained in our facility indicate that boundary layer effects are minimal for our large-diameter tube.

A major design decision was the selection of the method for heating the tube and its contents. Our goal was to obtain a uniform elevated temperature. Three methods were considered: electric resistance heating using heater tapes, direct electric resistance heating of the tube, and steam heating using a jacketed tube. The steam heating idea was dropped due to potential cost and complexity. In particular, passing transducers through a coaxial jacket posed a problem. Direct heating of the tube would require enormous currents at very low voltages, and was deemed impractical. Use of electric resistance tapes was the simplest method. A major concern was the uniformity of temperature that could be achieved. A heat transfer analysis indicated that the temperature variations in the tube due to the finite spacing of the tapes and heat loss through the insulation would be small (see Appendix F).

Originally, it was decided to support the tube from chains hung on a steel framework and support the insulation in wooden boxes. The design became too complex and costly. In the end, simple V block wooden-faced supports mounted on concrete-filled barrels were inexpensively made and have proven to be effective. These supports are similar to those used for shock tubes. It was

expected that there would be some motion of the tube back and forth in the guides, but no such motion has been evident. Apparently frictional forces are sufficient to prevent the large, but fast alternating axial forces from moving the tube. Fiberglass insulation was wrapped around the tube and was covered with plastic sheet to shield it from rain.

Construction of the Heated Detonation Tube (HDT) was concurrent with another project, the FLAME combustion channel [1]. The HDT was designed to use the same computer-controlled data acquisition system designed for FLAME. The needs of the two facilities for data acquisition are somewhat different but considerable use was made of the FLAME data acquisition system. High-speed digital data acquisition equipment used for DOE programs were available and also used.

2.2 HDT DESCRIPTION

The HDT is shown in Fig. 2-1 and Fig. 2-2, before and after the installation of the insulation. The HDT is composed of the main detonation tube, gas injection/recirculation secondary piping, computer-controlled heaters, explosive initiator circuit, instrumentation, and data acquisition system.

The detonation tube is composed of three pipe sections attached end-to-end. All are made of type 304 stainless steel and have a 45.7-cm (18-in) outer diameter. Two sections are 6.1 m (20 ft) long and have a 1.27-cm (0.5-in) thick wall and the third is 0.91 m (3 ft) long with a 2.54-cm (1-in) thick wall. The short, heavy-walled section serves as the initiation end. Transient initiation pressures due to the high explosive are much greater than the gaseous detonation pressure. Flat endplates cover each end of the detonation tube and are made of 3.18-cm (1.25-in) thick, type 304 stainless steel.

A schematic of the secondary piping is shown in Fig. 2-3. The piping provides for evacuation, injection and circulation of the gaseous mixture. The secondary piping consists of an inline filter, circulation pump, and appropriate tubing, fittings and valves. The gas flow is from the outlet port on the terminal end of the main tube, through a shutoff valve, the filter, the pump, past the high-point vent and the gas and steam injection ports, along the main tube to the shutoff valve on the inlet port at the initiation end of the main tube.

Gases, with the exception of steam, are introduced into the secondary piping from standard gas cylinders. Steam is introduced from a specially designed steam generator. The steam generator is a 1-liter stainless steel sample cylinder that has a 500-W flexible rod heater wrapped around the bottom of the vessel. The heater and cylinder were immersed in a molten lead bath contained in a larger cylinder to provide a thermal mass. A premeasured amount of water is introduced into the vessel prior

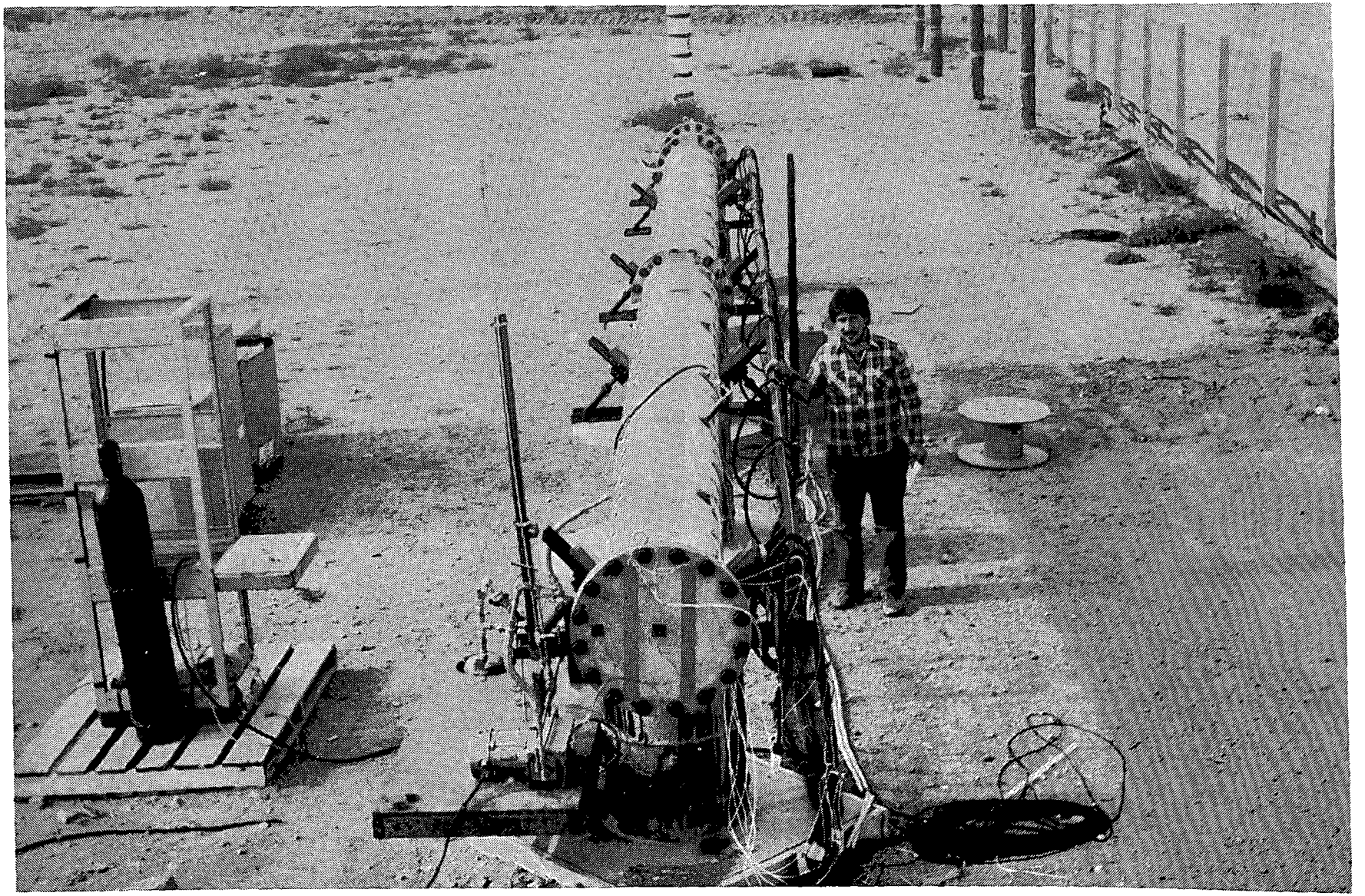

Figure 2-1. Heated Detonation Tube Without Thermal Insulation

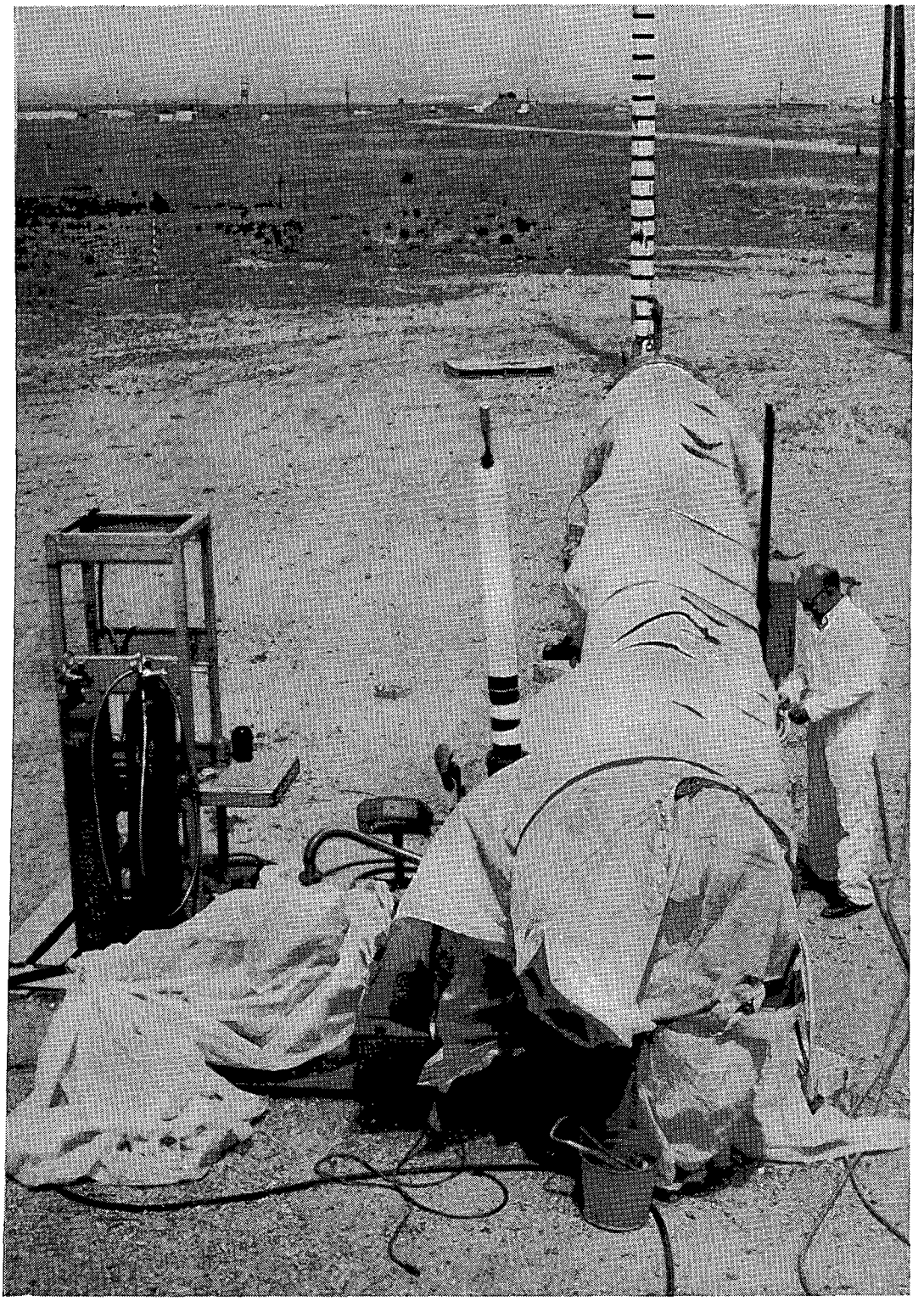

Figure 2-2. Heated Detonation Tube With Thermal Insulation Layer

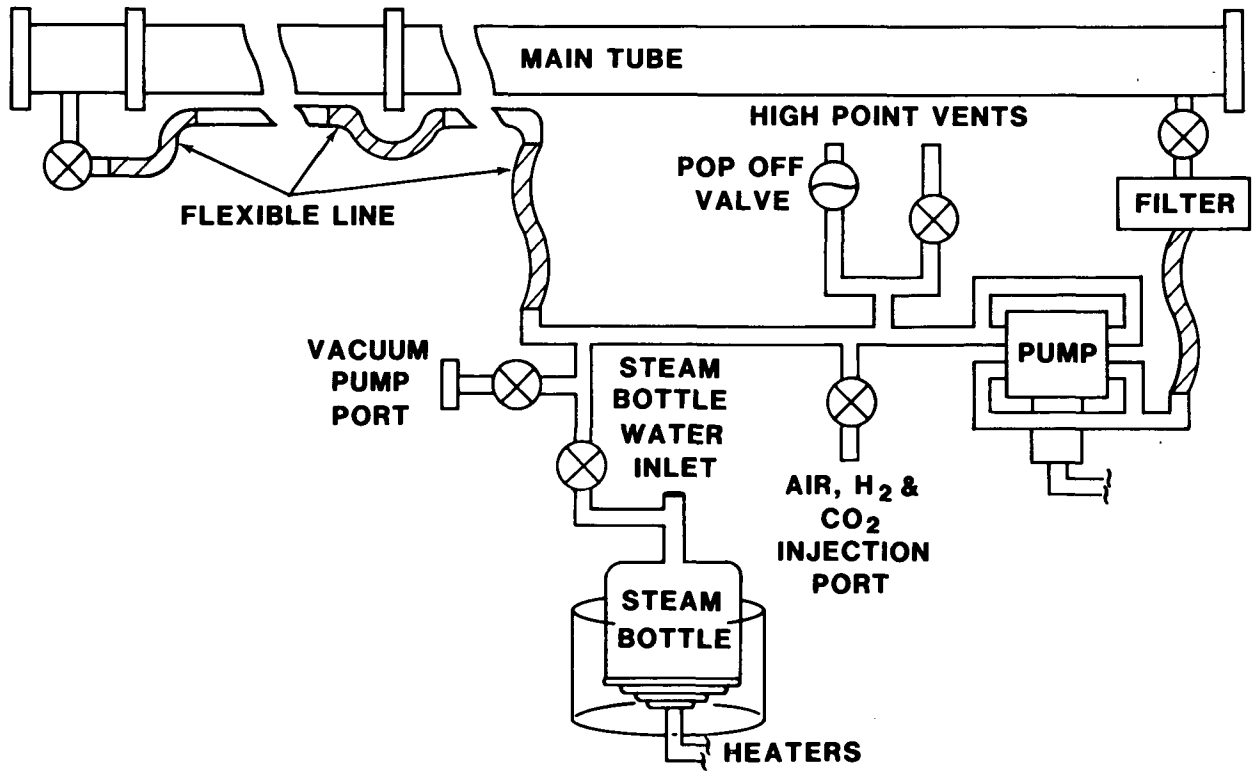

Figure 2-3. Schematic of the Secondary Piping.

to a test and is completely boiled out into the circulation line leading to the detonation tube.

The detonation tube heating system is composed of 15 individually controlled sections of resistance heaters on the surface of the main tube, one section on the steam heating bottle, and one section on the secondary piping. The heaters on the detonation tube and secondary piping are resistance-type, silicone-rubber strip heaters. These heaters are held against the surface of the detonation tube with fiberglass cord or RTV adhesive. All heater sections except on the secondary piping are under computer control. Each section contains several heaters of various sizes, wired in series and parallel, to achieve the desired power level.

Each section also has three Chromel-Alumel, type-K thermocouples to measure the anticipated hottest, coldest and an intermediate temperature in each section. The anticipated hottest temperature is underneath a heater tape, the coldest temperature is midway between heater tapes, and the intermediate temperature is midway between the hot and cold thermocouples. The hot thermocouple is used to control the heating process, while the other two measure the nonuniformity in temperature.

The heating system is controlled by on-off, set-point-logic controlled relays which supply power to the heater strips. Control feedback is maintained by monitoring the temperature of the thermocouple underneath a heater strip in each section and comparing it to the desired set-point temperature. The thermal inertia of the system is high enough that on-off control is sufficiently stable to maintain the detonation tube temperature. A schematic of the control circuit is shown in Fig. 2-4. The control decisions are made by a BASIC program running in the Digital LSI-11/23 computer. To ensure that the heaters are turned off in case of a computer failure, a Standard Engineering Corp. "Watch Dog Timer" is used to monitor the computer system.

The insulation used to cover the detonation tube and secondary piping is Certainteed Snap Wrap foil-backed fiberglass which has a thermal conductivity of 0.048 W/m°K (R - value of 3 (hr ft^2 °F)/(Btu in)). The detonation tube is covered with 8.9 cm (3.5 in) of this insulation. A plastic sheet is used to protect the insulation from moisture. Pre-formed 2.5-cm (1-in) thick cylindrical sections of insulation are used on the secondary piping. The endplates are covered by large insulating endcaps. The endcaps are made to slip over the flanges and are intended to be easily removable because they must be removed after each test. The endcaps are fabricated from a 20-gage galvanized sheet metal outer shell in the form of a cup. The diameter of the shell is 94 cm (37 in) and the sides are 45.7 cm (18 in) deep. The inside is lined with 15.2 cm (6 in) of insulation in the base and sides.

The most convenient method of initiating a gaseous detonation in the HDT is to use high explosive. This eliminates the

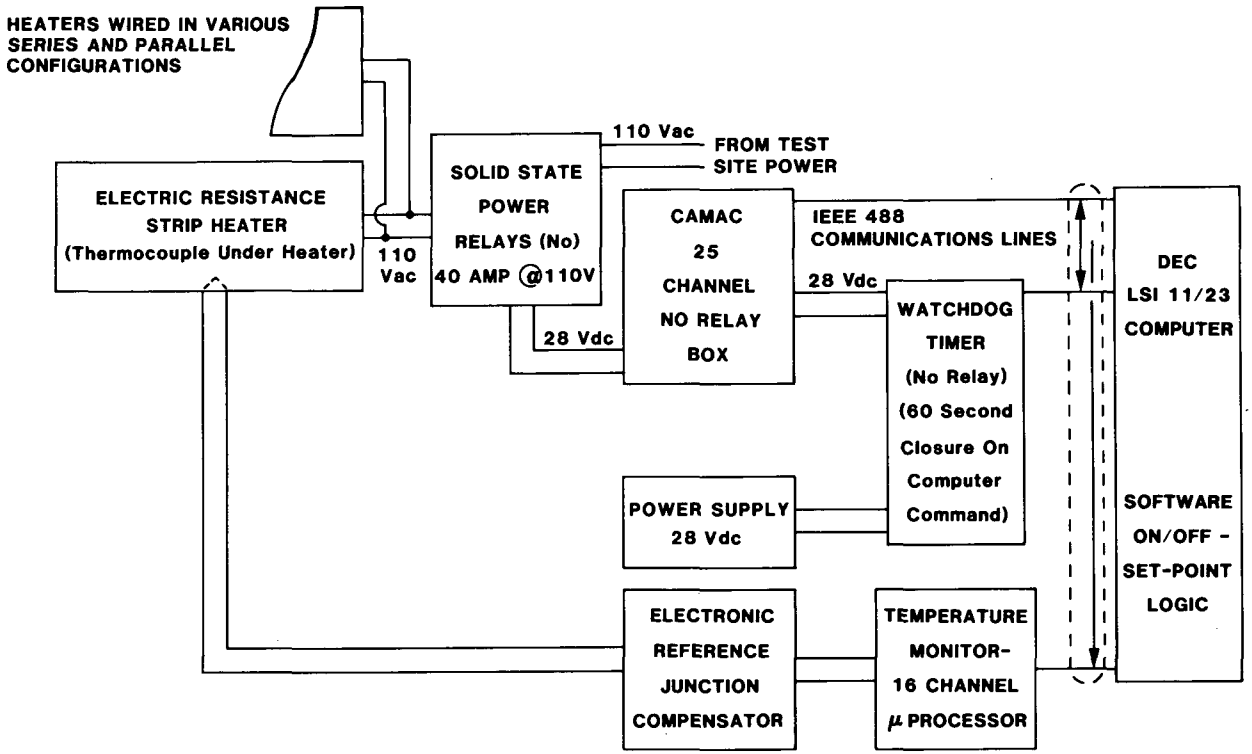

Figure 2-4. Schematic of the Heater Control Circuit.

need for long run-up distances required for DDT devices such as Shchelkin spirals. The disadvantage of using high explosives is that the gaseous detonation will be overdriven for a certain distance. This is due to the very high pressures initially generated by detonating the high explosive. To minimize overdriving, we used a thin (1-mm thick) sheet of DuPont Detasheet high explosive cut into a 25.4-cm (10-in) diameter spoked-wheel shape to both minimize the amount of high explosive and to effect almost planar initiation. The explosive is initiated by an exploding bridgewire detonator.

The instrumentation used on the HDT includes pressure gages, thermocouples, and gas bottles to determine the initial gas composition. To measure detonation properties, we use pressure transducers mounted flush in the tube wall at various axial locations and at one azimuthal position, and a thin smoked aluminum cylindrical section (foil) placed around the inner circumference of the tube at the end farthest from the driver. The pressure gage used to determine gas pressure is either a Wallace & Tiernan 0 to 800 mm Hg gage for one total atmosphere (101 kPa) tests, or a Wallace & Tiernan 0 to 50 psia gage for superatmospheric (>101 kPa) tests. The gas temperature measurement was made with a K-type thermocouple probe mounted through the wall of the detonation tube.

To measure detonation pressure, fast response quartz piezoelectric transducers are used. Normally, from 6 to 10 pressure transducers have been used in each test. The main value of their data has been to provide detonation time of arrival. Data from the transducer couplers travels about 100 m (300 ft) over coaxial cable to the instrumentation building. The pressure signals are recorded simultaneously on two high-impedance data acquisition systems. The FLAME data acquisition system is based on the use of two BiRa 5906 transient digitizer modules mounted in CAMAC (Computer Automated Measurement and Control) crates. The system is controlled by a Digital LSI 11/23 computer which communicates to the CAMAC crates with a GPIB (General Purpose Interface Bus) interface.

Each BiRa transient digitizer is run with four active channels, giving a maximum sampling rate of 40 kilosample/second (25 μs period) and a memory of 8K (8196 points) per channel. For detonations travelling at 1600 m/s, typical of a leaner hydrogen mixture, the time between recorded samples corresponds to a travel of 40 mm. The pressure transducers are capable of faster response, and a faster sampling rate would produce superior results.

In addition to the CAMAC digitizers, the HDT uses 3 Tektronix 7612D transient digitizers, each with two data channels. These units are capable of sampling speeds up to 200 megasample/second (5 ns), with preprogrammed changes in sampling speed. Typically, we use these units with sampling rates up to 2 MHz (0.5 μs). For detonations travelling at 1600 m/s, the time

between samples of 0.5 μs corresponds to a travel of 0.8 mm. A limitation of these units is the limited memory, 2K (2048 points) per channel. To extend the data sampling "window" while maintaining the same sampling speed during the detonation, slower sampling speeds are used both before and after the period in which the detonation arrival at the gage is expected. The 7612D's are also on the GPIB network and are partially controlled by the LSI 11/23 computer. The 7612D's use two 7A16A amplifiers. Several settings such as amplifier gains must be set by hand on these units. Further details and a description of the controlling software are given in Appendix G.

To measure detonation cell width, a smoked aluminum sheet (foil) is used. The sheet is 1.2 m (4 ft) wide by 3.7 m (12 ft) long and approximately 0.5 mm (0.020 in) thick. For tests without steam, the sheet is smoked with a MAPP (stabilized methylacetylene-propadiene) torch using no oxygen to produce black soot. For tests with steam, the best results were obtained using furnace oil in a wicked flame holder to produce soot on a foil with a surface preparation coating which consisted of a mixture of one-third Dow Corning Sylgard 186 and two-thirds Xylene. This surface preparation prevents spotting of the soot which occurred without the preparation. The sheet is rolled into a long cylinder around stiffening rings attached at each end and placed around the inside circumference of the HDT at the end opposite the explosive initiator.

2.3 REFERENCES FOR CHAPTER 2

1. Sherman, M. P., Tieszen, S. R., Benedick, W. B., Fisk, J. W., Carcassi, M., "The Effect of Transverse Venting on Flame Acceleration and Transition to Detonation in a Large Channel," AIAA Progress in Astronautics and Aeronautics Series, Vol. 106, pp. 66-89, 1986.

CHAPTER 3

PROCEDURE

The test procedures used for the Heated Detonation Tube experiments were developed and improved upon as the test program developed. The data have been categorized into 7 test series listed in Table 3-1. The general procedures for each test series are discussed in this chapter. Specific procedures for each series, including variations in procedure for each series are discussed in Appendix B.

All experiments in the HDT began by preparing a smoked foil and by assembling the explosive initiator. After a foil has been smoked, it is attached to stiffening rings at each end and inserted into the HDT. The endplate is then bolted in place. At the other end of the tube, the assembled explosive initiator is inserted into a protective coaxial tube and installed into the HDT. The detonator is connected to an electrical feed-through in the endplate, and the plate is bolted in place.

After the smoked foil and explosive initiator are installed in the detonation tube and the endplates secured and insulated, gases are then introduced. For each test series, air is the first gas introduced into the detonation tube followed by hydrogen, except for series #2. In test series #2, CO_2 is introduced before the hydrogen. In tests prior to HT49, ordinary ambient air, whose relative humidity had been measured, was used. From test 49 on, bottled dry air is used. Steam is added after heating the detonation tube.

To ensure a homogeneous mixture, the circulation bellows pump runs continuously from the introduction of the first gas until just before the detonation initiation sequence to ensure homogeneous mixture. At least one detonation tube volume of gas is allowed to circulate during the addition of each gas to the recirculation line and at least one additional tube volume of gas is allowed to circulate prior to recording the temperature and pressure of the gas mixture. One tube volume of gas takes approximately 15 minutes to circulate. Temperature and pressure measurements are used to determine gas composition. For mixtures without steam, perfect gas is assumed for calculating compositions; for mixtures with steam, a virial equation of state is used.

For test series #1, #2, and #6, the partial pressure of each gas was adjusted so that the total initial pressure prior to detonation was 101 kPa (1 atm). For test series #3, #4, and #5, the air pressure was adjusted so that the air density was 41.6 moles/m^3. This density corresponds to air at 101 kPa (1 atm) and

Table 3-1

Test Series

Series #	Description	# of Tests in Series
1	H_2-Air @ P=1 atm, T=20°C	16
2	H_2-Air-CO_2 @ P=1 atm, T=20°C	10
3	H_2-Air @ ρ_{air}=41.6 moles/m^3, T=100°C	16
4	H_2-Air-H_2O @ ρ_{air}=41.6 moles/m^3, T=100°C	18
5	H_2-Air @ ρ_{air}=41.6 moles/m^3, T=20°C	6
6	H_2-Air @ X_{H2}=0.17, P=1 atm	4
7	H_2-Air @ X_{H2}=0.17, ρ=42 moles/m^3	3

20°C. For test series #7, the partial pressure of each gas was adjusted so that the total initial gas density was 42 moles/m^3.

For test series #1, #2, and #5, the detonation tube was not heated but maintained at ambient temperature while the composition was varied. For test series #3, the temperature was held at 100°C and the composition was varied. For test series #6 and #7, the temperature was varied while the composition was held fixed. Typically, heating took approximately 5 hours to reach 100°C.

The detonation initiation sequence is the same for all tests. After the temperature and pressure are measured for the last gas injected into the tube and it has reached its equilibrium temperature, the secondary piping is isolated from the detonation tube to protect the pump. The manifold to the static pressure gage is closed, the power supplies to the dynamic pressure transducers are turned on, and the detonator lines are connected. All personnel are then required to leave the vicinity of the detonation tube and enter the control room in Bldg. 9920. For elevated temperature tests, the heaters are turned off. The computer is then configured to control the data acquisition equipment. The area is cleared and the high voltage capacitor in the firing circuit is charged. A trigger pulse discharges the high voltage capacitor into the exploding bridgewire detonator that initiates the detonation and simultaneously starts the data acquisition equipment. The time between secondary piping isolation and the initiation of the detonation is typically 12 minutes. The time between turning off the heaters and the initiation of the detonation is typically 8 minutes.

CHAPTER 4

RESULTS

Detonation cell width, velocity and pressure are measured in the HDT. The detonation cell width and velocity results will be discussed in the following sections. Tabular results are presented in Appendix C. The detonation pressure is not reported because of uncertainty associated with the data (see Appendix D).

4.1 DETONATION CELL SIZE, λ

Results of the tests performed in the detonation tube are shown in Figs. 4-1 through 4-7. Smoked foil records from H_2-air detonations show a somewhat irregular cell structure as in Fig. 4-1. As noted in the literature review, most experimenters quote a single detonation cell width for a given mixture. A current area of active research is to test the validity of the assumption that a given mixture has a given unique detonation cell width, as opposed to a range of detonation cell widths. Testing completed for this report was not intended to address this question. For this report, a single detonation cell width has been selected for a given mixture using established methods of selecting detonation cell width.

Two methods of selecting a single detonation cell width are described by Moen, et al. [1], the single cell method and the dominant mode method. Both methods depend on observer interpretation of the detonation cell tracks on the the smoked foil record, and are subject to observer bias. In the single cell method the observer measures a large sample of individual cells (diamond shapes). Subjectivity enters into deciding what constitutes a detonation cell. The dominant cell method is really an extension of the single cell method. In the dominant cell method, the criteria for what constitutes a cell is defined by the number of cells between parallel bands, usually in one direction. These methods are discussed in Appendix D. Subjectivity enters into deciding what are parallel lines. Most lines are wavy and vary in contrast along the length of the line. In this method a few parallel bands are measured using the longest running parallel lines with the highest contrast.

In this report, the dominant mode method is used to determine the detonation cell width. The "U"-shaped curve of detonation cell width versus equivalence ratio is assumed to be smooth to assist in the selection of the detonation cell width. It must be noted that the process of selecting detonation cell width is subjective. Details and uncertainty estimates are given in Appendix D.

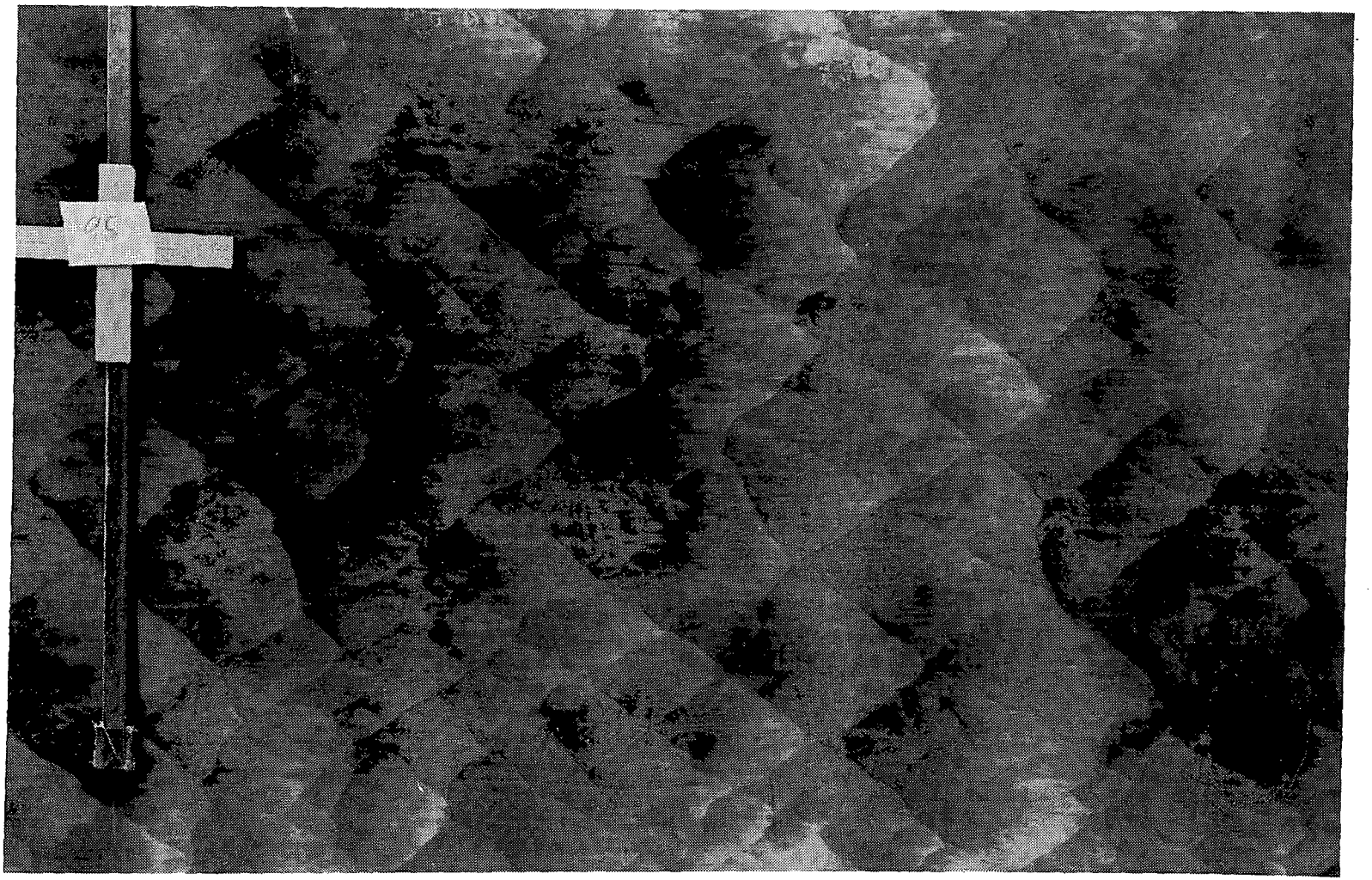

Figure 4-1. Typical Smoked Foil from HDT.

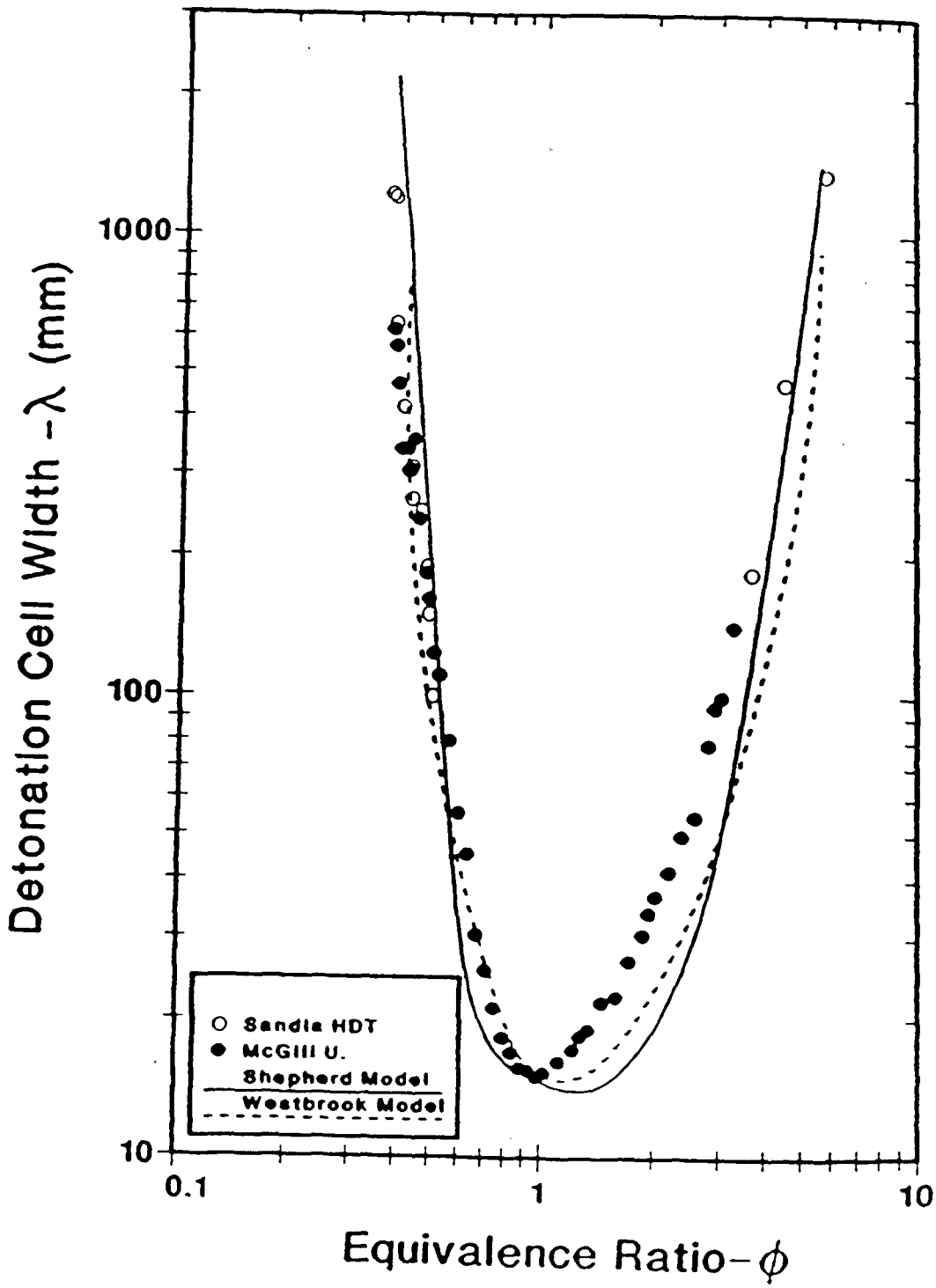

Figure 4-2. Detonation Cell Width vs. Equivalence Ratio for Test Series #1. (H_2-Air at P=1 atm, T=20°C)

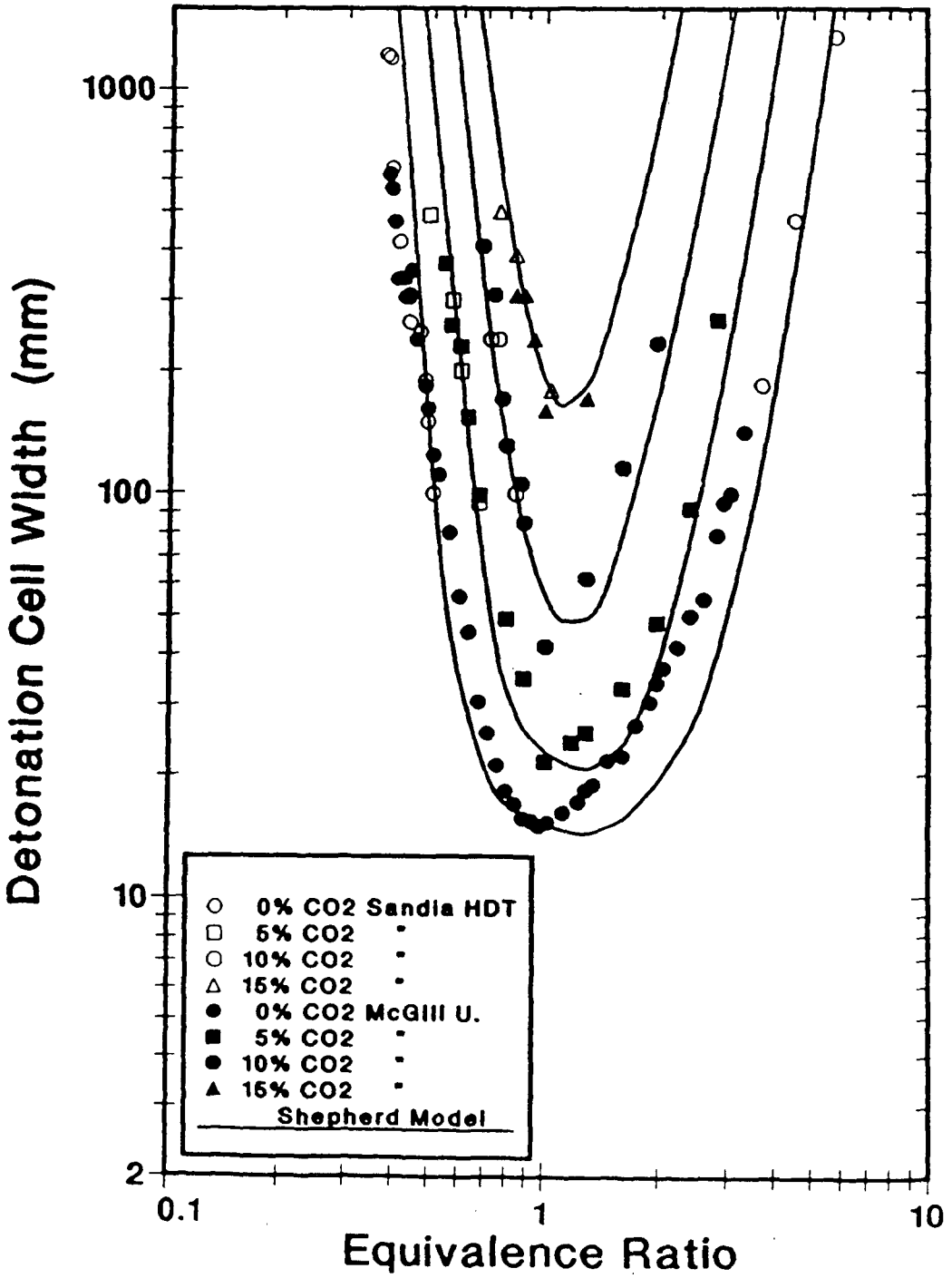

Figure 4-3. Detonation Cell Width vs. Equivalence Ratio for Test Series #2. (H_2-Air-CO_2 at P=1 atm, T=20°C)

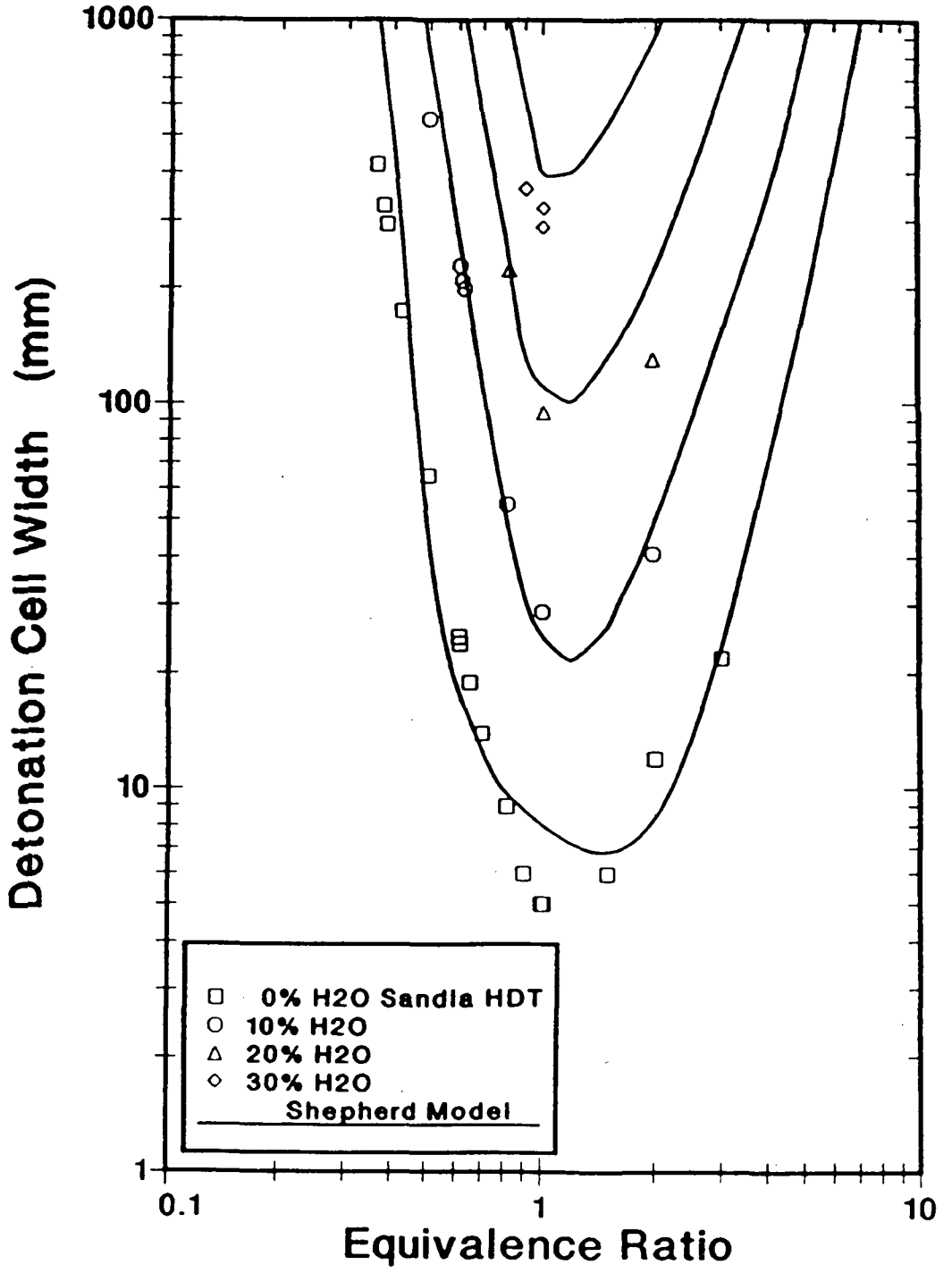

Figure 4-4. Detonation Cell Width vs. Equivalence Ratio for Test Series #3, 4. (H_2-Air-H_2O at ρ_{air}=41.6 moles/m^3, T=100°C)

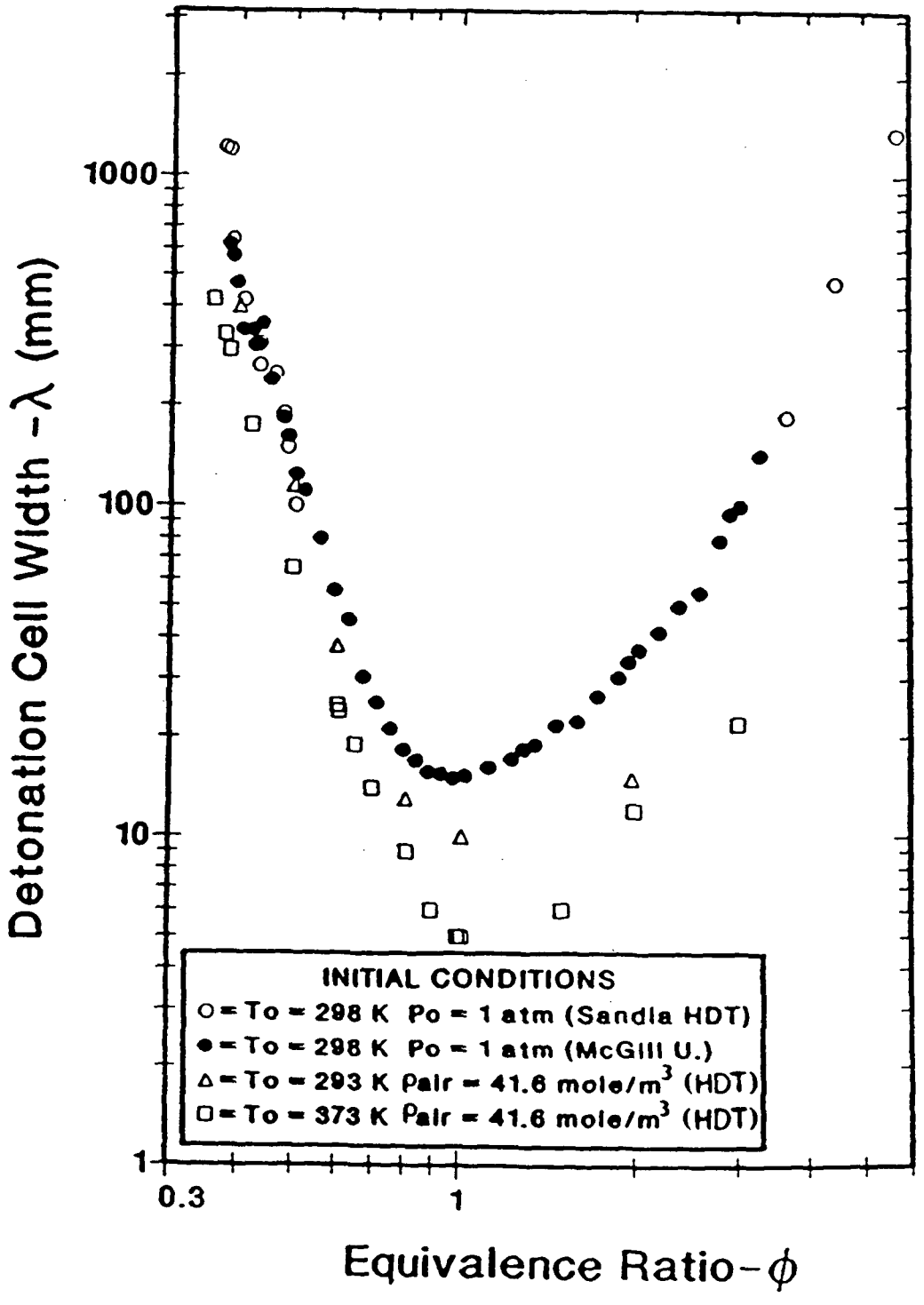

Figure 4-5. Effect of Initial Conditions on Detonation Cell Width of H_2-Air Mixtures.

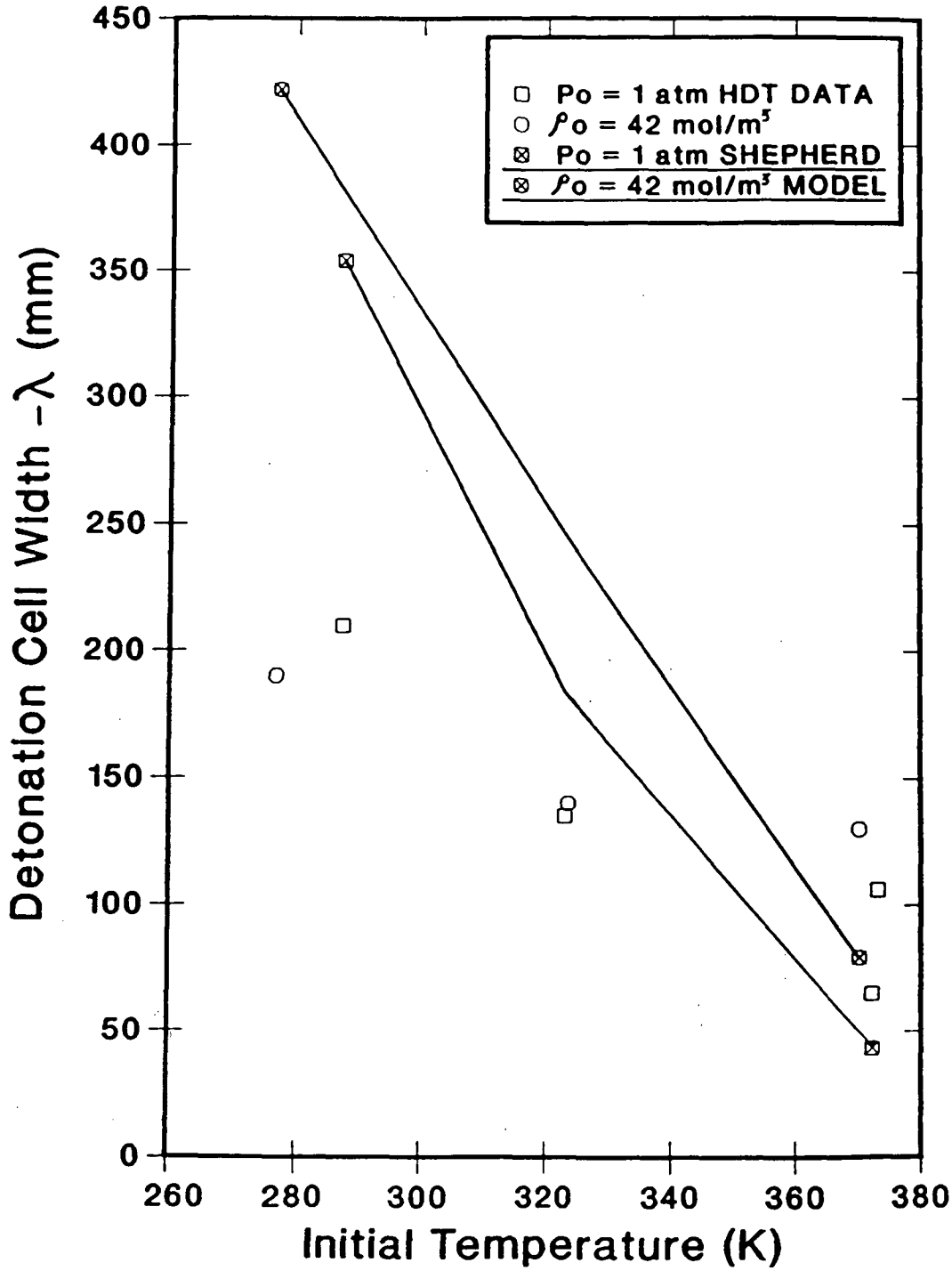

Figure 4-6. Detonation Cell Width vs. Temperature Ratio for Test Series #6, 7. (H_2-Air at X_{H2}=0.17)

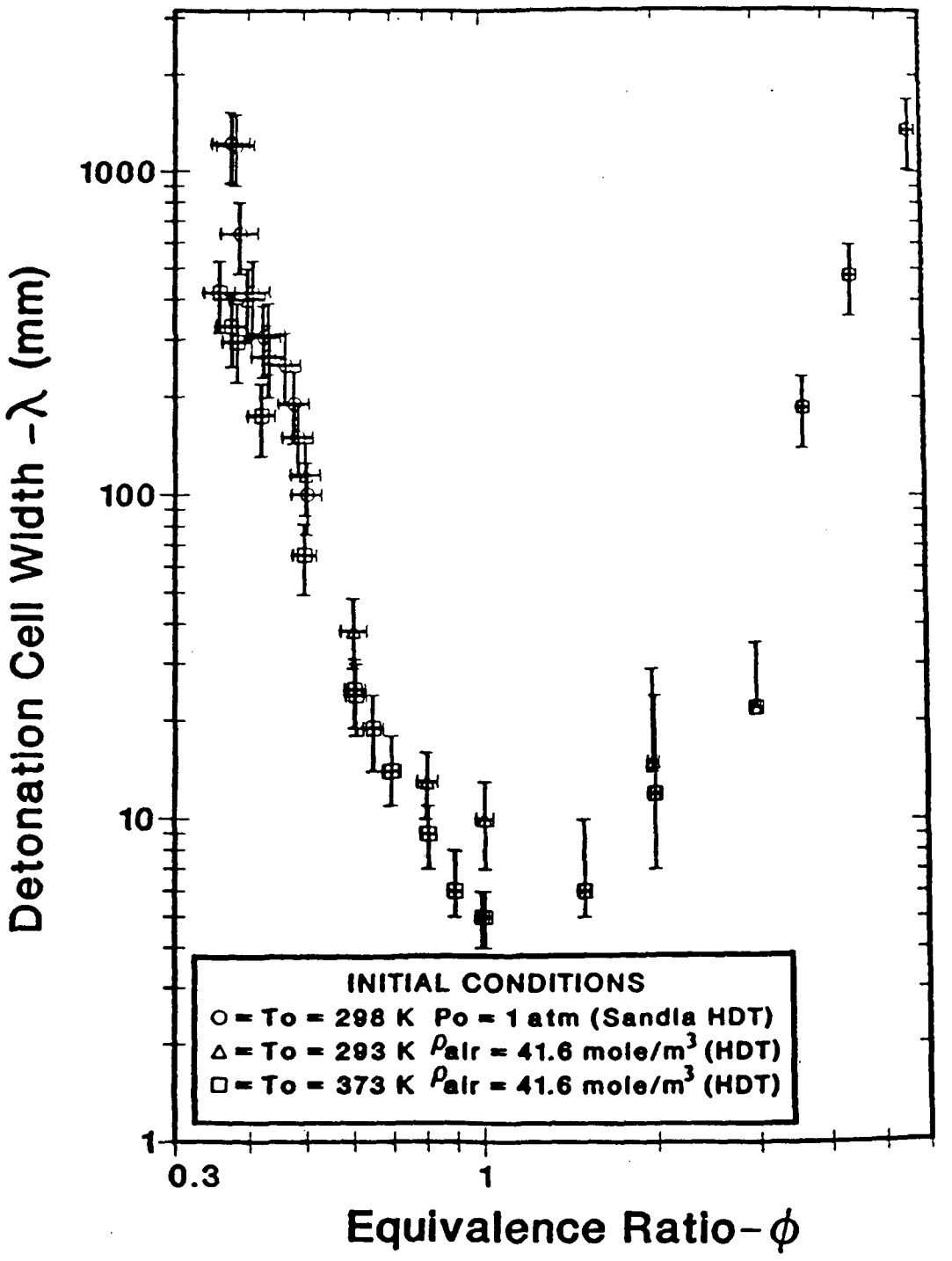

Figure 4-7. Uncertainty Ranges for the HDT Data in Figure 4-5.

A relative uncertainty bound can be estimated to be +/-25% for measured detonation cell width when a comparison is to be made among data in the report. An "absolute" uncertainty bound can be estimated to be a factor of 2 for comparison with data from other reports. Since subjectivity is involved in measuring detonation cell width, subjectivity is also involved in the estimation of uncertainty bounds. For the purpose of a conservative detonability hazard analysis, it is strongly recommended that the detonation cell width in this report be divided by 2.

For clarity in identifying the functional relationship between detonation cell width and equivalence ratio, diluent mole fraction, and initial thermodynamic state, the uncertainty bars have been deleted from Figs. 4-2 through 4-6. Fig. 4-7 shows the relative uncertainty bars for the data in Fig. 4-5. A complete listing of the data and relative uncertainty estimates is given in Appendix C. The details used to establish the values in Appendix C are discussed in Appendix D. A short discussion of uncertainty in irregular H_2-air detonation cell measurement is also given in Ref. [2].

For Figs. 4-2 through 4-5, the detonation cell width is plotted versus the equivalence ratio, ϕ. The equivalence ratio is defined as the fuel (H_2) to air molar ratio divided by the same ratio at stoichiometry. This ratio is invariant with respect to the type and amount of added diluent. Some values of equivalence ratio are listed in Table 4-1. Various thermodynamic relationships including the relation between ϕ and the mole fraction of H_2 are developed in Appendix E.

4.1.1 Modeling

The detonation cell width data presented in Figs. 4-2 through 4-4 and 4-6 have been compared by Shepherd [3] with a characteristic reaction zone length computed from a Zel'dovich-von Neumann-Döring (ZND)-type model. The model integrates a set of hydrogen oxidation reactions (reaction rates given in [4]) along the Rayleigh line. As first suggested by Shchelkin and Troshin [5], the characteristic reaction zone length, L, is believed to be approximately proportional to the cell size, λ,

$$\lambda = A\ L$$

The validity of this relation has been discussed by Lee, et al., [6] and by Westbrook and Urtiew [7]. For the model used in this report, the length of the reaction zone, L, is defined as the distance behind the shock wave where the flow Mach number M = 0.75. The constant A is determined by requiring the predictions to match the data at the stoichiometric point for H_2-air detonations in test series #1. A value of A = 22 was determined in this manner. Alternative definitions of L and a complete discussion of the model and its validity is found in Ref. [3].

Table 4-1

Equivalence Ratio as a Function of Steam and H_2 Concentrations in Total Mixture by Volume

	% H_2O in mixture by volume			
%H_2 in mixture by volume	0	10	20	30
10	0.27	0.30	0.34	0.40
15	0.42	0.48	0.55	0.65
20	0.60	0.68	0.80	0.95
25	0.80	0.92	1.08	1.33
30	1.03	1.19	1.43	1.79
40	1.59	1.91	2.39	3.18
50	2.39	2.98	3.98	5.97
60	3.58	4.77	7.16	14.32
70	5.57	8.35	16.71	∞

The calculations shown in Figs. 4-2 through 4-5 were made for a limited number of points corresponding to the detonation cell width measurements. Spline interpolation was used to generate continuous curves. Unless otherwise noted, nominal values (see Table 3-1) were used for initial conditions. Calculations were also made for the exact initial conditions for each test. These results are listed in Appendix C.

4.1.2 H_2-Air; P,T = Constant (Test Series #1)

Detonation cell width (λ) measurements for the H_2-air system, at one atmosphere total pressure and 20°C, derived from laboratory-scale experiments at McGill University and from the HDT measurements at Sandia, are displayed in Fig. 4-2. These experimental results for the hydrogen-air system represent the widest known compositional range for the detonation cell width in any fuel-air mixtures. The leanest and the richest compositions (i.e., 13.5% H_2-air and 70% H_2-air) have detonation cell patterns that have one set of dominant tracks indicating that the mixtures are close to mixtures that correspond to the onset of a single-head spin in the 43 cm diameter HDT. These limits are much wider than the previously believed 18-59% discussed by Lewis and Von Elbe [8], which were influenced by the small size of the experimental tube rather than any intrinsic limit of the H_2-air system.

Note that the results of the HDT (43-cm dia.) are close to those obtained in the largest tube (30-cm dia.) at McGill University. Since subjectivity is involved in estimating λ, R. Knystautas of McGill University measured the detonation cell width from the smoked foils for this test series and at McGill University. By determining the detonation cell width for both sets of experiments, differences in the application of the criteria for determining detonation cell width between different observers were reduced. During this test series, Knystautas instructed the authors in the methods of measuring detonation cell width from smoked foils. These data compare to within +/-25% as discussed in Appendix D.

The detonation cell measurements are correlated with both the Westbrook [7] and Shepherd [3] kinetic models. The correlation requires the establishment of an empirical link between the calculated reaction zone length, as calculated by Westbrook or by Shepherd, and the detonation cell width. This is done via the single-point matching at the stoichiometric composition. It is clear that the kinetic models recover the qualitative trend and, to some extent, the quantitative trend of the cell width measurements. However, using single-point matching for both the Westbrook and the Shepherd models, there is significant discrepancy between calculation and experiment on the rich side of the compositional range, and for the very lean and very rich compositions.

4.1.3 H_2-Air-CO_2; P,T = Constant (Test Series #2)

As a prelude to H_2-air-steam detonation measurements, and to assess the inhibiting effect of an inert diluent on the detonability of H_2-air mixtures, a series of detonation experiments using H_2-air-CO_2 mixtures was carried out using smaller diameter tubes at McGill University and the HDT. Fig. 4-3 shows the effect of CO_2 dilution on the detonability of H_2-air mixtures as represented by the detonation cell width λ. The immediate effect that can be observed is the severe desensitization of the mixtures with even modest additions of CO_2. For example, the addition of 5, 10 and 15% CO_2 to a stoichiometric H_2-air mixture increases the detonation cell width by approximately a factor of 1.5, 2.8, and 12.8, respectively. Because detonation sensitivity, according to the Zel'dovich criterion, is inversely proportional to the cube of the chemical length scale and hence λ, CO_2 decreases the detonability by the corresponding factors of 3.4, 22, and 2100.

The experimental measurements for the detonation cell width have been correlated with the numerical calculations of reaction zone length by Shepherd [3] for the H_2-air-CO_2 system. The correlation is based on the single-point matching at stoichiometry described previously for the H_2-air system. It is remarkable to observe that in spite of the fact that the single-point matching was done for a stoichiometric mixture of H_2-air, the quantitative calculations from this model and cell width measurements for the

H_2-air-CO_2 mixtures are within 100-200%. This degree of correlation is acceptable considering the crudeness of the model and the uncertainty involved in detonation cell width measurements. More elaborate correlation using the existing H_2-air results gives better agreement for the H_2-air-CO_2 mixtures [3].

4.1.4 H_2-Air-Steam; ρ_{air},T = Constant (Test Series #3,#4)

An extensive series of tests was carried out to measure the detonation sensitivity of H_2-air-steam mixtures. All experiments were carried out at elevated initial temperature, nominally at T = 100°C in the HDT. To simulate the nuclear reactor environment in the event of hydrogen release, the initial air partial density of the mixture was fixed for air conditions at NTP (i.e., an initial air density of 41.6 moles/m^3). The hydrogen and steam were then added, resulting in an initial mixture pressure which was superatmospheric, ranging from 1.5 to 3 atm depending on the amounts of H_2 and steam added. A range of H_2-air mixtures, to which 10, 20 and 30% steam had been added, were studied in the HDT. Results for these tests are displayed in Fig.4-4, where the detonation cell width, λ, is plotted as a function of equivalence ratio and steam mole fraction. It can be observed that the role of steam is to desensitize the mixture by a substantial factor. As an example, for stoichiometric compositions of H_2-air, the addition of 10, 20 and 30% of steam leads to an increase in the detonation cell width, λ, by the corresponding factors of 6, 20 and 60. According to the Zel'dovich criteria of dependence of the mixture sensitivity on the inverse cube of the chemical length scale, this corresponds to a reduction in detonability by factors of 220, 8000 and 2.2×10^5, respectively. As discussed in Chapter 1, a prediction made by Shapiro and Moffette [9] indicated that steam concentration had a negligible effect on detonability below about 25% steam. The data do not support this prediction.

Detonations were recorded with 30% steam for equivalence ratios of 0.9 and 1.0. Predictions by Shapiro and Moffette were that 32% steam would completely inert a detonation. For the stoichiometric mixture at 100°C, saturation corresponds to a steam mole fraction of 35.6%. In the present tests with a stoichiometric H_2-air mixture and 30% steam dilution, the measured detonation cell width is well below the detonation limit of the tube. Consequently, we believe that a stoichiometric steam-saturated mixture could be detonated in our facility. The detonation cell width data measured in the HDT for the H_2-air-steam mixtures have been correlated with the ZND model results of Shepherd [3] in the manner described for the H_2-air-CO_2 mixtures. The agreement is remarkably good in spite of the preliminary nature of this type of empirical correlation. The chemical kinetics model again appears to recover the essential qualitative features of the experimental results.

4.1.5 H_2-Air; ρ_{air},T = Constant (Test Series #5)

Note that the effectiveness of steam addition to H_2-air mixtures in reducing detonation sensitivity is affected by the initial temperature and pressure. The addition of steam in significant quantities to a fixed volume of H_2-air requires (a) elevated temperatures and (b) elevated pressures. Evidence indicates that both of these conditions, the increased initial temperature and pressure above STP, tend to sensitize the detonable mixture. A comparison of the three sets of experimental points, and corresponding theoretical curves using the ZND model, are shown in Fig. 4-5. For the lower two sets of points and curves, the difference in detonation cell width at a given equivalence ratio is due to the temperature difference at constant mixture density. For the upper two sets of points and curves, the difference in detonation cell width at a given equivalence ratio is due to the difference in mixture density at constant temperature.

4.1.6 H_2-Air; X_{H2},P = Constant (Test Series #6)
ρ = Constant (Test Series #7)

Test series #6 and #7 examine the effect of temperature at constant pressure and constant density, respectively, for one composition, X_{H2}=0.166. The detonation cell width results are shown in Fig. 4-6 along with the ZND model of Shepherd predictions [3] using the exact test initial conditions. There is a large uncertainty associated with the detonation cell width measurements in this series due to the small number of tests. Because of the uncertainty, care must be taken in drawing conclusions from this small sample. However, the general trend is a decrease in detonation cell width with temperature for both constant density and constant pressure.

The constant density results are in agreement with the results of test series #5 and both constant density and constant pressure results are in qualitative agreement with the Shepherd model for this off-stoichiometric composition. However, previous predictions by both Westbrook and Urtiew [7] and Shepherd [3] show that detonation cell width increases slightly with increasing temperature when the pressure is held constant for a stoichiometric H_2-air mixture. They note that the increase in detonation cell width is due to two effects. The primary effect is that the post-shock reactant density decreases with increasing temperature when the pressure is held fixed. The second effect is that the post-shock temperature decreases slightly with increased initial temperature.

If the effect predicted by Westbrook and Urtiew [7] can be substantiated, then the temperature effect is compositionally dependent. For near stoichiometric mixtures, an increase in temperature at constant pressure will produce an increase in detonation cell size. For off-stoichiometric (or at least lean)

mixtures, an increase in temperature at constant pressure produces a decrease in detonation cell size. A mechanism exists for such a composition-dependent initial temperature effect; the controlling chemical kinetic mechanism changes for H_2-air mixtures between stoichiometric and lean limit compositions [3].

4.2 DETONATION VELOCITY MEASUREMENTS

Detonation velocity measurements have also been made in the HDT for H_2-air-diluent mixtures. The results are displayed in Figs. 4-8 through 4-11, together with the Chapman-Jouguet (C-J) velocity calculated from the Gordon-McBride code [10]. The calculations are made for a limited number of data points corresponding to the actual test conditions. Spline interpolation was used to generate continuous curves (except for Figure 4-11). The calculations used the exact initial conditions, not nominal values. For Figs. 4-8 through 4-11, the detonation velocity is plotted versus the equivalence ratio, ϕ. This ratio is invariant with respect to the type and amount of added diluent. Various thermodynamic relationships, including the relation between ϕ and the mole fraction of H_2, are developed in Appendix E.

All the results indicate that the measured detonation velocities, even in marginal H_2-air-steam mixtures, is within a few percent of the calculated C-J values. No velocity deficit can be observed in any of the present tests. This is in agreement with the observations of Dupre, et al. [11] described in a recent paper where detonation propagation has been studied in a range of detonation tube diameters. It was observed that the velocity deficit does not exist for tube diameters in excess of 5 cm and atmospheric initial pressures. It has been postulated that the velocity deficit is related to the wall boundary layer effect in small diameter tubes and/or low initial pressures, where the Reynolds number is such that the boundary layer effect is significant. At the larger tube diameters and at high initial pressures, the Reynolds number is large and the relative effect of the boundary layer growth in the detonation propagation begins to vanish. This is most certainly indicated in the present measurements.

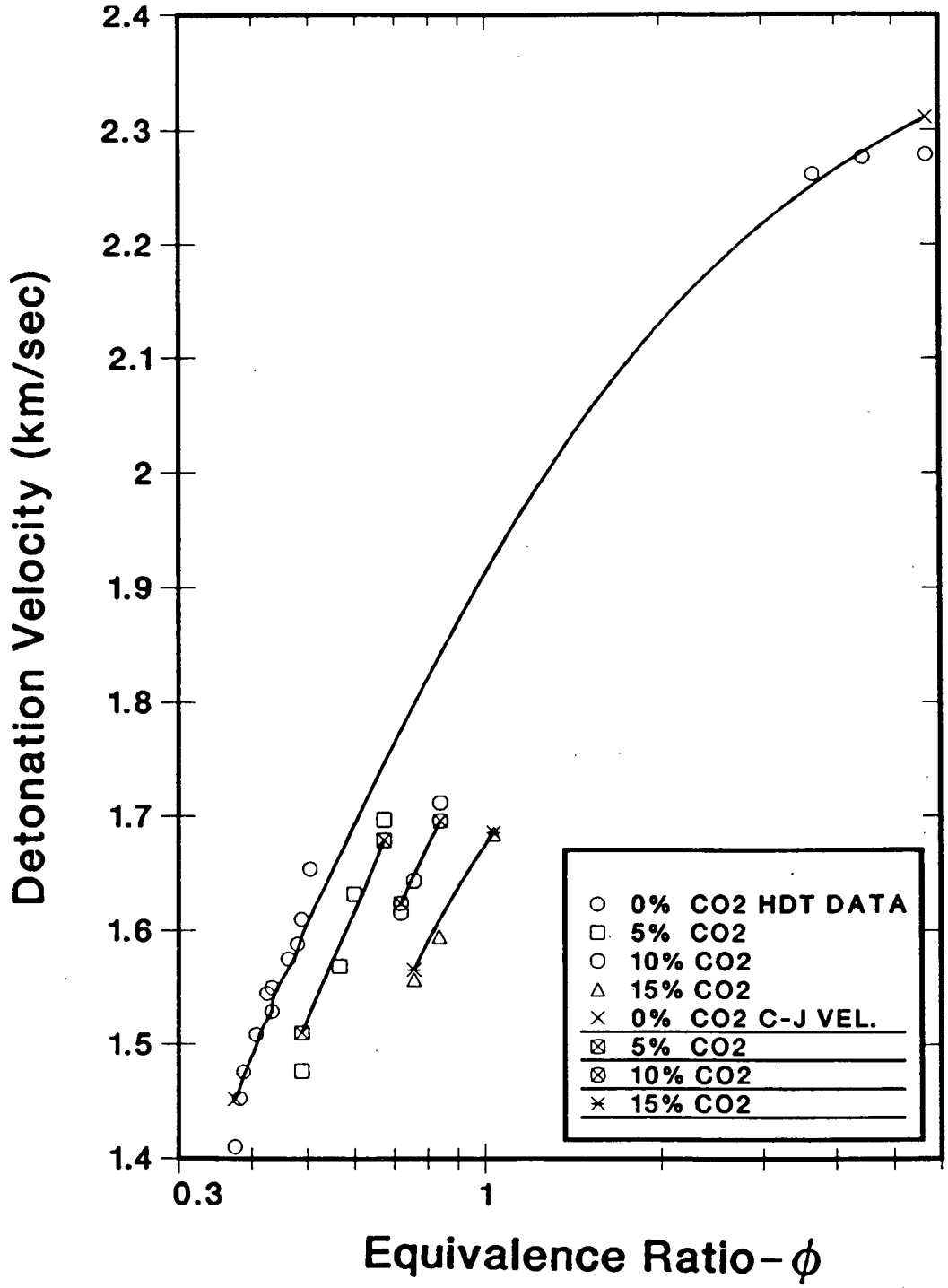

Figure 4-8. Detonation Velocity vs. Equivalence Ratio for Test Series #1, 2. (H_2-Air-CO_2 at P=1 atm, T=20°C)

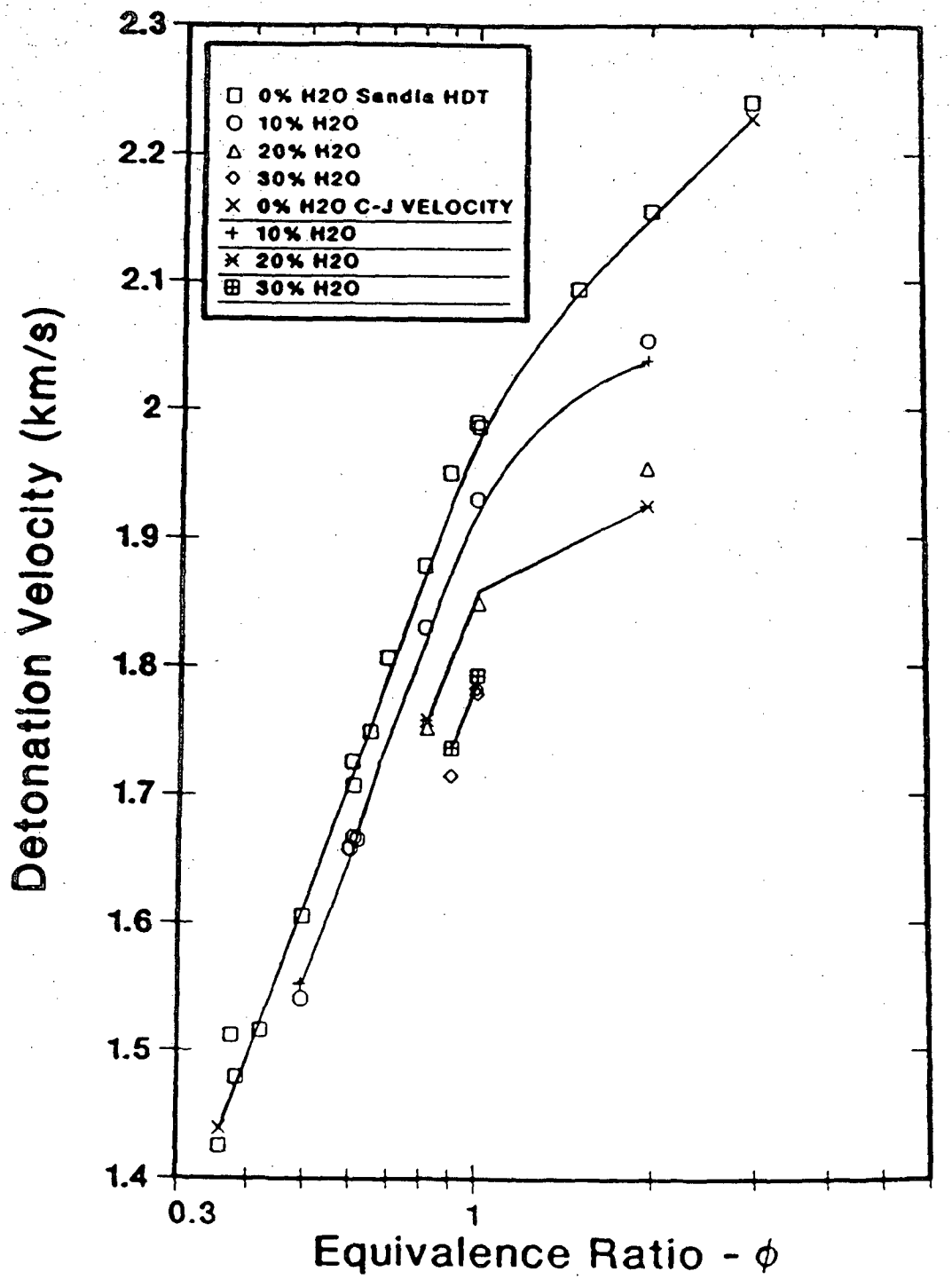

Figure 4-9. Detonation Velocity vs. Equivalence Ratio for Test Series #3, 4. H_2-Air-H_2O at ρ_{air}=41.6 moles/m^3, T=100°C)

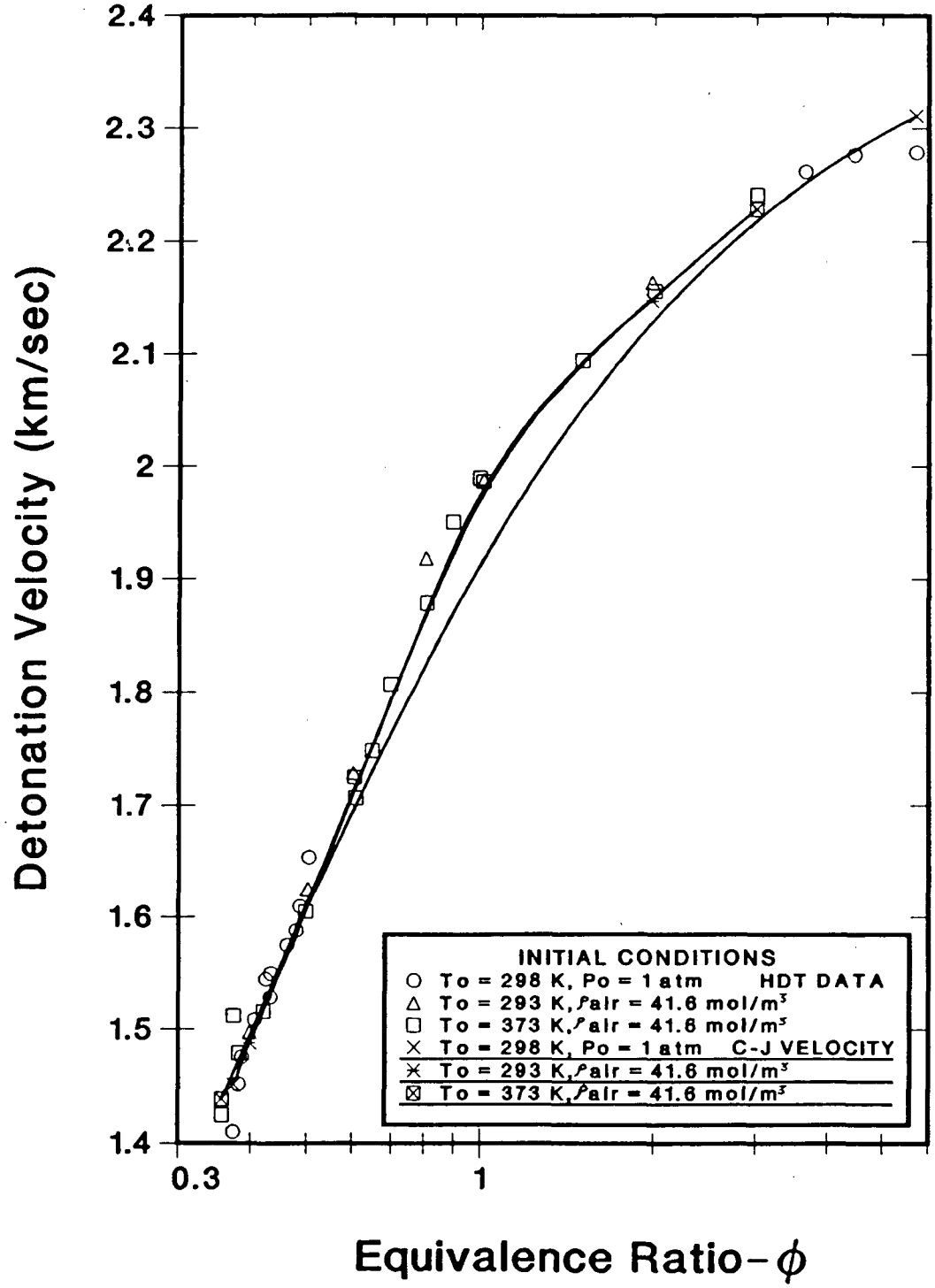

Figure 4-10. Effect of Initial Conditions on Detonation Velocity of H_2-Air Mixtures.

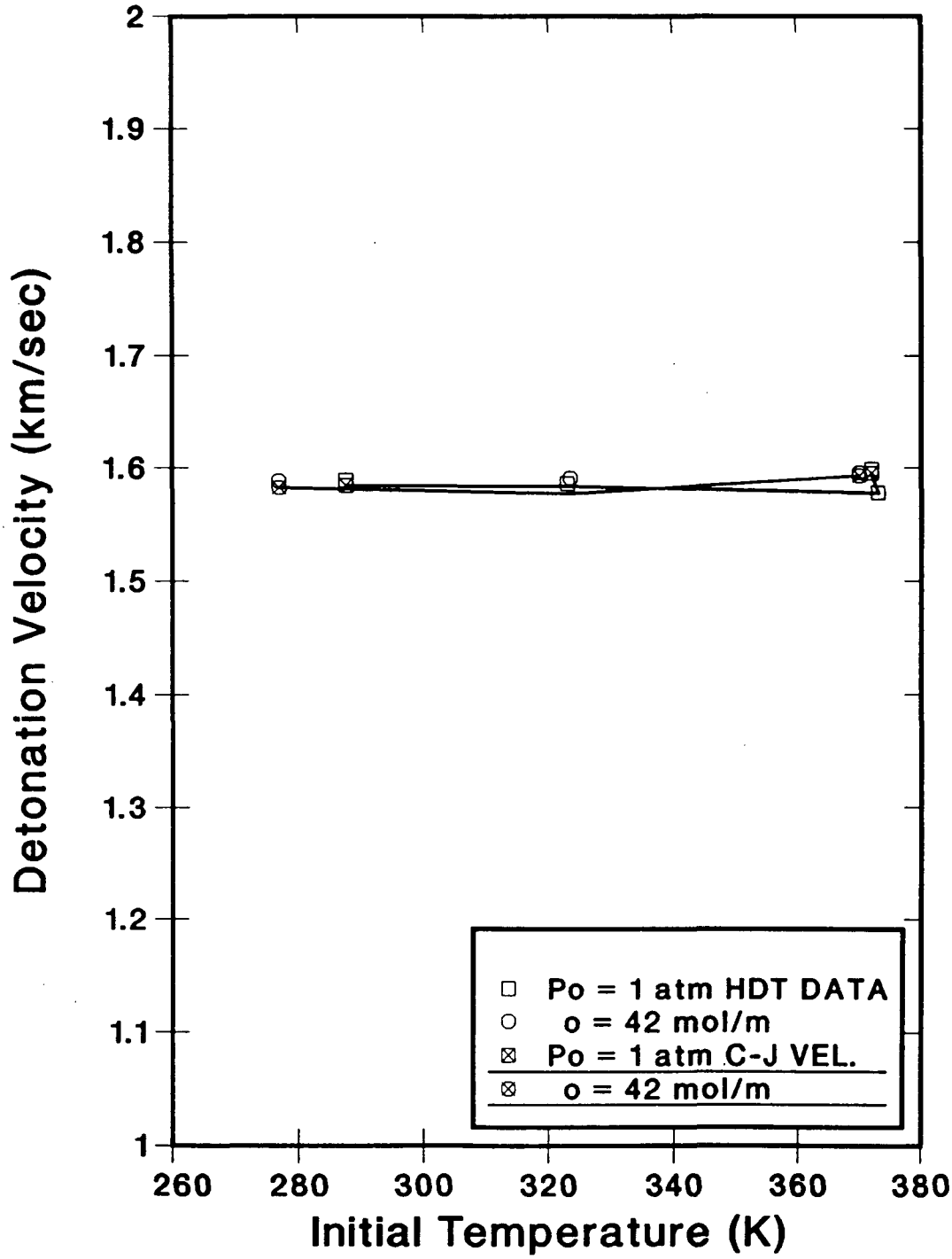

Figure 4-11. Detonation Velocity vs. Temperature for Test Series #6, 7. (H_2-Air at X_{H2}=0.17)

4.3 REFERENCES FOR CHAPTER 4

1. Moen, I. O., Murray, S. B., Bjerketvedt, D., Rinnan, A., Knystautas, R., Lee, J. H., "Diffraction of Detonation From Tubes Into A Large Fuel-Air Explosive Cloud," 19th Symp. (Int'l.) on Combustion, The Combustion Institute, Pittsburgh, PA, 1982, pp 635 - 645.

2. Bull, D. C., Elsworth, J. E., Shuff, P. J., "Detonation Cell Structures in Fuel/Air Mixtures," Combustion and Flame, V. 45, 1982, pp 7-22.

3. Shepherd, J. E., "Chemical Kinetics and Hydrogen-Air-Diluent Detonations," AIAA Progress in Astronautics and Aeronautics Series, Vol. 106, pp. 263-293, 1986.

4. Miller, J. A., Mitchell, R. E., Smooke, M. D., and Kee, R. J., "Towards a Comprehensive Kinetic Mechanism for Oxidation of Acetylene," 19th Symposium (International) on Combustion, The Combustion Institute, Pittsburgh, Pa., 1983, pp 181-196.

5. Shchelken, K. I. and Troshin, Ya. K., Gasdynamics of Combustion, Mono Book Corp., Baltimore, Md., 1965.

6. Lee, J. H., Knystautas, R., Guirao, C., Benedick, W. B., Shepherd, J. E., "Hydrogen-Air Detonations," Proceedings of the Second International Conference on the Impact of Hydrogen on Water Reactor Safety, NUREG/CP-0038, EPRI RP 1932-35, SAND82-2456, October 1982, pp 1007-1026.

7. Westbrook, C. K., and Urtiew, P. A., "Chemical Kinetic Prediction of Critical Parameters in Gaseous Detonation," 19th Symp. (Int'l.) on Combustion, The Combustion Institute, Pittsburgh, PA, 1982, pp 615 - 623.

8. Lewis, B., and Elbe, G. von, Combustion, Flames and Explosions of Gases, 2nd Ed., New York, Academic Press, 1961.

9. Shapiro, Z. M. and Moffette, T. R., Hydrogen Flammability Data and Application to PWR Loss-of-Coolant Accident, WAPD-SC-545, Bettis Plant, September 1957.

10. Gordon, S., and McBride, B. J., "Computer Program for Calculation of Complex Chemical Equilibrium Compositions, Rocket Performance, Incident and Reflected Shocks, and Chapman-Jouguet Detonations," NASA SP-273, 1971.

11. Dupre, G., Knystautas, R., and Lee, J. H., "Near Limit Propagation of Detonation in Tubes," AIAA Progress in Astronautics and Aeronautics Series, Vol. 106, pp. 244-260, 1986.

CHAPTER 5

DISCUSSION AND CONCLUSIONS

5.1 DISCUSSION

The data from the HDT tests can be used to analyze the possibility of detonation propagation in reactor containment buildings. In the past this type of analysis has often made use of the predicted hydrogen-air-steam detonability limit by Shapiro and Moffette[1]. Shapiro and Moffette plotted their detonability limits on ternary mixture coordinates. This is common for deflagration analysis since deflagration limits are strong functions of mixture concentration and only weak functions of other variables, such as temperature and pressure, in the range of interest. These other variables are often shown parametrically on the ternary diagrams.

Chapter 1 reviewed detonation studies completed since Shapiro and Moffette which conclusively show that detonation limits are a strong function of geometric scale and pressure in addition to mixture concentration. The hydrogen-air-steam data from the HDT tests also show that the detonation limits are a function of mixture temperature. The detonation limit prediction by Shapiro and Moffette is invalid since it does not address these additional variables. A single ternary mixture diagram is not sufficient to plot all the variables. However, for a given mixture temperature and pressure (or density), contours of constant detonation cell width can be plotted on ternary mixture coordinates.

Figure 5-1 shows these contours for a mixture temperature of 100°C and an air molar density of 41.6 moles/m^3. For comparison, the theoretical prediction by Shapiro and Moffette is also shown. The lines of constant cell width correspond to lines of constant detonation sensitivity. As the detonation cell width increases, the smallest room dimension which will allow detonation propagation increases. A large room will allow a broader range of mixtures to propagate a detonation compared to a smaller room.

To evaluate which mixtures will propagate a detonation in a given geometry, the detonation cell width is compared to geometric propagation correlations discussed in Chapter 1. For convenience, the detonation propagation correlations given in Figure 1-4 have been copied again as Figure 5-2. As an example, take a long duct of square cross-section, 1 m by 1 m. From Figure 5-2, the proper detonation propagation correlation is that between parallel plates. Therefore the detonation cell width that will just marginally propagate in the duct is 1 m, the same dimension as the duct. This means that the area to the left of the 1 m contour in Figure 5-1 is detonable for the given temperature and air density. If the duct were only 0.5 m on a side, then the area to the left of the 0.5 m contour would be the detonable region, etc.

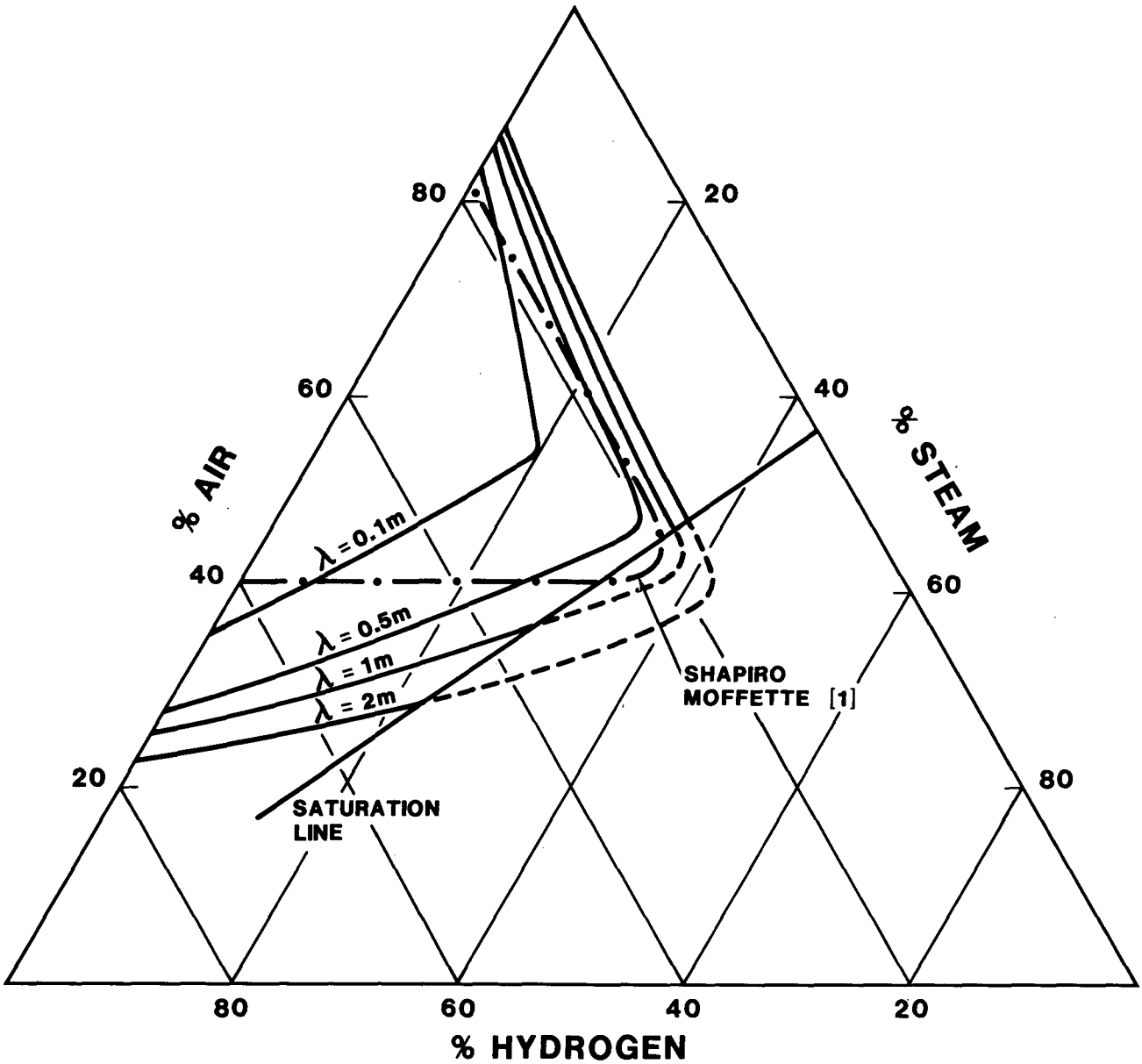

Figure 5-1. Constant Detonation Cell Width on Mixture Coordinates. (For T = 100°C, Air Density = 41.6 mole/m^3)

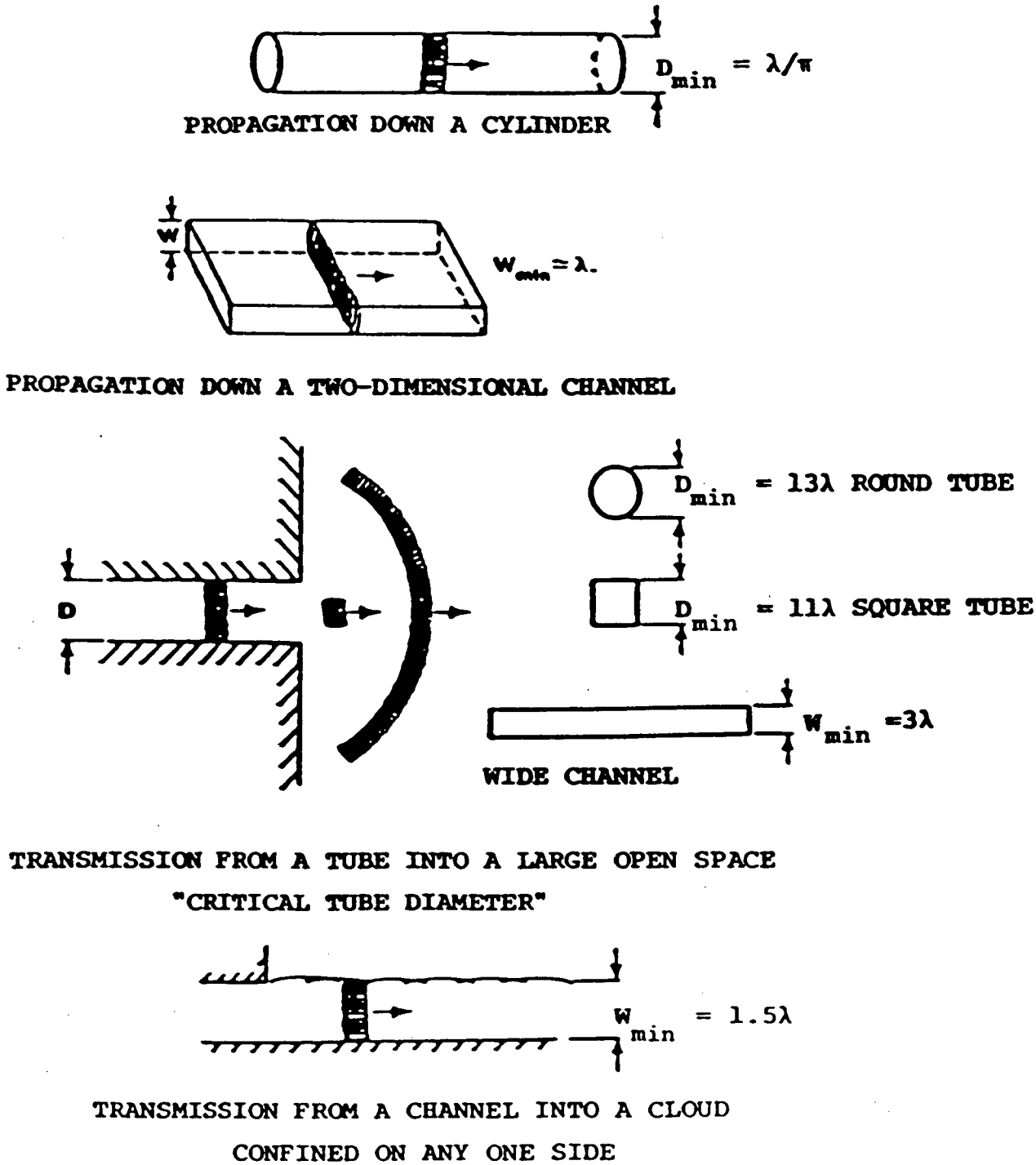

Figure 5-2. Effect of Geometry on Propagation of Detonation Waves.

It is not necessary to use the ternary mixture diagram to evaluate detonability. For a given mixture, the plot of detonation cell width as a function of equivalence ratio can be used, e.g. Figure 4-4. For convenience, Figure 4-4 has been copied to Figure 5-3. For example if a mixture is formed at 100°C with an initial air density of 41.6 moles/m^3 with 30% H_2O and 29.5% H_2, Fig. 5-3 shows that the dominant mode detonation cell width is 300 mm. From Fig. 5-2 the minimum channel width for propagation of a detonation is 300 mm. Any channel narrower than this will not continue to propagate a detonation in this mixture. Similarly, the smallest tube diameter for propagation is 100 mm. The smallest tube diameter that will allow a detonation to propagate from the tube into free space is 3.9 m, etc. For accident conditions that have not been directly tested in the HDT, the test data can be interpolated. For example, a mixture of 21% H_2 (ϕ = 0.63) and 15% H_2O at 100°C can be anticipated to have a dominant mode detonation cell width of approximately 400 mm.

Two qualifications need to be considered when using the data. First, great care should be taken in trying to extrapolate trends in the data. A state-of-the-art chemical kinetics model [2] is used in this report to extrapolate the data to obtain the one and two meter detonation contours in Fig. 5-1. The model is discussed briefly in Chapter 4, but it is beyond the scope of this report to evaluate the predictive capability and uncertainty associated with this class of models. However, the chemical kinetics model shows that changes in initial conditions, equivalence ratio, and diluent concentration can change the rate-controlling reactions. Therefore, an attempt to extrapolate trends from the data could lead to very large errors.

Secondly, there are large uncertainties in the measurement of detonation cell width and in the detonation propagation correlations based on detonation cell width. The analyst using the detonation cell width data in this report is urged to read Appendix D. A range of detonation cell widths appears on a smoked foil record. The characterization of this range is an area of current research and may have a significant impact on safety analysis. Mixtures with broad distributions (irregular) may have different propagation criteria than those with narrow (regular) distributions. For this reason, the authors strongly recommend that safety analysts divide the dominant mode detonation cell widths in this report by a factor of two for use in safety calculations. For example, the one meter detonation cell width contour in Fig. 5-1 should be considered as a 0.5 m contour in safety calculations. In some cases dividing by a factor of two may be conservative and in other cases it may not be. The factor of two is recommended because there is almost always structure that could be interpreted as a detonation cell width that is a factor of two smaller than the dominant mode measured on smoked foil records. Other researchers have termed this smaller cell width "substructure" and have noted its existence for many fuel-air mixtures [3,4].

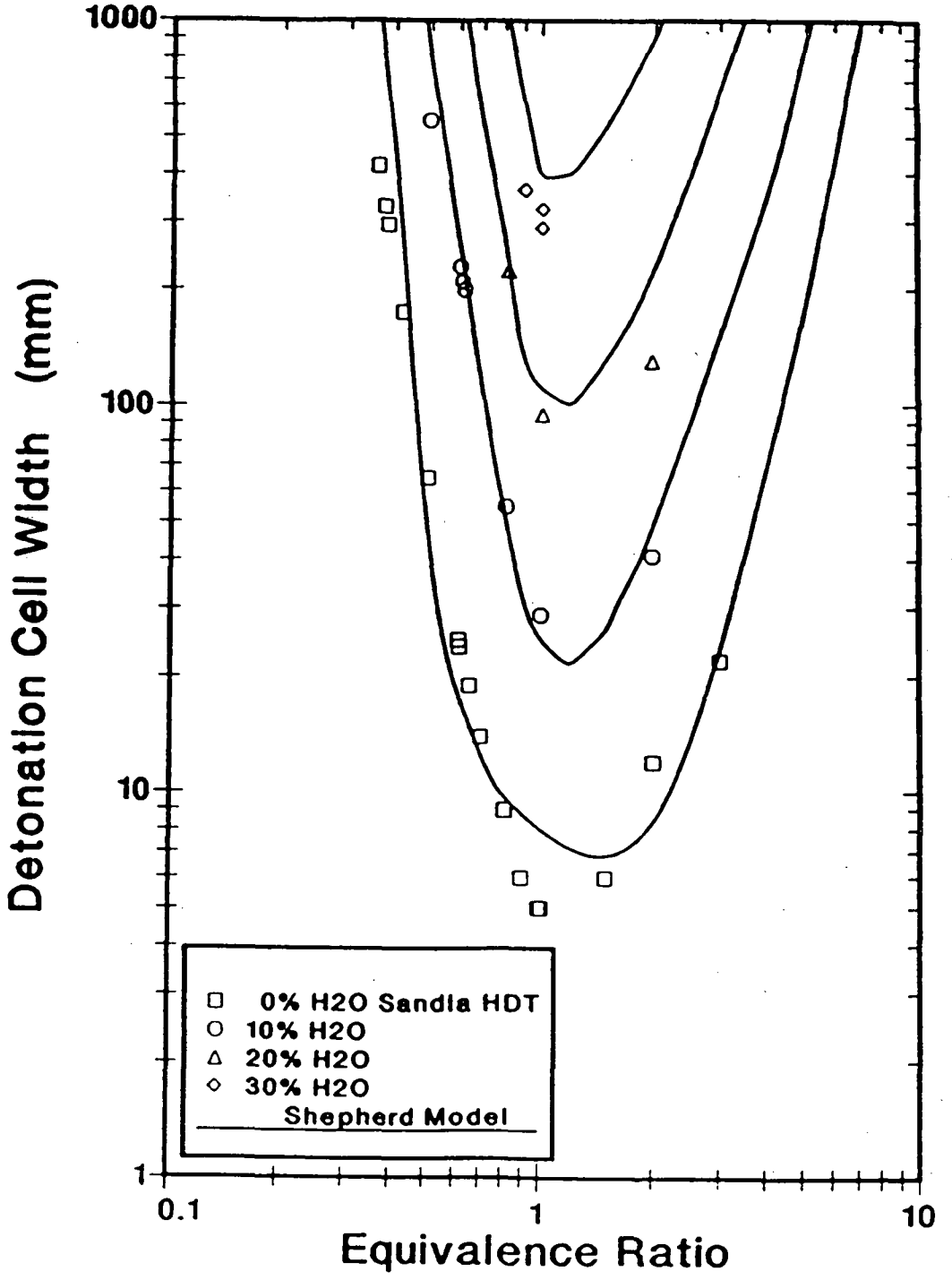

Figure 5-3. Detonation Cell Width vs. Equivalence Ratio for Test Series #3,4. (H_2-Air-H_2O at ρ_{air}=41.6 mole/m^3, T=100°C).

The nonlinear nature of the chemical processes complicates a direct comparison of the effectiveness of CO_2 and H_2O directly from the data taken in this report. The H_2O data are at higher initial temperature and pressure than the CO_2 data. It was expected that the effect of CO_2 and H_2O dilution on detonation cell width would be similar because of similar heat capacities. However, the chemical kinetics model used in this report indicates that CO_2 and steam affect the hydrogen-oxidation reactions chemically as well as thermally, and it predicted that steam should be less effective than CO_2 as a diluent.

5.2 CONCLUSIONS

1. For H_2-air mixtures at 20°C and a total pressure of 101 kPa, detonations have been achieved between 13.5% and 70% H_2 mole fraction. This compositional range is wider than the detonability limits previously reported for smaller tubes.

2. The addition of CO_2 to H_2-air mixtures greatly reduces the detonability of the mixture.

3. For given initial temperature, air density and equivalence ratio, the addition of steam to an H_2-air mixture greatly decreases the detonability of the mixture.

4. At 100°C and an air density of 41.6 moles/meter^3, detonation of H_2-air mixtures with up to 30% steam have been recorded.

5. For H_2-air mixtures, the detonability increases with increasing initial temperature at constant density. Consequently, the diluent effect of the addition of steam to a fixed volume of a H_2-air mixture in reducing detonability is partially offset if there is a concomitant temperature increase.

6. At 100°C and an air density of 41.6 moles/meter^3, a 13.0% H_2-air mixture has been detonated.

7. Within the measurement uncertainty, the detonation velocities in the HDT agree with the velocities predicted by the Chapman-Jouguet theory.

5.3 FUTURE WORK

The purpose of this work has been to determine the detonability of H_2-air-diluent mixtures, particularly H_2-air-steam mixtures for conditions of interest in nuclear reactor safety. We have developed a data base that covers some of the range of temperatures and pressures of interest. The current research has focused on the need to validate theoretical models by identifying specific effects such as temperature, density, H_2 concentration and diluent concentration. The tests have been conducted at

constant molar air density which is a valid condition assuming globally uniform mixing. To evaluate the threat of localized detonations due to transient mixing, tests will have to be conducted at constant pressure. Hydrogen rich conditions will exist locally around the source. Much of the testing to date has been done for lean to stoichiometric conditions. Further work will need to be conducted on the hydrogen rich side.

Isolating individual effects has contributed substantially to code validation. Chemical kinetics modeling has shown promise as a tool to interpolate and potentially extrapolate experimental results. Given the broad range of possible initial thermodynamic states and compositions that may develop as a result of an accident, particularly early in an accident prior to complete mixing, this type of research should continue. Some testing is planned to compare H_2O and CO_2 diluents directly.

The experimental technique to obtain detonation cell width information has not improved significantly for more than a decade. Measurement of detonation cell width still requires experimental judgement in interpreting the pattern on the smoked foil. Work is beginning that uses modern digital image processing to lessen human judgement in the measurement process.

The largest uncertainty in predicting whether a detonation will occur is the deflagration-to-detonation transition (DDT) problem. Detonation cell width has been related to the minimum spherical charge (energy) required to detonate a mixture but has not yet been solidly linked to turbulence parameters. Detonation tube experiments such as those in the HDT can be used to identify the detonation cell width but will not yield DDT criteria directly.

5.4 REFERENCES FOR CHAPTER 5

1. Shapiro, Z. M. and Moffette, T. R., Hydrogen Flammability Data and Application to PWR Loss-of-Coolant Accident, WAPD-SC-545, Bettis Plant, September 1957.

2. Shepherd, J. E., "Chemical Kinetics and Hydrogen-Air-Diluent Detonations," AIAA Progress in Astronautics and Aeronautics Series, Vol. 106, pp. 263-293, 1986.

3. Moen, I. O., Murray, S. B., Bjerketvedt, D., Rinnan, A., Knystautas, R., Lee, J. H., "Diffraction of Detonation From Tubes Into A Large Fuel-Air Explosive Cloud," 19th Symp. (Int'l.) on Combustion, The Combustion Institute, Pittsburgh, PA, 1982, pp 635 - 645.

4. Bull, D. C., Elsworth, J. E., Shuff, P. J., "Detonation Cell Structures in Fuel/Air Mixtures," Combustion and Flame, V. 45, 1982, pp 7-22.

APPENDIX A

DETAILS OF THE EXPERIMENTAL APPARATUS

This appendix describes in detail the structural, electrical, and thermal aspects of the Heated Detonation Tube (HDT), the explosive initiator circuit, and instrumentation.

A.1 STRUCTURE

The HDT can be divided into three structural segments, the main tube, the secondary piping, and the tube and piping supports. Each will be described and the appropriate structural limits identified.

A.1.1 The Main Tube

The main tube is composed of three pipes, one short thick-walled section used for initiation of the detonation followed by two long sections for propagation. All are made of 304 stainless steel and have a 45.7-cm (18-in) outer diameter. The short initiator section is 0.91 m (3 ft) long with a 2.54-cm (1-in) thick wall. The two long sections are 6.1 m (20 ft) long and have a 1.27-cm (0.5-in) thick wall. The short thick initiator section has one penetration for gas recirculation. The two long sections each have 7 penetrations for transducers. The second long section also has one penetration for gas recirculation. Figure A-1 shows a cross-section of a gas recirculation penetration. Figure A-2 shows a cross-section of a transducer penetration. The gas recirculation penetrations are 90° clockwise from the vertical and the transducer penetrations are 64° counter-clockwise from the vertical as viewed from the initiation end.

The pipes are bolted together, and endplates are bolted to the ends of the connected pipes, through flanges that have been welded on the ends of each pipe. A cross-section of the flange is shown in Figure A-3. The O.D. of the flange is 63.5 cm (25 in) and is 4.45 cm (1.75 in) thick. Sixteen 3.18 cm (1.25 in) unthreaded bolt holes are on a 57.79 cm (22.75 in) bolt hole circle. The bolts used are 2.86 cm (1.125 in) diameter, ASTM 325 hardened, UNC-7 thread, 12.7 cm (5 in) long with matching nuts and 0.36 cm (9/64 in) thick by 5.08 cm (2 in) O.D. washers.

A gas seal between the pipes and pipe/endplate is provided by an O-ring. O-ring grooves are cut into the face of the flanges on the initiator section and the second long section. The mating flanges and endplate faces have no grooves. The O-ring grooves are 8.69 mm (0.342 in) wide at the base by 5.21 mm (0.205 in) deep and 50.902 cm (20.04 in) in diameter. The O-ring material is high temperature grade ethylene-propylene, Parker #2-468E692-75 rated at 260°C.

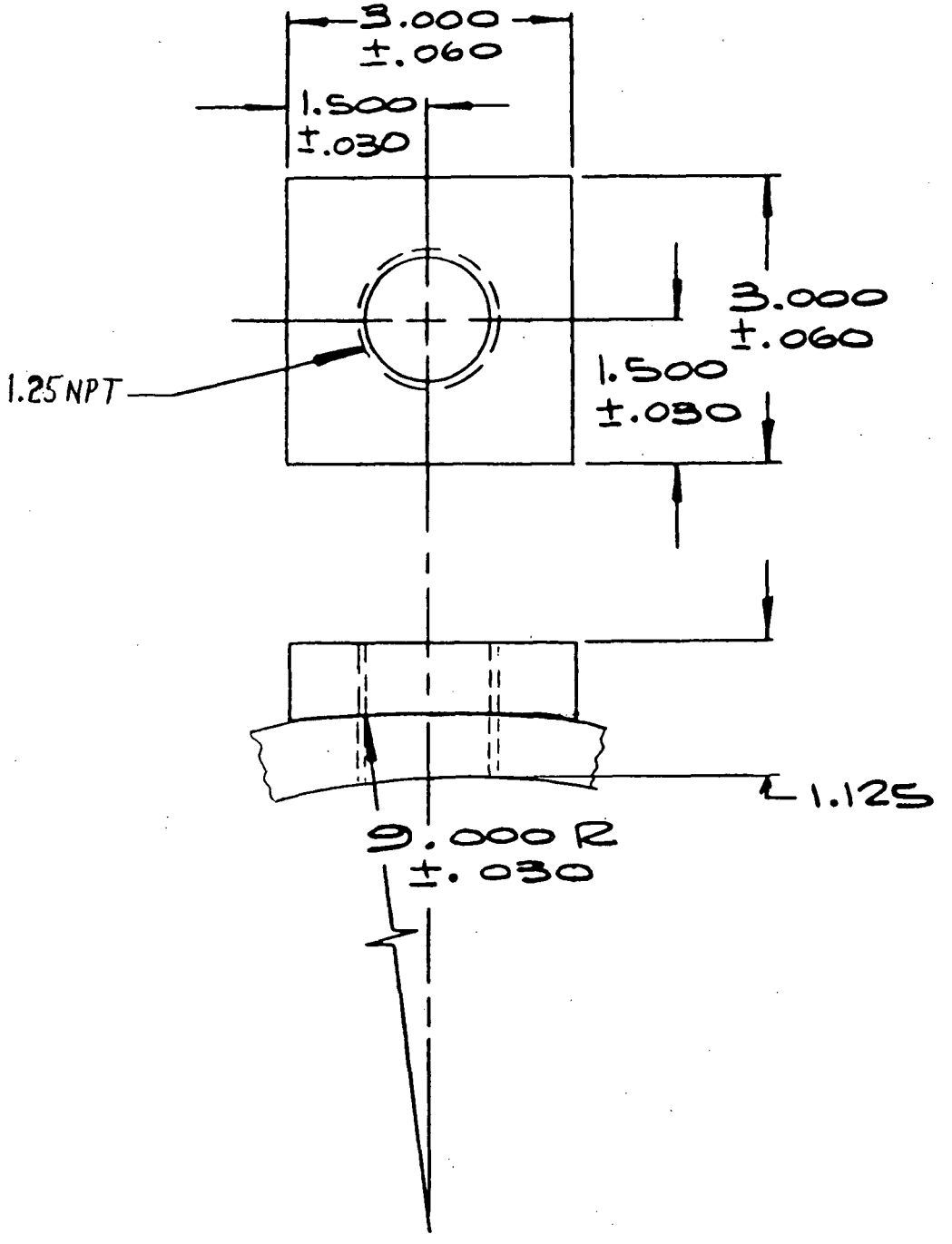

Figure A-1. Cross-Section of a Gas Recirculation Penetration.

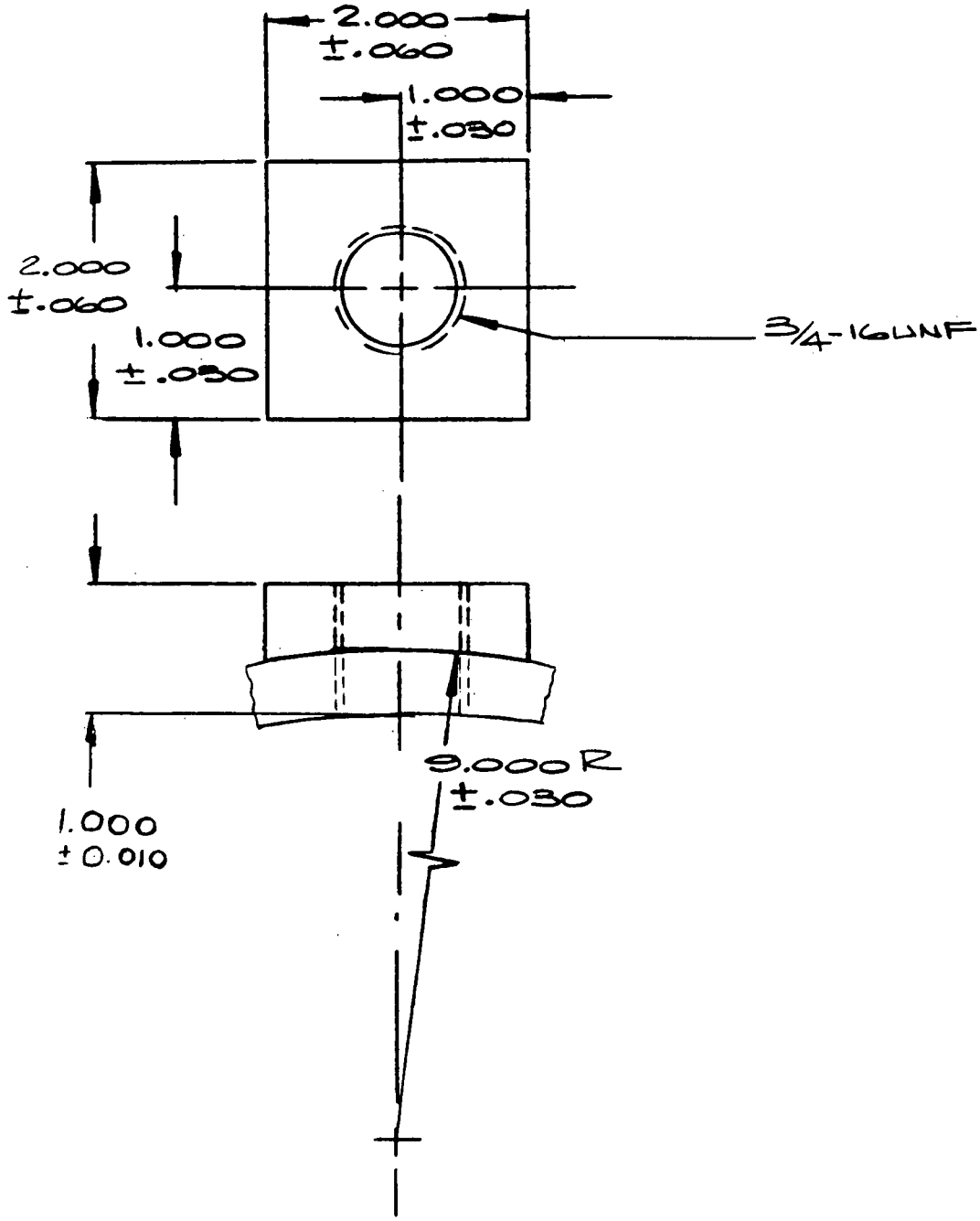

Figure A-2. Cross-Section of a Transducer Penetration.

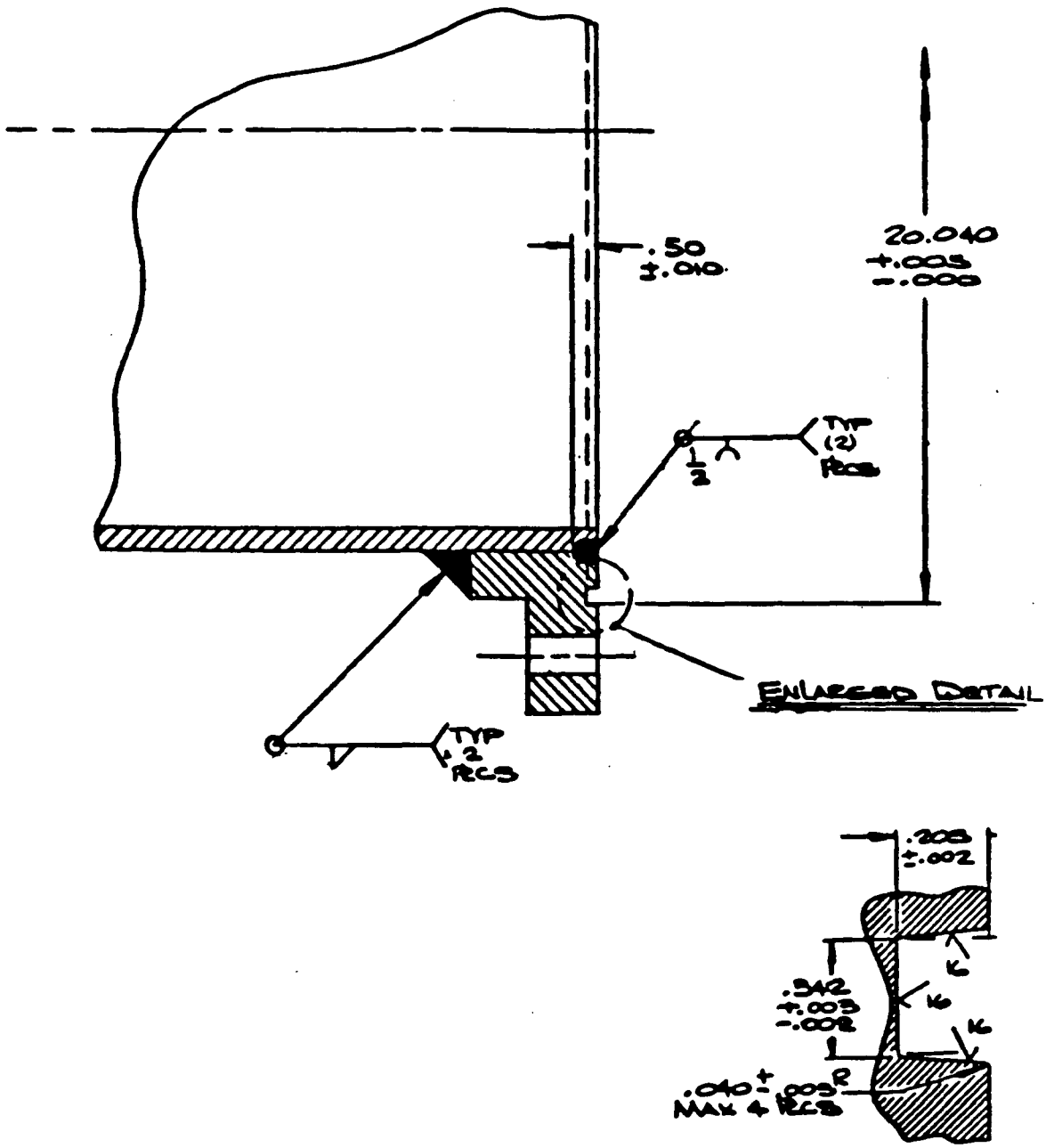

Figure A-3. Cross-Section of a Pipe Flange.

The endplates are 3.18 cm (1.25 in) thick 304 stainless steel disks 63.5 cm (25 in) diameter having the same bolt hole pattern as the pipe flanges. The plate on the initiation end has a hole for a 2.54 cm (1 in) pipe thread for a detonation initiator cable feed-through. The plates have a 3.8 cm (1.5 in) diameter, 1.27 cm (0.5 in) thick eyelets welded on the upper edge for lifting purposes.

The long pipes have a theoretical yield pressure under static loading of 11.5 MPa (1667 psi) and a burst pressure of 28.7 MPa (4167 psi). The initiation section has a yield pressure of 23 MPa (3333 psi) and a burst pressure of 57.5 MPa (8333 psi). The yield and burst values for dynamic loading can conservatively be taken as 1/2 the static values. The endplates are more limited in strength. Reference A-1 gives the following formula for statically loaded flat heads under uniform pressure rigidly bolted to the flange:

$$h = d\sqrt{\frac{C\ P_s}{S_d}} \qquad \text{(Eq. A-1)}$$

where:
- h = plate thickness (in)
- d = bolt hole circle (in)
- C = 0.162
- P_s = static pressure (psi)
- S_d = Allowable stress with safety factor.

Rearranging,

$$P_s = \frac{S_d}{C}\left(\frac{h}{d}\right)^2 \qquad \text{(Eq. A-2)}$$

The dynamic pressure can be considered to be twice the static pressure, or

$$P_d = \frac{S_d}{2C}\left(\frac{h}{d}\right)^2 \qquad \text{(Eq. A-3)}$$

where P_d is the dynamic pressure

The diameter, d, in equation A-3 is to the bolt hole circle. However, for small deflections, the pressure does not extend to the bolt hole circle but stops at the O-ring groove. The allowable stress can be taken as the static yield stress which is

290 MPa (42000 psi). The dynamic yield stress is approximately 1.4 times this value. Using the static value of 290 MPa gives a safety factor of 1.4.

$$P_d = \frac{42000}{2(.162)} \left(\frac{1.25}{20}\right)^2 = 506 \text{ psi} = 3.4 \text{ MPa} = 34 \text{ atm}$$

H_2-Air detonations have pressure ratios between 10 and 15 times the initial pressure depending on the mixture. Therefore, the maximum initial pressure is between 2.3 atm and 3.4 atm absolute.

A.1.2 The Secondary Piping

A schematic of the secondary piping is shown in Figure A-4. The piping provides for evacuation, injection and circulation of the gaseous mixture. The secondary piping consists of a circulation pump, inline filter, and the appropriate tubing, fittings and valves. The gas flow is from the outlet penetration on the terminal (foil) end of the main tube, through a shutoff valve, a filter, a pump, past a high point vent and gas and steam injection ports, along the main tube to a shutoff valve on the inlet penetration at the initiation end of the main tube. The main shutoff valves are use to isolate the secondary piping prior to initiating a detonation to protect the secondary side from the detonation pressures. The valves are Swagelock SS-65F12 ball valves.

The pump and gas injection/evacuation port and vents are mounted on a wooden platform suspended from a main tube support. Flexible tubing is used to connect these components to the rest of the secondary piping which is attached to the main tube. The flexible lines allow for motion between the secondary piping attached to the main tube and the components attached to the fixed main tube support.

The secondary tubing attached to the main tube is mounted against the main tube wall and held in place with large diameter steel hose clamps. It is mounted between heating tapes and the main tube wall so that it is maintained at the main tube temperature. At the flanges on the main tube, flexible lines are used instead of rigid piping to circumvent the flange in order to minimize the number of sharp bends that create pressure losses.

All rigid piping throughout the secondary except the pump manifold is 1.91 cm (0.75 in) diameter, 1.25 mm (0.049 in) wall thickness, 304 stainless steel tubing. The flexible lines are braided stainless steel with a teflon core. The pump has two pumping chambers which are piped in parallel by inlet and exit manifolds. The manifolds are made of 1.27 cm (0.5 in) diameter, 304 stainless steel, 0.89 mm (0.035 in) wall thickness tubing.

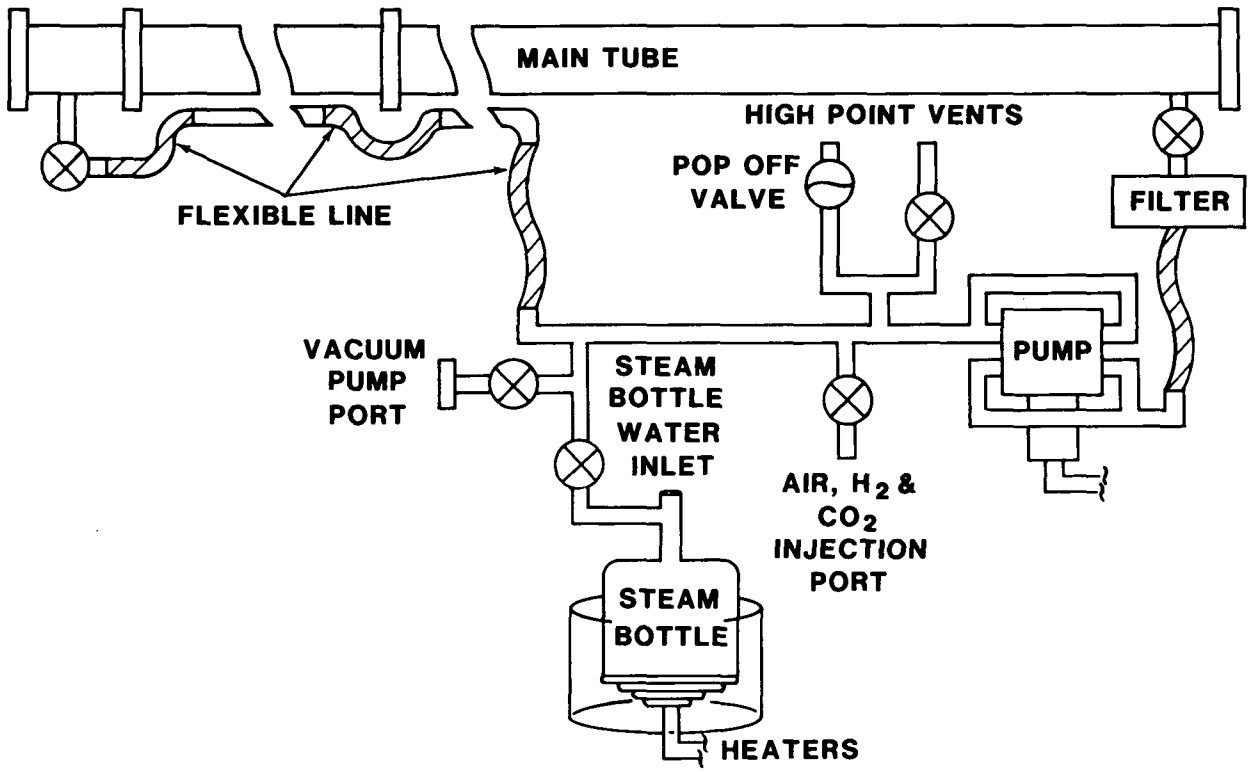

Figure A-4. Schematic of the Secondary Piping.

Swagelock tube fittings are used throughout except the first reducing bushing at the main tube penetrations.

The pump is a Metal Bellows Corp. sealed bellows pump Model MB-602-XP. It is rated at 2.83 std. L/s (6 scfm) with no back pressure. The inline filter protects the pump from particle debris resulting from the explosive initiator products. The filter is a Balston type 62A-3/4 case with a type 150-19-CQ filter cartridge made of borosilicate and removes 8 μm particles. This material does not absorb moisture. The filter is positioned immediately downstream of the main shutoff valve on the outlet gas recirculation port of the tube.

Downstream of the filter and pump is the high point vent tee. Venting can occur through two paths. One is through a manual valve used to release gases after a test which has a temperature rating of 205°C (400°F). The other path has a pop-off type relief valve set at 345 kPa (50 psig). Both pipes are 1.27 cm (0.5 in) diameter tubing and vent approximately 3 m (10 ft) above the ground. Downstream of the tee leading to the high point vents are the gas injection port tee and steam injection/ evacuation tee respectively.

The gas injection port has a ball valve for flow control and 0.64 cm (0.25 in) Swagelock double shutoff quick disconnect stem to accommodate the transfer line from the gas supply bottles. The gas transfer line is a 0.64 cm (0.25 in) flexible hose with a teflon inner liner. The gas supply bottles are standard, nominal 5.67 m^3 (200 ft^3), pressurized cylinders with appropriate two stage regulators with secondary side pressures of 690-1380 kPa (100-200 psi). The regulator outlets are connected to a needle valve for flow regulation and a Swagelock 0.64 cm (0.25 in) quick disconnect body to accommodate the transfer line.

The steam bottle is a 1-liter gas sample cylinder that has a 500 W flexible rod heater wrapped around the bottom of the vessel. The heater and cylinder were immersed in a molten lead bath that was allowed to harden in a larger cylinder. The 1 liter vessel sets under a 1.91 cm (0.75 in) diameter vertical pipe with two tees. The vertical pipe has a pipe plug which is removed to introduce a premeasured amount of water into the steam vessel. One tee leads to a BS & B 2.54 cm (1 in) diameter UA-2 burst disk holder with a 2.4 MPa (350 psi) vacuum supported burst disk. For early tests, 345 kPa (50 psi) disks were used. The other tee connects the steam bottle with the secondary piping through a ball type shut off valve. (Note: this type of valve does not provide enough flow control and will be replaced in future testing.)

The evacuation line tees into the line running from the steam bottle to the secondary piping. The evacuation line also contains a ball-type shutoff valve and a special O-ring type fitting to connect the vacuum pump line. The vacuum pump is a

Leybold-Heraeus model E-150. It is designed to handle some condensed liquids but is being used beyond its liquid handling capacity to handle the water generated from the H_2-Air detonations. The oil is changed frequently to maintain the vacuum pump.

The primary pressure restriction on the secondary system is the circulation pump. The pump has a design pressure of 276 kPa (40 psig). The remainder of the system can take detonation level overpressures with the possible exception of the filter casing. The filter casing has a working pressure of 1.7 MPa (250 psi). The 1.91 cm (0.75 in) secondary tubing has a static yield of 27 MPa (3900 psi), the flexible lines have a static yield of 6.7 MPa (975 psi), the 1.27 cm (0.5 in) tubes on the pump manifold have a static yield of 29 MPa (4200 psi). The fittings used, both brass and stainless, have similar or higher yield pressures than the tubing. It was found that the pump would not restart once it had stopped if the pressure in the system was above 136 kPa (20 psia).

The popoff relief valve on the high point vent was installed to protect the pump from accidental overpressure. In the case of an accidental detonation, the pump bellows will be destroyed before the pressure can be vented to a safe level. To protect personnel from shrapnel, a 6.3 mm (0.25 in) thick box was placed over the pump bellows.

A.1.3 The Structural Supports

The detonation tube is held in place by "V" block type supports mounted on 55 gallon drums that have a concrete base as shown in Figure A-5. The V blocks are made of 10.2 cm (4 in) structural steel channel with a 10.2 cm (4 in) square cross-sectional wood block setting in the channel. The wood provides an insulating surface for the heated detonation tube to set on. The channels that form the V are hinged and can be adjusted by a hinged 3.79 cm (1.25 in) diameter threaded rod assembly shown in Figure A-6. Adjusting the length of the threaded rod provides alignment for adjustment of the detonation tube. The threaded rod assembly and V blocks are hinged to a horizontal 15.3 cm (6 in) structural steel channel. The hinges are made by 1.27 cm (0.5 in) diameter steel dowels inserted through holes in the mating pieces and held in place by cotter pin restrained washers.

The V-block assembly is mounted on the top of the 55 gallon drums which are filled with concrete and are bolted to two 3.79 cm (1.25 in) diameter threaded rods that are embedded deep into the concrete. The base of the 55 gallon drums are set in a 1.22 m (4 ft) square by 15.3 cm (6 in) deep concrete pad. Four holes were cut in the sides of the 55 gallon drums approximately 7.6 cm from the bottom at 90° angles and two 3.79 cm (1.25 in) threaded rod was inserted through the barrel. The threaded rod and "chicken wire" served as rebar for the concrete pad and to

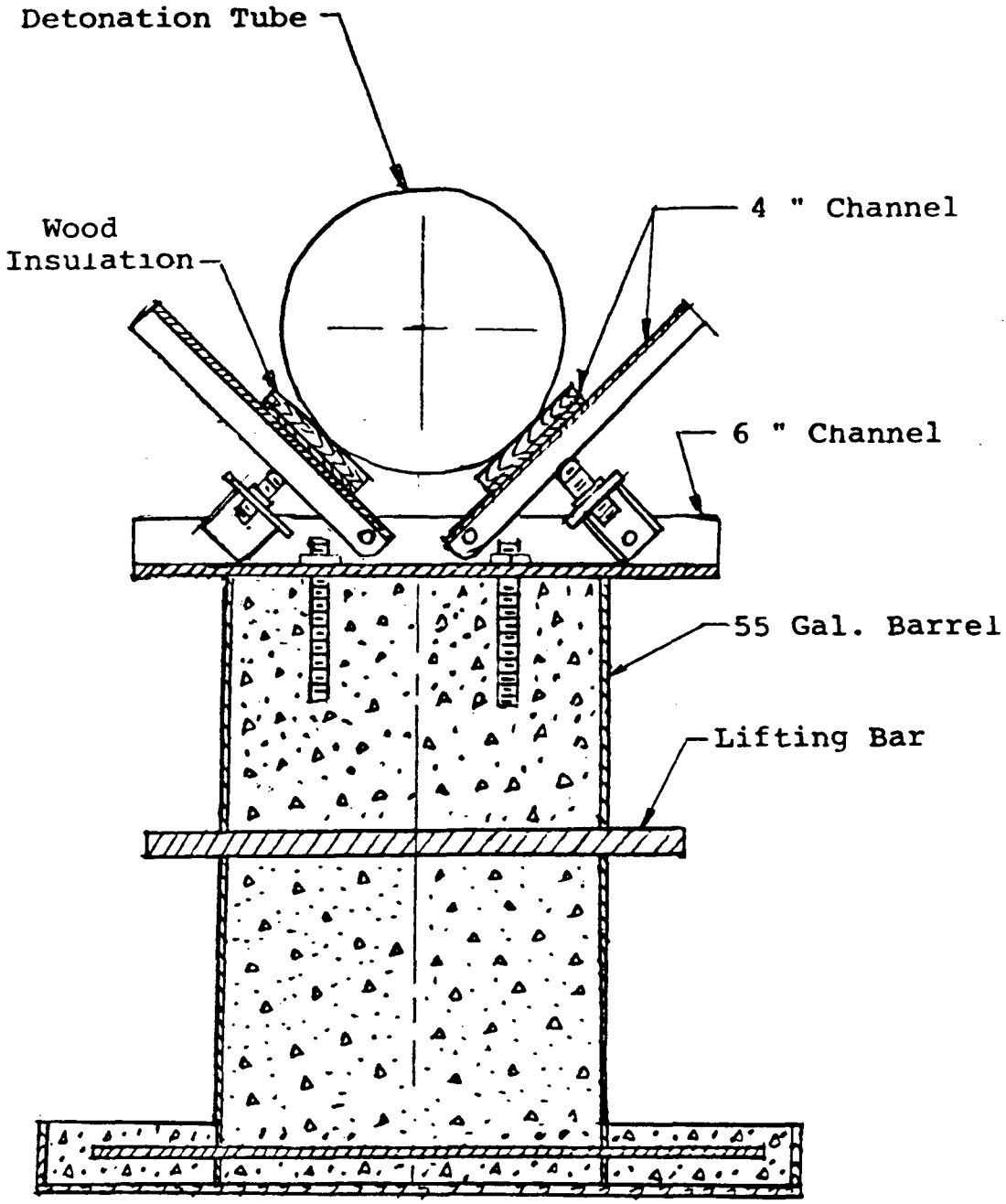

Figure A-5. Detonation Tube Supports.

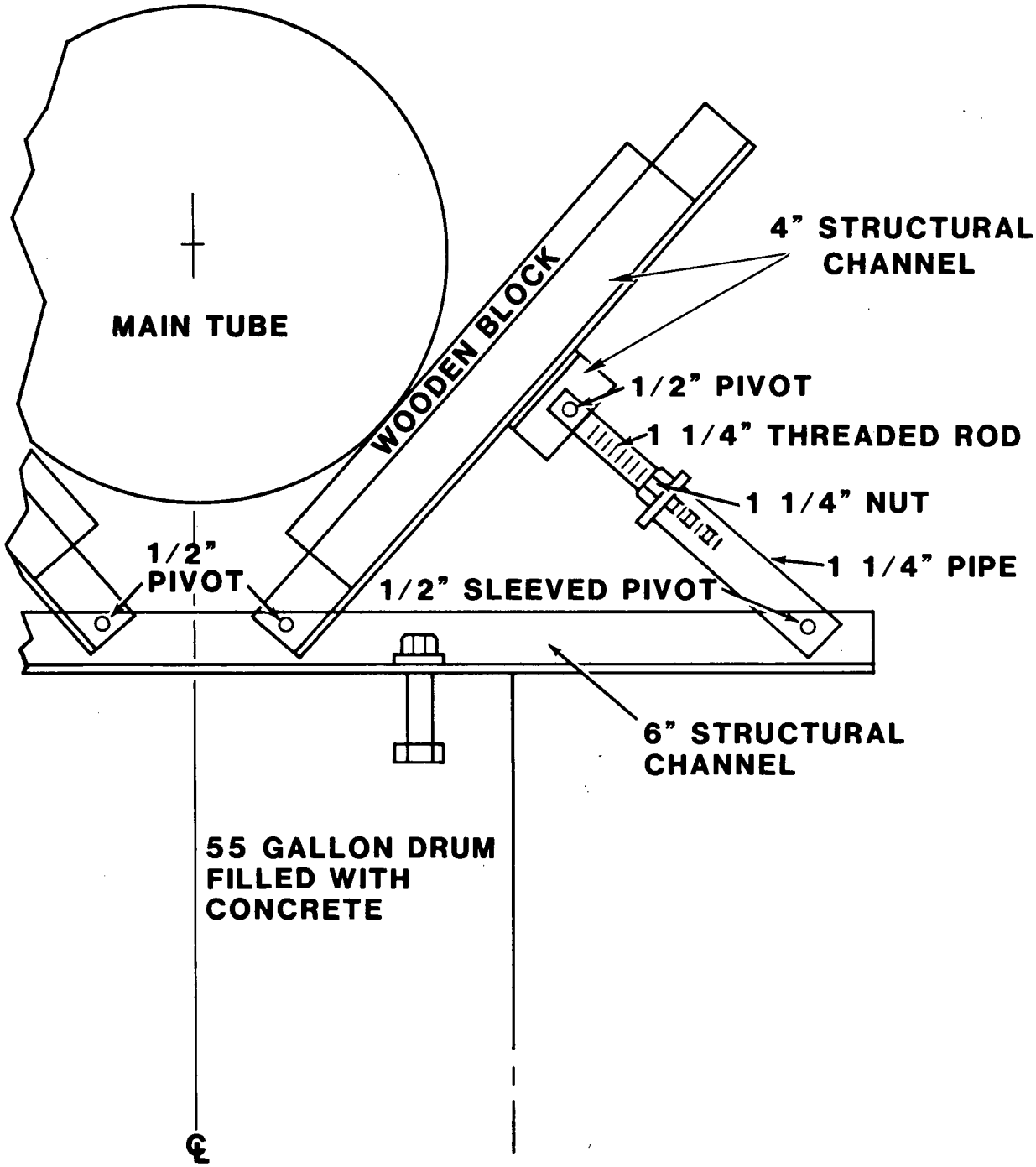

Figure A-6. Tube Support V-Block Positioning Device.

hold the pad to the 55 gallon drums. The square pads are oriented so the maximum force required to tip the supports is parallel and perpendicular to the axis of the detonation tube.

Five supports are used to hold the detonation tube, two each per long section of pipe and one on the short section. Since there are five supports, the load distribution is statically indeterminate. Assuming that the load is spread evenly to the supports, the weight of the tube on each support is 500 kg (1100 lb). Static analysis shows that it requires a 5.69 kN (1280 lb) force at a height corresponding to the elevation of the detonation tube (1.4 m - 56 in) to tip the 500 kg (1100 lb) weight of the tube per support and 545 kg (1200 lb) weight of the support, either parallel or perpendicular to the axis of the tube.

The largest tipping moment parallel to the detonation tube axis is provided by the detonation of gases in the tube. The coefficient of friction between the wood and detonation tube can conservatively be estimated as 0.6. For the 500 kg (1100 lb) tube weight per support, the tipping force is 2.94 kN (660 lb) giving a safety factor of 1.9 for tipping parallel to the tube.

Perpendicular to the axis of the tube, the maximum tipping moment will come from wind or blast loading. A maximum wind speed can be estimated to be no more than 129 km/hr (80 mph) which yields a force of 1.1 kN (250 lb). Blast loading can occur due to the other experiments conducted at the 9920 Firing Site. In particular, the detonation tube is located parallel to the FLAME facility. Blast loading has high pressures but the total impulse is low because of the short duration. The detonation tube has suffered no noticeable effects from several detonations in the FLAME facility.

Structurally the weakest member of the tube support is the 1.27 cm (0.5 in) diameter pin hinge between the 3.18 cm (1.25 in) threaded rod and the 10.2 cm (4 in) V structural channel. The safety factor due to the tube weight alone is 5. The pin hinge between the base of the threaded rod and the 15.3 cm (6 in) horizontal channel was sleeved to reduce the bending moment and has a higher safety factor. Sleeving the other pin hinge will improve its safety factor as well.

The pump and gas injection/evacuation manifold is supported from a platform from the 55 gallon drum nearest the foil end of the detonation tube. The platform is a 1.9 cm (0.75 in) thick plywood platform 0.76 m (2.5 ft) by 1.5 m (5 ft) mounted on a wooden 5 cm by 10 cm (2 by 4 in) frame supported by a welded metal frame attached to the 55 gallon drum. The steam bottle is separately supported by insulating bricks stacked on the ground.

The gas bottles are on a pallet tied to a rack in which the static pressure gage and gas temperature reference are mounted.

The pallet is weighted by sand bags to prevent it from tipping over.

A.2 ELECTRICAL

The electrical system can be divided into two parts. The first is general power to supply the pumps, manually controlled heaters and instrumentation. The second is the computer controlled heating system.

A.2.1 General Power

Power to supply the heated detonation tube originates from a 2.5 kV, 400 kW, 3 phase trunk line passing through the 9920 Firing Site. A transformer on the east side of building 9920 reduces the voltage to 220 V before the line passes through a fuse box with 100 amp fuses on each phase. A 100 amp, 220 V, 3 phase line is buried underground along the south side of 9920 to the termination building at the detonation tube. The line terminates in a breaker box and is split into one 220 V line to interior and exterior outlets, and into several 110 V single phase lines. The 110 V power supplies an exterior double duplex box and two interior double duplex boxes in the termination building. All three phases also go to the power relay box described in the next section to heat the detonation tube, and to three additional relay controlled exterior double duplex outlets.

Power is supplied to the circulation pump, a Digitec temperature reference and a variac controlling a secondary line heater by an extension cord from an external outlet on the termination building. The pump is rated at 372 W (1/2 HP). The secondary line heater is rated at 400 W. The temperature reference draws little power.

A.2.2 Detonation Tube Heating System

The detonation tube heating system is composed of 17 individually controlled sections of resistance heaters and control/measurement thermocouples mounted on the surface of the detonation tube, secondary piping and steam bottle. With the exception of the heater on the steam bottle, all heaters are resistance wires embedded in a silicon rubber strip and have a power density of 0.775 W/cm^2 (5 W/in^2) made by Watlow. Sixteen of these sections are under computer control. Each section contains several heaters of various sizes wired in both series and parallel to achieve the desired power level. The heaters are mounted by either 1.6 mm (1/16 in) diameter fiberglass cord or Dow Corning 736 RTV silicone rubber adhesive.

Each section also has three Chromel-Alumel, K-type, thermocouples to measure the anticipated hottest, coldest and an intermediate temperature in each section. The anticipated hottest

temperature is underneath a heater tape, the coldest temperature is midway between heater tapes, and the intermediate temperature is measured midway between the hot and cold thermocouples. The hot thermocouple is used to control the heating process, while the other two measure the nonuniformity in temperature.

The thermocouples are made from 0.25 mm (10 mil) kapton coated wire. The beads have been pressed to form a disk for better contact with the pipe. The thermocouples are mounted by using kapton tape. One layer is placed against the pipe to provide an electrical isolation barrier. The flattened bead is pressed against this layer of tape by a second layer of tape placed over the bead. The wires are held in place by Dow Corning 736 RTV (silicone adhesive) to prevent the bead from being accidentally pulled loose.

The sixteen individual computer-controlled heater sections can be divided into five different configurations. Each of these configurations, a manually controlled heater section, and the computer control system are described below.

Long pipe sections, sides and bottom - Of the sixteen individually controlled sections, eight are configured to heat the sides and bottom of the two long sections of pipe. Figure A-7 shows the electrical schematic of this configuration. Each section is 1.49 m (58.75 in) long, 1/4 of the length of one long section of pipe, and covers an arc of 255° around the underside of the pipe. The heaters are 5.1 cm wide by 1 m long (2 in by 40 in) and are wrapped circumferentially around the underside of the pipe with the 1 m (40 in) length covering the 255°. Axially, the heaters are spaced 24.9 cm (9.8 in) center to center or 19.8 cm (7.8 in) between tapes. The heater tapes are laced tightly to the pipe by fiberglass cord tied to eyelets in the silicone rubber at each end of the heater. Each heater is rated at 400 W @ 110 V and the overall power for the six heater tapes in each section is 600 W.

Three thermocouples are mounted in each section. One thermocouple is mounted underneath a heater tape. The second is mounted axially midway between the heaters, 9.9 cm (3.9 in) from the edge of a heater. The third is axially midway between the second thermocouple and the heater edge.

Long pipe section, top - Two individually controlled heater sections are used to heat the top of the two long sections of pipe, one heater section for each pipe section. The individual heater tapes are 15.2 cm wide by 1 m long (6 by 40 in) and six are laid end to end to form a 15.2 cm (6 in) wide row covering the top of each section of pipe. They are held in place by the fiberglass cords used to tie the ends of bottom and side heaters together. Each section is intended to heat the top 105° of circumference (41.9 cm or 16.5 in) not heated by the tapes which cover the underside of the pipes. Each heater tape is rated at

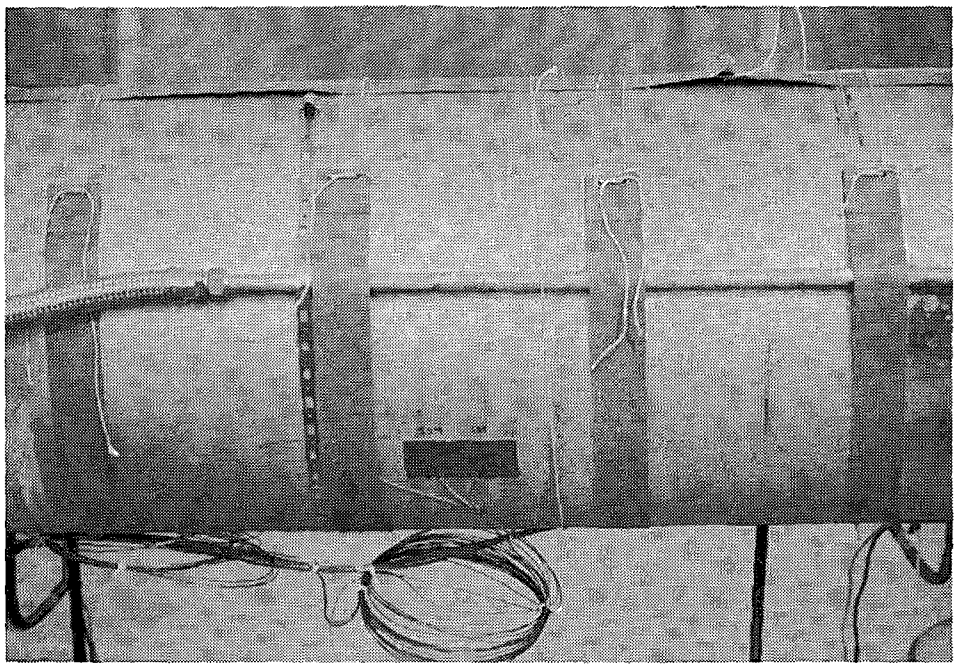

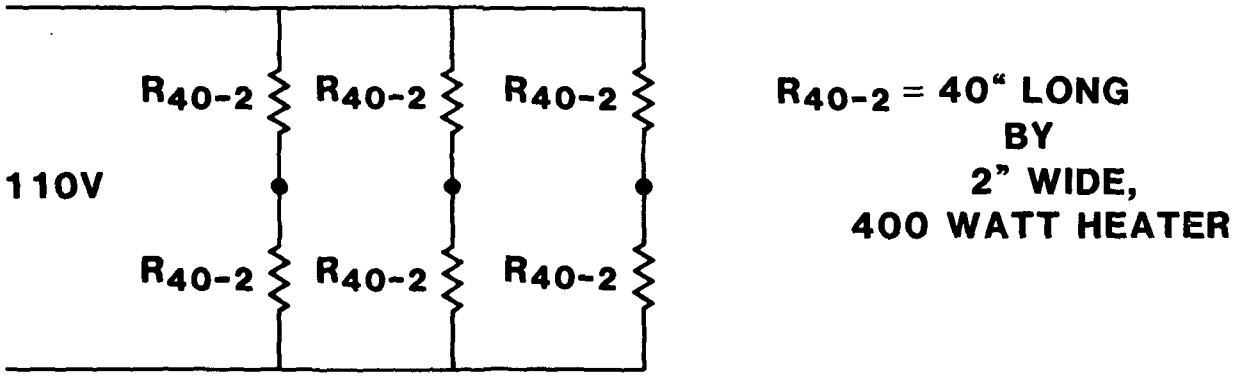

Figure A-7. Heater Section Schematic - Long Pipe Section, Sides and Bottom.

1200 W @ 110 V. Figure A-8 shows the wiring schematic. The overall power of the six heater tapes in each section is 800 W.

Three thermocouples are mounted in each section. One is mounted underneath the row of 15.2 cm (6 in) wide heater tapes covering the top of the pipes. The second is mounted half way between this row of heaters and a heater strip mounted circumferentially around the pipe to heat the sides and bottom of the long pipes (See previous section). The third thermocouple is spaced equidistant from the top row of heaters and two of the circumferentially spaced heaters, nominally 10 cm (4 in) from each.

Pipe to pipe flanges - Two individually controlled heater sections are used to heat the pipe to pipe flanges, one for each flange. The heaters used are 5.1 cm by 1 m (1 in by 40 in) and two are laid end to end and wrapped completely around the 2 m flange circumference for each 4.5 cm wide flange. They are held in place with RTV adhesive. Figure A-9 shows the wiring schematic. The four individual heaters are 400 W @ 110 V and the total power is 400 W per section.

Three thermocouples are mounted in each section. One is mounted underneath the row of heaters on the edge of the flange. The second thermocouple is mounted halfway down the side of the 4.5 cm wide section of the flange approximately 3.8 cm (1.5 in) from the heaters. It is mounted circumferentially at a nominal 17 cm (6.7 in) from the edge of the top heaters. The third thermocouple is mounted on the thick circumferential weld used to mount the flange. It is approximately 7.6 cm (3 in) from the flange heaters. For the flange between the long pipes, it is nominally 7.6 cm (3 in) from the top heaters. For the flange between the long and short pipe, it is nominally 13 cm (5 in) from the top heaters.

Short pipe section - One individually controlled heater section is used to heat the short initiator section of piping. Four 15.2 cm wide by 1 m long (6 in by 40 in) heater strips are mounted spirally along the 0.91 m length of the short section of pipe. The heaters are held in place with fiberglass cord and the maximum spacing between the heaters is 0.3 m (12 in) at the top center. Figure A-10 shows the wiring schematic. The heaters are 1200 W @ 110 V and the total power for the section is 1200 W.

Three thermocouples are mounted in the section. The thermocouples are mounted axially in a place where there is nominally 20 cm (8 in) between heaters. One thermocouple is mounted under a heater, the second is mounted 10.2 cm (4 in) from the heater edge, and the third is midway 5.1 cm (2 in) between the heater edge and the second thermocouple.

Endplates, flanges - Two individually controlled heater sections are used to heat the endplates and flanges, one for each

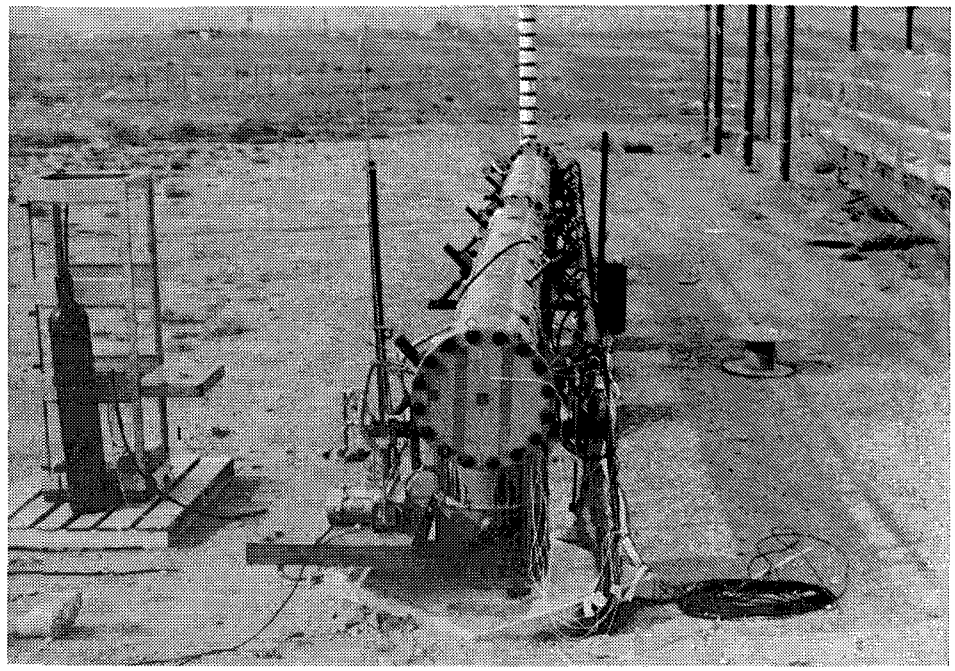

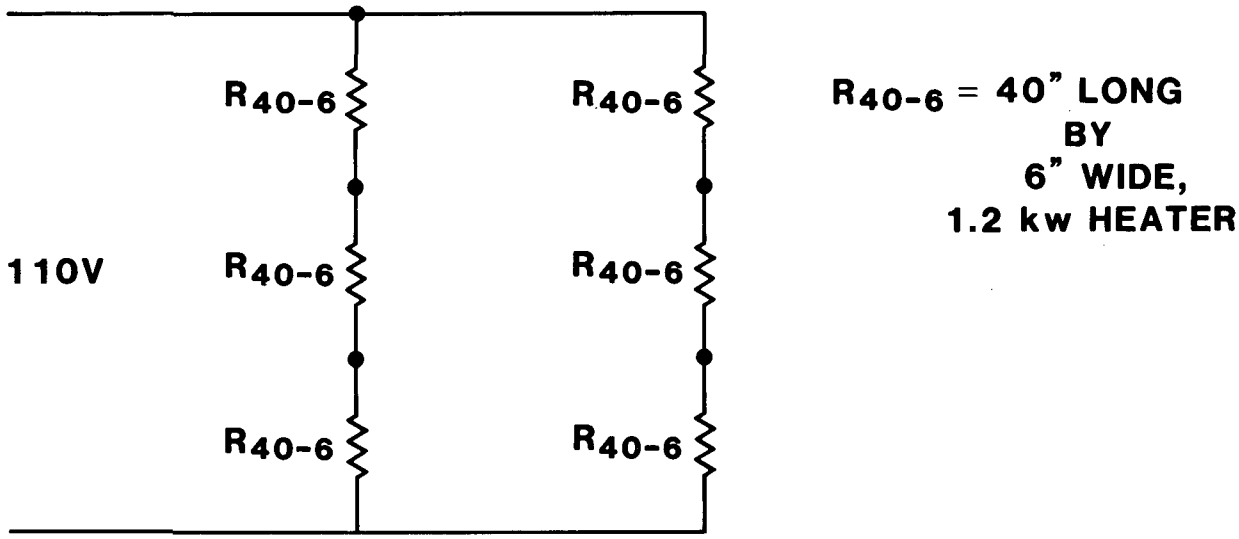

Figure A-8. Heater Section Schematic - Long Pipe Section, Top.

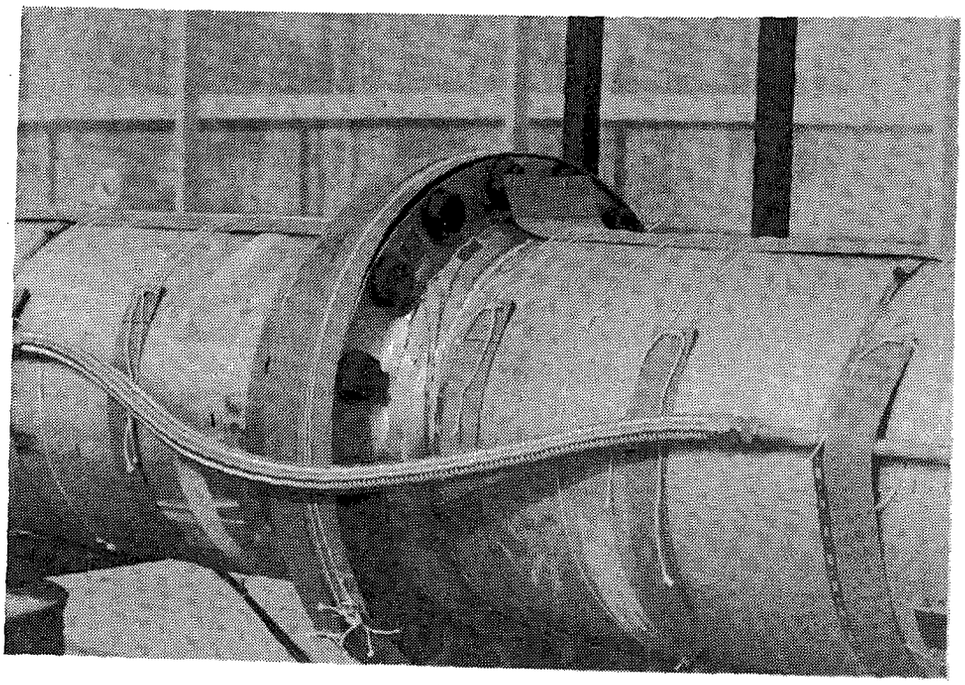

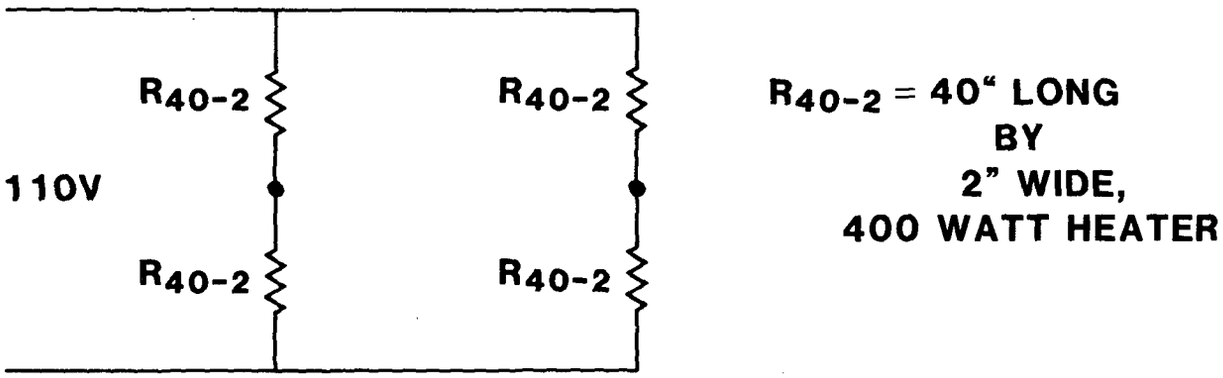

Figure A-9. Heater Section Schematic - Pipe to Pipe Flanges.

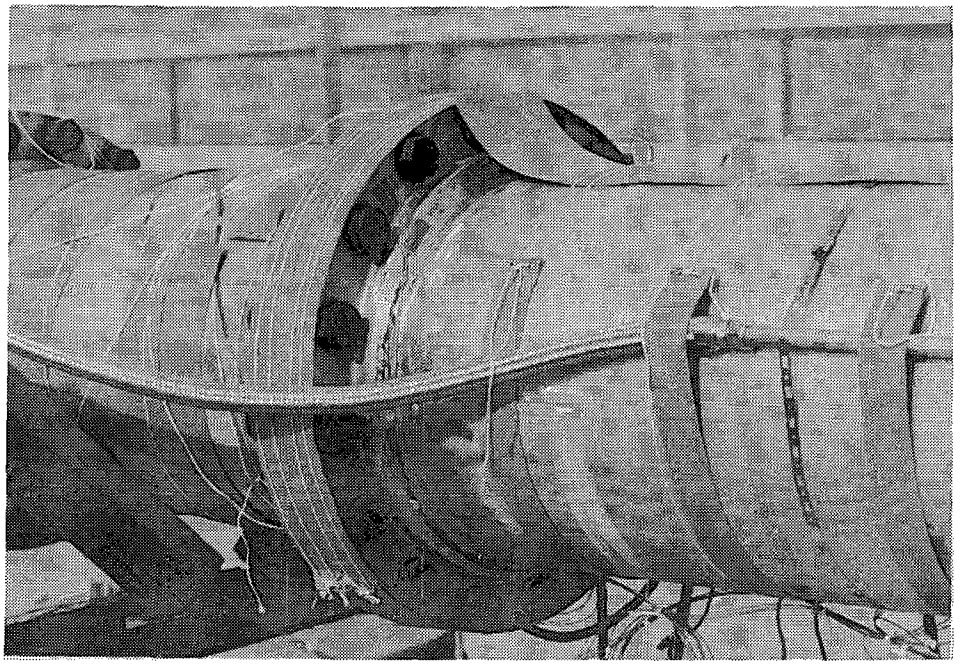

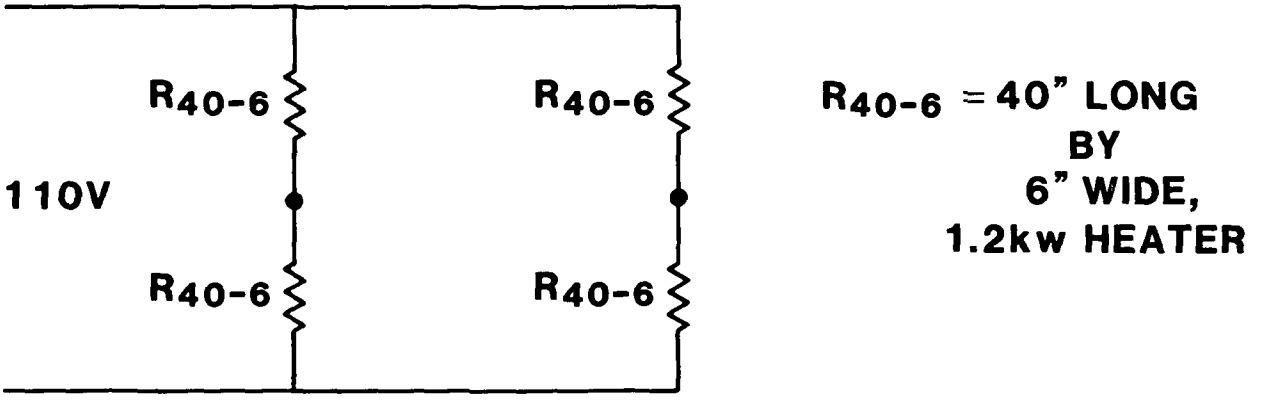

Figure A-10. Heater Section Schematic - Short Pipe.

end of the detonation tube. The initiation end plate has a single 5.1 cm wide by 1 m long (2 in by 40 in) heater mounted in the form of a V with RTV adhesive. The other endplate has two shorter heaters placed vertically 20.3 cm between centers. The heaters are 5.1 cm wide by 0.5 m long (2 in by 20 in). The flanges on each end are covered by four 2.54 cm wide by 1 m long (1 in by 40 in) heaters. The arrangement is the same as the pipe to pipe flanges, i.e., two heaters each laid end to end around the circumference of the pipe flange and endplate. All heaters are held in place with RTV adhesive. Figure A-11 shows the wiring schematic. The 1 m long heaters are 400 W @ 110 V and the 0.5 m heaters are 200 W @ 110 V. The total power for each section is 600 W.

Three thermocouples are mounted in each section. For the ignition endplate, the first thermocouple is mounted on the face of the endplate under the V heater. The second thermocouple is mounted on the face of the endplate near the base of the V shaped heater, 1.27 cm (0.5 in) from the bottom rim of the endplate The third thermocouple is mounted on the face of the endplate at the top of the V heater, 11.4 cm (4.5 in) equidistant from each leg of the V and the top rim of the endplate. For the other endplate, the first thermocouple is mounted on the face of the endplate in the middle of one of the short vertically mounted heaters. The second thermocouple is mounted on the face of the endplate 7.6 cm (3 in) from either heater strip and 1.9 cm (0.75 in) from the bottom rim of the end plate. The third thermocouple is mounted on the face of the endplate between one heater and the plate rim, 9.5 cm (3.25 in) from the rim and 8.3 cm (3.75 in) from the heater.

Steam Bottle - One individually controlled heater section is used to control the temperature of the steam bottle. One 500 W rod type heater embedded in lead and spirally wound around the bottom of the steam bottle is used to heat the vessel. The windings are tight leaving no space between them. The heater covers the base and approximately 2.5 cm (1 in) of the side of the vessel. The heater and vessel are completely immersed in approximately 23 kg (50 lb) of lead.

Three thermocouples are mounted in this section. Two thermocouples are in 3.2 mm (0.125 in) stainless steel sheaths with 0.5 mm (20 mil) ungrounded tips. The first is embedded in the lead so that the tip is touching the lead side surface of the edge of the heater coil. The second thermocouple is mounted through the plug on the top of the pipe leading to the steam bottle. The tip of the thermocouple is suspended in the piping approximately 2.5 cm (1 in) from the top of the vessel to measure gas temperature. The third thermocouple is made from 0.25 mm (10 mil) kapton coated wire and is mounted just below the upper surface of the lead bath surrounding the steam bottle approximately 2.5 cm (1 in) from the surface of the steam bottle.

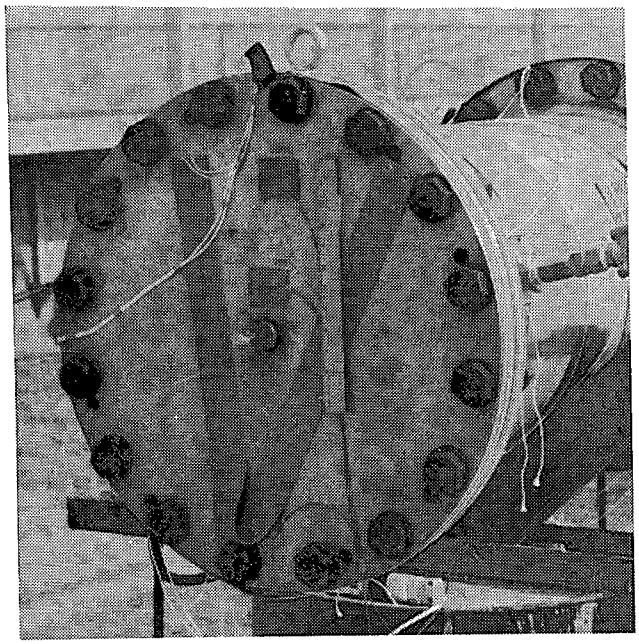

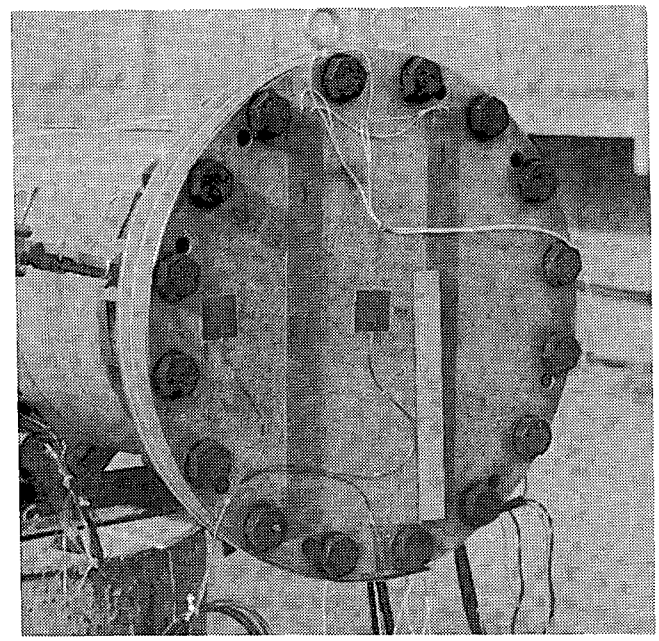

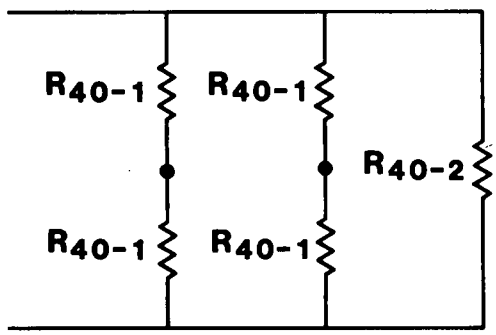

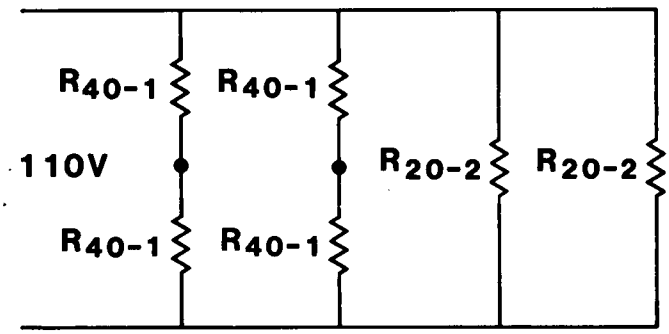

R_{40-2} = 40" LONG BY 2" WIDE
400 WATT HEATER

R_{20-2} = 20" LONG BY 2" WIDE
200 WATT HEATER

R_{40-1} = 40" LONG BY 1" WIDE
200 WATT HEATER

INITIATION END **TERMINATION END**

Figure A-11. Heater Section Schematic - Endplates, Flanges

Secondary piping - One heater is used to heat the secondary piping between the steam bottle and the vertical flexible line leading from the manifolding on the pump table to the piping along the surface of the tube (see structural discussion). This heater is not computer controlled and was added to prevent condensation from occurring in the secondary piping. The heater is a 5.1 cm wide by 1 m long (2 in by 40 in) 400 W @ 110 V strip heater that is wrapped around the 1.9 cm diameter secondary piping. The heater is controlled by a variac mounted on the pump table.

One thermocouple is used in this section. It is a K-type, 0.5 mm (20 mil) ungrounded tip in a 3.2 mm (0.125 in) stainless steel sheath. It is mounted in a plug in a tee with the tip centered in the lowest elevation of the 1.9 cm diameter secondary piping.

Heating System Control - The heating system is controlled by on-off set-point-logic relays which supply power to the heater strips. Control feedback is maintained by monitoring the temperature of the thermocouple underneath a heater strip in each section and comparing it to the desired set-point temperature. The thermal inertia of the system is high enough that on-off control is sufficiently stable to maintain the detonation tube temperature.

A schematic of the control circuit is shown in Figure A-12. The control decisions are made by a BASIC program running in the Digital LSI-11/23 computer. The program is designed to run in two modes, continuous operation and delayed start. In the continuous mode, the program acquires temperature data from a temperature monitor and compares these values to user assigned set-point temperatures. If the measured temperature is below the set point, the computer sends a signal for a relay to close. If the measured temperature is above the set point, then the computer sends a signal for the relay to open.

The relay unit is a Kinetic Systems Model 3074-A1A, 24 bit isolated output register with reed relays and is a module in a CAMAC crate. The communications interface between the module and the computer is a LeCroy 8901 GPIB Crate Controller communicating with a Tektronix CP4100/IEEE 488 board on the back-plane of the LSI-11/23. The 10 volt-amp reed relays are not sufficient to switch the power needed to heat the detonation tube. They are used to switch 28 Vdc power to close solid-state power relays which are used to switch power to the detonation tube heaters. The 28 Vdc power supply is a Harrison Labs Model 6266A located in the control building, 9920.

The relays which control the power to the detonation tube heaters are Teledyne Model 615-5 solid state, optically isolated, relays rated at 40 amps @ 110 V. The relays are normally open and can be closed with 3 to 32 Vdc input. These relays are

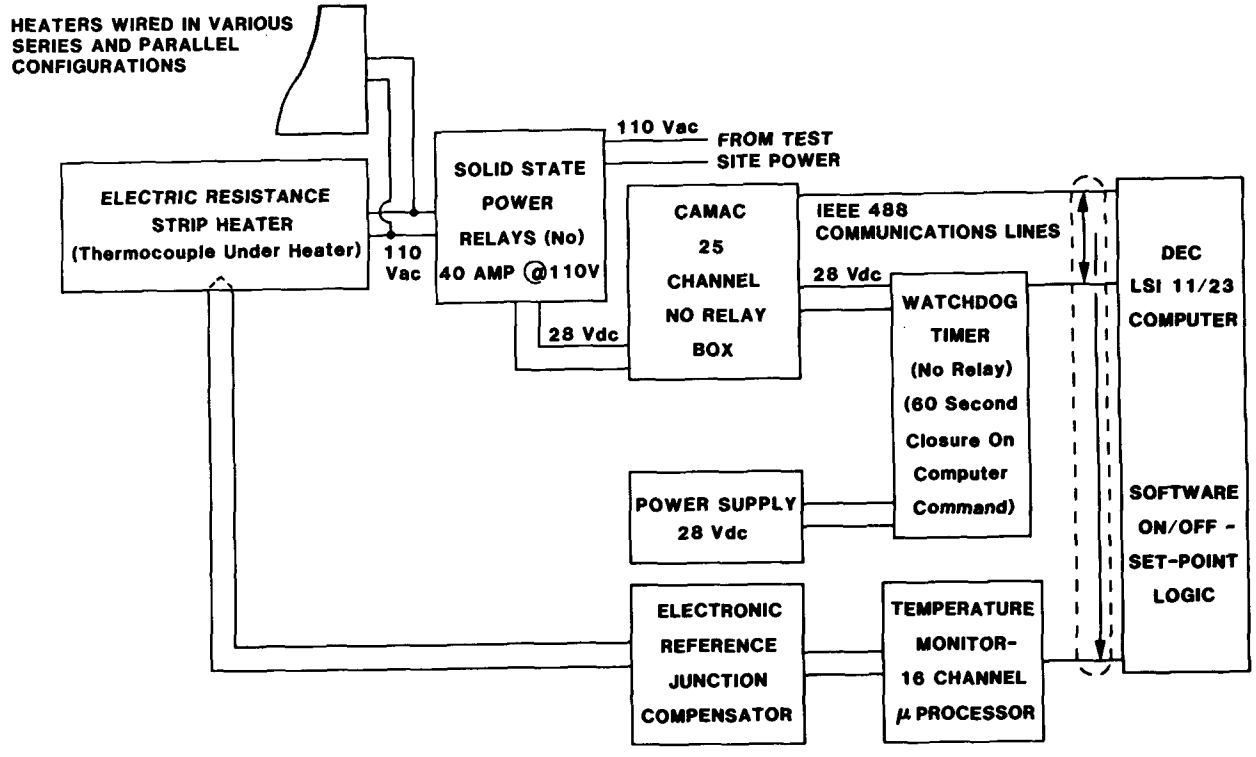

Figure A-12. Heater Control Circuit Schematic.

controlled by the 28 Vdc signal coming from the Kinetics relay module and are located in the termination building near the heated detonation tube. The cable between the Kinetics relays and the power relays is a 9-pair cable and is located in the south trench (see reference A-2 for layout of instrumentation cabling trenches).

Sixteen relays are used to control the sixteen individual sections of the detonation tube described in the last section. The source of the 110 V power to heat the detonation tube was described in the general power subsection. Sixteen cables run from the power relays in the termination building in an underground cable trench which surfaces at the base of the foil end tube support. The cables are #12 SO three wire cables with standard neoprene insulation. These cables are run along the the length of the detonation tube and are tied to a horizontal unistrut that runs the length of the tube to provide mechanical isolation to prevent a cable from being pulled loose. The ground wires on all sixteen leads are tied to the horizontal unistrut which is in turn electrically connected to the detonation tube to provide a grounding path in case of an electrical short against the tube wall.

The insulation of these cables is not sufficient to take the temperature of the detonation tube. These cables are spliced to #16 teflon-coated wire just outside of the insulation on the tube. This teflon-coated wire is spliced to the pig tail leads on the heater strips. The splices used are a plastic-coated crimp-type splice with a temperature rating of 105°C. These splices have been coated with Dow Corning 736 RTV for mechanical isolation and increased temperature resistance.

The feedback mechanism to control the heaters is the comparison of the heater temperature as measured by the thermocouple under a heater strip in a given section to the user supplied setpoint temperature in the computer program. The thermocouples and mounting were described in the heating system section. The thermocouple wiring runs along the base of the detonation tube between the tube wall and the surrounding insulation. The insulation of the thermocouple wire is rated at 230°C. The wiring terminates at a Nema 4 type enclosure mounted midway down the length of the detonation tube on vertical unistruts.

Two twenty-four pair K-type thermocouple extension cables connect to the 16 control and 32 measurement thermocouple wires. These 24 pair cables terminate in a patch panel in the termination building. From the termination building two 24 pair K-type run underground to the control room in building 9920 (See Reference A-2 for details). One of the two 24 pair cables carrying the 16 control temperatures is split off and terminated in a temperature monitored Kinetics Model 1991 isothermal panel. Copper-copper wire is used to connect this reference junction to a Kinetics Systems 16 Channel Temperature Monitor Model 3525-A1K

mounted in a CAMAC crate. This module converts the voltage data from the thermocouples to temperature.

The LSI-11 computer interrogates this module to compare the measured temperature and the set point temperature for each section. Based on the comparison, the computer commands the Kinetics relay module to open or close the power relays which control the power to the detonation tube heaters. This cycle occurs approximately once every 20 seconds. For convenience, the program displays the measured and set-point temperatures and the time each cycle. The time is obtained from a Borer Model 1413 Clock which is mounted in the CAMAC crate.

The second mode in which the computer program operates is the delayed start mode. In this mode the user enters a time at which the heating process is to begin. The computer compares the time from the Borer clock to the set point. When the set-point time is reached the program switches to back to the first mode.

To provide a fail safe condition, a Standard Engineering Corp. WDT 1000 "Watch Dog Timer" is used to monitor the heating system. The watch dog timer controls the 28 V dc line between the power supply and the Kinetics reed relay module and is mounted in a CAMAC crate. The watch dog timer is a timer-controlled relay device which is normally open, preventing power to be switched by the Kinetics module to the control lines leading to the power relays. The watch dog relay will close only if it is communicated with by the computer every 64 seconds.

In normal operation the computer communicates with the watch dog timer every cycle and the relay remains closed allowing the detonation tube to heat. If a power failure occurs, the computer program will not restart and the watch dog timer will open the circuit to the power relays in 64 seconds. The thermal inertia in the detonation tube will prevent failure due to uncontrolled heating for this short period of time. The watch dog timer is connected to two alarm buzzers which are activated if the watch dog timer relay becomes open. The buzzers are located in buildings 9920 and 9926.

A.3 THERMAL ASPECTS

Several options were considered in the design of the heating system for the detonation tube. One design was a shell within a shell using hot water under pressure in the annulus between the coaxial tubes. This design was rejected because of the difficulty in instrumenting the tube with pressure transducers through the coaxial tube. Another design was to heat the tube by induction. This design was rejected because the impedance of the thick wall detonation tube is to low. The internal impedance of the generator would have to have been very low requiring massive coils.

The heating system chosen is based on using strip heaters under insulation. Analysis indicated that the temperature non-uniformity present in this type of heating would be acceptable if the insulation was sufficient. The heating system was described in the last section. A description of the insulation, temperature monitoring thermocouples, and thermal limits are discussed in this section. The analysis which led to the design is contained in Appendix F.

A.3.1 Insulation

The insulation used to cover the detonation tube and secondary piping is Certainteed Snap-Wrap which has a thermal conductivity of 0.048 W/m°K (R - value of 3 (hr ft^2 °F)/(BTU in)). The insulation was purchased in two thicknesses, 5.1 cm and 3.8 cm (2 in and 1.5 in) in 91.4 cm (36 in) wide rolls for use on the detonation tube. Pre-formed 2.5 cm (1 in) thick cylindrical sections of insulation are used on the secondary piping.

Two layers of insulation is used to wrap around the detonation tube pipes, one layer of 5.1 cm (2 in) and one layer of 3.8 cm (1.5 in) thick insulation. The layers are offset axially so that the seams do not overlap on the long pipes where 6 sections are used which cover 5.5 m of the 6.1 m length. With the two layers of insulation, the outer diameter of the insulation is the same as the pipe flanges. Two layers of insulation are placed over the flanges between the pipes so that the flange insulation overlaps the insulation over the pipe body.

The endplates are covered by large endcaps. The endcaps are made to slip over the flanges and are intended to be easily removable, as they must be removed after each test. The endcaps are fabricated out of a 20 gage galvanized shell, 94 cm (37 in) in outer diameter by 45.7 cm (18 in) deep lined with 15.2 cm (6 in) of insulation in the base and sides. It was found with use that the endcaps are heavy enough to "sag" and the gas seal gained by having the endcap slide over the insulation on the pipe body is compromised. Ambient, cold air could circulate around the gap in insulation and cool the endplate. This effect was enhanced by the need to cut a hole in the insulation in the endcap to slide over the lifting lug on the endplate.

Several attempts were made to eliminate this leakage problem; none were entirely satisfactory. Better results were obtained by replacing the endcaps with loose fiberglass insulation placed over the endplates and tightly sealed with plastic. Future tests will have a different endcap design.

A.3.2 Temperature Monitoring Thermocouples

Three thermocouples are located in each temperature controlled heating section of the HDT. One thermocouple is used to control the heaters and the other two measure the nonuniformity

in temperature. The thermocouples, mounting and cabling to the control room in building 9920 are described in the Electrical section, A.2.2.

The reference junction for the 32 measurement thermocouples is a Sandia Laboratory design constant temperature block. The temperature of the block is measured and the voltage measurements are compensated for the reference junction temperature. The temperatures are recorded on fan folded paper tape from a Vidar AutoData Eight datalogger.

A.3.3 Thermal Limits

Table A-1 lists the temperature limits of various components of the heated detonation tube.

Table A-1

Temperature Limits of Detonation Tube Components

Component	Temperature (°C)
304 Stainless Steel	650*
O-rings (#2-468E-692-70)	260
Dow Corning Compound 4 O-ring grease	204
ASTM 325 hardened bolts	400*
Swagelock Swack pipe joint compound	180
Gordon Thermocouple Feed-Thru's (TFE Gland)	230
Dow Corning 736 RTV (RED)	260
Delrin transducer fittings	82**
Nylon transducer fittings	82-93***
Transducer O-rings (#2-019E692-75)	260
Pressure Transducer (electronics)	135
High purity Goop O-ring grease	204
Silicone Rubber Heaters	260
Fiberglass Heater Cord	250
Teflon Heater Wire Insulation	230
EL506 Explosive (DTA)	93
RP-2 Initiator	121
Brass Secondary pipe fittings	>200*
Circulation Pump	<230****
Insulation	230
Burst Disk	*****
Valves (Teflon packing)	230

* 15% loss of strength
** Melting point is 175°C
*** Melting point is 250°C
**** TFE seal temperature - motor will probably overheat before this temperature
***** Continuous loss of strength with temperature

A.4 EXPLOSIVE INITIATOR CIRCUIT

The most convenient method of initiating a gaseous detonation is to use high explosive. The disadvantage of this method is that the gaseous detonation will be overdriven for some distance due to the very high pressures associated with high explosives. To overcome this disadvantage, we used a thin (1 mm thick) sheet of DuPont Detasheet high explosive cut into a 25.4 cm (10 in) diameter spoked-wheel shape to both minimize the amount of high explosive and to effect an almost planar initiation. The explosive is initiated by a detonator at the hub of the spoked wheel as shown in Figure A-13, where the detonation proceeds radially outward at about 7.2mm/μsec. The gaseous detonation proceeds at about 2mm/μsec so the high explosive initiation is quasi-planar.

To mount the explosive perpendicular to the detonation tube axis, the sheet explosive is attached to a thin mylar sheet which is suspended from lugs at four points using nylon braid. The lugs are welded inside a 35.6 cm (14 in) diameter stainless steel pipe which is 40.6 cm (16 in) long. This inner pipe has four spacers which provide coaxial placement of the pipe within the detonation tube. The purpose of this inner pipe is to prevent detonator shrapnel from impinging on the inner wall of the detonation tube and to prevent very high pressure loading of the detonation tube. The explosive charge is located approximately 30 cm (12 in) forward of the endplate to minimize shock loading on the endplate.

The nominal explosive weight is 40 grams for all gaseous mixtures except the very insensitive mixtures. The less sensitive mixtures require a high explosive charge which more fully covers the 25.4 cm (10 in) diameter. The explosive charge weight is nominally 80 grams for these mixtures.

The detonator used to initiate the high explosive is a Reynolds Industries exploding bridgewire (EBW) type RP-2. Transition to the DuPont EL506C1 Detasheet explosive is by means of a few grams of plastic explosive type Composition C-4. This transition charge is held in place with a fabric tape which is stapled to the sheet explosive using a specially modified paper stapler. Electric wires to the detonator are teflon insulated twisted pair. These wires are crimp connected to wires passing through an insulated feed-thru in the endplate. The connection is covered with teflon tubing.

High voltage, low impedance type "C" coaxial cable is connected to the feed-thru connector outside the insulated endplate. To initiate the high explosive detonation, the EBW is subject to the discharge of a 3 μfd capacitor charged to 4-5 kilovolts which is located in the control room in Bldg. 9920.

Figure A-13. High Explosive Initiator.

A.5 INSTRUMENTATION

Four types of instrumentation are used on the detonation tube. The initial thermodynamic state is established by static pressure and temperature measurements. Detonation properties are obtained by smoke foil measurement of detonation cell width. Pressure measurements are used to obtain time-of-arrival to establish the detonation velocity. There are 14 access ports in the detonation tube for instrumentation. Table A-2 lists the axial location of these ports with respect to the initiation endplate. Circumferentially, the ports are all located 64° from the top of the detonation tube.

Table A-2

Axial Location of Instrumentation Ports Relative to the Initiation Endplate Inside Face

Port #	Distance (m)	Port #	Distance (m)
1	1.039	8	7.201
2	1.689	9	7.810
3	2.603	10	8.725
4	3.823	11	9.944
5	4.737	12	10.853
6	5.956	13	12.078
7	6.871	14	12.992

A.5.1 Static Pressure Instrumentation

The static pressure measurement is taken from port 12. A high pressure 15.2 MPa (2200 psi) black rubber hose with a plug valve connects this port to a pressure gage or manifold on an instrumentation rack. Tables A-3, 4 list the static pressure gages for each test. For tests HT-11 to 30 a Wallace & Tiernan, Model 61A-10-0800, Serial #SS-14109, 0 - 800 mm Hg, absolute pressure gage was used to measure the pressure. This gage has a 1 mm Hg resolution and an accuracy of 0.8 mm Hg. For tests 31,32 and 33, this gage was used to establish ambient pressure and a 0-100 psig, Heise pressure gage, Serial #47971, was used for gage pressure. The Heise gage has a 0.1 psig resolution and an accuracy of 0.1 psig. From test 34 - 96, a Wallace & Tiernan, Model 61A-1A-0050, Serial #TT11757, 0 - 50 psia, absolute pressure gage was used to measure the pressure. This gage has a resolution of 0.05 psia and an accuracy of 0.1 psia for measurements above 4 psia. Prior to initiation of the detonation, port 12 is isolated from the pressure gage by the plug valve to prevent over-ranging of the gages.

A.5.2 Temperature Instrumentation

For tests HT-11 to 19 and 73, the gas temperature was taken to be the average of the tube temperature as measured by the thermocouples described in the previous section. Tables A-3, 4 list the type and location of the gas temperature measurement for each test. From test 20 to 96 (excluding 73), the temperature was measured by a thermocouple inserted in port 6. The thermocouple is a Chromel-Alumel, K-type, in a 3.2 mm (0.125 in) stainless steel sheath made with 0.51 mm (20 mil) wire. The thermocouple is inserted through a Gorden Th-2571-T-125 feedthrough that is mounted in a "blank" transducer fitting (see dynamic pressure instrumentation for fitting description).

For tests 20 to 72 the thermocouple tip was inserted approximately 3.2 mm (0.125 in) into the gas mixture. For tests 74 to 96, the thermocouple tip was inserted approximately 2.5 cm (1 in) into the gas mixture. When the thermocouple was removed after test 96 it was noted that the detonations had bent the thermocouple to a 45° angle.

For test 20 to 81 excluding 79, the temperature reference junction was a hand held Fluke DMM Model 8024B, Serial #3275848, with a temperature readout for K-type thermocouples. The resolution of the unit is 1°C with an accuracy of 3°C. For tests 79, 81 to 96, the reference junction was a Digitec Model 2831, Serial #53930983, self-calibrating thermocouple reference junction with digital temperature readout. The resolution of the Digitec is 0.1°C with an accuracy of 0.3°C.

A.5.3 Smoked Foil Instrumentation

During the first ten shakedown tests of the HDT (HT-1 to 10), the smoke foil size and shape were determined. Early foils were 1.2 m (4 ft) wide and 1.2 m (4 ft) long made of ~1 mm aluminum sheet. The sheet was machine rolled into a 43.2 cm (17 in) diameter cylinder for insertion into the HDT. With this thickness of sheet, the post-test foils were permanently set by the detonation into the cylindrical shape and were hard to handle.

For tests HT-11 through HT-96, the smoked foils were made of aluminum sheets 1.2 m (4 ft) wide by 3.7 m (12 ft) long and ranged between 0.4 mm (0.016 in) and 0.64 mm (0.025 in) in thickness. The longer length was found to give a better record and the thinner material could be flattened out after a test for storage. In addition, the thinner material did not have to be machine rolled into a cylindrical shape. However, the sheets had to be reinforced with stiffening rings at each end of the sheet to hold it against the HDT wall to keep it from crumpling. The best overall thickness of aluminum sheet was found to be 0.51 mm (0.02 in).

TABLE A-3

TYPE AND LOCATION OF
INITIAL THERMODYNAMIC STATE MEASUREMENTS

Test #	Series #	TEMPERATURE Point or Average	TEMPERATURE Depth Position	TEMPERATURE Ice Point Reference	Static Pressure	Humidity Measurement
11*	1,6	A**	-	-	1	1
12	1	A	-	-	1	1
13	1	A	-	-	1	1
14	1	A	-	-	1	1
15	1	A	-	-	1	1
16	2	A	-	-	1	1
17	2	A	-	-	1	1
18	2	A	-	-	1	1
19	2	A	-	-	1	1
20	2	P	1	1	1	1
21	2	P	1	1	1	1
22	2	P	1	1	1	1
23	2	P	1	1	1	1
24	2	P	1	1	1	1
25	2	P	1	1	1	1

* Tests 1-10 are system development.

**Refer to TABLE A-4 for instrumentation.

TABLE A-3 (Cont'd)
TYPE AND LOCATION OF
INITIAL THERMODYNAMIC STATE MEASUREMENTS

Test #	Series #	TEMPERATURE Point or Average	Depth Position	Ice Point Reference	Static Pressure	Humidity Measurement
26	U	P	1	1	1	1
27	U	P	1	1	1	1
28	U	P	1	1	1	1
29	U	P	1	1	1	1
30	U	P	1	1	1	1
31	U	P	1	1	1&2	1
32	U	P	1	1	1&2	1
33	U	P	1	1	1&2	1
34	U	P	1	1	3	1
35	U	P	1	1	3	1
36	U	P	1	1	3	1
37	U	P	1	1	3	1
38	U	P	1	1	3	1
39	3	P	1	1	3	1
40	U	P	1	1	3	1
41	3	P	1	1	3	1
42	3	P	1	1	3	1

TABLE A-3 (Cont'd)
TYPE AND LOCATION OF
INITIAL THERMODYNAMIC STATE MEASUREMENTS

Test #	Series #	Point or Average	TEMPERATURE Depth Position	Ice Point Reference	Static Pressure	Humidity Measurement
43	U	P	1	1	3	1
44	6	P	1	1	3	1
45	6	P	1	1	3	1
46	5	P	1	1	3	1
47	5	P	1	1	3	1
48	5	P	1	1	3	1
49	5	P	1	1	3	2
50	3	P	1	1	3	2
51	3	P	1	1	3	2
52	3	P	1	1	3	2
53	3	P	1	1	3	2
54	3	P	1	1	3	2
55	3	P	1	1	3	2
56	3	P	1	1	3	2
57	3	P	1	1	3	2
58	3	P	1	1	3	2
59	3	P	1	1	3	2
60	3	P	1	1	3	2

TABLE A-3 (Cont'd)
TYPE AND LOCATION OF
INITIAL THERMODYNAMIC STATE MEASUREMENTS

Test #	Series #	TEMPERATURE Point or Average	Depth Position	Ice Point Reference	Static Pressure	Humidity Measurement
61	3	P	1	1	3	2
62	3	P	1	1	3	2
63	1	P	1	1	3	2
64	1	P	1	1	3	2
65	1	P	1	1	3	2
66	1	P	1	1	3	2
67	1	P	1	1	3	2
68	1	P	1	1	3	2
69	1	P	1	1	3	2
70	1	P	1	1	3	2
71	1	P	1	1	3	2
72	1	P	1	1	3	2
73	3	A	-	-	3	2
74	3	P	2	1	3	2
75	3	P	2	1	3	2
76	3	P	2	1	3	2
77	3	P	2	1	3	2

TABLE A-3 (Cont'd)
TYPE AND LOCATION OF
INITIAL THERMODYNAMIC STATE MEASUREMENTS

Test #	Series #	TEMPERATURE Point or Average	Depth Position	Ice Point Reference	Static Pressure	Humidity Measurement
78	3	P	2	1	3	2
79	3	P	2	2	3	2
80	3	P	2	1	3	2
81	3	P	2	2	3	2
82	3	P	2	2	3	2
83	3	P	2	2	3	2
84	3	P	2	2	3	2
85	3	P	2	2	3	2
86	3	P	2	2	3	2
87	3	P	2	2	3	2
88	3	P	2	2	3	2
89	3	P	2	2	3	2
90	3	P	2	2	3	2
91	4	P	2	2	3	2
92	4	P	2	2	3	2
93	4	P	2	2	3	2
94	4	P	2	2	3	2
95	4	P	2	2	3	2
96	4	P	2	2	3	2

Table A-4

Temperature, Pressure and Humidity Instrumentation

Temperature:

Average: Instruments: Thermocouples, Type K, used to control heater tapes overall uncertainty estimate 3°C.

Point: Instrument: Thermocouple, Type K, 1/8" diameter ss sheath, magnesium oxide insulated, ungrounded tip.

Location: Port 6

Depth: Position 1 - tip is 1/8" from the wall ± 1/16"

Position 2 - tip is 1" from the wall ± 1/4"

Reference/Recorder:

1 Fluke Multimeter 8024B
Serial #3275848
Accuracy: 3°C)mfg. calibration
Resolution: 1°C)" "

2 Digitec Model 2831
Accuracy: 0.3°C)mfg. calibration
Resolution: 0.1°C)" "

Pressure-Static:

Instrument:

1 Absolute Pressure Gage, 0-800 mm Hg
Wallace & Tiernan, Model 61A-1D-0800
Serial #SS-14109
Resolution: 1 mm Hg division
Accuracy: 0.8mm Hg
Sandia cal 7/13/83
exp 1/31/85

2 Pressure Gage, 0-100 psig
Heise, Serial #47971
Resolution: 0.1 psig
Accuracy: 0.1 psig
Sandia field cal 2/18/82

Table A-4 (cont'd.)

Pressure-Static: (cont'd.)

Instrument:	3	Absolute Pressure Gage, 0-50 psia Wallace & Tiernan, Model 61A-1A-0050 Serial #TT11757 Resolution: 0.05 psia divisions Accuracy: 0.1 limited range (0.4 full range) Sandia cal 6/21/84 exp 7/30/85
Location:	Port 12	

Humidity

1.	Ambient Air:	Humidity measured with Environmental Systems, Inc., Model 22012 Uncertainty 3%
2.	Dry Air:	Dew Point -75 F No humidity measurement taken

Several types of stiffening rings were used. Early rings were made of 3.2 mm (1/8 in) carbon steel and were approximately 2.5 cm (1 in) wide. Later rings were made of two layers of 0.25 mm (0.01 in) spring steel welded together. The ring at the initiation end of the foil widened to approximately 15 cm (6 in). The aluminum sheet was attached to the ring by rolling the sheet over the ring and riveting the foil to the ring with low-profile-head rivets.

Because the smoked foil is only 121.9 cm wide and the circumference of the HDT is 135.7 cm wide, the foil does not form a complete cylinder. A 13.8 cm slot is formed along the length of the cylinder. When the smoked foil is inserted into the HDT, the slot is placed along the axis of the pressure transducers so there is no interference. However, a 3.81 cm (1.5 in) hole is cut in the sheet 16.5 cm (6.5 in) from the end of the foil in contact with the endplate to allow gas to enter the recirculation line. The hole is cut 39.4 cm (15.5 in) from the edge of the foil to have the proper orientation with the recirculation line and have the slot over the pressure transducer ports.

During the test program, the method of smoking the foils has been modified and improved. Initially, the foils were rolled into a cylinder and were stood on end where a MAPP (stabilized Methylacetylene-Propadiene) gas torch was used to smoke them. Attempts to improve the smoking technique led to the use of furnace oil. The furnace oil was placed in an approximately 1/3 m long by 2 cm wide and deep trough which held a ceramic wick. The foil was laid flat and supported on a wooden rack in a semi-enclosed area. For the heated tests (Test Series #3,4,6, and 7), particularly with steam, it was found that the furnace oil alone would leave "spots" on the foil as if the oil had evaporated and left a residue. This problem was eliminated by first coating the surface of the foil with a mixture of 1/3 Dow Corning Sylgard 186 and 2/3 Xylene and then buffing the surface dry. A side effect of this procedure was a reduction of the contrast of the detonation tracks on the smoked foil. Therefore, for steam dilution tests (Test Series #4), the furnace oil with coating was used. In all other tests, the foil was smoked with a MAPP gas torch.

It was found in both cases that the semi-enclosed area did not provide enough protection from the winds in Albuquerque and a permanent enclosure was built, the "smoke house." In the smoke house, the foil is clamped flat to an aluminum frame and suspended form the ceiling. In this position, either furnace oil or MAPP can be used to smoke the foil.

A.5.4 Dynamic Pressure Instrumentation

Dynamic pressure is measured by transducers from two manufacturers, Kistler and PCB. Both gages are piezoelectric fast

response gages with identical mounting requirements. Tables A-5, 6 list the type, number and digitizing frequency for the gages used in each test. Five to six Kistler gages were used in each test from HT-11 to 96. One to three PCB transducers were used from test 31 through 34 and 42 through 96.

The Kistler transducers are Model 211B3 with a pressure range of 0 - 3.4 MPa (0 - 500 psi). The rise time is 2 μs with a resonant frequency of 250 kHz. The transducers have electronic charge converters in the back of the transducer. The transducers are powered by battery operated Kistler Model 5112, 2 mA power supply couplers. The power supply has a decoupling capacitor so the D.C. signal is not transmitted to the data recording equipment.

Two types of PCB transducers are used. One type of PCB transducer is Model 113A24 with a pressure range of 0 - 6.8 MPa (0 - 1000 psi). The second type is Model 113A26 with a 5.1 cm (2 in) extender between the transducer and the electronic charge converter. This distance places the temperature limited electronics outside of the insulation. The Model 113A26 has a range of 0 - 3.4 MPa (0 - 500 psi). The rise time for both transducers is 1μs with a resonant frequency of 450 kHz. The transducers are powered by PCB Model 480B power supply couplers which are similar to the Kistler coupler and have been interchanged.

The transducers are mounted in specially designed fittings. Figure A-2 shows a cross-section of a pressure transducer penetration in the detonation tube piping. Figure A-14 shows the fitting designed to mount pressure transducers in the transducer penetration. Originally, brass fittings were made but the vibration of the transducer mount caused excessive noise on the pressure data. Delrin and nylon fittings were used to isolate the transducer from the detonation tube vibration. Nylon has a higher temperature softening point but the surface subjected to detonation temperatures tended to char. The nylon is also stronger than delrin. The delrin mounts tended to fail at the neck of the mount near the O-ring groove. The O-rings are Parker #2-019E692-75 ethylene-propylene.

To plug the instrumentation ports not being used, brass "blanks" were made. These blanks are the same as the fittings in Figure A-14 except they are not drilled and tapped for the pressure transducers. These fittings are used to accommodate other instrumentation such as the thermocouple to measure gas temperature.

A.5.5 Humidity

For test HT-11 through HT-48, ambient Albuquerque air was used. An Environmental Systems Inc. Series #22010 Psychrometer was used to measure the humidity.

TABLE A-5
TYPE, NUMBER AND DIGITIZING FREQUENCY
FOR DYNAMIC PRESSURE MEASUREMENT

Test #	Series #	Type of Gage	# of Gages per Type	RECORDS 7612 #	7612 Resolution (μs)	CAMAC #	CAMAC Resolution (μs)
11*	1,6	1**	6	5	10	5	25
12	1	1	6	5	10	5	25
13	1	1	6	6	10	6	25
14	1	1	6	6	10	5	25
15	1	1	6	6	10	6	25
16	2	1	6	6	10	6	25
17	2	1	6	6	10	6	25
18	2	1	6	6	10	6	25
19	2	1	6	5	10	5	25
20	2	1	6	6	10	6	25
21	2	1	6	6	10	6	25
22	2	1	6	6	10	6	25
23	2	1	6	6	10	6	25
24	2	1	6	6	10	6	25
25	2	1	6	6	10	5	25
26	U	1	6	6	10	6	25

* Tests 1-10 are system development.

**Refer to TABLE A3 for Instrumentation.

TABLE A-5 (Cont'd)
TYPE, NUMBER AND DIGITIZING FREQUENCY
FOR DYNAMIC PRESSURE MEASUREMENT

Test #	Series #	Type of Gage	RECORDS # of Gages per Type	7612 #	7612 Resolution (μs)	CAMAC #	CAMAC Resolution (μs)
27	U	1	6	0	10	0	25
28	U	1	6	6	10	6	25
29	U	1	6	5	10	4	25
30	U	1	6	0	10	0	25
31	U	1,2	5,1	5	10	5	25
32	U	1,2	5,1	5	10	6	25
33	U	1,2	5,1	5	10	5	25
34	U	1,2	5,1	6	10	6	25
35	U	1	6	6	10	6	25
36	U	1	6	6	10	6	25
37	U	1	6	6	10	0	25
38	U	1	6	6	10	6	25
39	3	1	6	6	10	6	25
40	U	1	6	6	10	6	25
41	3	1	6	5	10	5	25
42	3	1,2	5,1	5	10	5	25
43	U	1,2	5,1	6	10	6	25
44	6	1,2	5,1	6	10	6	25

TABLE A-5 (Cont'd)
TYPE, NUMBER AND DIGITIZING FREQUENCY
FOR DYNAMIC PRESSURE MEASUREMENT

Test #	Series #	Type of Gage	# of Gages per Type	RECORDS 7612 #	7612 Resolution (μs)	CAMAC #	CAMAC Resolution (μs)
45	6	1,2	5,1	6	10	6	25
46	5	1,2	5,1	4	10	4	25
47	5	1,2	5,1	6	10	6	25
48	5	1,2	5,1	5	10	5	25
49	5	1,2	5,1	6	10	6	25
50	3	1,2	5,1	6	10	6	25
51	3	1,2	5,1	5	1	5	25
52	3	1,2	5,1	6	1	6	25
53	3	1,2	5,1	5	1	5	25
54	3	1,2	5,1	5	1	5	25
55	3	1,2	5,1	5	1	5	25
56	3	1,2	5,1	6	1	6	25
57	3	1,2	5,1	6	1	6	25
58	3	1,2	5,1	6	1	6	25
59	3	1,2	5,1	6	1	6	25
60	3	1,2	5,1	6	1	6	25
61	3	1,2	5,1	6	1	6	25
62	3	1,2	5,1	6	1	6	25
63	1	1,2	5,1	6	1	6	25

TABLE A-5 (Cont'd)
TYPE, NUMBER AND DIGITIZING FREQUENCY
FOR DYNAMIC PRESSURE MEASUREMENT

Test #	Series #	Type of Gage	# of Gages per Type	RECORDS 7612 #	7612 Resolution (μs)	CAMAC #	CAMAC Resolution (μs)
64	1	1,2	5,1	6	1	6	25
65	1	1,2	5,1	6	1	6	25
66	1	1,2	5,1	5	1	5	25
67	1	1,2	5,1	6	1	6	25
68	1	1,2	5,1	6	1	6	25
69	1	1,2	5,1	6	1	6	25
70	1	1,2	5,1	6	1	6	25
71	1	1,2	5,1	6	1	6	25
72	1	1,2	5,1	6	1	6	25
73	3	1,2,3	6,1,2	3	1	5	25
74	3	1,2,3	6,1,2	3	1	8	25
75	3	1,2,3	6,1,2	3	1	8	25
76	3	1,2,3	6,1,2	3	1	8	25
77	3	1,2,3	6,1,2	3	1	8	25
78	3	1,2,3	6,1,2	2	1	7	25
79	3	1,2,3	6,1,2	4	1	9	25
80	3	1,2,3	6,1,2	4	1	9	25
81	3	1,2,3	6,1,2	5	1	1	25
82	3	1,2,3	6,1,2	6	1	9	25

TABLE A-5 (Cont'd)
TYPE, NUMBER AND DIGITIZING FREQUENCY
FOR DYNAMIC PRESSURE MEASUREMENT

Test #	Series #	Type of Gage	# of Gages per Type	RECORDS 7612 #	7612 Resolution (μs)	CAMAC #	CAMAC Resolution (μs)
83	3	1,2,3	6,1,2	5	1	8	25
84	3	1,2,3	6,1,2	5	1	8	25
85	3	1,2,3	6,1,2	6	1	9	25
86	3	1,2,3	6,1,2	6	1	9	25
87	3	1,2,3	6,1,2	5	1	8	25
88	3	1,2,3	6,1,2	5	1	8	25
89	3	1,2,3	6,1,2	6	1	9	25
90	3	1,2,3	6,1,2	3	1	7	25
91	4	1,2,3	6,1,2	4	1	8	25
92	4	1,2,3	6,1,2	5	1	9	25
93	4	1,2,3	6,1,2	5	1	9	25
94	4	1,2,3	6,1,2	5	1	9	25
95	4	1,2,3	6,1,2	5	1	9	25
96	4	1,2,3	6,1,2	5	1	9	25

Table A-6

Dynamic Pressure Instrumentation

Pressure - Dynamic

Instrument:

1. Pressure: Kistler Piezotron Pressure Transducer
   Model 211B3
   Rise time (10-90%) = 2 μs
   Linearity = 1% FS
   Resonant frequency - 250 kHz
   Pressure range: 0-500 psi

   Coupler: Kistler Model 5112, 2mA power supply

2. Pressure: PCB Pressure Transducer
   Model 113A24 with 401A charge converter
   Rise time = 1 μs
   Linearity = 1% FS
   Resonant frequency - 450 kHz
   Pressure range: 0-1000 psi

   Coupler: Used with either 1 or 3

3. Pressure: PCB Pressure Transducer
   Model 113A26 with 074A247
   2" extender & 401A charge converter
   Rise time = 1 μs
   Linearity = 1% FS
   Resonant frequency - 450 kHz
   Pressure range: 0-500 psi

   Coupler: PCB
   Model 480B (Frequency response is essentially that of the transducer)

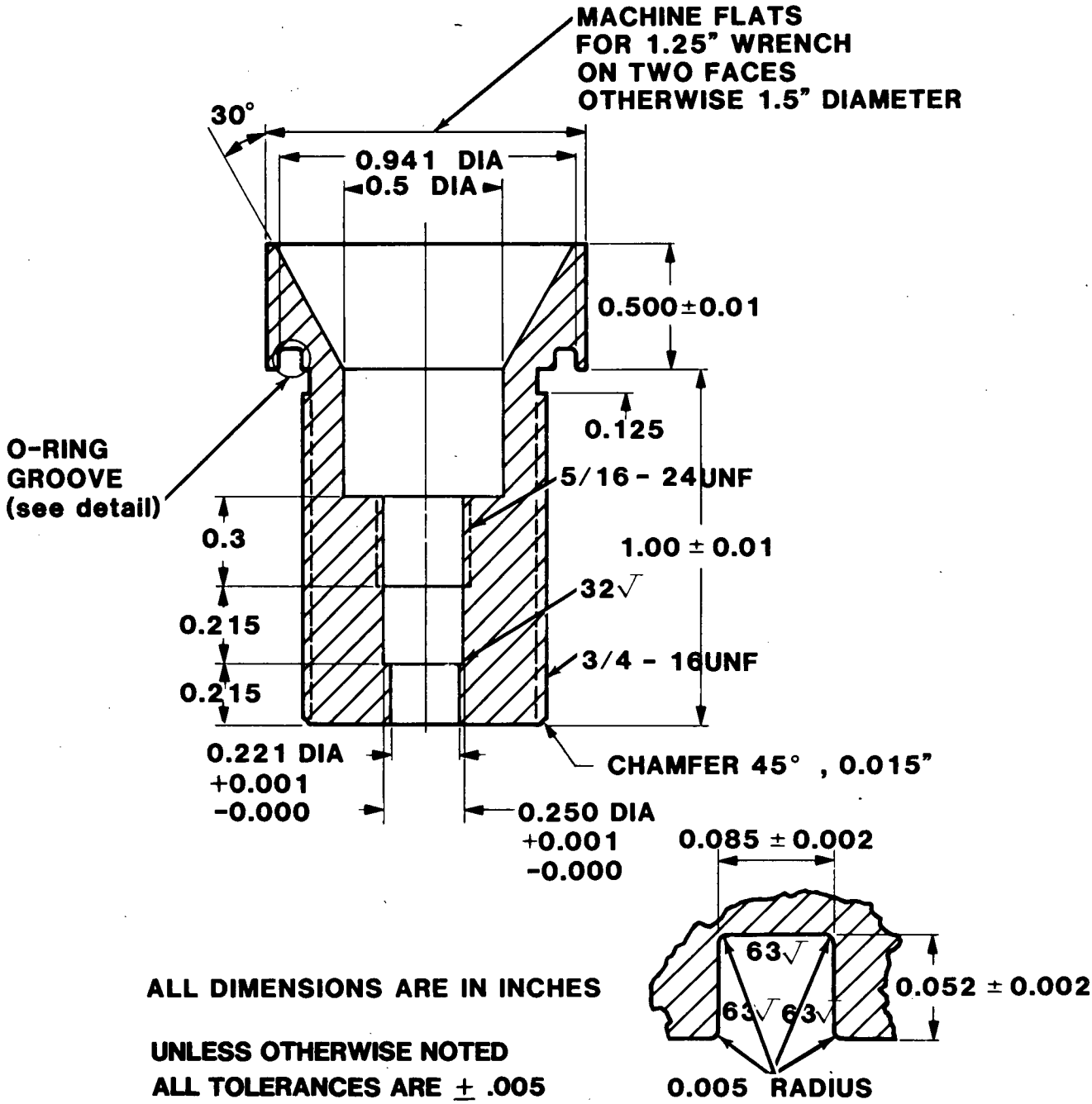

Figure A-14. Transducer Fitting Cross-Section.

A.6 REFERENCES FOR APPENDIX A

A-1. Maleev, V. L., Hartman, J. B., Machine Design, Third Edition, International Tex., pp 334 - 335.

A-2. Sherman, M. P., et al., "The FLAME Facility - The Effect of Transverse Venting on Flame Acceleration and Transition to Detonation," SAND REPORT 85-1264, (to be published).

FIGURES

Figure A-1. Cross-section of a Gas Recirculation Penetration.

Figure A-2. Cross-section of a Transducer Penetration.

Figure A-3. Cross-section of a Pipe Flange

Figure A-4. Schematic of the Secondary Piping

Figure A-5. Detonation Tube Supports

Figure A-6. Tube Support V-Block Positioning Device

Figure A-7. Heater Section Schematic - Long Pipe Section, sides and bottom

Figure A-8. Heater Section Schematic - Long Pipe Section, top

Figure A-9. Heater Section Schematic - Pipe to Pipe Flanges

Figure A-10. Heater Section Schematic - Short Pipe

Figure A-11. Heater Section Schematic - Endplates, Flanges

Figure A-12. Heater Control Circuit Schematic

Figure A-13. High Explosive Initiator

Figure A-14. Transducer Fitting Cross-section

APPENDIX B

DETAILS OF PROCEDURE

The test procedures used in the Heated Detonation Tube were developed and improved as the test program developed. The data have been categorized into 7 test series listed in Table B-1. The specific procedures will be discussed for each series, including variations in procedure for each series. The hardware is described in Appendix A, and the effect of the change in procedure/hardware on the data uncertainty is discussed in Appendix D.

All tests begin with smoking a foil. The technique of smoking a foil is discussed in Appendix A. After the foil is smoked, it is rolled around steel stiffening rings and riveted to the rings. A slot is formed along one side of the cylinder because the foil is not as wide as the circumference of the HDT. When the smoked foil is inserted into the HDT, the slot is placed along the axis of the pressure transducers so there is no interference. The endplate is then bolted in place.

Next, the explosive initiator is assembled. An RP-2 detonator is attached to the precut detasheet charge in the explosives assembly igloo. The complete initiator is mounted into the coaxial pipe and inserted into the HDT. The initiator is connected with the feed-through connector on the endplate and the endplate is bolted in place. The explosive initiator is not connected to the firing circuit until after the gases have been entered and the test is ready for detonation initiation.

After the smoked foil and explosive initiator are installed into the detonation tube and the endplates bolted in place, gases are then introduced into the recirculation line. The circulation pump runs continuously from the introduction of the first gas to the detonation initiation sequence to ensure a homogeneous mixture. Temperature and pressure are measured after the introduction of each gas to determine the composition. The specific details for each test series are discussed following the next paragraph.

After the temperature and pressure are measured for the last gas injected into the tube, the secondary piping is isolated from the detonation tube to protect the pump. The manifold to the pressure gage is closed, the power supplies to the dynamic pressure transducers are turned on, and the detonator lines are connected. All personnel are then required to leave the detonation tube and enter the control room in Bldg. 9920. For elevated temperature tests, the heaters are turned off. The computer is then configured to control the data acquisition equipment. The area is cleared and the firing circuit is charged. The discharge

Table B-1

Test Series

Series #	Description	# of tests in series
1	H_2-Air @ P=1 atm, T=20°C	16
2	H_2-Air-CO_2 @ P=1 atm, T=20°C	10
3	H_2-Air @ ρ_{air}=41.6 moles/m^3, T=100°C	16
4	H_2-Air-H_2O @ ρ_{air}=41.6 moles/m^3, T=100°C	18
5	H_2-Air @ ρ_{air}=41.6 moles/m^3, T=20°C	6
6	H_2-Air @ X_{H2}=0.17, P=1 atm	4
7	H_2-Air @ X_{H2}=0.17, ρ=42 moles/m^3	3

from the firing circuit simultaneously initiates the detonation and triggers the data acquisition equipment. The time between secondary piping isolation from the detonation tube and initiation of the detonation is typically 12 minutes. The time between turning off the heaters and the initiation of the detonation is typically 8 minutes.

B.1 TEST SERIES #1: H_2-Air @ P=1 atm, T=20°C

The first test series is composed of tests HT11 through 15 and 62 through 72. After the explosive initiator and smoked foil were placed in the detonation tube, air was introduced. In tests 11 through 15, the humid ambient air in the tube at the time the endplates were put on was used. The air was typically at 84 kPa (12.2 psia). Wet and dry bulb measurements were recorded to determine the humidity. The air was then partially evacuated to a level at which the addition of H_2 would bring the total pressure to one atmosphere. For tests 62 through 72, the tube was evacuated to less than 3.4 kPa (0.5 psia) prior to injecting compressed dry bottled air. The air pressure was set to a level at which the addition of H_2 would bring the total pressure to one atmosphere.

The air was allowed to stabilize for at least 15 minutes (typically 30 minutes) from the time the air pressure first reached its pre-determined pressure. The air pressure was adjusted while the gas achieved thermal equilibrium with the detonation tube. At least 5 minutes (typically 15 minutes) were

allowed where no changes were made in the pressure. The temperature and pressure were then recorded.

Hydrogen was then introduced to bring the total pressure up to one atmosphere. Hydrogen was introduced into the recirculation line at a rate slow enough that one equivalent tube volume of mixture had circulated through the secondary piping, approximately 15 minutes. The pressure was adjusted while the gas mixture achieved thermal equilibrium with the detonation tube. The mixture was allowed at least 15 minutes to stabilize prior to recording the temperature and pressure.

The temperature of the detonation tube was not controlled but was in equilibrium with the ambient air. The standard detonation initiation sequence was then begun.

B.2 TEST SERIES #2: H_2-Air-CO_2 @ P=1 atm, T=20°C

The second test series is composed of tests HT16 through 25. The air used in these tests was the ambient air in the tube after the explosive initiator and smoked foil installed. The air was typically at 84 kPa (12.2 psia). Wet and dry bulb measurements were recorded to determine the humidity. The air was then partially evacuated to a level at which the addition of CO_2 and H_2 would bring the total pressure to one atmosphere. The air was allowed to stabilize for at least 15 minutes (typically 30 minutes) from the time the air pressure first reached its predetermined pressure. The air pressure was adjusted while the gas achieved thermal equilibrium with the detonation tube. At least 5 minutes (typically 15 minutes) were allowed where no changes were made in the pressure. The temperature and pressure were then recorded.

Carbon dioxide was then introduced into the recirculation line at a rate slow enough that one equivalent tube volume of mixture had circulated through the secondary piping, approximately 15 minutes. The pressure was adjusted while the gas mixture achieved thermal equilibrium with the detonation tube. The mixture was allowed at least 15 minutes to stabilize prior to recording the temperature and pressure.

Hydrogen was then introduced into the recirculation line to bring the total pressure up to one atmosphere. Hydrogen was introduced at a rate slow enough that one equivalent tube volume of mixture had circulated through the secondary piping, approximately 15 minutes. The pressure was adjusted while the gas mixture achieved thermal equilibrium with the detonation tube. The mixture was allowed at least 15 minutes to stabilize prior to recording the temperature and pressure.

The temperature of the detonation tube was not controlled but was in equilibrium with the ambient air. The standard detonation initiation sequence was then begun.

B.3 TEST SERIES #3 and #4: H_2-Air-H_2O @ ρ_{air}=41.6 moles/m^3, T=100°C

The third and fourth test series are composed of tests HT39, 41, 42, 50 through 61, and 73 through 90. For all tests except 39, 41, and 42, the explosive initiator and smoked foil were placed in the detonation tube, and then the tube was evacuated to less than 3.4 kPa (0.5 psia). Dry bottled air was injected. The air pressure was set so that the air molar density, ρ_{air}, was 41.6 moles/m^3. The actual pressure depended on the detonation tube temperature at the time of air injection, being superatmospheric for any temperature over 20°C. For the third test series, the steam bottle was isolated from the secondary recirculation line and for the fourth test series, a premeasured volume of water was then poured into the steam bottle.

The detonation tube and steam bottle were then heated to 100°C. From test 74 to 90 the detonation tube was allowed to heat unattended overnight using the "watchdog" timer device. Normal heating times were 5 hours. Typical temperature profiles are shown in Appendix F. For tests prior to 74, the circulation pump was run continuously during the heating process; for overnight heating the pump was turned on in the morning. After the tube reached 97°C or 98°C, and the circulation pump had run for at least 30 minutes, any final adjustments were made to the air pressure to achieve the desired air density. At least 5 minutes (typically 15 minutes) were allowed where no changes were made in the pressure. The temperature and pressure were then recorded.

Hydrogen was then introduced into the recirculation line at a rate slow enough that one equivalent tube volume of mixture had circulated through the secondary piping, approximately 15 minutes. The pressure was adjusted while the gas mixture achieved thermal equilibrium with the detonation tube. The mixture was allowed at least 15 minutes to stabilize prior to recording the temperature and pressure. For tests 39, 41, and 42, the air and hydrogen were added and then the tube was heated. For test series #3, the standard firing sequence was begun, for test series #4, steam was introduced into the HDT.

To produce steam in the superatmospheric conditions in the detonation tube, the temperature of the steam bottle was raised, typically between 150°C and 200°C. The steam bottle was then opened to the secondary piping and allowed to flow in. Condensation in the secondary line was a problem on most tests because of the poor metering characteristics of the ball valve between the steam bottle and secondary piping. The condensate would reevaporate as detected by a thermocouple at the low point in the

secondary line and a concurrent increase in pressure. Future tests will use a metering valve for better injection control.

The water in the steam bottle was determined to have completely evaporated when there was no change in the detonation tube pressure and the temperature controller indicated that the heater on the steam bottle was no longer cycling around the set point temperature but was off for long periods, ~3 minutes. The mixture was allowed at least 15 minutes to stabilize prior to recording the temperature and pressure. The standard detonation initiation sequence was then begun.

B.4 TEST SERIES #5: H_2-Air @ ρ_{air}=41.6 moles/m^3, T=100°C

The fifth test series is composed of tests HT91 through 96. After the explosive initiator and smoked foil were placed in the detonation tube, the tube was evacuated to less than 3.4 kPa (0.5 psia). Dry bottled air was injected and the air pressure was set so that the air molar density, ρ_{air}, was 41.6 moles/m^3. The actual pressure depended on the detonation tube temperature at the time of air injection. The air pressure was adjusted while the gas achieved thermal equilibrium with the detonation tube. At least 5 minutes (typically 15 minutes) were allowed where no changes were made in the pressure. The temperature and pressure were then recorded.

These tests were done in the fall of the year and the ambient air temperature was below 20°C during the night and was approximately that temperature during the day. The detonation tube does not have refrigeration coils. Two tests were run each day for three days. The heaters were programmed to turn on early in the morning with a set point of 18°C. This allowed two degrees of heating which occurred as during gas injection and circulation. For the second test of the day the heaters were turned off and the tube obtained the ambient temperature of the day. The test temperatures varied between 19.2°C and 22.7°C.

Hydrogen was then introduced into the recirculation line at a rate slow enough that one equivalent tube volume of mixture had circulated through the secondary piping, approximately 15 minutes. The pressure was adjusted while the gas mixture achieved thermal equilibrium with the detonation tube. The mixture was allowed at least 15 minutes to stabilize prior to recording the temperature and pressure. The standard detonation initiation sequence was then begun.

B.5 TEST SERIES #6: H_2-Air @ X_{H2}=0.17, P=1 atm

The sixth test series is composed of tests HT46 through 49. After the explosive initiator and smoked foil were placed in the detonation tube, the endplates were put on. The humid air in the

tube at the time the endplates were placed on the detonation tube was used as the air in the test. The air was typically at 84 kPa (12.2 psia). Wet and dry bulb measurements were recorded to determine the humidity. The air was then partially evacuated to a level at which the addition of H_2 would bring the total pressure to one atmosphere and the H_2 mole fraction to 0.17.

The air was allowed to stabilize for at least 15 minutes (typically 30 minutes) from the time the air pressure first reached its pre-determined pressure. The air pressure was adjusted while the gas achieved thermal equilibrium with the detonation tube. At least 5 minutes (typically 15 minutes) were allowed where no changes were made in the pressure. The temperature and pressure were then recorded.

Hydrogen was then introduced into the recirculation line to bring the total pressure up to one atmosphere. Hydrogen was introduced at a rate slow enough that one equivalent tube volume of mixture had circulated through the secondary piping, approximately 15 minutes. The pressure was adjusted while the gas mixture achieved thermal equilibrium with the detonation tube. The mixture was allowed at least 15 minutes to stabilize prior to recording the temperature and pressure. For test HT46, the standard detonation initiation sequence was then begun.

For tests 47, 48 and 49, detonation tube was then heated. For test 47 the tube was heated to 50°C, and for 48 and 49 the tube was heated to 100°C. The temperature was allowed to come to equilibrium around the set point temperature typically with no detectable change in temperature in 15 minutes. The standard detonation initiation sequence was then begun.

B.6 TEST SERIES #7: H_2-Air @ X_{H2}=0.17, ρ=42 moles/m^3

The seventh test series is composed of tests HT11, 44 and 45. Test HT11 is described in test series #1. The procedure for tests 45 and 46 are described here. After the explosive initiator and smoked foil were placed in the detonation tube, the endplates were put on. The humid air in the tube at the time the endplates were placed on the detonation tube was used as the air for the test. The air was typically at 84 kPa (12.2 psia). Wet and dry bulb measurements were recorded to determine the humidity. Additional air was introduced from a compressed air source at the 9920 site to bring the air density to a level at which the addition of H_2 would bring the total mixture density to 42 moles/m^3 and the H_2 mole fraction to 0.17.

The air was allowed to stabilize for at least 15 minutes (typically 30 minutes) from the time the air pressure first reached its pre-determined pressure. The air pressure was adjusted while the gas achieved thermal equilibrium with the detonation tube. At least 5 minutes (typically 15 minutes) were

allowed where no changes were made in the pressure. The temperature and pressure were then recorded.

Hydrogen was then introduced into the recirculation line to bring the total pressure up to one atmosphere. Hydrogen was introduced at a rate slow enough that one equivalent tube volume of mixture had circulated through the secondary piping, approximately 15 minutes. The pressure was adjusted while the gas mixture achieved thermal equilibrium with the detonation tube. The mixture was allowed at least 15 minutes to stabilize prior to recording the temperature and pressure.

The detonation tube was then heated. For test 45 the tube was heated to 50°C, and for 44 the tube was heated to 100°C. The temperature was allowed to come to equilibrium around the set point temperature typically with no detectable change in temperature in 15 minutes. The standard detonation initiation sequence was then begun.

APPENDIX C

TABULATED DATA

The data are tabulated by test series. Uncertainty estimates are included in the tables. For each variable listed, three columns are defined, LB which is the lower bound, MP which is the most probable, and UB which is the upper bound (see Appendix D). Table C-1 lists the test series. Table C-2 lists the detonation cell width for each series. Within each series, the data are listed in increasing equivalence ratio and increasing diluent mole fraction. Table C-2 also lists the results of the model calculations (See Chapter 4). The Z.75 column is the length required to reach Mach 0.75. The DCW/Z.75 column is the most probable detonation cell width divided by this length scale. The final column is 22 times the Z.75 column which is the predicted detonation cell width using a single point fit for the constant A in the model. Table C-3 lists the detonation velocity for each series. Within each series, the data are listed in increasing equivalence ratio and increasing diluent mole fraction. Table C-3 also lists the data acquisition equipment used, number of gages recording data, and the Chapman-Jouguet theory predicted velocity. Table C-4 lists the full initial thermodynamic state for each test series. Within each test series, the data are listed in increasing test number.

Table C-1

Test Series

Series #	Description	# of Tests in Series
1	H_2-Air @ P=1 atm, T=20°C	16
2	H_2-Air-CO_2 @ P=1 atm, T=20°C	10
3	H_2-Air @ ρ_{air}=41.6 moles/m^3, T=100°C	16
4	H_2-Air-H_2O @ ρ_{air}=41.6 moles/m^3, T=100°C	18
5	H_2-Air @ ρ_{air}=41.6 moles/m^3, T=20°C	6
6	H_2-Air @ X_{H2}=0.17, P=1 atm	4
7	H_2-Air @ X_{H2}=0.17, ρ=42 moles/m^3	3

Table C-2

Detonation Cell Width Data

TEST SERIES #1

The 2S limits for T,P for the entire series are:

275. < T (K) < 306.
99.1 < P (kPa) < 101.7

TEST	EQUIVALENCE RATIO			DETONATION CELL WIDTH (MM)			Z.75 (MM)	MODEL DCW/Z.75	22*Z.75 (MM)
	LB	MP	UB	LB	MP	UB			
15	0.3465	0.3743	0.4021	915.	1220.	1525.	179.	6.82	3938.
14	0.3529	0.3812	0.4094	900.	1200.	1500.	159.	7.67	3498.
67	0.3583	0.3868	0.4152	480.	640.	800.	95.0	6.74	2090.
68	0.3788	0.4071	0.4353	315.	420.	525.	53.3	9.85	1173.
66	0.3965	0.4248	0.4531	229.	305.	381.	34.5	8.84	759.
12	0.4046	0.4334	0.4622	233.	310.	388.	48.7	6.37	1071.
69	0.4048	0.4335	0.4621	199.	265.	331.	30.0	8.83	660.
65	0.4334	0.4623	0.4912	188.	250.	313.	16.1	15.5	354.
11	0.4498	0.4792	0.5085	143.	190.	238.	19.2	9.90	422.
64	0.4575	0.4867	0.5158	113.	150.	188.	9.52	15.8	209.
63	0.4737	0.5037	0.5336	75.	100.	125.	7.77	12.9	171.
70	3.5773	3.6647	3.7521	139.	185.	231.	4.99	37.1	110.
71	4.3527	4.4655	4.5783	356.	475.	594.	15.6	30.4	343.
72	5.5574	5.7129	5.8684	1013.	1350.	1688.	73.5	18.4	1617.

Table C-2 (cont'd.)

TEST SERIES #2

The 2S limits for T,P for the entire series are:

275. < T (K) < 299.
106.5 < P (kPa) < 106.9

TEST	EQUIVALENCE RATIO			CO2 MOLE FRACTION			DETONATION CELL WIDTH (MM)			MODEL Z.75 (MM)	DCW/Z.75	22*Z.75 (MM)
	LB	MP	UB	LB	MP	UB	LB	MP	UB			
16	0.4589	0.4877	0.5165	0.0406	0.0500	0.0594	368.	490.	613.	62.0	7.90	1364.
22	0.5369	0.5652	0.5936	0.0408	0.0498	0.0588	225.	300.	375.	15.2	19.7	334.
17	0.5672	0.5977	0.6282	0.0409	0.0505	0.0601	150.	200.	250.	13.4	14.9	295.
25	0.6430	0.6723	0.7017	0.0396	0.0486	0.0577	86.	95.	198.	3.95	24.1	86.9
21	0.6863	0.7182	0.7502	0.0914	0.0999	0.1085	125.	240.	260.	12.3	19.5	271.
18	0.7227	0.7558	0.7889	0.0912	0.1000	0.1088	180.	240.	300.	9.96	24.1	219.
24	0.8048	0.8379	0.8709	0.0916	0.1001	0.1086	100.	100.	200.	5.20	19.2	114.
23	0.7208	0.7559	0.7909	0.1419	0.1500	0.1581	340.	500.	520	35.9	13.9	790.
20	0.7983	0.8342	0.8700	0.1425	0.1505	0.1585	293.	390.	488.	20.3	19.2	447.
19	0.9953	1.0338	1.0723	0.1428	0.1509	0.1590	180.	180.	290.	9.99	18.0	220.

Table C-2 (cont'd.)

TEST SERIES #3

The 2S limits for T, air density for the entire series are:

366. < T (K) < 375.
40.4 < Air Density (moles/m^3) < 42.1

TEST	EQUIVALENCE RATIO			STEAM MOLE FRACTION			DETONATION CELL WIDTH (MM)			MODEL Z.75 (MM)	DCW/Z.75	22*Z.75 (MM)
	LB	MP	UB	LB	MP	UB	LB	MP	UB			
74	0.3355	0.3575	0.3794	0.0000	0.0000	0.0000	315.	420.	525.	51.9	8.1	1142.
73	0.3526	0.3747	0.3967	0.0000	0.0000	0.0000	247.	330.	413.	33.3	9.9	733.
77	0.3606	0.3827	0.4048	0.0000	0.0000	0.0000	221.	295.	389.	28.2	10.5	620.
62	0.3990	0.4213	0.4437	0.0000	0.0000	0.0000	131.	175.	219.	12.0	14.6	264.
76	0.4751	0.4981	0.5212	0.0000	0.0000	0.0000	49.	65.	81.	2.73	23.8	60.1
60	0.5820	0.6059	0.6297	0.0000	0.0000	0.0000	19.	25.	31.	0.779	32.1	17.1
78	0.5848	0.6088	0.6327	0.0000	0.0000	0.0000	18.	24.	30.	0.774	31.0	17.0
42	0.6253	0.6501	0.6750	0.0038	0.0038	0.0038	14.	19.	24.	0.623	30.5	13.7
80	0.6738	0.6985	0.7232	0.0000	0.0000	0.0000	11.	14.	18.	0.537	26.1	11.8
56	0.7830	0.8085	0.8339	0.0000	0.0000	0.0000	7.	9.	11.	0.442	20.4	9.7
82	0.8701	0.8964	0.9226	0.0000	0.0000	0.0000	5.	6.	8.	0.399	15.0	8.8
84	0.9687	0.9957	1.0228	0.0000	0.0000	0.0000	4.	5.	6.	0.368	13.6	8.1
53	0.9826	1.0098	1.0369	0.0000	0.0000	0.0000	4.	5.	6.	0.367	13.7	8.0
86	1.4687	1.5000	1.5313	0.0000	0.0000	0.0000	5.	6.	10.	0.309	19.5	6.8
50	1.9618	1.9974	2.0329	0.0000	0.0000	0.0000	7.	12.	24.	0.375	32.0	8.3
88	2.9632	3.0077	3.0522	0.0000	0.0000	0.0000	22.	22.	35.	1.09	20.2	24.0

Table C-2 (cont'd.)

TEST SERIES #4

The 2S limits for T, Air Density for the entire series are:

367. < T (K) < 376.
40.9 < Air Density (moles/m^3) < 42.0

TEST	EQUIVALENCE RATIO			STEAM MOLE FRACTION			DETONATION CELL WIDTH (MM)			MODEL Z.75 (MM)	DCW/Z.75	22*Z.75 (MM)
	LB	MP	UB	LB	MP	UB	LB	MP	UB			
75	0.4713	0.4943	0.5173	0.0903	0.0975	0.1046	413.	550.	688.	37.7	14.6	829.
79	0.5779	0.6018	0.6256	0.0898	0.0970	0.1041	173.	230.	288.	10.6	21.7	233.
41	0.5829	0.6102	0.6374	0.0955	0.1033	0.1110	158.	210.	263.	11.3	18.6	249.
61	0.5955	0.6195	0.6435	0.0919	0.0990	0.1062	150.	200.	250.	9.29	21.5	204.
58	0.7857	0.8111	0.8366	0.0904	0.0975	0.1046	41.	55.	69.	2.09	26.3	46.0
54	0.9765	1.0036	1.0306	0.0901	0.0972	0.1043	22.	29.	36.	1.05	27.6	23.1
51	1.9369	1.9724	2.0078	0.0956	0.1026	0.1095	31.	41.	51.	2.20	18.6	48.4
81	0.6687	0.6932	0.7178	0.1446	0.1514	0.1581	153.	207.	260.	12.0	17.3	264.
85	0.9753	1.0024	1.0295	0.1495	0.1562	0.1628	49.	74.	99.	26.1	28.4	57.4
90	0.6724	0.6969	0.7214	0.1792	0.1856	0.1921	265.	310.	500.	19.7	15.7	433.
59	0.7930	0.8185	0.8440	0.1901	0.1965	0.2028	169.	225.	281.	10.3	21.8	227.
55	0.9812	1.0082	1.0353	0.1896	0.1960	0.2023	60.	95.	180.	4.54	20.9	99.9
52	1.9350	1.9704	2.0057	0.1956	0.2018	0.2080	98.	131.	164.	10.1	13.0	222.
39	0.7862	0.8167	0.8472	0.2415	0.2483	0.2550	210.	280.	350.	22.5	12.4	495.
83	0.8742	0.9003	0.9265	0.2566	0.2624	0.2683	221.	295.	369.	16.6	17.8	365.
89	0.8767	0.9028	0.9290	0.2903	0.2959	0.3015	350.	365.	1070.	25.8	14.1	568.
87	0.9751	1.0021	1.0291	0.2892	0.2948	0.3004	280.	290.	700.	16.7	17.4	367.
57	0.9781	1.0051	1.0322	0.2821	0.2877	0.2934	170.	325.	330.	15.3	21.2	337.

Table C-2 (cont'd.)

TEST SERIES #5

The 2S limits on T, Air density for the entire Series are:

290. < T (K) < 298.
41.0 < Air Density (moles/m^3) < 42.0

TEST	EQUIVALENCE RATIO			DETONATION CELL WIDTH (MM)			MODEL		
	LB	MP	UB	LB	MP	UB	Z.75 (MM)	DCW/Z.75	22*Z.75 (MM)
96	0.3709	0.3989	0.4270	300.	400.	500.	70.0	5.7	1540.
95	0.4719	0.5011	0.5303	86.	115.	144.	9.36	12.3	206.
94	0.5733	0.6036	0.6340	29.	38.	48.	2.07	18.4	45.5
93	0.7714	0.8038	0.8361	10.	13.	16.	0.550	23.6	12.1
92	0.9771	1.0116	1.0461	7.	10.	13.	0.417	24.0	9.1
91	1.9329	1.9776	2.0223	14.	15.	29.	0.567	26.5	12.5

TEST SERIES #6

2S limits for EQR and P for the entire series are:

0.446 < EQR < 0.511
100.1 < P (kPa) < 101.7

TEST	TEMPERATAURE (K)			DETONATION CELL WIDTH (MM)			MODEL		
	LB	MP	UB	LB	MP	UB	Z.75 (MM)	DCW/Z.75	22*Z.75 (MM)
46	285.6	287.6	289.6	158.	210.	263.	16.1	13.0	354.
47	321.1	323.1	325.1	130.	135.	230.	8.35	16.2	184.
48	371.1	373.1	375.1	81.	106.	140.	2.61	40.6	57.
49	370.1	372.1	374.1	60.	65.	120.	1.97	33.0	43.

Table C-2 (cont'd.)

TEST SERIES #7

2S limits for EQR and AIR DENSITY for the entire series are:

0.448 < EQR < 0.510
34.0 < AIR DENSITY> (MOLES/M^3) < 34.8

TEST	TEMPERATAURE (K)			DETONATION CELL WIDTH (MM)			MODEL Z.75 (MM)	DCW/Z.75	22*Z.75 (MM)
	LB	MP	UB	LB	MP	UB			
11	274.9	276.9	278.9	143.	190.	238.	19.2	9.90	422.
45	321.6	323.6	325.6	90.	140.	150.	11.1	12.6	244.
44	368.1	370.1	372.1	82.	130.	137.	3.59	36.2	79.

Table C-3

Detonation Velocity Data

(Note: Velocity Sources - 1 = 7612D's , 2 = CAMAC)

TEST SERIES #1

2S limits for T,P for the entire series are:

275. < T (K) < 306.
99.1 < P (kPa) < 101.7

TEST	EQUIVALENCE RATIO			#	DETONATION VELOCITY (KM/S)				CHAPMAN-JOUGUET VELOCITY (KM/S)
	LB	MP	UB	OBS.	LB	MP	UB	SOURCE	
15	0.3465	0.3743	0.4021	5	1.3964	1.4103	1.4245	1	1.4520
14	0.3529	0.3812	0.4094	5	1.3707	1.4523	1.5443	1	1.4611
67	0.3583	0.3868	0.4152	5	1.4516	1.4758	1.5009	1	1.4716
68	0.3788	0.4071	0.4353	5	1.5040	1.5086	1.5131	1	1.4986
66	0.3965	0.4248	0.4531	4	1.5007	1.5447	1.5914	1	1.5211
12	0.4046	0.4334	0.4622	4	1.5073	1.5287	1.5507	1	1.5279
69	0.4048	0.4335	0.4621	5	1.5307	1.5496	1.5690	1	1.5313
65	0.4334	0.4623	0.4912	5	1.5707	1.5749	1.5791	1	1.5655
11	0.4498	0.4792	0.5085	4	1.5314	1.5879	1.6488	1	1.5819
64	0.4575	0.4867	0.5158	5	1.5896	1.6099	1.6307	1	1.5934
63	0.4737	0.5037	0.5336	5	1.6487	1.6539	1.6591	1	1.6115
70	3.5773	3.6647	3.7521	5	2.2435	2.2610	2.2788	1	2.2511
71	4.3527	4.4655	4.5783	5	2.2091	2.2757	2.3464	1	2.2799
72	5.5574	5.7129	5.8684	6	2.2281	2.2782	2.3305	1	2.3109

Table C-3 (cont'd.)

TEST SERIES #2

The 2S limits for T,P for the entire series are:

275. < T (K) < 299.
106.5 < P (kPa) < 106.9

TEST	EQUIVALENCE RATIO			CO2 MOLE FRACTION			#	DETONATION VELOCITY (KM/S)				CHAPMAN-JOUGUET VELOCITY (KM/S)
	LB	MP	UB	LB	MP	UB	OBS.	LB	MP	UB	SOURCE	
16	0.4589	0.4877	0.5165	0.0406	0.0500	0.0594	5	1.4533	1.4766	1.5007	1	1.5100
22	0.5369	0.5652	0.5936	0.0408	0.0498	0.0588	5	1.5299	1.5682	1.6086	1	1.5874
17	0.5672	0.5977	0.6282	0.0409	0.0505	0.0601	5	1.6040	1.6321	1.6612	1	1.6154
25	0.6430	0.6723	0.7017	0.0396	0.0486	0.0577	5	1.6659	1.6969	1.7290	1	1.6790
21	0.6863	0.7182	0.7502	0.0914	0.0999	0.1085	5	1.6085	1.6156	1.6228	1	1.6239
18	0.7227	0.7558	0.7889	0.0912	0.1000	0.1088	5	1.6057	1.6437	1.6836	1	1.6488
24	0.8048	0.8379	0.8709	0.0916	0.1001	0.1086	5	1.6980	1.7115	1.7252	1	1.6959
23	0.7208	0.7559	0.7909	0.1419	0.1500	0.1581	5	1.5219	1.5567	1.5931	1	1.5655
20	0.7983	0.8342	0.8700	0.1425	0.1505	0.1585	5	1.5571	1.5949	1.6347	1	1.6091
19	0.9953	1.0338	1.0723	0.1428	0.1509	0.1590	5	1.6708	1.6845	1.6985	1	1.6857

TEST SERIES #3

The 2S limits for T, air density for the entire series are:

366. < T (K) < 375.
40.4 < Air Density (moles/m^3) < 42.1

TEST	EQUIVALENCE RATIO			STEAM MOLE FRACTION			#	DETONATION VELOCITY (KM/S)				CHAPMAN-JOUGUET VELOCITY (KM/S)
	LB	MP	UB	LB	MP	UB	OBS.	LB	MP	UB	SOURCE	
74	0.3355	0.3575	0.3794	0.0000	0.0000	0.0000	7	1.3939	1.4252	1.4580	2	1.4391
73	0.3526	0.3747	0.3967	0.0000	0.0000	0.0000	4	1.4113	1.5121	1.6284	2	1.4628
77	0.3606	0.3827	0.4048	0.0000	0.0000	0.0000	7	1.4687	1.4792	1.4898	2	1.4733

Table C-3 (cont'd.)

Test Series #3 (cont'd.)

62	0.3990	0.4213	0.4437	0.0000	0.0000	0.0000	5	1.4996	1.5160	1.5327	1	1.5222
76	0.4751	0.4981	0.5212	0.0000	0.0000	0.0000	7	1.5851	1.6052	1.6259	2	1.6103
60	0.5820	0.6059	0.6297	0.0000	0.0000	0.0000	5	1.6954	1.7255	1.7566	1	1.7154
78	0.5848	0.6088	0.6327	0.0000	0.0000	0.0000	6	1.6904	1.7071	1.7242	2	1.7180
42	0.6253	0.6501	0.6750	0.0037	0.0038	0.0040	5	1.7327	1.7491	1.7658	1	1.7514
80	0.6738	0.6985	0.7232	0.0000	0.0000	0.0000	4	1.7751	1.8070	1.8399	1	1.7924
56	0.7830	0.8085	0.8339	0.0000	0.0000	0.0000	5	1.8688	1.8787	1.8886	1	1.8700
82	0.8701	0.8964	0.9226	0.0000	0.0000	0.0000	6	1.9418	1.9507	1.9596	1	1.9220
84	0.9687	0.9957	1.0228	0.0000	0.0000	0.0000	5	1.9767	1.9898	2.0032	1	1.9695
53	0.9826	1.0098	1.0369	0.0000	0.0000	0.0000	4	1.9585	1.9865	2.0153	1	1.9752
86	1.4687	1.5000	1.5313	0.0000	0.0000	0.0000	6	2.0816	2.0943	2.1071	1	2.0911
50	1.9618	1.9974	2.0329	0.0000	0.0000	0.0000	5	2.1375	2.1555	2.1738	1	2.1508
88	2.9632	3.0077	3.0522	0.0000	0.0000	0.0000	5	2.2259	2.2406	2.2555	1	2.2281

TEST SERIES #4

The 2S limits for T, Air Density for the entire series are:

367. < T (K) < 376.
40.9 < Air Density (moles/m^3) < 42.0

	TEST EQUIVALENCE RATIO			STEAM MOLE FRACTION				DETONATION VELOCITY (KM/S)				CHAPMAN-JOUGUET VELOCITY (KM/S)
	LB	MP	UB	LB	MP	UB	# OBS.	LB	MP	UB	SOURCE	
75	0.4713	0.4943	0.5173	0.0903	0.0975	0.1046	7	1.5297	1.5408	1.5520	2	1.5524
79	0.5779	0.6018	0.6256	0.0898	0.0970	0.1041	4	1.6490	1.6586	1.6683	1	1.6562
41	0.5829	0.6102	0.6374	0.0955	0.1033	0.1110	4	1.6607	1.6672	1.6737	1	1.6597
61	0.5955	0.6195	0.6435	0.0919	0.0990	0.1062	5	1.5986	1.6653	1.7378	1	1.6704
58	0.7857	0.8111	0.8366	0.0904	0.0975	0.1046	5	1.8212	1.8306	1.8401	1	1.8166
54	0.9765	1.0036	1.0306	0.0901	0.0972	0.1043	4	1.9112	1.9303	1.9498	1	1.9191
51	1.9369	1.9724	2.0078	0.0956	0.1026	0.1095	4	2.0179	2.0542	2.0919	1	2.0383

Table C-3 (cont'd.)

Test Series #4 (cont'd.)

81	0.6687	0.6932	0.7178	0.1446	0.1514	0.1581	5	1.7029	1.7144	1.7261	1	1.6986
85	0.9753	1.0024	1.0295	0.1495	0.1562	0.1628	6	1.8734	1.8857	1.8983	1	1.8834
90	0.6724	0.6969	0.7214	0.1792	0.1856	0.1921	6	1.6649	1.6681	1.6712	2	1.6791
59	0.7930	0.8185	0.8440	0.1901	0.1965	0.2028	5	1.7409	1.7521	1.7634	1	1.7579
55	0.9812	1.0082	1.0353	0.1896	0.1960	0.2023	4	1.8099	1.8497	1.8914	1	1.8599
52	1.9350	1.9704	2.0057	0.1956	0.2018	0.2080	5	1.9349	1.9549	1.9752	1	1.9256
39	0.7862	0.8167	0.8472	0.2415	0.2483	0.2550	5	1.7129	1.7305	1.7484	1	1.7198
83	0.8742	0.9003	0.9265	0.2566	0.2624	0.2683	5	1.7350	1.7671	1.8003	1	1.7609
89	0.8767	0.9028	0.9290	0.2903	0.2959	0.3015	6	1.7045	1.7146	1.7248	1	1.7364
87	0.9751	1.0021	1.0291	0.2892	0.2948	0.3004	5	1.7711	1.7829	1.7948	1	1.7867
57	0.9781	1.0051	1.0322	0.2821	0.2877	0.2934	5	1.7563	1.7787	1.8016	1	1.7932

TEST SERIES #5

The 2S limits on T, Air density for the entire Series are:

290. < T (K) < 298.
41.0 < Air Density (moles/m^3) < 42.0

	TEST EQUIVALENCE RATIO				DETONATION VELOCITY (KM/S)				CHAPMAN-JOUGUET VELOCITY (KM/S)
	LB	MP	UB	# OBS.	LB	MP	UB	SOURCE	
96	0.3709	0.3989	0.4270	5	1.4799	1.4976	1.5158	1	1.4878
95	0.4719	0.5011	0.5303	5	1.6178	1.6254	1.6331	1	1.6092
94	0.5733	0.6036	0.6340	5	1.7162	1.7292	1.7424	1	1.7113
93	0.7714	0.8038	0.8361	5	1.8894	1.9182	1.9480	1	1.8688
92	0.9771	1.0116	1.0461	5	1.9771	1.9879	1.9989	1	1.9081
91	1.9329	1.9776	2.0223	4	2.1520	2.1632	2.1746	1	2.1468

Table C-3 (cont'd.)

TEST SERIES #6

2S limits for EQR and P for the entire series are:

0.446 < EQR < 0.511
100.1 < P (kPa) < 101.7

TEST	TEMPERATURE (K)			#	DETONATION VELOCITY (KM/S)				CHAPMAN-JOUGUET VELOCITY (KM/S)
	LB	MP	UB	OBS.	LB	MP	UB	SOURCE	
46	285.6	287.6	289.6	3	1.5819	1.5885	1.5950	1	1.5836
47	321.1	323.1	325.1	5	1.5748	1.5854	1.5961	1	1.5832
48	371.1	373.1	375.1	4	1.5715	1.5776	1.5838	1	1.5773
49	370.1	372.1	374.1	5	1.5903	1.5988	1.6073	1	1.5950

TEST SERIES #7

2S limits for EQR and AIR DENSITY for the entire series are:

0.448 < EQR < 0.510
34.0 < Air Density (Moles/m^3) < 34.8

TEST	TEMPERATURE (K)			#	DETONATION VELOCITY (KM/S)				CHAPMAN-JOUGUET VELOCITY (KM/S)
	LB	MP	UB	OBS.	LB	MP	UB	SOURCE	
11	274.9	276.9	278.9	4	1.5314	1.5879	1.6488	1	1.5819
45	321.6	323.6	325.6	5	1.5850	1.5905	1.5961	1	1.5762
44	368.1	370.1	372.1	5	1.5847	1.5955	1.6065	1	1.5926

Table C-4

Initial Thermodynamic State

TEST SERIES #1

TEST	TEMPERATURE (C)			PRESSURE (PA)			AIR DENSITY (MOLES)			EQUIVALENCE RATIO			STEAM MOLE FRACTION		
	LB	MP	UB	LB	MP	UB	LB	MP	UB	LB	MP	UB	LB	MP	UB
11	274.9	276.9	278.9	99174.	99284.	99394.	35.534	35.798	36.062	0.4498	0.4792	0.5085	0.0031	0.0031	0.0031
12	275.6	277.6	279.6	99863.	99974.	100084.	36.255	36.523	36.792	0.4046	0.4334	0.4622	0.0037	0.0037	0.0037
13	279.1	281.1	283.1	97864.	97974.	98084.	35.739	36.001	36.262	0.3534	0.3813	0.4092	0.0038	0.0038	0.0038
14	275.6	277.6	279.6	97795.	97905.	98016.	36.203	36.471	36.739	0.3529	0.3812	0.4094	0.0027	0.0027	0.0027
15	279.1	281.1	283.1	97312.	97423.	97533.	35.664	35.925	36.185	0.3465	0.3743	0.4021	0.0028	0.0028	0.0028
63	292.1	294.1	296.1	100112.	100801.	101490.	33.667	34.035	34.403	0.4737	0.5037	0.5336	0.0000	0.0000	0.0000
64	298.1	300.1	302.1	100249.	100939.	101628.	33.240	33.597	33.954	0.4575	0.4867	0.5158	0.0000	0.0000	0.0000
65	296.6	298.6	300.6	100043.	100732.	101422.	33.627	33.985	34.344	0.4334	0.4623	0.4912	0.0000	0.0000	0.0000
66	299.1	301.1	303.1	100318.	101008.	101697.	33.888	34.246	34.604	0.3965	0.4248	0.4531	0.0000	0.0000	0.0000
67	292.6	294.6	296.6	100112.	100801.	101490.	35.038	35.409	35.779	0.3583	0.3868	0.4152	0.0000	0.0000	0.0000
68	297.6	299.6	301.6	100112.	100801.	101490.	34.205	34.565	34.925	0.3788	0.4071	0.4353	0.0000	0.0000	0.0000
69	296.6	298.6	300.6	100180.	100870.	101559.	34.018	34.379	34.741	0.4048	0.4335	0.4621	0.0000	0.0000	0.0000
70	300.1	302.1	304.1	100180.	100870.	101559.	15.544	15.837	16.130	3.5773	3.6647	3.7521	0.0000	0.0000	0.0000
71	297.6	299.6	301.6	100249.	100939.	101628.	13.817	14.113	14.408	4.3527	4.4655	4.5783	0.0000	0.0000	0.0000
72	301.6	303.6	305.6	100249.	100939.	101628.	11.497	11.782	12.067	5.5574	5.7129	5.8684	0.0000	0.0000	0.0000

TEST SERIES #2

TEST	TEMPERATURE (K)			PRESSURE (PA)			AIR DENSITY (MOLES)			EQUIVALENCE RATIO			CO2 MOLE FRACTION		
	LB	MP	UB	LB	MP	UB	LB	MP	UB	LB	MP	UB	LB	MP	UB
16	283.4	285.4	287.4	106551.	106658.	106765.	35.084	35.337	35.590	0.4589	0.4877	0.5165	0.0406	0.0500	0.0594
17	275.0	277.0	279.0	106585.	106691.	106798.	34.846	35.104	35.362	0.5672	0.5977	0.6282	0.0409	0.0505	0.0601
18	281.2	283.2	285.2	106551.	106658.	106765.	30.674	30.897	31.121	0.7227	0.7558	0.7889	0.0912	0.1000	0.1088
19	277.8	279.8	281.8	106818.	106925.	107031.	26.923	27.124	27.324	0.9953	1.0338	1.0723	0.1428	0.1509	0.1590
20	284.5	286.5	288.5	106618.	106725.	106831.	27.953	28.155	28.358	0.7983	0.8342	0.8700	0.1425	0.1505	0.1585
21	289.5	291.5	293.5	106618.	106725.	106831.	30.153	30.367	30.580	0.6863	0.7182	0.7502	0.0914	0.0999	0.1085

Table C-4 (cont'd.)

Test Series #2 (cont'd.)

22	294.5	296.5	298.5	106685.	106791.	106898.	32.945	33.174	33.403	0.5369	0.5652	0.5936	0.0408	0.0498	0.0588
23	283.9	285.9	287.9	106551.	106658.	106765.	28.703	28.911	29.118	0.7208	0.7559	0.7909	0.1419	0.1500	0.1581
24	288.4	290.4	292.4	106551.	106658.	106765.	29.158	29.366	29.574	0.8048	0.8379	0.8709	0.0916	0.1001	0.1086
25	292.5	294.5	296.5	106551.	106658.	106765.	31.986	32.210	32.435	0.6430	0.6723	0.7017	0.0396	0.0486	0.0577

TEST SERIES #3,4

TEST	TEMPERATURE (C)			PRESSURE (PA)			AIR DENSITY (MOLES)			EQUIVALENCE RATIO			STEAM MOLE FRACTION		
	LB	MP	UB	LB	MP	UB	LB	MP	UB	LB	MP	UB	LB	MP	UB
39	367.1	369.1	371.1	225113.	225803.	226492.	40.955	41.333	41.711	0.7862	0.8167	0.8472	0.2415	0.2483	0.2550
41	367.1	369.1	371.1	177539.	178229.	178918.	41.127	41.487	41.847	0.5829	0.6102	0.6374	0.0955	0.1033	0.1110
42	368.1	368.1	370.1	160509.	161199.	161888.	40.424	40.745	41.066	0.6253	0.6501	0.6750	0.0038	0.0038	0.0038
50	371.1	373.1	375.1	236007.	236696.	237386.	41.220	41.535	41.851	1.9618	1.9974	2.0329	0.0000	0.0000	0.0000
51	370.1	372.1	374.1	260380.	261069.	261759.	41.138	41.454	41.771	1.9369	1.9724	2.0078	0.0956	0.1026	0.1095
52	369.6	371.6	373.6	291716.	292406.	293095.	41.218	41.534	41.849	1.9350	1.9704	2.0057	0.1956	0.2018	0.2080
53	369.6	371.6	373.6	181952.	182641.	183331.	41.220	41.535	41.851	0.9826	1.0098	1.0369	0.0000	0.0000	0.0000
54	369.1	371.1	373.1	200568.	201257.	201947.	41.162	41.476	41.791	0.9765	1.0036	1.0306	0.0901	0.0972	0.1043
55	371.1	373.1	375.1	225940.	226630.	227319.	41.053	41.366	41.680	0.9812	1.0082	1.0353	0.1896	0.1960	0.2023
56	370.6	372.6	374.6	171127.	171817.	172506.	41.110	41.424	41.738	0.7830	0.8085	0.8339	0.0000	0.0000	0.0000
57	371.1	373.1	375.1	254416.	255105.	255795.	41.109	41.423	41.737	0.9781	1.0051	1.0322	0.2821	0.2877	0.2934
58	370.6	372.6	374.6	189536.	190226.	190915.	41.052	41.365	41.679	0.7857	0.8111	0.8366	0.0904	0.0975	0.1046
59	370.1	372.1	374.1	212151.	212840.	213530.	40.920	41.233	41.546	0.7930	0.8185	0.8440	0.1901	0.1965	0.2028
60	370.1	372.1	374.1	160234.	160923.	161613.	41.165	41.480	41.794	0.5820	0.6059	0.6297	0.0000	0.0000	0.0000
61	369.1	371.1	373.1	177746.	178436.	179125.	41.117	41.432	41.746	0.5955	0.6195	0.6435	0.0919	0.0990	0.1062
62	370.1	372.1	374.1	149547.	150236.	150926.	40.958	41.269	41.581	0.3990	0.4213	0.4437	0.0000	0.0000	0.0000
73	371.1	373.1	375.1	147961.	148650.	149340.	41.096	41.413	41.729	0.3526	0.3747	0.3967	0.0000	0.0000	0.0000
74	369.6	371.6	373.6	146996.	147685.	148375.	41.253	41.569	41.885	0.3355	0.3575	0.3794	0.0000	0.0000	0.0000
75	370.1	372.1	374.1	171265.	171955.	172644.	41.249	41.565	41.881	0.4713	0.4943	0.5173	0.0903	0.0975	0.1046
76	370.1	372.1	374.1	154649.	155338.	156028.	41.275	41.591	41.907	0.4751	0.4981	0.5212	0.0000	0.0000	0.0000
77	370.1	372.1	374.1	148995.	149685.	150374.	41.375	41.692	42.009	0.3606	0.3827	0.4048	0.0000	0.0000	0.0000
78	368.6	370.6	372.6	159958.	160647.	161337.	41.219	41.536	41.852	0.5848	0.6088	0.6327	0.0000	0.0000	0.0000
79	369.8	371.8	373.8	177539.	178229.	178918.	41.327	41.644	41.960	0.5779	0.6018	0.6256	0.0898	0.0970	0.1041
80	369.1	371.1	373.1	165887.	166577.	167266.	41.442	41.760	42.078	0.6738	0.6985	0.7232	0.0000	0.0000	0.0000

Table C-4 (cont'd.)

Test Series #3,4 (cont'd.)

81	370.3	372.3	374.3	195328.	196017.	196707.	41.328	41.645	41.961	0.6687	0.6932	0.7178	0.1446	0.1514	0.1581
82	369.6	371.6	373.6	176091.	176781.	177470.	41.275	41.591	41.908	0.8701	0.8964	0.9226	0.0000	0.0000	0.0000
83	371.3	373.3	375.3	238489.	239178.	239868.	41.175	41.490	41.804	0.8742	0.9003	0.9265	0.2566	0.2624	0.2683
84	370.3	372.3	374.3	181883.	182573.	183262.	41.308	41.625	41.941	0.9687	0.9957	1.0228	0.0000	0.0000	0.0000
85	370.9	372.9	374.9	216150.	216839.	217529.	41.295	41.611	41.928	0.9753	1.0024	1.0295	0.1495	0.1562	0.1628
86	370.5	372.5	374.5	209324.	210014.	210703.	41.331	41.647	41.963	1.4687	1.5000	1.5313	0.0000	0.0000	0.0000
87	372.3	374.3	376.3	258277.	258966.	259656.	41.209	41.523	41.837	0.9751	1.0021	1.0291	0.2892	0.2948	0.3004
88	370.3	372.3	374.3	290061.	290751.	291440.	41.298	41.613	41.929	2.9632	3.0077	3.0522	0.0000	0.0000	0.0000
89	372.3	374.3	376.3	250141.	250830.	251520.	41.098	41.412	41.726	0.8767	0.9028	0.9290	0.2903	0.2959	0.3015
90	372.0	374.0	376.0	204222.	204911.	205601.	41.285	41.599	41.914	0.6724	0.6969	0.7214	0.1792	0.1856	0.1921

TEST SERIES #5

TEST	TEMPERATURE (K)			PRESSURE (PA)			AIR DENSITY (MOLES)			EQUIVALENCE RATIO			STEAM MOLE FRACTION		
	LB	MP	UB	LB	MP	UB	LB	MP	UB	LB	MP	UB	LB	MP	UB
91	293.9	295.9	297.9	186089.	186778.	187468.	41.127	41.526	41.925	1.9329	1.9776	2.0223	0.0000	0.0000	0.0000
92	290.9	292.9	294.9	143273.	143962.	144652.	41.126	41.527	41.927	0.9771	1.0116	1.0461	0.0000	0.0000	0.0000
93	291.4	293.4	295.4	134654.	135344.	136033.	41.140	41.541	41.942	0.7714	0.8038	0.8361	0.0000	0.0000	0.0000
94	290.4	292.4	294.4	126036.	126725.	127415.	41.210	41.612	42.014	0.5733	0.6036	0.6340	0.0000	0.0000	0.0000
95	292.6	294.6	296.6	122037.	122726.	123416.	41.057	41.456	41.855	0.4719	0.5011	0.5303	0.0000	0.0000	0.0000
96	293.3	295.3	297.3	117762.	118452.	119141.	40.946	41.343	41.741	0.3709	0.3989	0.4270	0.0000	0.0000	0.0000

TEST SERIES #6

TEST	TEMPERATURE (K)			PRESSURE (PA)			AIR DENSITY (MOLES)			EQUIVALENCE RATIO			STEAM MOLE FRACTION		
	LB	MP	UB	LB	MP	UB	LB	MP	UB	LB	MP	UB	LB	MP	UB
46	285.6	287.6	289.6	100112.	100801.	101490.	34.554	34.932	35.309	0.4506	0.4807	0.5107	0.0043	0.0043	0.0043
47	321.1	323.1	325.1	100318.	101008.	101697.	30.625	30.988	31.352	0.4480	0.4788	0.5096	0.0050	0.0050	0.0050
48	371.1	373.1	375.1	100180.	100870.	101559.	26.815	27.080	27.346	0.4461	0.4701	0.4942	0.0030	0.0030	0.0030
49	370.1	372.1	374.1	100180.	100870.	101559.	26.830	27.096	27.362	0.4606	0.4848	0.5091	0.0000	0.0000	0.0000

Table C-4 (cont'd.)

TEST SERIES #7

TEST	TEMPERATURE (K)			PRESSURE (PA)			AIR DENSITY (MOLES)			EQUIVALENCE RATIO			STEAM MOLE FRACTION		
	LB	MP	UB	LB	MP	UB	LB	MP	UB	LB	MP	UB	LB	MP	UB
11	274.9	276.9	278.9	98595.	99284.	99974.	35.402	35.798	36.194	0.4480	0.4792	0.5103	0.0031	0.0031	0.0031
44	368.1	370.1	372.1	127001.	127690.	128380.	33.978	34.269	34.561	0.4618	0.4853	0.5087	0.0061	0.0061	0.0061
45	321.6	323.6	325.6	111212.	111902.	112591.	34.108	34.444	34.779	0.4468	0.4736	0.5003	0.0074	0.0074	0.0074

APPENDIX D

ESTIMATE OF UNCERTAINTY BOUNDS

The uncertainty bounds associated with four measured quantities, detonation cell width, detonation pressure, detonation velocity and thermodynamic state of the mixture will be discussed.

D.1 DETONATION CELL WIDTH

Obtaining detonation cell size (or width) data from a smoked foil still remains more of an art than a science, and hence, the uncertainty of the measurement is difficult to estimate. In fact, the long accepted postulate that there exists a single dominant mode, or detonation cell width, for a given fuel-air mixture has been recently questioned [D1]. A typical smoked foil record from a detonation in a H_2-air mixture is shown in Figure D-1. Casual observation shows a range or distribution of structure. If this range of structure is interpreted as representing a detonation with a single dominant mode that is continually being perturbed, then an estimator of the variability in size, or width, of that mode has some meaning. If the range of structure is interpreted as representing a detonation with multiple modes, or length scales, then a single variance estimator is meaningless.

The experiments conducted in this report were not intended to address the question of detonation cell width distributions. The currently accepted procedure, i.e., to select a single detonation cell width for a given mixture at a given initial thermodynamic state, is the approach taken for this report. The method of estimating the uncertainty associated with the procedure is discussed below.

D.1.1 Method of Estimating Detonation Cell Width

The method used to determine the detonation cell size is termed the dominant mode method [D2]. The method is illustrated in Figure D-1. Long-running parallel lines (relative to the spacing between the lines) are used to determine the dominant mode as in Figure D-1(b). Long parallel lines typically run three to ten times the spacing between the lines. Unfortunately, the lines are never perfectly parallel and appear to fade in and out (change in contrast) along their length. Therefore, experimenter judgement is used to determine what degree of parallelness and contrast in variation are acceptable in determining a long running line. Typically, the space between three or four parallel lines is measured for each foil and averaged to determine the most probable detonation cell width.

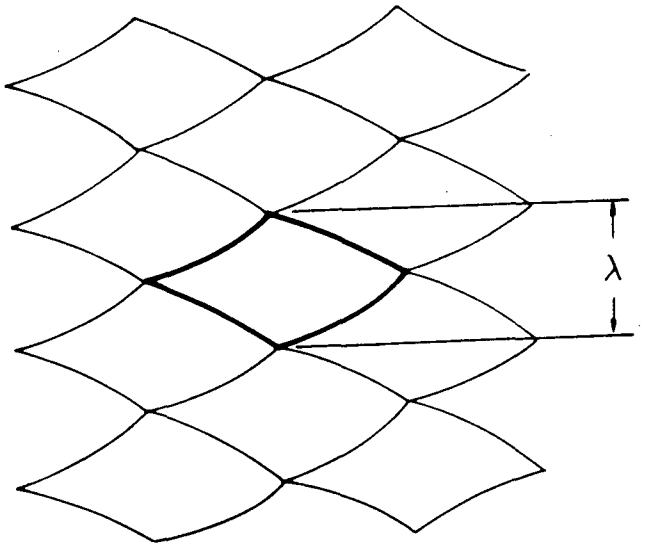

(a)

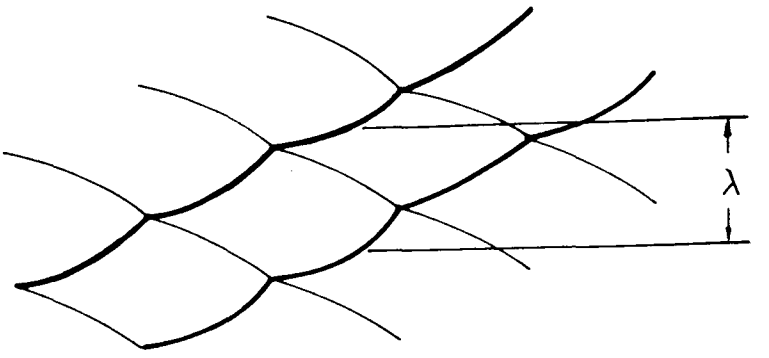

(b)

Figure D-1. Detonation Cell Width Measurement (a) Use of High Contrast Individual Cells, (b) Use of High Contrast Long Running Lines

Depending on how line length and contrast ratio are defined, and the relative weight given to each criterion, different values of detonation cell width can be selected. Since there is no fundamental physical reasoning which yields the proper balance of the two criteria, subjectivity is required. In other words, there is no a priori reason that a detonation cell width selected by one method over the other plays a more fundamental role in determining the propagation properties, or is more representative of the chemical-hydrodynamic coupling.

In general, one would expect that detonation cell width measurements would be more accurate for near-stoichiometric detonations where the cells are small compared to the size of the smoked foil. However, the advantage of a larger sample size is offset by lower contrast on the foil (due to weaker transverse structure) which makes the lines harder to distinguish. Because of these competing effects, it is not clear that detonation cell width can be more accurately measured for certain reactant concentrations than for others.

For the HDT tests, R. Knystautas of McGill University, Montreal, P.Q., Canada instructed the authors in his version of the dominant cell method. Because of the complexity of the pattern and the large change of length scales, the variability in line length and contrast is large over the spectrum of mixtures tested. For this reason it is not possible to assign quantitative values for the criteria used. Most of the smoked foil records have been independently reviewed by Benedick and Tieszen as discussed in the next section. Where multiple observers have reviewed a single foil, more than one detonation cell size is usually selected. In many cases, a range is selected because it is almost impossible to select a single value for detonation cell width. Heavy weight was given to the measurements made by R. Knystautas because of his experience in making detonation cell width measurements in many different laboratories.

To select a single value from a range of detonation cell widths, a technique commonly used by other researchers is used [D3]. In using this technique, the ranges of detonation cell width are plotted as part of a family of curves. Certain smoothness properties are assumed about the shape of the best fit curve that is drawn through the data. It is this "best fit line" which becomes the locus of detonation cell width values, called the "most probable" values in this appendix. Figures D-2 and D-3 show the range of data and the best fit line which yields the most probable detonation cell widths for test series #3 and #5.

The best fit line is established by appropriate weighting of two criteria. The first criterion is that, for a given test, a subjective confidence level is established for the data point by each individual. Individuals who independently review the foil may have low, medium, or high confidence in their ability to interpret the track spacing on the smoked foil based on their

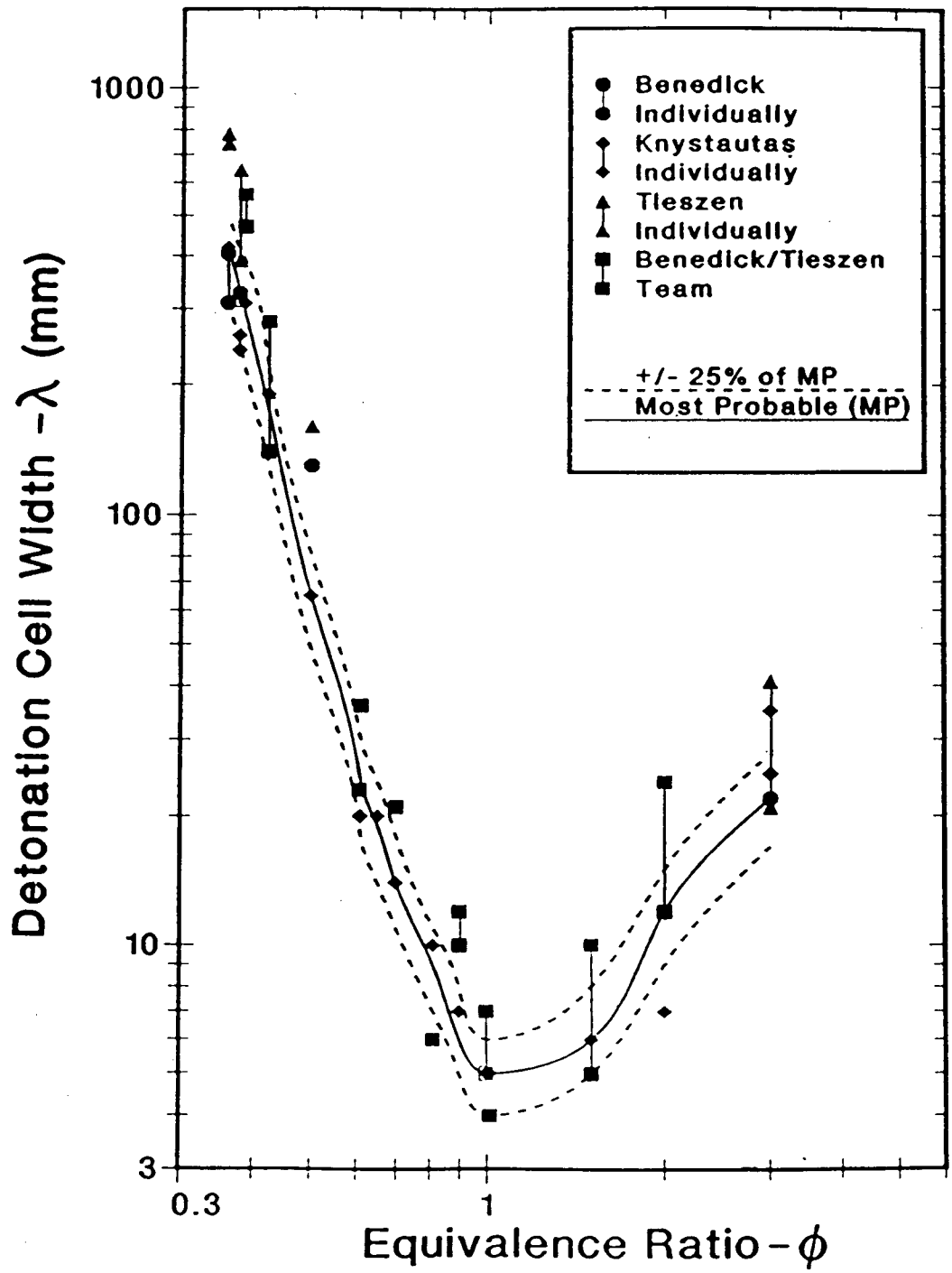

Figure D-2. Detonation Cell Width Measurements for HDT Test Series #3 (H_2-Air, ρ_{air} = 41.6 moles/m^3, T=100°C).

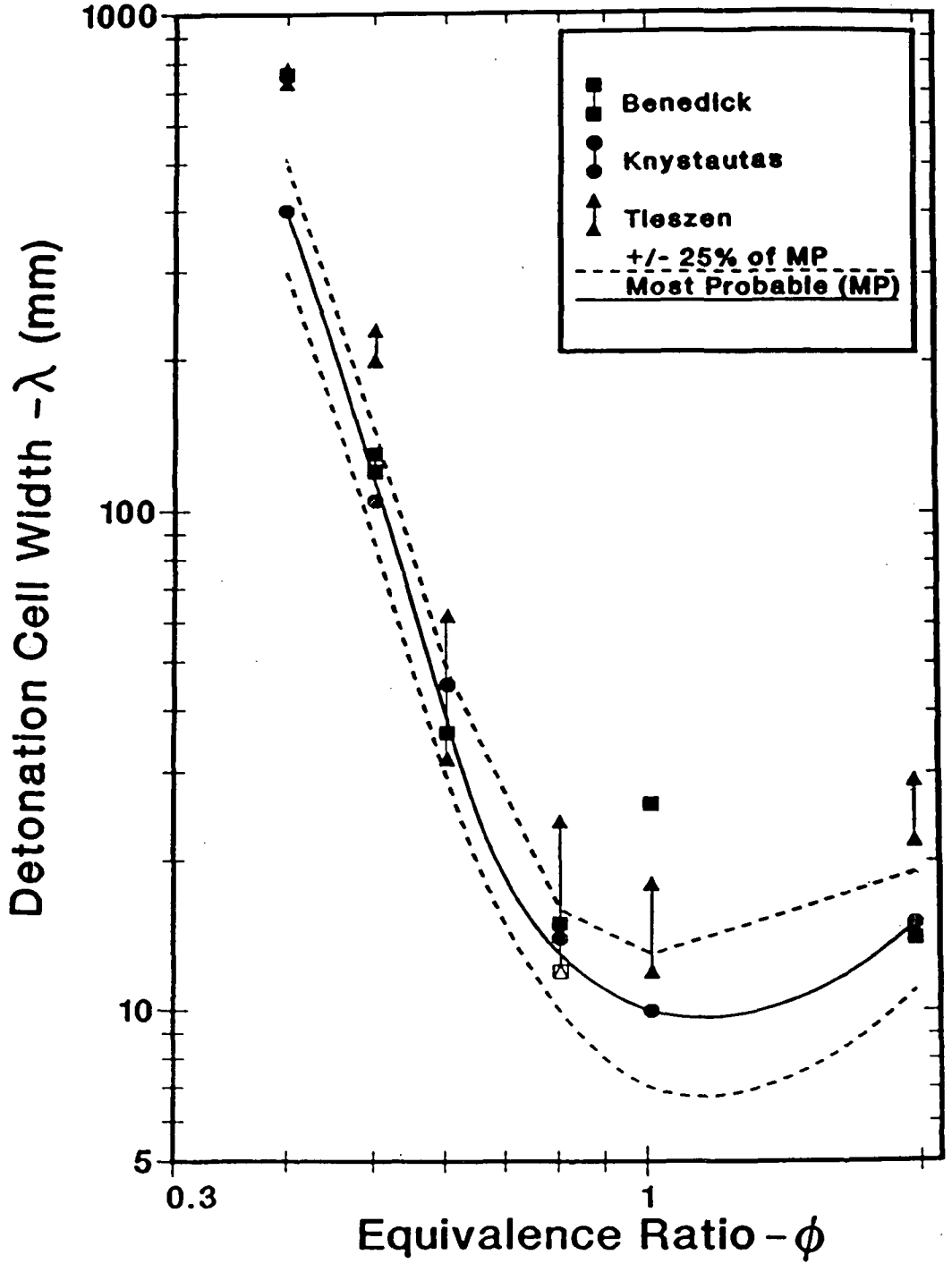

Figure D-3. Detonation Cell Width Measurements for HDT Test Series #5 (H_2-Air, ρ_{air} = 41.6 moles/m^3, T=20°C).

experience and the complexity of the pattern on the particular smoked foil. Additional weight was given to the estimates of R. Knystautas due to his experience.

The second criterion is that the functional dependence of detonation cell width on equivalence ratio is a smooth "U"-shape curve. The smoothness property can be stated as:

$$\frac{\partial^2 \lambda}{\partial \phi^2} \text{ is continuous and } > 0$$

For the case where $\phi < 1$, the gradient, $\partial\lambda/\partial\phi$, is negative and tends to zero. For the case where $\phi > 1$, the gradient is positive and for $\phi = 1$, the gradient is zero.

The application of the second criterion requires that data be examined as a whole while the first criterion examines each data point individually. Subjective judgement is then used to select the line through the data that best matches the two criterion. This is the method used to determine the most probable values of detonation cell width.

This technique can only be applied with confidence if there is a large number of points measured for a given family of curves, and if the range of data selected by independent observations for any one test is smaller than the differences between tests. Fortunately, detonation cell widths cover two to three orders of magnitude in the HDT. For those tests where it was subjectively felt that there was not enough data to justify a best fit function, weight was usually given to R. Knystautas's measurement. The exact criteria used for each test series is given in section D.1.3 following a discussion of uncertainty bounds.

D.1.2 Uncertainty Bounds for Detonation Cell Width Measurements

Establishing uncertainty bounds on the dominant mode detonation cell width is difficult because the definition of the dominant mode is subjective. As discussed above, in using the dominant mode method two criteria are applied (a) the length of parallel running bands and (b) the contrast ratio. Depending on the relative weight of these criteria different values of the dominant mode can be selected. Because of this reason, uncertainty bounds that consider both variability and bias are extremely difficult to establish.

One method of estimating the uncertainty bound is to assume that there is no bias error, i.e., the criteria used to select the detonation cell width is correct and consistently applied.

A single observer will probably give more self-consistent interpretations than will multiple observers because of bias.

Bounds obtained by this method are "relative" to the criteria used by the individual observer. They are useful for determining the significance of a change in detonation cell width as measured by a single observer. A different observer with a different bias may easily select detonation cell widths outside of the uncertainty bounds obtained by this method.

A bound estimator of detonation cell width that includes both variability and bias must be made with multiple observers making independent measurements. The multiple observers would use their individual criteria of line length and contrast ratio to determine the detonation cell width. This type of bound would be wider than that on a single observer because of the broader range of criteria application of the multiple observers. A bound determined by this method may be quite large and may hide real trends in the data simply because there is no accepted quantitative criteria available for the selection of detonation cell width.

However, in spite of the difficulties in establishing meaningful uncertainty bounds, the authors feel that some variability estimate is necessary to give safety analysts some qualitative "feel" for the uncertainties involved. Bounds will be estimated using a comparison between test apparatus, where the foil has been read by a single observer and by multiple observers of selected tests.

D.1.2.1 Comparison Between Test Apparatus

Figure D-4 shows a comparison between the detonation cell width measurements made for test series #1 where those measurements overlap the measurements at McGill University [D3]. The detonation cell width measurements in the HDT and at McGill University were made by R. Knystautas of McGill University. During test series #1, R. Knystautas instructed the authors in measuring detonation cell width. An uncertainty bound estimate of +/-25% of the McGill University data completely include the HDT data. The range of equivalence ratio in this comparison is not large, compared to the range covered in the HDT test series but the range of detonation cell width covered is a substantial fraction of the detonable range in the HDT, and as such, represents a fair comparison. This result suggests that relative bounds (i.e., neglecting bias error) can be estimated to be +/-25% of the data.

D.1.2.2 Multiple Observers

Figure D-5 shows the measured detonation cell width for all tests in the HDT where more than one individual measured the detonation cell width independently. The measured detonation cell width by the individual author has been divided by the measurement of R. Knystautas to normalize the data. For the dozen or so tests where R. Knystautas selected a range of detonation cell width, the center of the range was used to normalize

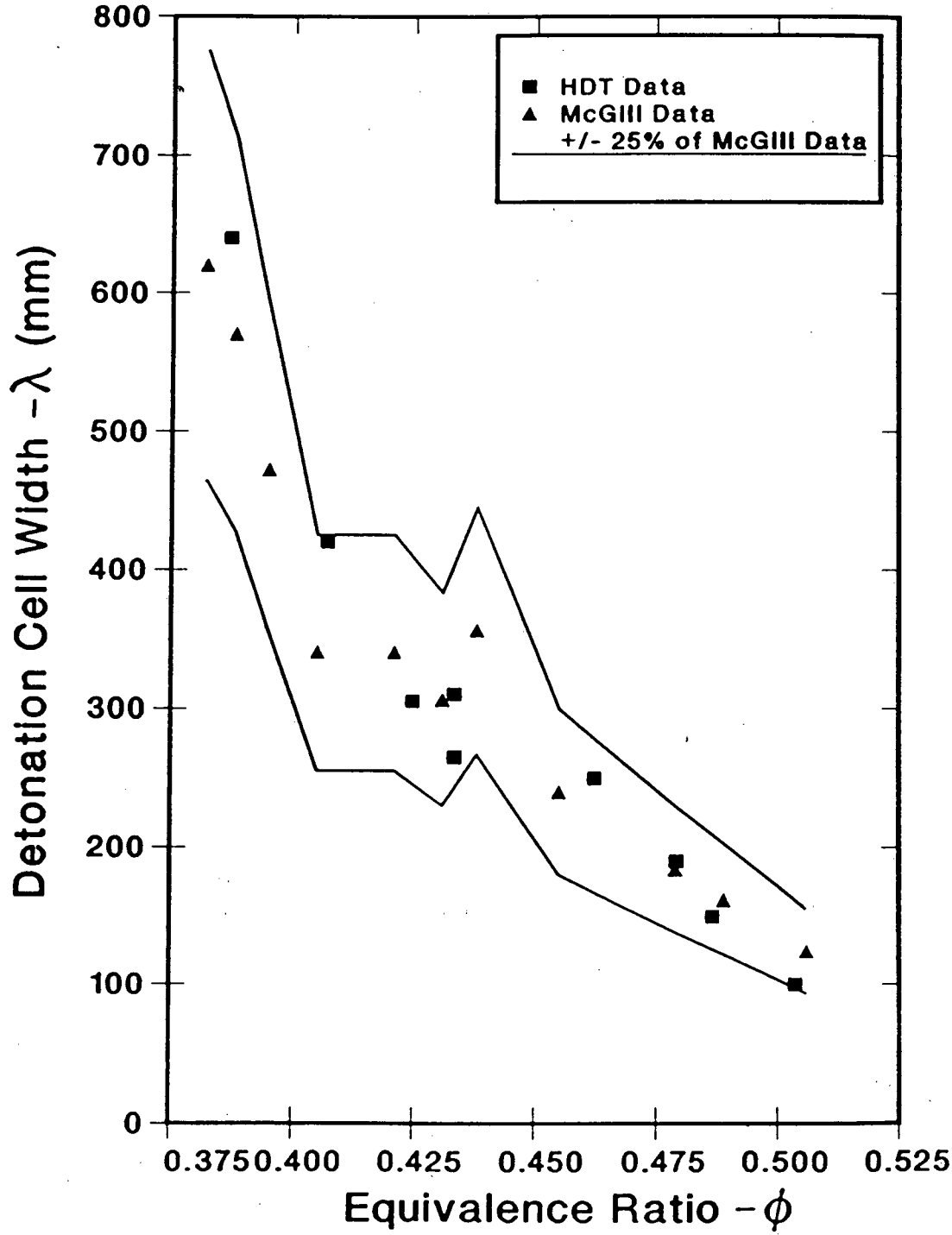

Figure D-4. Comparison of Detonation Cell Width Data Between the HDT and McGill University. (HDT Test Series #1, P=1 atm, T=25°C).

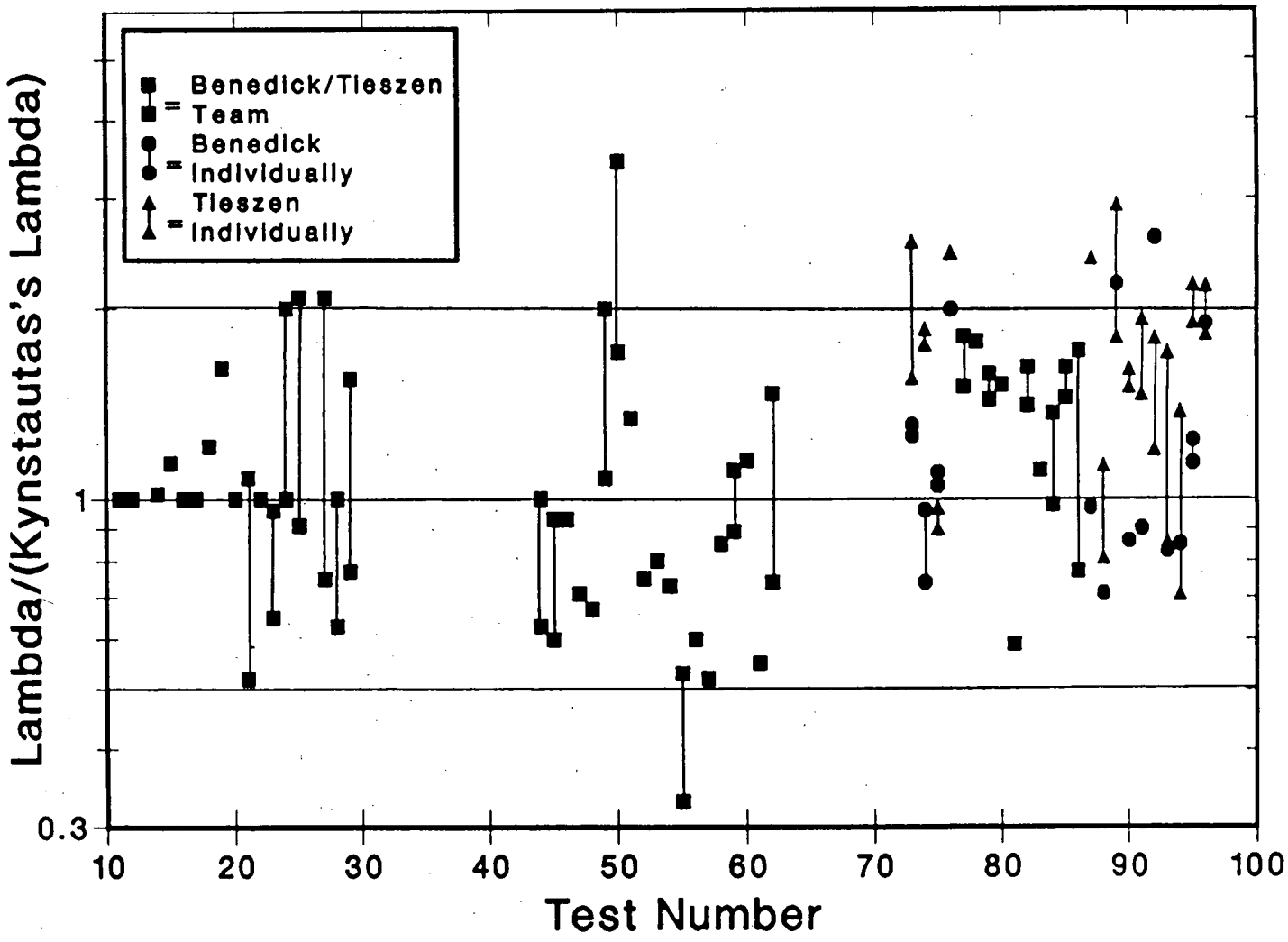

Figure D-5. Normalized Detonation Cell Width (λAuthor/λ Knystautas) vs. HDT Test Number.

the other individual's measurement. Where the individual selected a range, two symbols linked with a line are shown; where the individual selected a single detonation cell width only one symbol is shown. Often when a range is shown, the detonation cell width is not necessarily continuous across the range, but may appear to the individual to be in discrete subranges. This includes the cases where the individual decided the detonation was either one end of the range or the other.

As expected, the variability in the data is higher than that in the previous comparison between test apparatus where the smoked foils were measured by a single individual. The horizontal lines in Figure D-5 represent a factor of 2 of the normalized value. Most of the data only had two independent observations, R. Knystautas and a joint observation by S. Tieszen and W. Benedick, however, later tests had three independent measurements.

Some of the data haves been plotted in Figures D-2 and D-3 as a function of equivalence ratio. Relative bounds of +/-25% have been also been drawn. For the most part the +/-25% bounds cover the measurements made by R. Knystautas. In most instances, the measurements by S. Tieszen are higher than the values measured by the other individuals. This is an example of using different criteria to select detonation cell width. In informal discussion, it was found that S. Tieszen placed more emphasis on contrast than the other observers.

D.1.3 Bounds on the HDT Test Series

The numerical values for the estimated detonation cell widths (most probable, or MP values) and the corresponding estimates for the uncertainty bounds (LB and UB values) are listed in Appendix C by test series. The subjective judgement used to establish the most probable value of detonation cell width and the corresponding uncertainty bounds is described below.

For the first test series, the most probable values of detonation cell width is assumed to be the measured value of R. Knystautas, except for test HT-15 where Tieszen & Benedick's measurement is used. The uncertainty bounds are assumed to be +/-25% of the most probable value as in Figure D-4.

For test series #2, the most probable value of the detonation cell width is assumed to be the measured value of R. Knystautas, except for test HT-23 where the high end of the Tieszen & Benedick range is used. The uncertainty bounds are assumed to be +/-25% of the most probable value, or the range of individual measurements, whichever is larger.

For test series #3 and #4, the most probable value of the detonation cell width is assumed to be the value predicted by the best fit function (described in the last section) through the data. The uncertainty bounds are assumed to be +/-25% where the

data are "dense" and many tests are used to define the most probable curve, that is for $\phi \leq 1$ and $X_{H2O} \leq 0.1$. Elsewhere, if only one individual measured the smoked foil, then the bounds are assumed to be a factor of 2 of that reading. If more than one individual measured the foil, then the bounds are assumed to be +/-25% or the range of the individual measurements, whichever is larger. Data from test series #3 is shown in Figure D-2.

For test series #5, the most probable value of detonation cell width is assumed to be the value predicted by the best fit function through the data for $\phi \leq 1$ and the value measured by R. Knystautas for ϕ=2. The uncertainty bounds are assumed to be +/-25% where the data is relatively dense for $\phi \leq 1$, and the range of the individual measurements for ϕ=2. Data from test series #5 is shown in Figure D-3.

For test series #6 and #7, the most probable value of detonation cell width is assumed to be the value measured by R. Knystautas. The uncertainty bounds are assumed to be +/-25% or the range of the individual measurements, whichever is larger.

An emphasis has been placed on the +/-25% bounds for the detonation cell width in selecting the above criteria. The primary reason for emphasizing this criterion is that we feel that factor-of-2 bounds artificially hide real trends that exist in the data because there is no accepted way to select detonation cell size. However, for safety analysis, the authors strongly recommend that the factor-of-2 bounds be universally applied and that the detonation cell width (MP value) be divided by 2 for use in safety calculations. In some cases, this may be conservative and in other cases it may not be, but it is necessary to reduce the possible effect of observer bias.

D.2 DETONATION PRESSURE

Detonation pressure measurements are made with dynamic piezoelectric gages made by two companies, Kistler and PCB. The performance of the pressure gages to measure detonation pressure is rather erratic compared to values predicted by Chapman-Jouguet (C-J) values and, for this reason, pressures were not presented in the main text. From decades of research, the expected values of detonation pressure are 10 to 15% below those predicted by the C-J theory. In the HDT, typical measured pressure-peak deviations from the Chapman-Jouguet value are +/-20%. The sources of variability in the pressure measurements include the response time of the gages, digitizing frequency, calibration of the gages, excitation of the gages from the couplers, the effect of temperature, and vibration in the gage mount.

The face of each transducer is perpendicular to the direction of propagation of the detonation front. The gage faces are on the order of 2 mm in diameter. Since detonation cell width for stoichiometric H_2-air mixtures is on the order of 8 - 15 mm,

the transducers should be able to resolve the pressure distribution in a cell provided the rise time is sufficiently fast. The Chapman-Jouguet pressure is related to the average pressure in a cell and should easily be resolved.

Detonations in H_2-air mixtures propagate on the order of 2000 m/s. Since the transducer face is on the order of 2 mm, it takes about 1 μs to sweep the face of the transducer. The natural frequency of each type of transducer is quite high, 250 kHz for the Kistler and 500 kHz for the PCB. The rise time for each transducer is 1 μs. This rise time is fast enough to respond to the peak pressure averaged over the face of the transducer. The signals from the transducers are recorded on Textronix 7612D and BI RA digitizers. The digitizing rate on the 7612D's depended on the test, either 10 μs or 1 μs per point (see Table A-5) while the BI RA digitizers were fixed at 25 μs per point. The data digitized at 1 μs are sufficient to resolve the peak pressure averaged over the face of the transducer, and hence, the average pressure in a cell.

In addition to the standard uncertainty in the linearity and hysteresis of a gage, which are given by the manufacturer as <+/-1%, its calibration is sensitive to the input voltage provided to the gage by the couplers and the surrounding temperature. Sandia calibrations indicate that the manufacturers' estimates of linearity and hysteresis is good. However, during testing, the voltage supplied by the couplers was never recorded. Kistler indicates that their gages have a 0.5%/volt sensitivity. The PCB is assumed to have the same sensitivity. Voltage readings taken at random times during the testing, to verify that the batteries in the couplers were not too weak, indicated that the voltage ranged from 21V to 27V. Therefore, the calibration may be in error by 3% due to voltage supply.

The effect of temperature on each type of gage is different. On Kistler gages the sensitivity is -0.03%/°F and on PCB gages the sensitivity is +0.01%/°F. The temperature of the gages is assumed to be 100°C but the electronics in the back of the gages which are also temperature sensitive may be at a different temperature. The calibrations used in assigning engineering units to data plots have not taken the effect of the gage temperature into account; however plots from the BI RA data clearly show a negative drift for the Kistler gages and a positive drift for the PCB gages over a period of milliseconds for gages where the RTV face had decayed. It is assumed that data taken over the period of microseconds after the arrival of the detonation front are unaffected by temperature.

The combined effect of linearity, low voltage and hysteresis do not explain differences of +/-20% from the Chapman-Jouguet values. Typical pressure traces from PCB and Kistler transducers for tests with large and small cell width are shown in Figs. D-6 through D-9. It is obvious from the figures that there are large oscillations on the recorded pressure traces. These oscillations

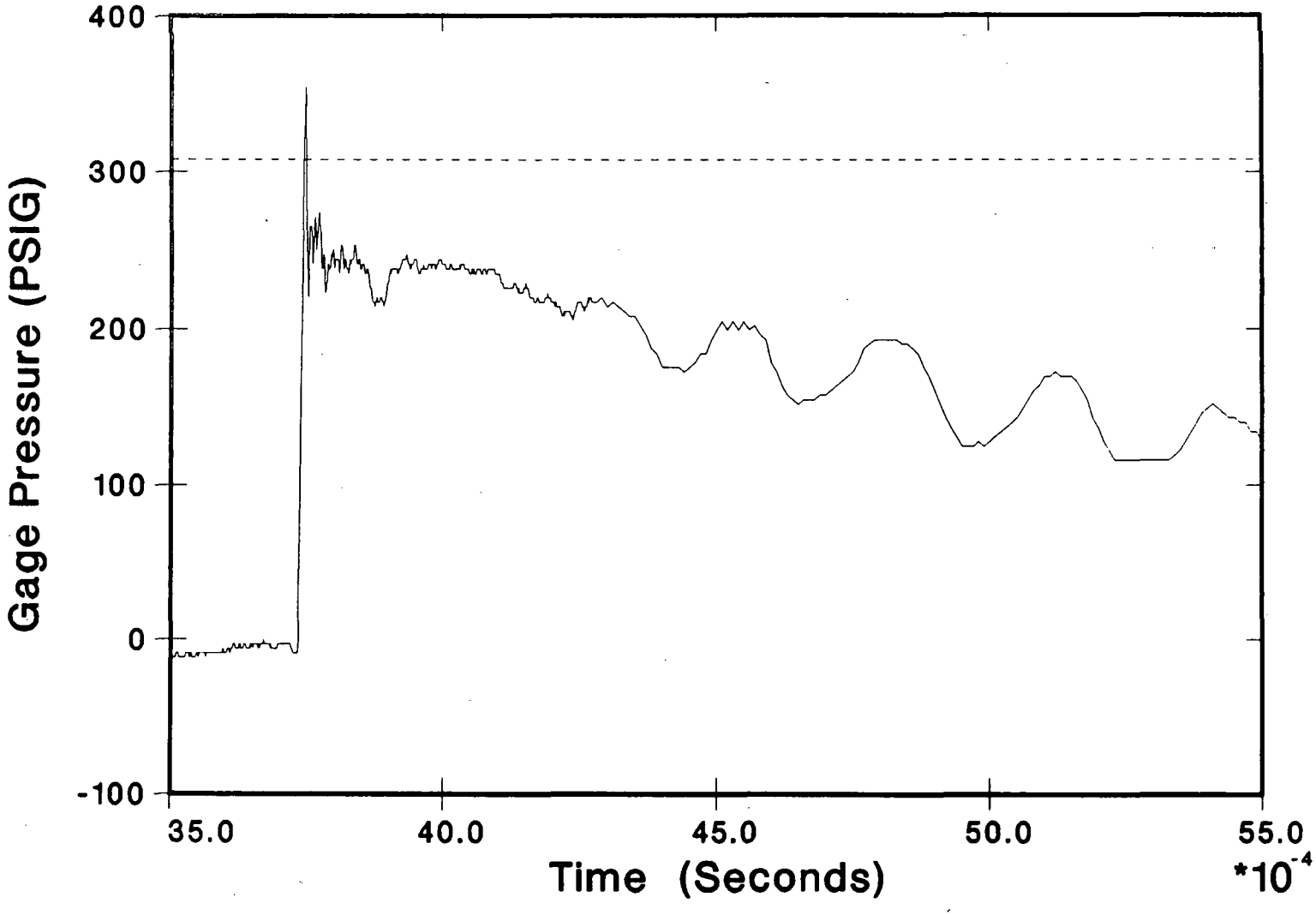

Figure D-6. Typical PCB Pressure Trace - Small Cell Width (λ = 5 mm, Test HT-84).

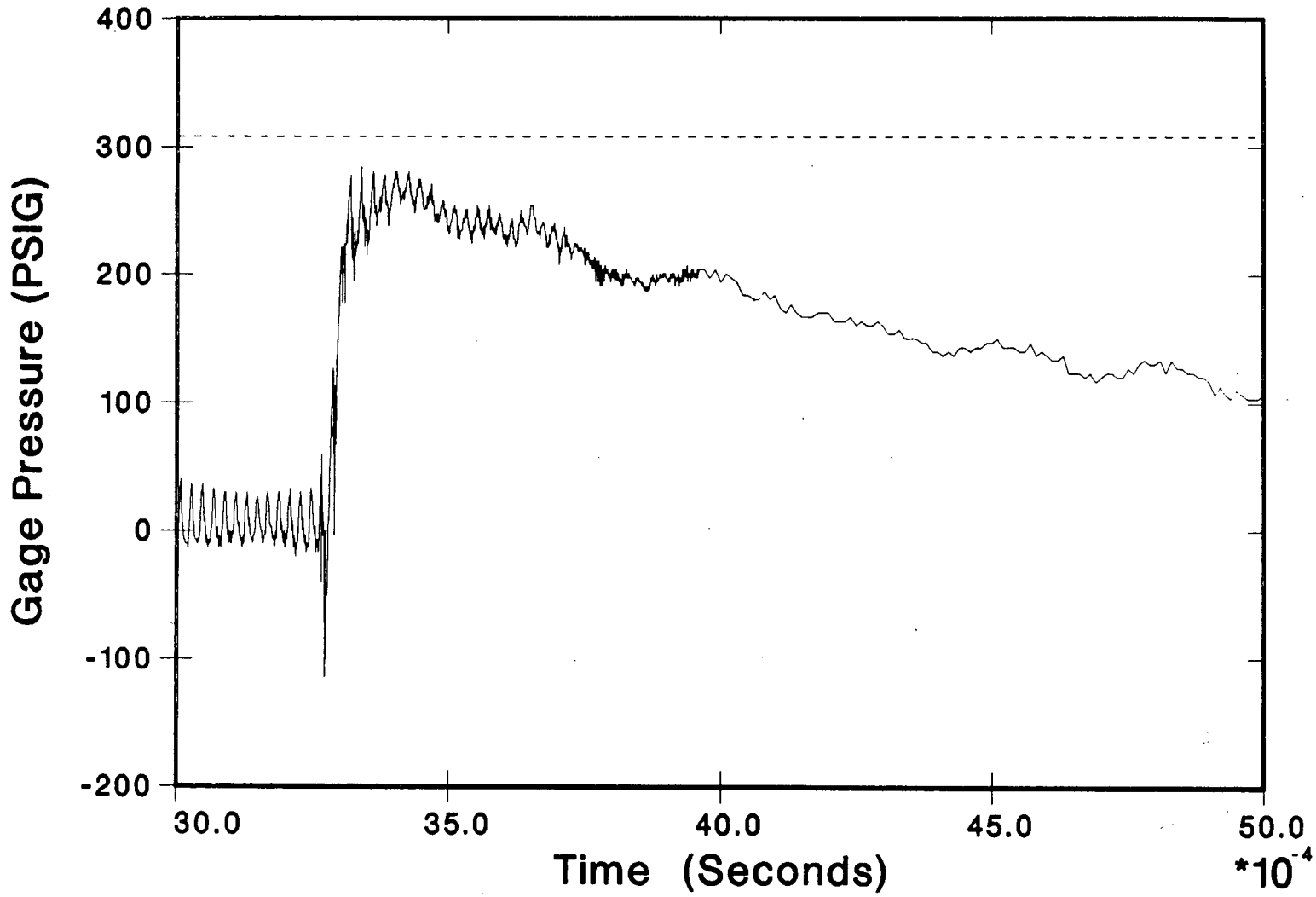

Figure D-7. Typical Kistler Pressure Trace - Small Cell Width
(λ = 5 mm, Test HT-84)

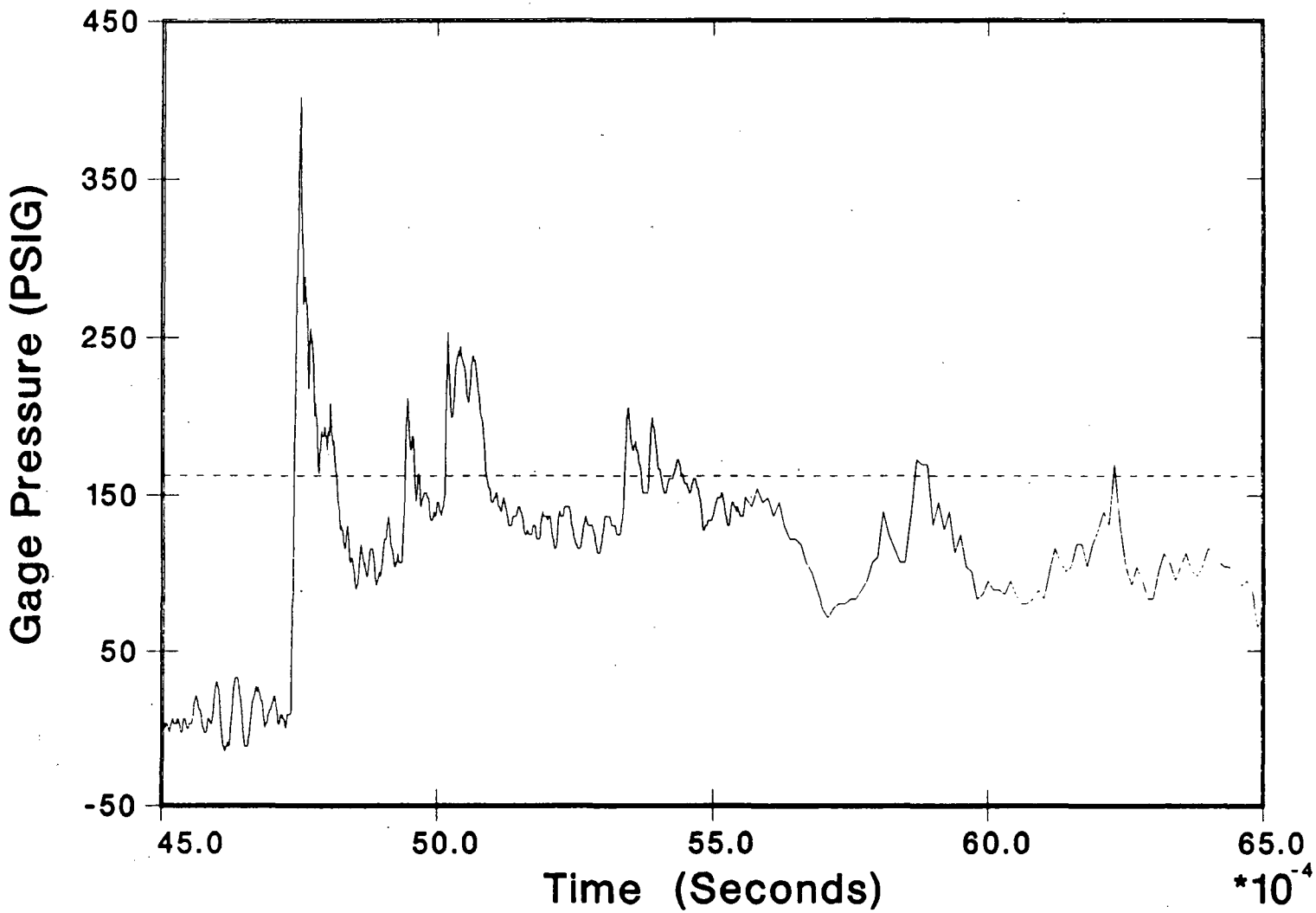

Figure D-8. Typical PCB Pressure Trace - Large Cell Width (λ = 400 mm, Test HT-96).

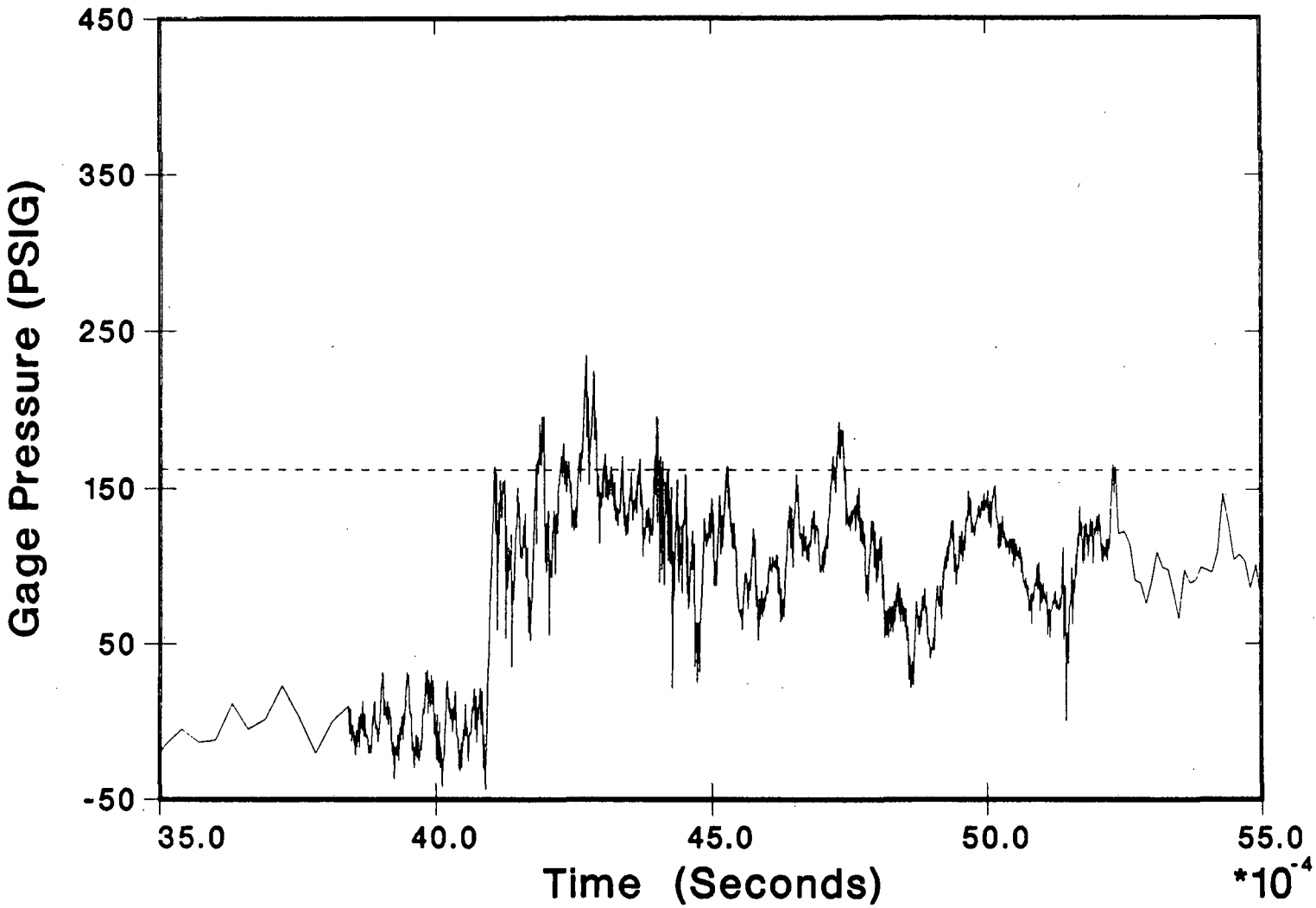

Figure D-9. Typical Kistler Pressure Trace - Large Cell Width (λ = 400 mm, Test HT-96).

can be attributed to the transverse waves in the three-dimensional detonation structure. However, the oscillations begin before the arrival of the pressure peak; therefore, the most probable source of the oscillations is vibration of the gage mount due to radial vibrations in the tube caused by the detonation. Because these oscillations can be +/-50% of the signal level, it was felt that spectral analysis would not completely separate the noise from the transverse wave structure.

Further, a comparison of the PCB and Kistler data shows that the PCB indicates a very large "overshoot." The overshoot can be explained as the von Neumann spike; however, the Kistler gages for the same test do not show this spike. Therefore, the most probable source for this overshoot is loading of the quartz gage face by the internal mount.

Because of the high degree of noise in the pressure data and the possible large variations from the Chapman-Jouguet value which can not be explained by standard calibration uncertainties, the peak pressure data taken during the tests are not reported.

D.3 DETONATION VELOCITY

Detonation velocity is determined by taking the time of arrival of the detonation as determined by the initial break in slope of the pressure transducer data divided by the distance of the transducer from a reference point. The variability of velocity measurements arises from the uncertainty in the location of the transducers, the digitizing frequency and the resolution of the break in slope on the data plots. The type, number and digitizing frequency of the transducers for each test is given in Table A-5 of Appendix A. Two types of recording devices were used. Both are discussed in Appendix A. One type is called CAMAC and the other is made by Tektronix (7612D).

The variability associated with determining detonation velocity from a single transducer is reduced by taking a linear regression of all time of arrival vs. distance data. For the analysis in this report, the independent variable was taken to be the location of the transducer and the dependent variable was taken to be the time of arrival. The slope of the linear regression line is the reciprocal of the detonation velocity. A standard deviation is calculated for the reciprocal of the detonation velocity and 95% confidence bounds are calculated using a standard statistical procedure. The calculations were made using a procedure from the SAS library [D4].

In the above analysis, the detonation velocity was assumed to be constant along the entire length of the tube, which it is not. Since the detonation is started from a high explosive charge, the detonation velocity is overdriven at the start. Constant detonation velocity indicates a steady-state wave has been reached. In test HT-11 through 72 the closest pressure

transducer to the explosive initiator was placed no closer than 1.3 m from the explosive. In tests HT-73 through 96 more pressure records were taken and the first transducer was located 0.749 m from the explosive and the second transducer was located 2.273 m from the explosive.

The latter data were used to establish that the detonation had reached steady state by 2.273 m from the explosive. A linear regression fit to the data from each test was made for six cases. Two different amounts of explosive were used to initiate the charge, nominally 40 grams and 80 grams. For each of these charge weights, three cases were considered. The first case used all the data including the data from the transducer at 0.749 m. The second case used all the transducer data except from the transducer 0.749 m from the explosive, and the third case used all the data except for the transducers at 0.749 m and 2.273 m from the explosive. The first transducer data used in the second (third) case came from the port located at 2.273 m (4.407 m) from the explosive.

Differences were taken of the detonation velocity between cases #1 and #2, and between #2 and #3 for each of the charge weights. The results are summarized in Table D-1. The difference in detonation velocity between cases #1 and #2 of 6.1 m/s

Table D-1

Effect of Initial Transient on Detonation Velocity

Initiation Charge Weight grams)	Case	Mean Difference in Velocity (m/sec)	STD Error of the Mean Diff. (m/s)
80	DIFF1	6.1	3.1
80	DIFF2	2.5	2.7
40	DIFF1	2.4	1.1
40	DIFF2	-0.17	1.6

DIFF1 ≡ Detonation velocity calculated with all data minus detonation velocity with all data except for the first transducer at 0.749 m from the initiator.

DIFF2 ≡ Detonation velocity calculated with all data except for the first transducer at 0.749 m from the initiator minus the detonation velocity with all data except the first two transducers at 0.749 m and 2.273 m from the initiator, respectively.

for the 80 gram initiating charge and 2.4 m/s for the 40 gram initiating charge show that the detonation had a higher velocity at the first transducer, located 0.749 m from the initiating charge, than at the remaining downstream transducers. These differences are judged to be significantly different from zero. The difference in detonation velocity between cases #2 and #3 of 2.5 m/s for the 80-gram initiating charge and -0.17 m/s for the 40-gram initiating charge are judged not to be significantly greater than zero. These results indicate that the estimated velocity is statistically the same whether the data from the second pressure transducer at 2.27 m from the initiator is included or excluded from the linear regression. Therefore, the detonation has reached steady state by 2.27 m from the initiator.

Table D-2 lists the upper and lower bounds for the velocity data for each test. These bounds are the the reciprocal of the confidence bounds calculated for the reciprocal of the velocity. Only data 2.273 m or farther from the explosive are used in the table.

The data from the Tektronix 7612D's almost always have smaller uncertainty bounds due to the higher digitizing frequency. Therefore, the data from the 7612D's were used when available. In some instances, no 7612D data was available; in these cases, the CAMAC data was used. The data with bounds are listed by Test Series in Appendix C.

D.4 THERMODYNAMIC STATE

Six variables are used in this report to specify the initial thermodynamic state of the gaseous mixtures. The six variables are: the temperature prior to initiation of detonation, T; the density of the air in the mixture, ρ_{air}; pressure prior to initiation of the detonation, P; the equivalence ratio, ϕ; the mole fraction of steam, X_{H2O}; and the mole fraction of carbon dioxide, X_{CO2}. For binary H_2-air mixtures only three thermodynamic variables are required to specify the initial state. For ternary H_2-air-H_2O, or H_2-air-CO_2 mixtures four variables are needed to specify the initial state. The variables chosen for each test series is listed in Table D-3.

Of the six variables used to specify the initial thermodynamic state of the mixtures, only two, the temperature and pressure prior to initiation of detonation, are measured directly. The other variables are inferred from temperature and pressure measurements. The relationships between various thermodynamic variables are derived in Appendix E. Table D-4 lists the temperature and pressure measurements made for each test and defines a numbered subscript for each measurement.

Table D-2

Upper and Lower Bounds on the Detonation Velocity (km/sec)

	7612				CAMAC			
Test	Sample size	Lower bnd.	Vel. est.	Upper bnd.	Sample size	Lower bnd.	Vel. est.	Upper bnd.
11	4	1.5314	1.5879	1.6488	4	1.5099	1.5756	1.6473
12	4	1.5073	1.5287	1.5507	5	1.5074	1.5261	1.5453
13	5	0.7918	0.8478	0.9123	5	0.7962	0.8506	0.9130
14	5	1.3707	1.4523	1.5443	5	1.3242	1.4434	1.5863
15	5	1.3964	1.4103	1.4245	5	1.3953	1.4178	1.4411
16	5	1.4533	1.4766	1.5007	5	1.4590	1.4716	1.4844
17	5	1.6040	1.6321	1.6612	5	1.6028	1.6322	1.6627
18	5	1.6057	1.6437	1.6836	4	1.6076	1.6603	1.7165
19	5	1.6708	1.6845	1.6985	4	1.5633	1.6707	1.7939
20	5	1.5571	1.5949	1.6347	5	1.5995	1.6226	1.6463
21	5	1.6085	1.6156	1.6228	5	1.6078	1.6098	1.6118
22	5	1.5299	1.5682	1.6086	5	1.5421	1.5606	1.5796
23	5	1.5219	1.5567	1.5931	5	1.5288	1.5606	1.5936
24	5	1.6980	1.7115	1.7252	5	1.6745	1.7032	1.7329
25	5	1.6659	1.6969	1.7290	4	1.6171	1.6759	1.7391
26	5	1.9085	1.9291	1.9500	5	1.8657	1.9274	1.9933
28	5	1.8325	1.8468	1.8614	5	1.8249	1.8494	1.8745
29	4	1.5850	1.6009	1.6172	3	1.2853	1.5961	2.1050
31	4	1.8357	1.8492	1.8628	4	1.6286	1.8070	2.0292
33	4	1.9743	1.9833	1.9924	4	1.9460	1.9943	2.0450
36	5	1.7868	1.7993	1.8119	5	1.7779	1.8173	1.8585
37	4	1.7285	1.7645	1.8021	.	.	.	.
38	.	.	.	.	5	1.7388	1.7779	1.8188
39	5	1.7129	1.7305	1.7484	5	1.7143	1.7322	1.7505
40	5	0.7797	0.8351	0.8989	5	0.7783	0.8358	0.9024
41	4	1.6607	1.6672	1.6737	4	1.6403	1.7077	1.7809
42	5	1.7327	1.7491	1.7658	5	1.7294	1.7361	1.7429
43	5	1.6148	1.6198	1.6250	5	1.6031	1.6358	1.6698
44	5	1.5847	1.5955	1.6065	5	1.5583	1.5910	1.6252
45	5	1.5850	1.5905	1.5961	5	1.5795	1.5879	1.5963
46	3	1.5819	1.5885	1.5950	3	1.5524	1.5993	1.6492
47	5	1.5748	1.5854	1.5961	5	1.5783	1.5975	1.6170
48	4	1.5715	1.5776	1.5838	4	1.5381	1.5654	1.5937
49	5	1.5903	1.5988	1.6073	5	1.5656	1.6395	1.7207
50	5	2.1375	2.1555	2.1738	5	2.1414	2.1619	2.1828
51	4	2.0179	2.0542	2.0919	4	1.9273	2.0285	2.1409
52	5	1.9349	1.9549	1.9752	5	1.9352	1.9529	1.9709
53	4	1.9585	1.9865	2.0153	4	1.9028	1.9803	2.0643
54	4	1.9112	1.9303	1.9498	4	1.8880	1.9425	2.0002

Table D-2 (cont'd.)

Upper and Lower Bounds on the Detonation Velocity (km/sec)

	7612				CAMAC			
Test	Sample size	Lower bnd.	Vel. est.	Upper bnd.	Sample size	Lower bnd.	Vel. est.	Upper bnd.
55	4	1.8099	1.8497	1.8914	4	1.8061	1.8419	1.8793
56	5	1.8688	1.8787	1.8886	5	1.8630	1.8750	1.8871
57	5	1.7563	1.7787	1.8016	5	1.7267	1.7663	1.8078
58	5	1.8212	1.8306	1.8401	5	1.8221	1.8331	1.8442
59	5	1.7409	1.7521	1.7634	5	1.7240	1.7543	1.7857
60	5	1.6954	1.7255	1.7566	5	1.6894	1.7283	1.7690
61	5	1.5986	1.6653	1.7378	5	1.6032	1.6454	1.6900
62	5	1.4996	1.5160	1.5327	5	1.4955	1.5062	1.5171
63	5	1.6487	1.6539	1.6591	5	1.5867	1.6223	1.6596
64	5	1.5896	1.6099	1.6307	5	1.5788	1.5911	1.6036
65	5	1.5707	1.5749	1.5791	5	1.5261	1.5702	1.6170
66	4	1.5007	1.5447	1.5914	4	1.4554	1.5154	1.5805
67	5	1.4516	1.4758	1.5009	5	1.4372	1.4633	1.4905
68	5	1.5040	1.5086	1.5131	5	1.5063	1.5231	1.5404
69	5	1.5307	1.5496	1.5690	5	1.5126	1.5434	1.5755
70	5	2.2435	2.2610	2.2788	5	2.1766	2.2267	2.2793
71	5	2.2091	2.2757	2.3464	5	2.2457	2.2764	2.3079
72	6	2.2281	2.2782	2.3305	5	2.2332	2.2757	2.3198
73	2	.	1.5056	.	4	1.4113	1.5121	1.6284
74	2	.	1.4300	.	7	1.3939	1.4252	1.4580
75	2	.	1.5520	.	7	1.5297	1.5408	1.5520
76	2	.	1.6354	.	7	1.5851	1.6052	1.6259
77	2	.	1.4881	.	7	1.4687	1.4792	1.4898
78	.	.	.	.	6	1.6904	1.7071	1.7242
79	4	1.6490	1.6586	1.6683	8	1.6468	1.6586	1.6706
80	4	1.7751	1.8070	1.8399	8	1.7892	1.8028	1.8165
81	5	1.7029	1.7144	1.7261	7	1.7018	1.7080	1.7141
82	6	1.9418	1.9507	1.9596	8	1.9219	1.9394	1.9572
83	5	1.7350	1.7671	1.8003	7	1.7398	1.7486	1.7574
84	5	1.9767	1.9898	2.0032	7	1.9720	1.9843	1.9966
85	6	1.8734	1.8857	1.8983	8	1.8610	1.8828	1.9052
86	6	2.0816	2.0943	2.1071	8	2.0878	2.1039	2.1202
87	5	1.7711	1.7829	1.7948	7	1.7683	1.7719	1.7755
88	5	2.2259	2.2406	2.2555	7	2.2275	2.2351	2.2427
89	6	1.7045	1.7146	1.7248	8	1.6850	1.7008	1.7169
90	3	1.5947	1.6821	1.7798	6	1.6649	1.6681	1.6712
91	4	2.1520	2.1632	2.1746	7	2.1170	2.1555	2.1953
92	5	1.9771	1.9879	1.9989	8	1.9758	1.9904	2.0053
93	5	1.8894	1.9182	1.9480	8	1.8793	1.8938	1.9086
94	5	1.7162	1.7292	1.7424	8	1.7057	1.7174	1.7294
95	5	1.6178	1.6254	1.6331	8	1.6111	1.6184	1.6257
96	5	1.4799	1.4976	1.5158	8	1.4882	1.4943	1.5005

Table D-3

Variables chosen to Specify the
Initial Thermodynamic State of the Mixture

Test Series	Variables
1	ϕ, T, P
2	ϕ, X_{CO2}, T, P
3	ϕ, T, ρ_{air}
4	$\phi, X_{H2O}, T, \rho_{air}$
5	ϕ, T, ρ_{air}
6	X_{H2}, T, P
7	X_{H2}, T, ρ_{air}

Table D-4

Measured Variables

Variables Measured	For CO_2 tests, variable measured for	For all other tests, variable measured for
T_0, P_0	Ambient Air	Ambient Air
T_1, P_1	Air only in HDT	Air only in HDT
T_2, P_2	CO_2-Air in HDT	H_2-air in HDT
T_3, P_3	H_2-CO_2-Air in HDT	H_2O-H_2-air in HDT
T_4, P_4	Prior to initiation	Prior to initiation

The technique used to establish uncertainty bounds for the reported variables is referred to as "Single Sample Uncertainty Analysis" [D5,D6]. The technique is used to estimate uncertainty bounds for test data where no repeat tests were conducted. The technique consists of the following procedures: The first step is to estimate the standard deviation of the measured variables, in this case the appropriate temperatures and pressures. The estimate is made by engineering judgement based on prior performance and calibration data. Next a Taylor series expansion is made of the relationship between the inferred (dependent) variables, such as equivalence ratio, and the measured (independent) temperature and pressure variables. The first term of the expansion is retained. An estimate of the variance of the inferred variable is the sum of the variances of the measured variables times the square of the gradient of the measured variable with respect to the inferred variable, i.e.:

given an inferred variable, V, that is a function, g, of the measured variables, X_i, or,

$$V=g(X_1,X_2, \ldots ,X_N) \tag{D-1}$$

then the mean of V is approximated by,

$$\mu_V = g(\mu_1,\mu_2, \ldots ,\mu_N) \tag{D-2}$$

and the variance of V is approximated by,

$$\sigma_g^2 \simeq \sigma_{X_1}^2 \left(\frac{\partial g}{\partial X_1} \Big| \mu_1,\mu_2,\ldots,\mu_N \right)^2 + \ldots + \sigma_{X_N}^2 \left(\frac{\partial g}{\partial X_N} \Big| \mu_1,\mu_2,\ldots,\mu_N \right)^2 \tag{D-3}$$

Upper and lower bound estimates are established on the six initial thermodynamic state variables and are calculated to be twice the standard deviation of the variable, i.e. an estimate of 2σ limits.

In single sample uncertainty, the estimator, $\bar{X}_i$, of the mean of each of the measured variables μ_i, is taken to be the actual measurement of the variable. Thus, the estimated mean is based on a sample size of one. For example, the mean value of temperature, μ_T, is estimated to be the actual temperature measurement, T. The estimator, s_i^2, of the variance of each of the measured variables, σ_i^2, is determined by engineering judgement of the accuracy of measurement.

D.4.1 Variance Estimates for Measured Variables

The measured thermodynamic variables for each test are the temperature and pressure of the mixture after the addition of

each component gas. The measurements are point measurements taken to reflect the average value in the gas volume. The variability in each of these measurements arise from the variability in the measurement itself and the uniformity and time variability of the mixture. Table D-5 summarizes the temperature and pressure standard deviation estimates. These estimates are based on engineering judgement which is discussed below.

Table D-5

Summary of
Standard Deviation Estimates of Measured Variables
(Using Engineering Judgement)

Test Series	Tests	δT (°C)	δP (psi)	$\delta(\Delta P)$ (psi)
1	11-15	1	0.008	0.005
	63-72	1	0.05	0.025
2	All	1	0.008	0.005
3	All	1	0.05	0.025
4	All	1	0.05	0.025
5	All	1	0.05	0.025
6	All	1	0.05	0.025
7	11	1	0.008	0.005
	44,45	1	0.05	0.025

D.4.1.1 Temperature Standard Deviation Estimate

The temperature measurement device and recorder for each test is listed in Table A-2, 3 in Appendix A. Early tests used an average of the surface temperature measurements made by the thermocouples used to control the temperature of the tube. The thermocouple tips were calibrated using ice and boiling point temperatures, but the electronic reference junctions were not calibrated. Sixteen thermocouples use a Kinetics Corp. Model 1991 reference junction while 32 thermocouples terminate in a Sandia designed, temperature monitored, constant temperature block. The discrepancy between readings of nominally the same temperature are on the order of 1°C.

After test HT19, a K-type ungrounded tip thermocouple in a 3 mm (1/8 in) sheath was used to measure the gas temperature. The thermocouple was inserted through the Heated Detonation Tube wall in port 6 and protruded only 3 mm (1/8 in) to prevent the

detonation from destroying the tip. At this depth, the thermocouple is subject to conduction effects from the tube wall. This influence is assumed to be minimal because the temperature is uniform in the tube wall and steady state is reached before the temperature measurement is taken. After test HT73, the thermocouple was inserted farther into the tube to a depth of approximately 2.5 cm (1 in). The fitting was removed after test HT96 and the thermocouple was found to be bent at the fitting in a 45° angle due to the pressure loading of the detonation wave. It can not be determined if the strain induced by the bend affected the calibration of the thermocouple.

For tests HT19 to HT79, the reference junction for the thermocouple was a Fluke Model 8024B Handheld DMM with a reference junction for a K-type thermocouple. The manufacturer's uncertainty estimate for the device is +/-3°C with a resolution of +/-1°C. After test HT79, the reference junction used is a Digitec model 2831. The manufacturer's uncertainty is +/-0.3°C with a resolution of +/-0.1°C.

The thermocouple and reference junctions were not calibrated prior to testing. An ice point and boiling point calibration was conducted after test HT96. Using the Fluke reference, the reading alternated between 0 and 1°C for the ice point and read 96°C at the boiling point (95.0°C at the time the calibration was taken). Using the Digitec reference, the ice point reading was 0.2°C and the boiling point reading was 95.6°C. No attempt was made to correct the data for the fixed error, and no estimate of thermocouple aging can be made.

Comparison of the average temperature of the thermocouples used to control the tube temperature and the thermocouple used to measure the gas temperature showed a variation of +/-1°C. Based on this information and the post test calibration, a reasonable estimate of the standard deviation is +/-1°C for each temperature measurement in each test.

D.4.1.2 Pressure Standard Deviation Estimate

The pressure gage(s) used to record the predetonation gas pressure are listed in Tables A-2, 3 in Appendix A. For tests prior to test HT31, a Wallace & Tiernan 0-800 mm Hg absolute gage was used. This gage was calibrated by Sandia Standards and the uncertainty is given as +/-0.8 mm Hg with a least division of 1 mm Hg. The +/-0.8 mm Hg uncertainty in calibration can be taken as a two sigma estimate, and therefore, the standard deviation is taken to be +/-0.4 mm Hg.

Tests HT31, 32 and 33 used the Wallace & Tiernan gage for an atmospheric reference and a Heise 0-100 psig gage was used for measuring the pressure in the tube. The Heise gage was calibrated by Sandia and has an uncertainty of 0.1 psig with a least division of 0.1 psig. The standard deviation of the Heise gage is estimated to be +/-0.05 psig.

For tests after HT33, a Wallace & Tiernan 0-50 psia gage was used. The gage was calibrated by Sandia Standards Lab and was assigned an uncertainty of 0.4 psia over the entire range of the gage. The gage was used in a range above 4 psia; below this value, the calibration error becomes large. In this limited range the uncertainty of the gage can reasonably be assumed to have a standard deviation of +/-0.05 psia. The gage has a least division of 0.05 psia.

Due to the high linearity of the pressure gages used, it is assumed that the relative uncertainty between any two pressure measurements is less than the absolute uncertainty which may contain some zero bias. The standard deviation for a relative pressure measurement in the tests prior to HT31 is assumed to be +/-0.25 mm Hg and after test HT33 it is assumed to be +/-0.025 psia. For tests HT31, 32 and 33 the standard deviation is assumed to be the square root of the sum of the squares of the two standard deviations or +/-0.05 psia.

D.4.1.3 Uncertainty in the Uniformity of the Gas Mixture

The temperature and pressure measurements are point measurements which may be affected by spatial nonuniformity of the gas. No compositional measurement is taken; composition is inferred from the temperature and pressure measurements.

Uniformity of Temperature - Temperature uniformity in the tube is maintained by 15 independently controlled sections of heaters on the tube. For details of the heating system see Appendix A. An analytical estimate of the nonuniformity of the inner surface of the wall in Appendix G predicts that the nonuniformity is +/-0.7°C. Typical variation in temperature at steady state at 100°C between the hot and cold measurements on the outer surface of the tube is +/-3°C excluding the endplates.

The temperature of the endplates varied with the ambient air temperature and date of test. The removable insulating endcaps lost their sealing quality with use and allowed ambient air to circulate around the endplates. For most elevated temperature tests, the endplates were lower in temperature than the rest of the tube, typically 5°C but sometimes as much as 20°C.

Attempts to introduce a steam mole fraction to produce saturation corresponding to the average tube temperature resulted in a mole fraction corresponding to saturation at a temperature approximately 5°C lower than the average tube temperature. Sufficient steam was introduced to produce condensation somewhere in the system. The secondary piping used to circulate the mixture is heated over most of its length. The only unheated segment is from the outlet port at the foil end of the tube, through the filter, pump, and a couple meters of pipe to where the secondary piping runs under the heating tapes along the main tube. The secondary piping is insulated along its entire length,

but the unheated portion is assumed to be the coldest point in the system.

While the largest temperature excursions of the tube wall and secondary piping are large compared to the point temperature measurement standard deviation of +/-1°C, these excursions are assumed to be confined to very narrow regions in the boundary layer of the gas and the temperature variability of the core region is assumed to be adequately characterized by +/-1°C.

Uniformity in Pressure - The pressure in the tube is uniform prior to the initiation of the detonation because there is no flow in the tube. Pressure measurements made between the addition of gases are made with the circulation pump running. The flow rate of the pump is 142 slm (5 cfm). This flow rate produces a velocity of approximately 15 mm/s (3 ft/min) in the detonation tube. The pressure drop is minimal and the measured static pressure can be considered the total pressure within the standard deviation of the point estimates.

Uniformity of mixture - The gas mixture is made homogeneous by continuous circulation of the gases in the tube during and after gas addition. At least one tube volume of gas is allowed to circulate through the secondary piping while gas is being added, and at least one additional tube volume of gas is allowed to circulate before adding additional gas or initiating the detonation. Since no compositional measurements are taken, there is no method of directly establishing the uniformity of the mixture.

D.4.1.4 Steady State Criteria

The temperature and pressure measurements which define the composition of the mixture are made only after steady state is obtained. Steady-state is defined by two criteria. The first is that there is no detectable change in temperature or pressure over a period of 15 minutes. This period is chosen because it is the time-constant of the tube with respect to a sudden change in temperature as discussed in Appendix B. (Pressure equilibration in the gas is very fast compared to this time scale.)

The second criterion is that the gas mixture be uniform. The circulation rate of the pump is 5 scfm (verified by a calibration test) and the tube volume is 1.92 m^3. A circulation of one tube volume of gas occurs every 13.5 minutes. To obtain uniformity in the gas mixture at least two tube volumes of gas are allowed to pass through the secondary piping. This is equivalent to waiting at least 27 minutes between the additions of gases.

Typical procedure was to wait approximately 1 hour between adding gases and a half an hour after the last gas was added to initiate the detonation. Using these times to achieve equilibrium, it is assumed that the time rate of change in temperature and pressure is minimal.

D.4.2 Standard Deviation Estimates of ρ_{air}, ϕ, X_{H2O}, and X_{CO2}

Equation D-3 is used to estimate the standard deviation of ρ_{air}, ϕ, X_{H2O}, and X_{CO2}, given the standard deviations of the measured variables established in the last section. The functional relation, g, for each of the variables is given below. The discussion of the equations will be divided into two categories: 1. H_2-air and H_2-air-H_2O, and 2. H_2-air-CO_2. This is necessitated because the order of gas entry for the CO_2 tests was air-CO_2-H_2 while the gas entry for the other tests was air-H_2-H_2O.

The following relations are based on the use of dry air. For tests prior to HT-49 ambient air containing some humidity was used. In all cases the final mole fraction of H_2O due to humidity in the ambient air is less than 0.01. The manufacturers estimate of the standard deviation of the humidity measuring device is +/-3%. In some cases, air from a compressor was used to boost the air density up to its required value. The compressor draws in ambient air, and therefore, the total air mixture in the HDT is assumed to have the same humidity as the ambient air.

The calculation of steam mole fraction requires interpolation of the steam tables. The estimated uncertainty in interpolation is +/-2% for a combined standard deviation of +/-3.6% for the humidity contained in the ambient air. This standard deviation is included in the final value of the standard deviation given for the mole fraction of steam for the appropriate tests where ambient air was used by taking the square root of the sum of the squares with the standard deviation for steam developed below.

H_2-air and H_2-air-H_2O Tests - As mentioned above, the mean value of a given variable, μ_i, is estimated by the measurement of that variable for a given test. The following mean value estimators are defined:

Air
Temperature: T_1 Pressure: P_1

H_2-air
Temperature: T_2 Pressure: P_2

H_2-air-H_2O
Temperature: T_3 Pressure: P3

Further, define a mean difference in pressure estimator as:

$$\Delta P_{H2} \equiv P_2 - P_1 \equiv \Delta P_{21}$$

$$\Delta P_{H2O} \equiv P_3 - P_2 \equiv \Delta P_{32}$$

The standard deviation estimator for each measurement is given in Table D-5. The symbol used in this appendix to identify a standard deviation estimate is δ; i.e., standard deviation in pressure: δP, standard deviation in temperature: δT; standard deviation in relative pressure: $\delta \Delta P$. Using these definitions the standard deviation in the air density, equivalence ratio, and steam mole fraction is as follows:

Temperature:

$$T = T_3 \tag{D-4}$$

$$\delta T = \delta T_3 \tag{D-5}$$

Air density:

$$\rho_{air} = \frac{P_1}{RT_1} \tag{D-6}$$

Taking the Taylor expansion of the air density and retaining the first term gives,

$$\partial \rho_{air} = \frac{\partial P_1}{RT_1} - \frac{P_1}{RT_1}\left(\frac{\partial T_1}{T_1}\right) \tag{D-7}$$

Taking square root of the sum of the squares, the standard deviation is,

$$\delta_{\rho_{air}} = \frac{P_1}{RT_1}\left[\left(\frac{\delta T_1}{T_1}\right)^2 + \left(\frac{\delta P_1}{P_1}\right)^2\right]^{1/2} \tag{D-8}$$

Equivalence ratio:

$$\phi = S \frac{X_{H_2}}{X_{air}} \quad \text{(see Appendix E)} \tag{D-9}$$

let S = 2.38691

Substituting (D-6) gives,

$$\phi = S \frac{n_{H_2}}{n_{air}} = S \left(\frac{\frac{P_2}{RT_2} - \frac{P_1}{RT_1}}{\frac{P_1}{RT_1}} \right) \tag{D-10}$$

Rearranging, and introducing relative pressure

$$\phi = S\left(\frac{T_1}{P_1} \right)\left[\frac{P_2}{T_2} \left(- \frac{P_1}{T_2} + \frac{P_1}{T_2} \right) - \frac{P_1}{T_1} \right]$$

$$= S\left(\frac{T_1}{P_1} \right)\left[\frac{\Delta P_{21}}{T_2} + \frac{P_1}{T_2} - \frac{P_1}{T_1} \right] \tag{D-11}$$

Rearranging, the equivalence ratio is

$$\phi = S\left[\frac{T_1}{T_2} \left(\frac{\Delta P_{21}}{P_1} + 1 \right) - 1 \right] \tag{D-12}$$

Taking the Taylor series and retaining the first term,

$$\partial\phi = S\left[\left(\frac{\Delta P_{21}}{P_1} + 1\right)\frac{\partial T_1}{T_2} - \left(\frac{\Delta P_{21}}{P_1} + 1\right)\left(\frac{T_1}{T_2}\right)\frac{\partial T_2}{T_2}\right.$$

$$\left. + \left(\frac{T_1}{T_2}\right)\frac{\partial \Delta P_{21}}{P_1} - \frac{T_1}{T_2}\frac{\Delta P_{21}}{P_1}\frac{\partial P_1}{P_1}\right] \qquad \text{(D-13)}$$

Taking the square root of the sum of the squares of each term, the standard deviation is,

$$\delta\phi = S\left(\frac{T_1}{T_2}\right)\left[\left(\frac{\Delta P_{21}}{P_1} + 1\right)^2\left(\left(\frac{\delta T_1}{T_1}\right)^2 + \left(\frac{\delta T_2}{T_2}\right)^2\right)\right.$$

$$\left. + \left(\frac{\Delta P_{21}}{P_1}\right)^2\left(\left(\frac{\delta \Delta P_{21}}{\Delta P_{21}}\right)^2 + \left(\frac{\delta P_1}{P_1}\right)^2\right)\right]^{1/2} \qquad \text{(D-14)}$$

Steam mole fraction: $X_{H_2O} \equiv \dfrac{n_{H_2O}}{n_{total}}$ (D-15)

Substituting (D-6) gives

$$X_{H_2O} = \frac{\left(\dfrac{P_3}{RT_3} - \dfrac{P_2}{RT_2}\right)}{\left(\dfrac{P_3}{RT_3}\right)} \qquad \text{(D-16)}$$

Rearranging,

$$X_{H_2O} = \left(1 - \frac{P_2\ T_3}{P_3\ T_2}\right) \tag{D-17}$$

Introducing relative pressure, the steam mole fraction is

$$X_{H_2O} = \left(1 - \left(\frac{T_3}{T_2}\right)\left(\frac{P_2}{P_3} + \frac{P_3}{P_3} - \frac{P_3}{P_3}\right)\right)$$

$$= \left(1 - \left(\frac{T_3}{T_2}\right)\left[1 - \frac{\Delta P_{32}}{P_3}\right]\right) \tag{D-18}$$

Taking the Taylor series expansion of the steam mole fraction and retaining the first term,

$$\partial X_{H_2O} = \left[1 - \frac{\Delta P_{32}}{P_3}\right]\frac{\partial T_3}{T_2} - \left[1 - \frac{\Delta P_{32}}{P_3}\right]\left(\frac{T_3}{T_2}\right)\frac{\partial T_2}{T_2}$$

$$- \left(\frac{T_3}{T_2}\right)\frac{\partial \Delta P_{32}}{P_3} + \left(\frac{T_3}{T_2}\right)\left(\frac{\Delta P_{32}}{P_3}\right)\frac{\partial P_3}{P_3} \tag{D-19}$$

Taking the square root of the sum of the squares, the standard deviation is,

$$\delta X_{H_2O} = \left(\frac{T_3}{T_2}\right)\left[\left(1 - \frac{\Delta P_{23}}{P_3}\right)^2\left(\left(\frac{\delta T_3}{T_3}\right)^2 + \left(\frac{\delta T_2}{T_2}\right)^2\right)\right.$$

$$\left. + \left(\frac{\Delta P_{32}}{P_3}\right)^2\left(\left(\frac{\delta \Delta P_{32}}{\Delta P_{32}}\right)^2 + \left(\frac{\delta P_3}{P_3}\right)^2\right)\right]^{1/2} \tag{D-20}$$

Upper and lower bound estimates on the initial thermodynamic state variables can be taken as $+/-2\delta$. The numerical values for the bounds are listed in Appendix C.

H_2-air-CO_2 Tests - The mean value of a given variable, μ_i, is estimated by the measurement of that variable for a given test. The following mean value estimators are defined:

Air
Temperature: T_1 Pressure: P_1

CO_2-Air
Temperature: T_2 Pressure: P_2

H_2-air-CO_2
Temperature: T_3 Pressure: P3

Further, define a mean difference in pressure estimator as:

$$\Delta P_{CO2} \equiv P_2 - P_1 \equiv \Delta P_{21}$$

$$\Delta P_{H2} \equiv P_3 - P_2 \equiv \Delta P_{32}$$

Define standard deviation as δ; i.e., standard deviation in pressure: δP; standard deviation in temperature: δT; standard deviation in relative pressure: $\delta \Delta P$. Using these definitions the standard deviation in the air density, equivalence ratio, and carbon dioxide mole fraction is as follows:

Temperature:

$$T = T_3 \tag{D-21}$$

$$\delta T = \delta T_3 \tag{D-22}$$

Air density:

$$\rho_{air} = \frac{P_1}{RT_1} \tag{D-23}$$

Taking the Taylor series expansion of air density, and the square root of the sum of the squares of the terms, the standard deviation is

$$\delta_{\rho_{air}} = \frac{P_1}{RT_1}\left[\left(\frac{\delta T_1}{T_1}\right)^2 + \left(\frac{\delta P_1}{P_1}\right)^2\right]^{1/2} \tag{D-24}$$

Equivalence ratio:

Using (D-6) and (D-9), the equivalence ratio is:

$$\phi = S\,\frac{n_{H_2}}{n_{air}} = S\left(\frac{\dfrac{P_3}{RT_3} - \dfrac{P_2}{RT_2}}{\dfrac{P_1}{RT_1}}\right) \tag{D-25}$$

Rearranging, and introducing relative pressure

$$= S\left(\frac{T_1}{P_1}\right)\left[\frac{\Delta P_{32} + P_1 + P_1}{T_3} - \frac{\Delta P_{21} + P_1}{T_2}\right] \tag{D-26}$$

Taking the Taylor series expansion, and the square root of the sum of the squares of each term, the standard deviation is:

$$\delta\phi = S\left(\frac{T_1}{P_1}\right)\left[\left(\frac{P_3}{T_3} - \frac{P_2}{T_2}\right)^2\left(\frac{\delta T_1}{T_1}\right)^2 + \left(\frac{P_2}{T_2}\right)^2\left(\frac{\delta T_2}{T_2}\right)^2\right.$$

$$+ \left(\frac{P_3}{T_3}\right)^2\left(\frac{\delta T_3}{T_3}\right)^2 + \left(\frac{P_1 - P_3}{T_3} - \frac{P_2 + P_1}{T_2}\right)^2\left(\frac{\delta P_1}{P_1}\right)^2$$

$$\left. + \left(\frac{\Delta P_{21}}{T_3} - \frac{\Delta P_{21}}{T_2}\right)^2\left(\frac{\delta \Delta P_{21}}{\Delta P_{21}}\right)^2 + \left(\frac{\delta \Delta P_{32}}{T_3}\right)^2\right]^{1/2} \tag{D-27}$$

CO_2 mole fraction: $$X_{CO_2} \equiv \frac{n_{CO_2}}{n_{total}} \tag{D-28}$$

Substituting (D-6) gives

$$X_{CO_2} = \frac{\left(\frac{P_2}{RT_2} - \frac{P_1}{RT_1} \right)}{\left(\frac{P_2}{RT_1} \right)} \tag{D-29}$$

Rearranging and introducing relative pressure, the steam mole fraction is,

$$X_{CO_2} = \left(1 - \left(\frac{T_3}{T_2} \right) \left[1 - \frac{\Delta P_{32}}{P_3} \right] \right) \tag{D-30}$$

Taking the partial derivative of the CO_2 mole fraction, and taking the square root of the sum of the squares, the standard deviation is,

$$\delta X_{CO_2} = \left(\frac{T_2}{T_1} \right) \left[\left(1 - \frac{\Delta P_{21}}{P_2} \right)^2 \left(\left(\frac{\delta T_2}{T_2} \right)^2 + \left(\frac{\delta T_1}{T_1} \right)^2 \right) \right.$$

$$\left. + \left(\frac{\Delta P_{21}}{P_2} \right)^2 \left(\left(\frac{\delta \Delta P_{21}}{\Delta P_{21}} \right)^2 + \left(\frac{\delta P_2}{P_2} \right)^2 \right) \right]^{1/2} \tag{D-31}$$

Upper and lower bound estimates on the initial thermodynamic state variables can be taken as $+/-2\delta$. The numerical values for the bounds are listed in Appendix C.

D.4.3 Standard Deviation Estimates of Detonation Cell Width and Velocity Due to Initial Thermodynamic State

The variance in detonation cell width and velocity due to the variance in thermodynamic state can be estimated by using the same technique used to establish the variance in the initial thermodynamic state variable described above. Estimates of the detonation cell width and velocity gradients with respect to the thermodynamic state variables can be estimated from the data. For,

$$\lambda = f(T, \rho_{air}, \phi, X_{H2O} \text{ or } X_{CO2})$$

(D-32)

$$V_D = g(T, \rho_{air}, \phi, X_{H2O} \text{ or } X_{CO2})$$

the first term of the Taylor expansion is,

$$d\lambda, V_D = \left(\frac{\partial \lambda, V_D}{\partial \rho_{air}} \right)_{T,\phi,X_{H_2O}} d\rho_{air} + \left(\frac{\partial \lambda, V_D}{\partial T} \right)_{\rho_{air},\phi,X_{H_2O}} dT$$

(D-33)

$$+ \left(\frac{\partial \lambda, V_D}{\partial \phi} \right)_{\rho_{air},T,X_{H_2O}} d\phi + \left(\frac{\partial \lambda, V_D}{\partial X_{H_2O}} \right)_{\rho_{air},T,\phi} dX_{H_2O}$$

The standard deviation estimate is,

$$\delta\lambda, V_D = \left[\left(\frac{\partial \lambda, V_D}{\partial \rho_{air}} \right)^2_{T,\phi,X_{H_2O}} \delta\rho^2_{air} + \left(\frac{\partial \lambda, V_D}{\partial T} \right)^2_{\rho_{air},\phi,X_{H_2O}} \delta T^2 \right.$$

(D-34)

$$\left. + \left(\frac{\partial \lambda, V_D}{\partial \phi} \right)^2_{\rho_{air},T,X_{H_2O}} \delta\phi^2 + \left(\frac{\partial \lambda, V_D}{\partial X_{H_2O}} \right)^2_{\rho_{air},T,\phi} \delta X^2_{H_2O} \right]^{1/2}$$

As the mixture approaches the lean limit, the gradient of detonation cell width with respect to equivalence ratio approaches infinity. Equation D-34 shows that the standard deviation in the detonation cell width also approaches infinity due to a finite standard deviation in equivalence ratio multiplied by the infinite gradient. The effect of the standard deviation in the remaining thermodynamic variables can be estimated from their respective gradients. The standard deviation in detonation velocity due to standard deviation in the initial thermodynamic state can be estimated by using C-J theory to predict the gradients of detonation velocity with respect to the gradients in the thermodynamic variable. Assuming that the detonation velocity does not deviate significantly from C-J theory, none of the gradients are large.

D.5 REFERENCES FOR APPENDIX D

D1. Moen, I. O., Funk, J. W., Ward, S. A.,Rude, G. M. and Thibault, P. A., "Detonation Length Scales for Fuel-Air Explosives," AIAA Progress in Astronautics and Aeronautics, Vol. 94, 1984, pp 55-79.

D2. Moen, I. O., Murray, S. B., Bjerketvedt, D., Rinnan, A., Knystautas, R., Lee, J. H., "Diffraction of Detonation From Tubes Into A Large Fuel-Air Explosive Cloud," 19th Symp. (Int'l.) on Combustion, The Combustion Institute, Pittsburgh, PA, 1982, pp 635-645.

D3. Bull, D. C., Elsworth, J. E., Shuff, P. J., "Detonation Cell Structures in Fuel/Air Mixtures," Combustion and Flame, V. 45, 1982, pp 7-22.

D4. Ray, A. A., Editor, "SAS Users Guide: Statistics," SAS Institute Inc., Cary N. C., 1982 Ed.

D5. Kline, S. J. and McClintock, F. A., "Describing Uncertainties in Single-Sample Experiments," Mechanical Engineering, Jan. 1953, pp 3-8.

D6. Moffat, R. J., "Contributions to the Theory of Single-Sample Uncertainty Analysis," Trans. ASME, Vol. 104, June 1982, pp 250-260.

FIGURES

D-1 Typical Smoked Foil Record from the HDT with Large Cells (HT-96).

D-2 Detonation Cell Width Measurements for HDT Test Series #3 (H_2-air, ρ_{air}=41.6 moles/m^3, T=100°C).

D-3 Detonation Cell Width Measurements for HDT Test Series #5 (H_2-air, ρ_{air}=41.6 moles/m^3, T=20°C).

D-4 Comparison of Detonation Cell Width Data Between the HDT and McGill University. (HDT Test Series #1, P=1 atm, T=25°C).

D-5 Normalized Detonation Cell Width (λ Author/λ Knystautas) Vs. HDT Test Number.

D-6 Typical PCB Pressure Trace - Small Cell Width (λ = 5 mm , Test HT-84).

D-7 Typical Kistler Pressure Trace - Small Cell Width (λ = 5 mm , Test HT-84).

D-8 Typical PCB Pressure Trace - Large Cell Width (λ = 400 mm , Test HT-96).

D-9 Typical Kistler Pressure Trace - Large Cell Width (λ = 400 mm , Test HT-96).

APPENDIX E

THERMODYNAMICS AND CELL SIZE

For binary H_2-air mixtures three independent variables are required to specify the initial thermodynamic state. An additional variable is needed for each diluent, such as steam or CO_2. The purpose of this appendix is to develop relations between the variables used in this report and a few of the other commonly used variables. In addition, the general thermodynamic relationship between detonation cell width and the thermodynamic variables is developed and the relationship of cell width vs. temperature for various thermodynamic processes is discussed.

E.1 THERMODYNAMIC RELATIONS

Thermodynamic variables are related by the equilibrium equation of state. For simplicity a perfect gas relation is used:

$$P = nRT = \frac{\rho}{mw} RT \qquad \text{(E-1)}$$

where P = pressure
n = molar density
R = universal gas constant
T = temperature
ρ = mass density
mw = molecular weight

This relation is very good except at high steam concentrations at high pressures and relatively low temperatures.

An additional relation is necessary for multicomponent mixtures, and that is that the sum of the mole fractions add up to unity:

$$X_{air} + X_{H_2} + X_{H_2O} = 1 \qquad \text{(E-2)}$$

where X_i is the mole fraction $= \frac{ni}{n}$

The composition of air is taken to be
20.95% O_2
79.05% N_2

The equivalence ratio, ϕ, can be related to the air and fuel mole fractions by its definition:

$$\phi = \frac{n_{H_2}/n_{air}}{\left(\frac{n_{H_2}}{n_{air}}\right)_{stoichiometric}} \qquad \text{(E-3)}$$

where stoichiometric $\frac{n_{H_2}}{n_{air}}$ is given by:

$$H_2 + \frac{1}{2}\left(O_2 + 3.77382N_2\right) \rightarrow H_2O + \frac{1}{2}\left(3.77382N_2\right) \qquad \text{(E-4)}$$

$$\text{Let } \frac{1}{S} = \left(\frac{n_{H_2}}{n_{air}}\right)_{stoich} = \frac{1}{1/2\ (1 + 3.77382)}$$

$$\text{or } S = 2.38691$$

where S is defined simply for convenience.

Previous researchers have expressed detonation cell width as a function of $\%H_2$ in dry H_2-air in place of equivalence ratio. It is useful to derive the relation between these variables and equvalence ratio, and the mole fractions of the diluted mixture. Superscripts will be used to identify whether the variable is defined for a diluted, X^d, or undiluted, X^u, mixture. From equation 3, the equivalence ratio, ϕ, is invariant to the addition of diluent.

For undiluted mixtures, the H_2 and air mole fractions sum to unity:

$$X^u_{air} + X^u_{H_2} = 1 \qquad \text{(E-5)}$$

where X^u_{air} and $X^u_{H_2}$ are the undiluted mole fractions.

By definition $X^u_{H_2} = \dfrac{n_{H_2}}{n_{air} + n_{H_2}}$ (E-6)

So $\dfrac{n_{H_2}}{n_{air}} = \dfrac{X^u_{H_2}}{1-X^u_{H_2}}$ (E-7)

Therefore, $\phi = S \left(\dfrac{X^u_{H_2}}{1-X^u_{H_2}} \right) = S \dfrac{X^u_{H_2}}{X^u_{air}}$ (E-8)

or $X^u_{H_2} = \dfrac{\phi}{\phi + S}$ (E-9)

and from (Eq. E-5)

$X^u_{air} = \dfrac{S}{\phi + S}$ (E-10)

To get ϕ in terms of the diluted mole fractions, Eq. E-2 is used. The relations are developed for steam dilution but are general for any diluent. Note that the H_2 to air molar ratio is the same in each mixture, or

$$\left.\frac{n_{H_2}}{n_{air}}\right|_{\text{diluted}} = \left.\frac{n_{H_2}}{n_{air}}\right|_{\text{undiluted}} \quad \text{(E-11)}$$

By dividing by the appropriate total densities (Eq. E-11) becomes

$$\frac{X^d_{H_2}}{X^d_{air}} = \frac{X^u_{H_2}}{X^u_{air}} \quad \text{(E-12)}$$

Substituting (Eq. E-12) into (Eq. E-2) to eliminate $X^d_{H_2}$ gives

$$X^d_{air} + X^u_{H_2}\left(\frac{X^d_{air}}{X^u_{air}}\right) + X^d_{H_2O} = 1 \qquad \text{(E-13)}$$

Rearranging (Eq. E-13) and using (Eq. E-5) gives

$$X^d_{air} = X^u_{air}\left(1-X^d_{H_2O}\right). \qquad \text{(E-14)}$$

Similarly, substituting (Eq. E-12) into (Eq. E-2) to eliminate X_{air} gives, with rearranging,

$$X^d_{H_2} = X^u_{H_2}\left(1-X^d_{H_2O}\right) \qquad \text{(E-15)}$$

Substituting (Eq. E-15) into (Eq. E-8) gives

$$\phi = S\left(\frac{X^d_{H_2}}{1-X^d_{H_2O}-X^d_{H_2}}\right) = S\,\frac{X^d_{H_2}}{X^d_{air}} \qquad \text{(E-16)}$$

Substituting (Eq. E-9) and (Eq. E-10) into (Eq. E-15) and (Eq. E-14) gives

$$X^d_{H_2} = \frac{\phi}{\phi + S}\left(1-X^d_{H_2O}\right) \qquad \text{(E-17)}$$

$$X^d_{air} = \frac{S}{\phi + S}\left(1-X^d_{H_2O}\right) \qquad \text{(E-18)}$$

(Eq. E-18) can be used to give the relationship between total molar density and air density, i.e.,

$$n^d_{air} = n^d\left(\frac{s}{\phi + s}\right)\left(1-X^d_{H_2O}\right) \tag{E-19}$$

Since $n^d = \frac{\rho^d}{mw}$

$$\rho^d_{air} = \rho^d\frac{(mw_{air})}{(mw_{mix})}\left(\frac{s}{\phi + s}\right)1-X^d_{H_2O} \tag{E-20}$$

E.2 GENERAL FUNCTIONAL RELATIONSHIP

Choosing air density, temperature, equivalence ratio and mole fraction of steam as the four independent variables gives

$$\lambda = f\left(\rho_{air}, T, \phi, X_{H_2O}\right) \tag{E-21}$$

The change in cell width with respect to a change in any/all of the independent variables can be defined by the integral of the total derivative of (Eq. E-21) with a defined reference state:

$$\lambda_o = f\left(\rho_{air_o}, T_o, \phi_o, X_{H_2O_o}\right) \tag{E-22}$$

The total derivative is,

$$d\lambda = \left(\frac{\partial\lambda}{\partial\rho_{air}}\right)_{T,\phi,X_{H_2O}} d\rho_a + \left(\frac{\partial\lambda}{\partial T}\right)_{\rho_{air},\phi,X_{H_2O}} dT$$

$$+ \left(\frac{\partial\lambda}{\partial\phi}\right)_{\rho_{air},T,X_{H_2O}} d\phi + \left(\frac{\partial\lambda}{\partial X_{H_2O}}\right)_{\rho_{air},T,\phi} dX_{H_2O} \tag{E-23}$$

Integrating (Eq. E-23) gives

$$\lambda-\lambda_o = \int_{\rho_{air_o}}^{\rho_{air}} \left(\frac{\partial\lambda}{\partial\rho_{air}} \right)_{T,\phi,X_{H_2O}} d\rho_a + \int_{T_o}^{T} \left(\frac{\partial\lambda}{\partial T} \right)_{\rho_{air},\phi,X_{H_2O}} dT$$

(E-24)

$$+ \int_{\phi_o}^{\phi} \left(\frac{\partial\lambda}{\partial\phi} \right)_{\rho_{air},T,X_{H_2O}} d\phi + \int_{X_{H_2O_o}}^{X_{H_2O}} \left(\frac{\partial\lambda}{\partial X_{H_2O}} \right) dX_{H_2O}$$

E.3 EFFECT OF TEMPERATURE

To isolate the effect of temperature, consider a process where ϕ and X_{H_2O} are constant, such as a premixed set of gases undergoing heating. Consider this heating taking place in three different ways, at constant air density, at constant total density, and at constant total pressure.

Constant air density

$$\rho_a = C_1$$
$$\phi = C_2$$
$$X_{H_2O} = C_3$$

(Eq. E-23) gives,

$$d\lambda = \left(\frac{\partial\lambda}{\partial T} \right)_{\rho_{air},\phi,X_{H_2O}} dT \qquad \text{(E-25)}$$

B) Constant total density

$$\rho = C_1$$
$$\phi = C_2$$
$$X_{H_2O} = C_3$$

For $\lambda = f\left(\rho, T, \phi, X_{H_2O}\right)$ (E-26)

$$d\lambda = \left(\frac{\partial\lambda}{\partial T}\right)_{\rho,\phi,X_{H_2O}} dT \qquad \text{(E-27)}$$

Note, however, that for fixed ϕ and X_{H2O}, constant ρ from (Eq. E-20) implies constant$[01306sr_{air}$ and hence,

$$\left(\frac{\partial\lambda}{\partial T}\right)_{\rho,\phi,X_{H_2O}} = \left(\frac{\partial\lambda}{\partial T}\right)_{\rho_{air},\phi,X_{H_2O}} \qquad \text{(E-28)}$$

Therefore, at constant composition, the effect of temperature is the same whether the process occurs at constant air density or constant total density.

C) Constant total pressure

$$P = C_1$$
$$\phi = C_2$$
$$X_{H_2O} = C_3$$

For $\lambda = f\left(P, T, \phi, X_{H_2O}\right)$ (E-29)

$$d\lambda = \left(\frac{\partial\lambda}{\partial T}\right)_{P,\phi,X_{H_2O}} dT \qquad \text{(E-30)}$$

In this case,

$$\left(\frac{\partial \lambda}{\partial T} \right)_{P,\phi,X_{H_2O}} \neq \left(\frac{\partial \lambda}{\partial T} \right)_{\rho,\phi,X_{H_2O}}$$

The relationship between the temperature effect at constant pressure and constant density can be determined by differentiating (Eq. E-29) for constant composition and density, and relating that to the equation of state (Eq. E-1) and (Eq. E-27).

For constant ϕ, X_{H_2O}

$$d\lambda = \left(\frac{\partial \lambda}{\partial P} \right)_{T,\phi,X_{H_2O}} dP + \left(\frac{\partial \lambda}{\partial T} \right)_{P,\phi,X_{H_2O}} dT \qquad \text{(E-31)}$$

Differentiating (Eq. E-1) gives,

$$dP = d\rho \ \frac{RT}{mw} + \frac{\rho R}{mw} \ dT \qquad \text{(E-32)}$$

Substituting (Eq. E-32) into Eq. 31) gives

$$d\lambda = \left(\frac{\partial \lambda}{\partial P} \right)_{T,\phi,X_{H_2O}} \left[d\rho \ \frac{RT}{mw} + \frac{\rho R}{mw} \ dT \right] + \left(\frac{\partial \lambda}{\partial T} \right)_{P,\phi,X_{H_2O}} dT \qquad \text{(E-33)}$$

Equating (Eq. E-33) with $d\rho = 0$ and (Eq. E-27) gives

$$\left(\frac{\partial \lambda}{\partial P} \right)_{T,\phi,X_{H_2O}} \frac{\rho R}{mw} \ dT + \left(\frac{\partial \lambda}{\partial T} \right)_{P,\phi,X_{H_2O}} dT = \left(\frac{\partial \lambda}{\partial T} \right)_{\rho,\phi,X_{H_2O}} dT$$

(E-34)

Noting from (Eq. E-1) that $\frac{P}{T} = \frac{\rho R}{mw}$

$$\left(\frac{\partial\lambda}{\partial T}\right)_{\rho,\phi,X_{H_2O}} = \left(\frac{\partial\lambda}{\partial P}\right)_{T,\phi,X_{H_2O}} \frac{P}{T} + \left(\frac{\partial\lambda}{\partial T}\right)_{P,\phi,X_{H_2O}} \tag{E-35}$$

Using (Eq. E-28) gives,

$$\left(\frac{\partial\lambda}{\partial T}\right)_{\rho_{air},\phi,X_{H_2O}} = \left(\frac{\partial\lambda}{\partial P}\right)_{T,\phi,X_{H_2O}} \frac{P}{T} + \left(\frac{\partial\lambda}{\partial T}\right)_{P,\phi,X_{H_2O}} \tag{E-36}$$

Finally, rearranging gives,

$$\left(\frac{\partial\lambda}{\partial T}\right)_{P,\phi,X_{H_2O}} = \left(\frac{\partial\lambda}{\partial T}\right)_{\rho_{air},\phi,X_{H_2O}} - \left(\frac{\partial\lambda}{\partial P}\right)_{T,\phi,X_{H_2O}} \frac{P}{T} \tag{E-37}$$

Data for cell width measurements has established that both

$\left(\frac{\partial\lambda}{\partial T}\right)_{\rho_{air},\phi,X_{H_2O}}$ and $\left(\frac{\partial\lambda}{\partial P}\right)_{T,\phi,X_{H_2O}}$ are negative.

APPENDIX F

ANALYSIS OF THE TEMPERATURE DISTRIBUTION AND THERMAL TRANSIENT RESPONSE OF THE HDT

To estimate the temperature non-uniformity and the rate of heating of the HDT using heater strips, a one dimensional transient model was developed. The model assumes that the HDT tube wall acts as a one dimensional fin between the heater tapes. The fin length is half the distance between heater tapes and is assumed to be insulated at the tip. The inside surface of the tube is assumed to be insulated due to symmetry and the low heat capacity of the gas, while the outside surface loses heat to the environment. The heat loss is approximated by a constant, q. The heating occurs in two stages. In the first stage, the heating tapes are at full power. The second stage starts when the temperature of the heaters reaches a set reference temperature, T_r, such as 100°C. During this stage the heaters are held at this temperature. In the HDT this temperature is held by computer controlled feedback of the thermocouple temperature under the heater tape.

F.1 NOMENCLATURE

English

A_c	Cross-sectional area of fin (tube wall)
A_p	Surface area of fin (tube wall)
A	Constant to be determined
B	Constant to be determined
C	Specific heat
d,e,f	Constants to be determined
H	Width of fin
J	Conveniently defined constant = Q/2kL
k	Thermal conductivity
K	Conveniently defined constant = q/kw
L	Length of fin (1/2 distance between heaters)
q	Heat loss per unit area through insulation

Q	Heat gain per unit area from heaters
s	Laplace variable
S	Laplace transform of temperature distribution
S_p	Particular solution to Laplace ODE
S_g	General solution to Laplace ODE
$S_{1,\#}$	First subscript refers to the term in the Laplace transform. Second subscript refers to the pole at which s is to be evaluated for inverse transformation
t	Time, zero time begins when heaters are first turned on
t^*	Time when heaters reach set-point temperature, usually 100°C and begin to cycle
t_2	Time, $t-t^*$, zero time begins when heaters reach set-point temperature
T	Temperature distribution (x,t)
$T_{1,\#}$	First subscript refers to term in Laplace transform that was inverse transformed. Second subscript refers to the pole that was evaluated.
T_r	Set-point temperature of heaters (usually 100°C) = $T^*(L,t^*)$
T^*	Temperature distribution at $t^* = T(x,t^*)$
X	Distance. Zero at tip of fin (midway between heaters), L at heaters.

<u>Greek</u>

α	Thermal diffusivity = $k/\rho c$
λ_m	Convenience variable $(m - 1/2)\pi/L$
ρ	Tube wall density

F.2 DERIVATION OF THE MODEL

Conservation of energy on the differential control volume in Fig. F-1 yields,

$$\left(- A_c k \frac{\partial T}{\partial x}\right)_x - \left(- A_c k \frac{\partial T}{\partial x}\right)_{x+\Delta x} + qH\Delta x = \rho c A_c \Delta x \frac{\partial T}{\partial t} \qquad \text{(F-1)}$$

Retaining first order terms gives,

$$A_c k \frac{\partial^2 T}{\partial x^2} \Delta x + qH\Delta x = \rho c A_c \Delta x \frac{\partial T}{\partial t} \qquad \text{(F-2)}$$

Dividing through by Δx gives,

$$\frac{\partial^2 T}{\partial x^2} + \frac{qH}{kA_c} = \left(\frac{\rho c}{k}\right) \frac{\partial T}{\partial t} \qquad \text{(F-3)}$$

Defining areas and noting the definition of thermal conductivity,

$$A_p = LW \quad , \quad A_c = HW \ , \ \alpha = \frac{k}{\rho c} \qquad \text{(F-4)}$$

The governing equation becomes,

$$\frac{\partial^2 T}{\partial x^2} + \frac{q}{kW} = \frac{1}{\alpha} \frac{\partial T}{\partial t} \qquad \text{(F-5)}$$

with boundary conditions,

$$x = 0; \ \frac{\partial T}{\partial x} = 0$$

$$\text{(F-6)}$$

$x = L$ either $\frac{\partial T}{\partial x} = \frac{Q}{k}$ Problem #1 - Heaters Full On

T_r $T - T_r = 0$ Problem #2 - Heaters at Constant

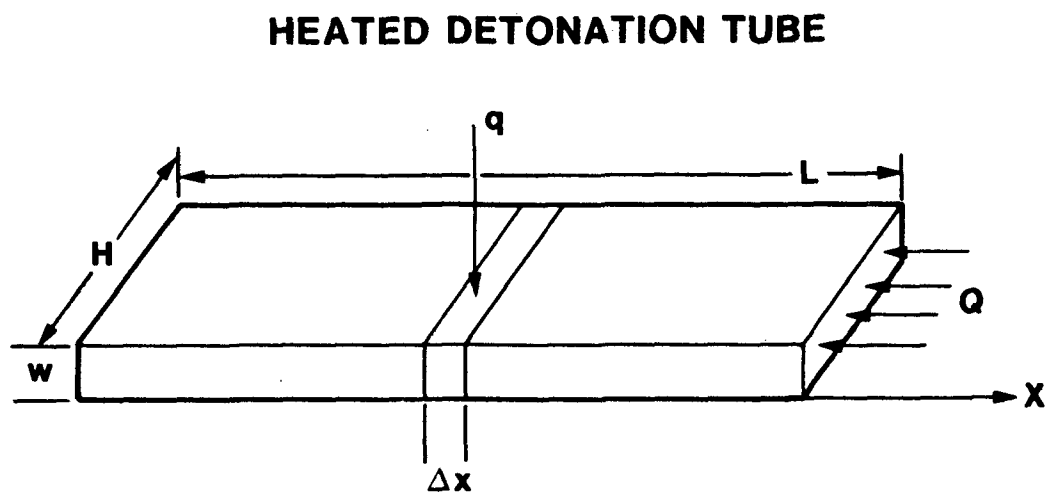

Figure F-1. Control Volume for the 1-D Unsteady Fin Model.

The heat loss per unit area from the surface, $\dot{q}$, and the heat gain from the heaters per unit area, Q, are assumed to be constant.

The initial conditions are,

$T(x,0) = 0$ Problem #1 - Heaters Full On

(F-7)

$T(x,t^*) = T^*(x,t^*)$ Problem #2 - Heaters at Constant T_r

where t^* is the time at which the heaters reach T_r.
$T^*(x,t^*)$ is the temperature distribution at t^*. Note: $T^*(L,t^*)=T_r$

A method of solution to the governing equation (Eq. F-5) subject to the initial and boundary conditions (Eq. F-6,7) is the Laplace Transform, L(T),

$$S \equiv \int_0^\infty e^{-st}\, T(x,t)dt = L(T) \qquad \text{(F-8)}$$

The transform of a time derivative is

$$L\left(\frac{\partial T}{\partial t} \right) = sS - T(x,0) \qquad \text{(F-9)}$$

F.3 SOLUTION TO PROBLEM #1 - HEATERS FULL ON

For convenience, define $K \equiv \frac{q}{kW}$

Taking the Laplace transform of the governing equation (Eq. F-5),

$$\frac{d^2S}{dx^2} + \frac{K}{s} = \frac{s}{\alpha} S \qquad \text{(F-10)}$$

The Laplace transform of the boundary conditions is,

$$\frac{dS}{dx} = 0 \text{ at } x = 0$$

$$\frac{dS}{dx} = \frac{Q}{sk} \text{ at } x = L \qquad \text{(F-11)}$$

Equation (F-10) is a second order ordinary differential equation in S which has:

particular solution $\quad Sp = \frac{\alpha K}{s^2}$ (F-12)

general solution

$$S_g = A \sinh \sqrt{\frac{s}{\alpha}}\, x + B \cosh \sqrt{\frac{s}{\alpha}}\, x + S_p \qquad \text{(F-13)}$$

Using the boundary conditions (Eq. F-11) yields,

$$\frac{dS}{dx} = 0 \text{ at } x = 0 \quad \Rightarrow A = 0 \qquad \text{(F-14)}$$

$$S_g = B \cosh \sqrt{\frac{s}{\alpha}}\, x + \frac{\alpha K}{s^2} \qquad \text{(F-15)}$$

Solving for B, using the second boundary condition,

$$B = \frac{Q}{sk\sqrt{\frac{s}{\alpha}}} \quad \frac{1}{\sinh \sqrt{\frac{s}{\alpha}}\, L} \qquad \text{(F-16)}$$

The Laplace transform of the solution to (Eq. F-10) is

$$S = \frac{Q}{sk\sqrt{\frac{s}{\alpha}}} \quad \frac{\cosh\sqrt{\frac{s}{\alpha}}\,x}{\sinh\sqrt{\frac{s}{\alpha}}\,L} + \frac{\alpha K}{s^2} \qquad \text{(F-17)}$$

which is of the form $S = S_1 + S_2$

Finding the inverse transform; $T = T_1 + T_2$

Second term has pole of order 2 at $s = 0$

$$T_2 = \alpha K t = \frac{\alpha q}{kW}\,t = \frac{qt}{\rho c W} = \left(\frac{q\,A_p}{\rho c\,W\,A_p}\right) t \qquad \text{(F-18)}$$

This term is the lumped mass cooling due to heat loss through the insulation.

First term has poles at $s = 0$, $sn = -\frac{n^2\pi^2 x}{L^2}$

<u>For $s \neq 0$</u>

$$S = \frac{p(s)}{q(s)} \quad \text{Residue at } s = sn \text{ for simple pole}$$

$$= \frac{p(sn)}{\frac{dq(sn)}{dsn}} \exp^{(snt)}$$

$$S_{1,sn} = \frac{Q}{k\ sn\sqrt{\frac{sn}{\alpha}}} \frac{\cosh\sqrt{\frac{sn}{\alpha}}\ x}{\sqrt{\frac{sn}{\alpha}}\ \frac{L}{2sn}\ \cosh\sqrt{\frac{sn}{\alpha}}\ L} \exp^{(snt)}$$

$$= \frac{-2QL}{kn^2\pi^2} \frac{\cos\left(n\pi\ \frac{x}{L}\right)}{\cos(n\pi)} \exp^{(snt)} \qquad \text{(F-19)}$$

Inverting (Eq. F-19) gives,

$$T_{1,n} = \frac{Q}{kL} \sum_{n=1}^{\infty} \frac{2(-1)^{n+1}\ L^2}{kn^2\pi^2} \cos\left(n\pi\ \frac{x}{L}\right) \exp\left(\frac{-\alpha n^2\pi^2 t}{L^2}\right) \qquad \text{(F-20)}$$

This term is initial transient response of the tube wall.

$$\text{For } s = 0,\ S_{1,0} = \frac{Q}{ks}\sqrt{\frac{\alpha}{s}}\ \frac{\cosh\sqrt{\frac{s}{\alpha}}\ x}{\sinh\sqrt{\frac{s}{\alpha}}\ L} \qquad \text{(F-21)}$$

$$\text{Expanding } S_{1,0} \simeq \frac{Q}{k} \frac{\sqrt{\alpha}}{s\sqrt{\frac{s}{\alpha}}} \frac{\left[1 + \frac{s}{\alpha}\frac{x^2}{2!} + \frac{s^2}{\alpha}\frac{x^4}{4!} + \text{--}\right]}{\left[\sqrt{\frac{s}{\alpha}}\ L + \left(\sqrt{\frac{s}{\alpha}}\right)\frac{L^3}{3!} + \left(\sqrt{\frac{s}{\alpha}}\right)^5 \frac{L^5}{5!}\right]}$$

$$S_{1,0} = \frac{Q}{kL}\frac{\alpha}{s^2}\left(1 + \frac{s}{2\alpha}x^2 - \frac{sL^2}{6\alpha} + \text{--}\ O\left(s^2\right)\right) \qquad \text{(F-22)}$$

Inverting gives,

$$T_{1,0} = \frac{\alpha Q}{kL} t + \frac{Q}{6kL}\left(3x^2 - L^2\right) \qquad \text{(F-23)}$$

The first term is the bulk heat gain from the heaters while the second term is the long time temperature distribution. Combining terms gives the complete solution to problem #1,

$$T = \left(\frac{q\,A_p}{\rho c(WA_p)}\right) t + \left(\frac{Q\,A_c}{\rho c(LA_c)}\right) t + \frac{Q}{6kL}\left(3x^2 - L^2\right)$$

$$+ \frac{2QL}{k\pi^2} \sum_{n=1}^{\infty} \frac{(-1)^{n+1}}{n^2} \cos\left(n\pi \frac{x}{L}\right) \exp\left(-\alpha n^2 \pi^2 t/L^2\right) \qquad \text{(F-24)}$$

F.4 SOLUTION TO PROBLEM #2 - HEATERS AT CONSTANT TEMPERATURE, T_r

For boundary and initial conditions,

Match conditions from Problem 1
Assume transient term in Problem #1 has died away

$$T = \left(\frac{q\,A_p}{\rho c(WA_p)}\right) t + \left(\frac{Q\,A_c}{\rho c(LA_c)}\right) t + \frac{Q}{6kL}\left(3x^2 - L^2\right)$$

Define t^* such that T at L is T_r at time of matching

$$T_r = \left(\frac{q\,A_p}{\rho c(WA_p)}\right) t^* + \left(\frac{Q\,A_c}{\rho c(LA_c)}\right) t^* + \frac{Q}{6kL}\left(2L^2\right) \qquad \text{(F-25)}$$

The reference temperature, T_r, is typically 100°C.

Define $t_2 = t - t^*$

where time t is zero at the beginning of problem #1 and t_2 is zero at the beginning of problem 2.

Define a new variable $\theta = T - T^*$

at time 0 in problem 2 $t = t^*$

The initial condition becomes,

$$\theta(x,0) = \frac{Q}{\alpha k}\left(x^2 - L^2\right) \tag{F-26}$$

The boundary conditions become,

$$\frac{\partial\theta}{\partial x}(0,t_2) = 0$$

$$\theta(L,t_2) = 0 \tag{F-27}$$

and the governing equation becomes,

$$\frac{\partial^2\theta}{\partial x^2} + \frac{q}{kW} = \frac{1}{\alpha}\frac{\partial\theta}{\partial t} \tag{F-28}$$

For convenience define

$$K = \frac{q}{kW}, \quad J = \frac{Q}{2kL} \tag{F-29}$$

The Laplace transform of the governing equation (Eq.F-28) is,

$$\frac{\partial^2 S}{\partial x^2} + \frac{K}{s} = \frac{1}{\alpha} \left(sS - J(x^2 - L^2) \right)$$

Rearranging gives,

$$\frac{d^2 S}{dx^2} - \frac{s}{\alpha} S = - \frac{Jx^2}{\alpha} + \frac{J}{\alpha}^2 - \frac{K}{\alpha} \qquad \text{(F-30)}$$

Solving the ordinary differential equation in S gives:

Particular solution: $S_p = fx^2 + ex + d$ (F-31)

Substituting into the differential equation (Eq. F-30),

$$2f - \frac{s}{\alpha} \left(fx^2 + ex + d \right) = \frac{Jx^2}{\alpha} - \frac{K}{s} + \frac{J}{\alpha}^2$$

Solving for d, e, f,

$$e = 0$$

$$f = \frac{J}{s}$$

$$d = \frac{\alpha}{s} \left(\frac{2J}{s} + \frac{K}{s} - \frac{J}{\alpha}^2 \right) = \alpha \frac{(K + 2J)}{s^2} - \frac{J}{s}^2$$

Therefore, S_p is

$$S_p = \frac{J}{s} x^2 + \frac{\alpha(K + 2J)}{s^2} - \frac{J^2}{s} = \frac{J}{s}(x^2 - L^2) + \frac{\alpha(K + 2J)}{s^2} \qquad \text{(F-32)}$$

The general solution is,

$$S_g = A \sinh \sqrt{s/\alpha}\, x + B \cosh \sqrt{s/\alpha}\, x + S_p(x) \qquad \text{(F-33)}$$

Using the Laplace transformed boundary conditions give,

$$\frac{\partial S}{\partial x}(0,s) = 0 \quad \Rightarrow \quad A = 0$$

$$S\,(L,s) = 0 \quad \Rightarrow \quad 0 = B\cosh \sqrt{s/\alpha}L + S_p(L)$$

Therefore,

$$B = \frac{F_p(L)}{\cosh \sqrt{s/\alpha}\, L}$$

the transform of the solution is,

$$S = \frac{J}{s}\,(x^2 - L^2) + \frac{\alpha}{s^2}\,(K + 2J)\left(1 - \frac{\cosh \sqrt{s/\alpha}x}{\cosh \sqrt{s/\alpha}L}\right) \qquad \text{(F-34)}$$

which is of the form $S = S_1 + S_2$

Inverting, there are poles at $s = 0$, and $s = n\pi/2$

<u>For $s \neq 0$</u>

The second term has a simple pole at $\cosh\left(\frac{n\pi}{2}\right)$ etc $n = 1,3,5$ etc

or, when

$$\sqrt{s/\alpha}\, L = (m - 1/2)\pi \qquad s_m = -\alpha(m - 1/2)^2 \frac{\pi^2}{L^2}, m = 1,2,3,$$

define $\lambda_m = (m - 1/2)\pi/L \quad \Rightarrow \quad s_m = -\alpha\lambda_m^2$

Pole has form $S_{2,\lambda_m} = \frac{1}{s^2}\frac{P(s)}{Q(s)} = -\frac{\alpha(K + 2J)}{s^2}\frac{\cosh\sqrt{s/\alpha}\,x}{\cosh\sqrt{s/\alpha}\,L}$ (F-35)

Inverting gives,

$$T_{2,\lambda_m} = \sum_{m=1}^{\infty}\frac{1}{x^2\lambda_m^4}\frac{P(\alpha\lambda m^2)}{\frac{\partial Q}{\partial s}(\alpha\lambda m^2)}e^{-\alpha\lambda_m^2 t_2} \qquad \text{(F-36)}$$

where $\partial Q/\partial s$ is evaluated as,

$$\frac{dQ}{ds} = \frac{d}{ds}\left[\cosh\sqrt{s/\alpha}L\right] = \left(\sinh\sqrt{s/\alpha}L\right)\frac{L}{2\sqrt{\alpha s}}$$

$$\left.\frac{dQ}{ds}\right|_{\alpha\lambda_m^2} = \frac{L}{2\alpha\lambda m}\sinh\left(-\lambda_m L\right) = \frac{L}{2\alpha\lambda m}(-1)^{m+1}$$

$$T_{2,\lambda_m} = -2(K + 2J)\sum_{m=1}^{\infty}\frac{(-1)^{m+1}e^{-\alpha\lambda_m^2 t_2}}{\lambda_m^3}\lambda\cos\lambda_m x \qquad \text{(F-37)}$$

This term is the initial temperature transient

<u>For s = 0</u>

To evaluate the second term of S it is necessary to expand the cosh terms to evaluate,

$$\cosh \sqrt{s/\alpha}\, x = 1 + \frac{s}{2}\,\frac{x^2}{\alpha} + \frac{s^2 x^4}{24\alpha^2} + \ldots\ldots$$

$$\frac{\cosh \sqrt{\frac{s}{\alpha}}\, x}{\cosh \sqrt{\frac{s}{\alpha}}\, L} = 1 + \frac{s\left(x^2 - L^2\right)}{2\alpha} + \frac{s^2}{24\alpha}\left(x^2 - 5L^2\right)\left(x^2 - L^2\right) + \ldots\ldots$$

$$1 - \frac{\cosh \sqrt{s/\alpha}\; x}{\cosh \sqrt{s/\alpha}\; L} = \frac{s\left(x^2 - L^2\right)}{2\alpha} + O\left(s^2\right)$$

Therefore, at s = 0, S becomes;

$$S_{1\&2,0} = \frac{J}{s}\left(x^2 - L^2\right) + \frac{(K + 2J)}{s^2}\left[\frac{-s(x^2 - L^2)}{2} + O(s^2)\right] \qquad \text{(F-38)}$$

Inverting,

$$T_{1\&2,0} = -\frac{K}{2}\left(x^2 - L^2\right) \qquad \text{(F-39)}$$

This term is the steady state temperature distribution in the tube wall.

Adding the terms,

$$T(x,t) = T_0 + T_{2,\lambda_m}$$

Noting that,

$$K = q/kW,\ J = Q/2kL,\ \text{and}\ \lambda_m = (m - 1/2)\,\frac{\pi}{L}$$

and $t_2 = t - t^*$

The solution is,

$$\theta(x,t) = \frac{q}{2kW}(x^2 - L^2) - 2\left(\frac{q}{kw} + \frac{Q}{kL}\right) \sum_{m=1}^{\infty} \frac{(-1)^{m+1} e^{-\alpha\lambda_m^2 t_2}}{\lambda_m^3} \cos \lambda_m x \qquad \text{(F-40)}$$

for $t > t^*$

F.5 COMPARISON BETWEEN THE MODEL AND THE HDT

The location of the Heaters are listed in Appendix A. The model is compared to the heater sections on the sides and bottom of the long pipes. Table F-1 lists the numerical values for the parameters used in the model. The heat loss ,q, is estimated from an assumed 80°C temperature drop across the insulation. The heat gain is estimated from the heater power and area of heat transfer to the fin. The length of the fin is taken as 1/2 of the length between the midplane of the heater area in contact with the fin.

Table F-1

Numerical Values of the Model Parameters

Parameter	Description and Units	Numerical Value
q	Heat Loss out Insulation (W/m^2)	-47.3
k	Metal Conductivity (W/m°C)	17.
W	Tube Wall Thickness (m)	0.0127
α	Thermal Diffusivity (m^2/s)	4.73E-06
Q	Heat Gain from Heater (W/m^2)	3875.
L	Half Length Between Heaters (m)	0.112

Figure F-2 shows the comparison between the model and actual thermocouple measurements from test HT-53 (Test Series #3). The initial temperature value used in the model is 17°C and the set point temperature used 101°C. The model predicts temperatures at three locations that correspond roughly to the location of the three thermocouples in heater tape section #5 that are shown in Figure F-2.

The initial transient dies out in approximately 15 minutes leaving a steady increase in temperature. The model predicts the time decay of the transient quite well. However, the temperature difference between the hot and the cold values are much higher

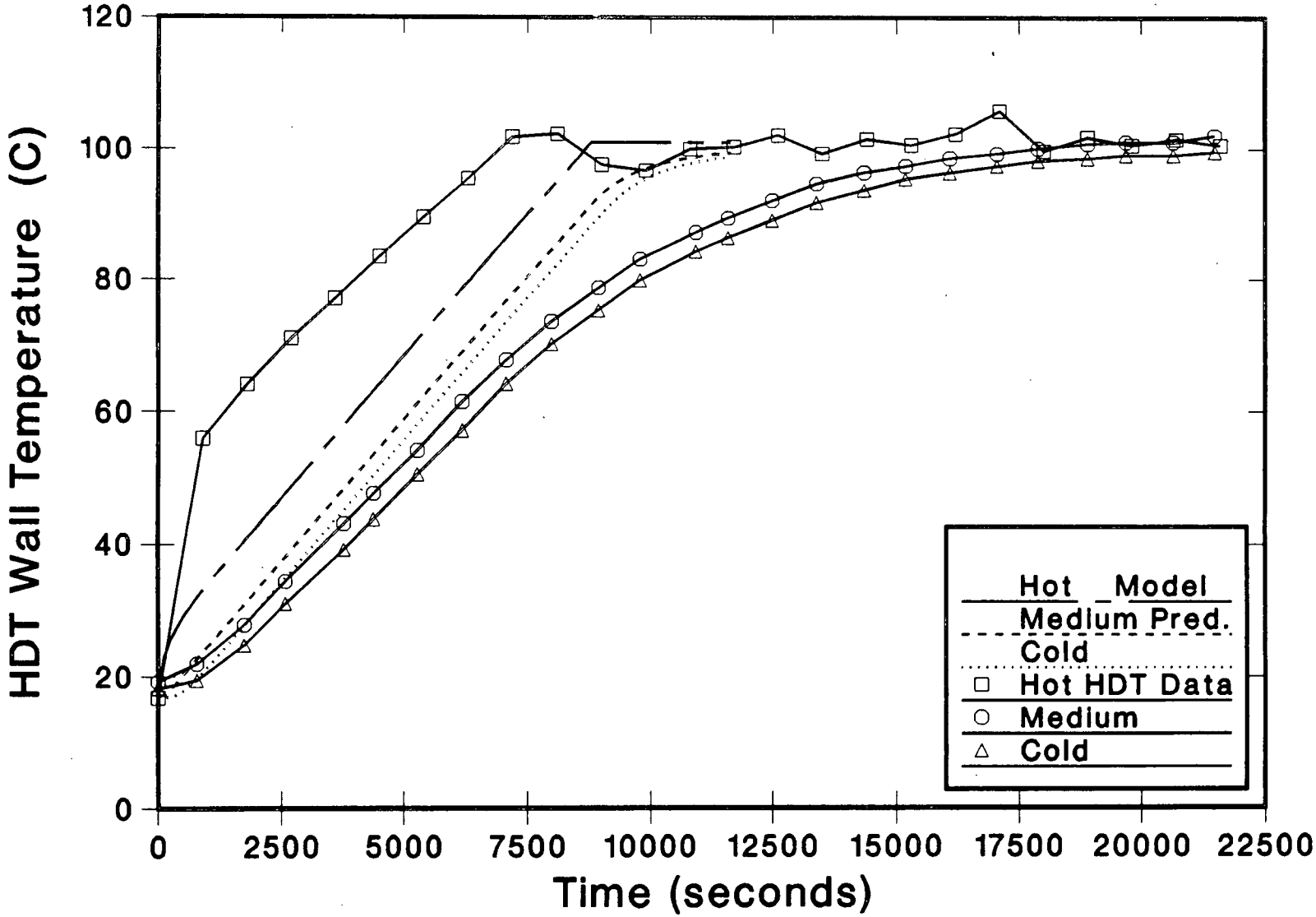

Figure F-2. Comparison of Temperature Distribution and Transient Response of the HDT and 1-D Unsteady Model.

for the HDT data than the model. The model does predict that the intermediate thermocouple is closer in temperature to the cold thermocouple than to the hot thermocouple as is the case in the data. The model also does an adequate job of predicting the time at which the heaters reach the set point temperature of 100°C.

Because of the under-prediction of the temperature difference between the heater temperature and the tube wall temperature midway between the heaters (tip of the fin in the model), the model also predicts a much shorter time to reach steady state than the data shows. If the temperature difference predicted by the model was greater at the time the set point temperature of 101°C was reached, then the time to reach steady state would also be longer. The model makes an adequate prediction of the final steady state temperature distribution.

Figures

F-1. Control Volume for the 1-D Unsteady Fin Model.

F-2. Comparison of Temperature Distribution and Transient Response of the HDT and 1-D Unsteady Model.

APPENDIX G

DATA ACQUISITION SYSTEM DETAILS

The data acquisition system used to acquire time of arrival (pressure) signal in the HDT tests is a general purpose system developed originally for another test apparatus, FLAME [G1]. The hardware consists of a Digital Equipment Corp. LSI 11/23 computer using an IEEE-488 (GPIB) communication bus to control two independent transient digitizer setups, Tektronix 7612D's and a CAMAC (Computer Automated Measurement and Control) rack. The software to control the systems and process the data was custom written. Relevant details of the hardware and software are described in this appendix.

G.1 HARDWARE

The data acquisition system hardware can be divided into three sections corresponding to separate tasks. During a test, data is recorded by two independent transient digitizer systems. The primary system is Tektronix 7612D's transient digitizers with the CAMAC system used as backup. Post-test, the data is transferred from the volatile memory storage onboard the digitizers and transferred to permanent storage.

G.1.1 Tektronix 7612D Transient Digitizers

The HDT uses three Tektronix 7612D's with each unit having two channels. The 7612's provide signal amplification, analog to digital conversion, and volatile memory for each channel. The input voltage range is 40 mV to 40 V full scale for the 7A16A plug in amplifiers currently being used. Each voltage range is converted to 256 digital steps (or "grey levels"). The 7612's can sample as fast as a 5 ns/sample to as slow as 1 s/sample with a total recordable sample size of 2048 samples. The time between samples (or sampling frequency) can be programmed to change at pre-set sample locations. (Note: The period in which the 7612 samples is set at 5ns. If samples are taken every 100ns, the sample is not the average value over the 100 ns.)

For use in the HDT, the 7612's were originally setup to sample every 10 μs/sample. From test HT-51 through HT-96, the sampling rate was preprogrammed for each channel to increase to 1 μs/sample at the expected time of arrival of the detonation front (as predicted by Chapman-Jouguet theory). For the first two channels closest to the initiator, the sample rate at the time of arrival of the detonation was set to 0.5 μs/sample.

It should be noted that the 7612's have high impedance inputs and the cable length to the heated detonation tube from the

digitizer is ~ 100 m (300 ft). The cable is RG-58 coaxial cable with a wave travel time of ~ 1.5 ns/ft. Therefore, the cable resonance period is on the order of 1 μs.

G.1.2 CAMAC Transient Digitizers

The term CAMAC is a generic term for a set of standards for data acquisition and control systems. In the system used as backup for the HDT, no signal amplification is needed. The analog to digital conversion is done by Bi Ra Inc. Model 5908 transient digitizers. These digitizers have variable performance parameters depending on the number of channels of data being used. For the HDT, two to three units are used, each with four channels. The highest sampling rate is 25 μs/sample. The Bi Ra digitizers do not have internal volatile storage, but use separate Bi Ra 5903 external memory units. One unit is used in the HDT tests with a corresponding maximum number of recordable samples per channel of 8192. The digitizing frequency can be changed by an external clock to lower frequencies but this feature is not used for the HDT. The input voltage range is internally selectable and is set at +/-5 V and the analog signal is divided into 4096 grey levels.

In the CAMAC standard, the Bi Ra digitizers cannot communicate directly with the IEEE-488 bus. In the setup for the HDT tests, a LeCroy 8901 bus controller is used for communication between the LSI 11/23 computer and the Bi Ra digitizers.

G.1.3 Storage/Processing Hardware

During a test in the HDT, data is digitized and stored in temporary volatile memory in the digitizers. This data is transferred to permanent storage and further processing by a DEC LSI 11/23 computer. The permanent storage devices are a DSD Inc. Model 880 Winchester hard disk and two DEC double density floppy disk drives. The computer can be addressed, and data plotted, on a Tektronix's 4010 display terminal with a hard copy unit. A Datamedia DT80 is also used as a display terminal.

G.2 SOFTWARE

The software to control the HDT, and to acquire, store and initially process the data is custom written using Tektronix's SPS BASIC language. The language is tied to DEC LSI 11 hardware is currently has a limited 32K words of program memory.

G.2.1 HDT Control Program

The temperature of the HDT is controlled by a program that interrogates the HDT temperature from a CAMAC temperature monitor

(see Appendix A for hardware details) and compares it to user-selected limit or set-point temperatures.* The interrogation, comparison, and relay closure cycle for all 16 measured temperatures occur once every 20 seconds. During each cycle, the program also interrogates a CAMAC clock and the user can select a time interval between printouts. The program can operate in a delayed start mode where only the clock is interrogated. The interrogated time is compared to a user-specified turn-on time. When that time is reached, the program reverts to its normal cycle. This feature is used to begin heating the HDT at night. The computer also communicates each cycle with a watchdog timer device that will open circuit the power if not contacted every 64 seconds. This feature protects the HDT in case of a computer failure.

G.2.2 Data Acquisition Programs

Two data acquisition programs have been written, one to acquire data from the Tektronix 7612D's and the other from the CAMAC system. The first communicates through a Tektronix custom driver which talks only to Tektronix equipment. The second program communicates through a more standard IEEE-488 driver. The programs are used to setup the programmable settings on the hardware as well as retrieve the data. The programmable settings are stored for processing the data.

G.2.3 Data Storage Formats

Tektronix SPS basic provides three storage formats. Data from the 7612D's is stored with the WRITE command format which is a BCD format with special data descriptors (which make it uncompatible to be read by any other language except SPS basic). Data from the CAMAC system is stored with the WRITEU command format which is a record addressable BCD format. The third format is the PRINT command format which stores ASCII output. This format is used to transfer data to other computers for further processing.

G.2.4 Data Processing Programs

Only simple data processing is done on the LSI 11/23 with SPS basic. Engineering units are assigned to the data and plots are made of both the raw and processed data. This facility is sufficient for obtaining the time of arrival data measured in the HDT experiments.

---

*The program then tells a CAMAC relay module to open or close (switching power to the HDT).

G.3 REFERENCES FOR APPENDIX G

G1. Sherman, M. P., Tieszen, S. R., Benedick, W. B., Fisk, J. W., and Berman, M., "The FLAME Facility - The Effect of Transverse Venting on Flame Acceleration and Transition to Detonation," SAND85-1264, NUREGXX-XXXX, (to be published).

DISTRIBUTION:

U.S. Government Printing Office
Receiving Branch (Attn: NRC Stock)
8610 Cherry Lane
Laurel, MD 20707
(250 Copies for R3)

U.S. Nuclear Regulatory Commission (12)
Division of Accident Evaluation
Office of Nuclear Regulatory Research
Washington, DC 20555
Attn: B. W. Morris T. Lee
P. Worthington J. Mitchell
B. Burson R. Meyer
W. S. Farmer J. Telford
M. Fleishman R. W. Wright
M. Silberberg C. W. Nilsen

U. S. Nuclear Regulatory Commission (8)
Office of Nuclear Reactor Regulation
Washington, DC 20555
Attn: V. Benaroya K. I. Parczewski
W. R. Butler Z. Rosztoczy
J. T. Larkins T. M. Su
R. Palla C. G. Tinkler

U.S. Department of Energy
R. W. Barber
Office of Nuclear Safety Coordination
Washington, DC 20545

U. S. Department of Energy (2)
Albuquerque Operations Office
P.O. Box 5400
Albuquerque, NM 87185
Attn: J. R. Roeder, Director
Transportation Safeguards
J. A. Morley, Director
Energy Research Technology
For: C. B. Quinn
R. N. Holton

Argonne National Laboratory (2)
9700 South Cass Avenue
Argonne, IL 60439
Attn: Dae Cho
R. Anderson

Battelle Columbus Laboratory
505 King Avenue
Columbus, OH 43201
Attn: R. Denning

Battelle Pacific Northwest Laboratory (2)
P.O. Box 999
Richland, WA 99352
Attn: M. Freshley
G. R. Bloom

Brookhaven National Laboratory (2)
Upton, NY 11973
Attn: T. Ginsberg
G. Greene

University of California
Nuclear Energy Laboratory (2)
405 Hilgard Avenue
Los Angeles, CA 90024
Attn: Prof. I. Catton
Prof. D. Okrent

Duke Power Company (2)
P. O. Box 33189
Charlotte, NC 28242
Attn: F. G. Hudson
A. L. Sudduth

EG&G Idaho (3)
Willow Creek Building, W-3
P. O. Box 1625
Idaho Falls, ID 83415
Attn: D. Croucher
R. Hobbins
Server Sadik

Electric Power Research Institute (4)
3412 Hillview Avenue
Palo Alto, CA 94303
Attn: J. Haugh
W. Loewenstein
B. R. Sehgal
R. Vogel

Factory Mutual Research Corporation
P. O. Box 688
Norwood, MA 02062
Attn: R. Zalosh

Fauske & Associates
16W070 West 83rd St.
Burr Ridge, IL 60521
Attn: R. Henry

General Electric Corporation
175 Curtner Avenue
Mail Code N 1C157
San Jose, CA 95125
Attn: K. W. Holtzclaw

General Electric Corporation
Advanced Reactor Systems Dept.
P.O. Box 3508
Sunnyvale, CA 94088
Attn: M. I. Temme, Manager
Probabilistic Risk Assessment

Institute of Nuclear Power Operation
1100 Circle 75 Parkway, Suite 1500
Atlanta, GA 30339
Attn: Henry Piper

International Technology Corporation
Attn: Mario H. Fontana
575 Oak Ridge Turnpike
Oak Ridge TN 37830

Los Alamos National Laboratory (7)
P. O. Box 1663
Los Alamos, NM 87545
Attn: F. J. Edeskuty
R. Gido
J. Carson Mark
G. Schott
M. Stevenson
J. Travis
K. D. Williamson, Jr.

Massachusetts Institute of Technology
Nuclear Engineering Dept.
Cambridge, MA 02139
Attn: N. C. Rasmussen

University of Michigan
Department of Aerospace Engineering
Ann Arbor, MI 47109
Attn: Prof. M. Sichel

University of Michigan
Nuclear Engineering Department
Ann Arbor, MI 48104

Mississippi Power & Light
P. O. Box 1640
Jackson, MS 39205
Attn: S. H. Hobbs

Northwestern University
Chemical Engineering Department
Evanston, IL 60201
Attn: Prof. S. G. Bankoff

NUS Corporation
4 Research Place
Rockville, MD 20850
Attn: R. Sherry

Oak Ridge National Laboratory (2)
NRC Programs
P.O. Box X, Bldg. 4500S
Oak Ridge, TN 37831
Attn: A. P. Malinauskas
T. Kress

Power Authority State of NY
10 Columbus Circle
New York, NY 10019

Gladys Shaw (15)
Sandia National Laboratories
P.O. Box 5800
Albuquerque, NM 87185

Dr. J. E. Shepherd
Department of Mechanical Engineering
Aeronautical Engineering and Mechanics
Rensselaer Polytechnic Institute
Troy, NY 12180-3590

Stratton & Associates, Inc.
2 Acoma Lane
Los Alamos, NM 87544
Attn: W. Stratton

Dr. Roger Strehlow
505 South Pine Street
Champaign, IL 61820

Texas A & M University
Nuclear Engineering Dept.
College Station, TX 77843

Prof. T. G. Theofanous
Chemical and Nuclear Engineering Dept.
University of California
Santa Barbara, CA 93106

Westinghouse Corporation (3)
P. O. Box 355
Pittsburgh, PA 15230
Attn: N. Liparulo
J. Olhoeft
V. Srinivas

University of Wisconsin
Nuclear Engineering Department
1500 Johnson Drive
Madison, WI 53706
Attn: Prof. M. L. Corradini

Belgonucleaire S.A.
Rue de Champ de Mars 25
B-1050 Brussels
BELGIUM
Attn: H. Bairiot

CEC
Director of Research, Science & Education
Rue De La Loi 200
1049 Brussels
BELGIUM
Attn: B. Tolley

Atomic Energy Ltd. (2)
Whiteshell Nuclear Research Establishment
Pinawa, Manitoba
CANADA
Attn: D. Liu
D. Wren

Atomic Energy Canada Ltd.
Chalk River, Ontario K0J 1J0
CANADA
Attn: P. Fehrenbach

McGill University
315 Querbes
Outremont, Quebec H2V 3W1
CANADA
Attn: Prof. John H. S. Lee

Institute of Nuclear Energy Research
P.O. Box 3
Lungtan
Taiwan 325
REPUBLIC OF CHINA
Attn: Sen-I-Chang

Battelle Institut E. V. (3)
Am Roemerhof 35
6000 Frankfurt am Main 90
FEDERAL REPUBLIC OF GERMANY
Attn: Dr. Werner Geiger
Dr. Guenter Langer
Dr. Manfred Schildknecht

Gesellschaft für Reaktorsicherheit (GRS)
Postfach 101650
Glockengasse 2
5000 Koeln 1
FEDERAL REPUBLIC OF GERMANY

Gesellschaft für Reaktorsicherheit (2)
8046 Garching
Forschungsgelande
FEDERAL REPUBLIC OF GERMANY
Attn: Dr. E. F. Hicken
Dr. H. L. Jahn

Institute für Kernenergetik und
Energiesysteme (2)
University of Stuttgart
Stuttgart
FEDERAL REPUBLIC OF GERMANY
Attn: M. Buerger
H. Unger

Projekt Schneller Brueter (3)
Kernforschungszentrum Karlsruhe
Postfach 3640
7500 Karlsruhe
FEDERAL REPUBLIC OF GERMANY
Attn: Dr. Kessler
Dr. Heusener
Dr. M. Reimann

Kraftwerk Union
Hammerbacherstrasse 12 & 14
Postfach 3220
D-8520 Erlangen 2
FEDERAL REPUBLIC OF GERMANY
Attn: Dr. M. Peehs

Technische Universität München
8046 Garching
FEDERAL REPUBLIC OF GERMANY
Attn: Dr. H. Karwat

ENEA Nuclear Energ Alt Disp (2)
Via V. Brancati
00144 Roma
ITALY
Attn: P. L. Ficara
G. Petrangeli

Universita Degli Studi Di Pisa
Dipartmento Di Costruzioni
Meccaniche E. Nucleari
Facolta Di Ingegneria
Via Diotisalvi 2
56100 Pisa
ITALY
Attn: M. Carcassi

Japan Atomic Energy Research Institute
Attn: Dr. K. Soda, Manager
Chemical Engineering Safety Laboratory
Dept. of Nuclear Fuel Safety
Tokai-mura, Naku-gun Ibaraki-ken
319-11
JAPAN

Japan Atomic Energy Research Institute
Attn: Dr. T. Fujishiro, Manager
Dept. of Fuel Safety Research
Tokai-mura, Naka-gun, Ibaraki-ken
319-11
JAPAN

Japan Atomic Energy Research Institute
Attn: Mr. Kazuo Sato, Director
Dept. of Reactor Safety Research
Tokai-mura, Naka-gun Ibaraki-ken
319-11
JAPAN

Power Reactor Nuclear Fuel
Development Corp. (PNC)
FBR Project
9-13, 1-Chome, Akasaka
Minato-Ku, Tokyo
JAPAN
Attn: Dr. Watanabe

Korea Advanced Energy Research
Institute
P.O. Box 7
Daeduk Danji, Chungnam
KOREA
Attn: H. R. Jun

Netherlands Energy Research Foundation
P.O. Box 1
1755ZG Petten NH
NETHERLANDS
Attn: K. J. Brinkmann

Statens Karnkraftinspektion
P.O. Box 27106
S-10252 Stockholm
SWEDEN
Attn: L. Hammar

Studsvik Energiteknik AB
S-611 82 Nykoping
SWEDEN
Attn: K. Johansson

Swedish State Power Board
S-162 Fach 87 Vallingby
SWEDEN
Attn: Wiktor Frid

AERE Harwell (2)
Didcot
Oxfordshire OX11 ORA
UNITED KINGDOM
Attn: J. R. Matthews, TPD

National Nuclear Corp. Ltd.
Cambridge Road
Whetestone, Leicester, LE8 3LH
UNITED KINGDOM
Attn: R. May

Simon Engineering Laboratory
University of Manchester
M139PL
UNITED KINGDOM
Attn: Prof. W. B. Hall

UKAEA Safety & Reliability Directorate (2)
Wigshaw Lane, Culcheth
Warrington WA3 4NE
Cheshire
UNITED KINGDOM
Attn: J. H. Gittus
M. R. Hayns

UKAEA, Culham Laboratory (2)
Abingdon
Oxfordshire OX14 3DB
UNITED KINGDOM
Attn: F. Briscoe
D. Fletcher

UKAEA AEE Winfrith (5)
Dorchester
Dorset DT2 8DH
UNITED KINGDOM
Attn: M. Bird
S. Board
T. Butland
R. Potter
A. Wickett

Sandia Distribution:

1131	W. B. Benedick
1510	J. W. Nunziato (1)
	Attn: 1512 J. C. Cummings
1530	L. W. Davison
	Attn: 1534 J. R. Asay
6000	D. L. Hartley
6400	D. J. McCloskey
6412	A. L. Camp
6414	A. S. Benjamin
6415	F. E. Haskin
6419	K. D. Bergeron
6420	J. V. Walker
6422	D. A. Powers
6425	W. J. Camp
6425	M. F. Young
6427	M. Berman
6427	D. F. Beck
6427	J. T. Hitchcock
6427	B. W. Marshall, Jr.
6427	L. S. Nelson
6427	M. P. Sherman
6427	S. E. Slezak
6427	D. W. Stamps
6427	S. R. Tieszen (20)
6427	C. C. Wong
6440	D. A. Dahlgren
3141	S. A. Landenberger (5)
3151	W. L. Garner

NRC FORM 335 (2-84) NRCM 1102, 3201, 3202

U.S. NUCLEAR REGULATORY COMMISSION

BIBLIOGRAPHIC DATA SHEET

SEE INSTRUCTIONS ON THE REVERSE

1 REPORT NUMBER (Assigned by TIDC, add Vol. No., if any)

NUREG/CR-4905
SAND85-1263

2 TITLE AND SUBTITLE

DETONABILITY OF H_2-AIR-DILUENT MIXTURES

3 LEAVE BLANK

4 DATE REPORT COMPLETED

MONTH	YEAR
MARCH	1987

5 AUTHOR(S)

Sheldon R. Tieszen, Martin P. Sherman
William B. Benedick, Marshall Berman

6 DATE REPORT ISSUED

MONTH	YEAR
JUNE	1987

7 PERFORMING ORGANIZATION NAME AND MAILING ADDRESS (Include Zip Code)

Sandia National Laboratories
Reactor Safety Research Department
Severe Accident Containment Response Div.
Albuquerque, NM 87185

8 PROJECT/TASK/WORK UNIT NUMBER

9 FIN OR GRANT NUMBER

A-1246

10 SPONSORING ORGANIZATION NAME AND MAILING ADDRESS (Include Zip Code)

Division of Reactor System Safety
Office of Nuclear Regulatory Research
Accident Evaluation Branch
U.S. Nuclear Regulatory Commission
Washington, DC 20555

11a TYPE OF REPORT

Technical

b PERIOD COVERED (Inclusive dates)

----

12 SUPPLEMENTARY NOTES

13 ABSTRACT (200 words or less)

This report describes the Heated Detonation Tube (HDT). Detonation cell width and velocity results are presented for H_2-air mixtures, undiluted and diluted with CO_2 and H_2O for a range of H_2 concentration, initial temperature and pressure. The results show that the addition of either CO_2 or H_2O significantly increases the detonation cell width and hence reduces the detonability of the mixture. The results also show that the detonation cell width is reduced (detonability is increased) for increased initial temperature and/or pressure.

14 DOCUMENT ANALYSIS - a KEYWORDS/DESCRIPTORS

b IDENTIFIERS/OPEN ENDED TERMS

15 AVAILABILITY STATEMENT

Unlimited

16 SECURITY CLASSIFICATION

(This page)

Unclassified

(This report)

Unclassified

17 NUMBER OF PAGES

212

18 PRICE

☆ U.S. GOVERNMENT PRINTING OFFICE: 1987—773-049/41050

120555003909 1 1AN1R3
US NRC-ASLAP
CHAIRMAN
EWW-532
WASHINGTON DC 20555

WASHINGTON DC 20555